ISSN 1068-9761/e-2541-9935

LIGHT & ENGINEERING

Volume 28, Number 5, 2020

Editorial of Journal
"Light & Engineering" (Svetotekhnika), Moscow

The purpose and content of «Light & Engineering» is to develop the science of light within the framework of ray, photometric concepts and the application of results for a comfortable light environment, as well as for visual and non-visual light technologies, including medicine. The light engineering science is a field of science and technology and its subject is the development of methods for generation and spatial redistribution of optical radiation, as well as its conversion to other forms of energy and use for various purposes.

The scope of journal includes articles in the following areas:

- Sources of light;
- Light field theory;
- Photometry, colorimetry and radiometry of optical radiation;
- Visual and non-visual effects of radiation on humans;
- Control and regulation devices for light sources;
- Light devices, their design and production technology;
- Light devices for the efficient distribution and transportation of the light energy: hollow light guides, optical fibers;
- Lighting and irradiation installations;
- Light signaling and light communication;
- Light remote sensing;
- Mathematical modelling of light devices and installations;
- Energy savings in light installation;
- Innovative light design solutions;
- Photobiology, including problems of using light in medicine;
- Disinfection of premises, drinking water and smell elimination by UV radiation technology;
- Light transfer in the ocean, space and other mediums;
- Light and engineering marketing;
- Legal providing and regulation of energy effective lighting;
- Light conversion to other forms of energy;
- Standardization in field of lighting;
- Light in art and architecture design;
- Education in field of light and engineering.

Journal “Light & Engineering” had been founded by Prof. Julian B. Aizenberg in 1993

LIGHT & ENGINEERING

СВЕТОТЕХНИКА

Editorial of Journal “Light & Engineering/Svetotekhnika”

Moscow, 2020

Publishing House: Editorial of Journal "Light & Engineering" (Svetotekhnika), Moscow

Editorial Office:

Russia, VNISI, Rooms 327 and 334
106 Prospekt Mira, Moscow 129626

Tel: +7.495.682.26.54
Tel./Fax: +7.495.682.58.46
E-mail: lights-nr@inbox.ru
http://www.l-e-journal.com

Light & Engineering" is an international scientific Journal subscribed to by readers in many different countries. It is the English edition of the journal "Svetotekhnika" the oldest scientific publication in Russia, established in 1932.

Establishing the English edition "Light and Engineering" in 1993 allowed Russian illumination science to be presented the colleagues abroad. It attracted the attention of experts and a new generation of scientists from different countries to Russian domestic achievements in light and engineering science. It also introduced the results of international research and their industrial application on the Russian lighting market.

The scope of our publication is to present the most current results of fundamental research in the field of illumination science. This includes theoretical bases of light source development, physiological optics, lighting technology, photometry, colorimetry, radiometry and metrology, visual perception, health and hazard, energy efficiency, semiconductor sources of light and many others related directions. The journal also aims to cover the application illumination science in technology of light sources, lighting devices, lighting installations, control systems, standards, lighting art and design, and so on.

"Light & Engineering" is well known by its brand and design in the field of light and illumination. Each annual volume has six issues, with about 80–120 pages per issue. Each paper is reviewed by recognized world experts.

CONTENTS

VOLUME 28 NUMBER 5 2020

LIGHT & ENGINEERING

Light & Engineering
Vol. 28, No. 5, pp. 4–8, 2020

https://doi.org/10.33383/2020-036
Svetoteknnika #5, 2020, pp. 5–8

PRESENT AND FUTURE ACTIVITIES OF THE INTERNATIONAL COMMISSION ON ILLUMINATION (CIE)

Peter Blattner

The Optics Laboratory at the Swiss Federal Institute of Metrology (METAS), Bern-Wabern, Switzerland
Email: peter_blattner@bluewin.ch

ABSTRACT

The article describes the main activities of the International Commission on Illumination in recent years. The most important publications are reflecting recent developments in lighting science and industry, including LED sources and luminaires test methods, fundamental recommendations concerning colorimetry, discomfort caused by glare from luminaires with a non-uniform luminance, as well as intelligent control of lighting systems. Human centric lighting and the non-visual effects of light on humans was highlighted. To promote standardization in the field of horticultural lighting the CIE is in the process of establishing a new JTC. In view of *COVID-19* pandemic outspread the use of germicidal UV radiation is of relevance to reduce both contact spread and airborne transmission of infectious agents. The CIE is responsible for worldwide standardization of the fundamentals, including metrology and vocabulary, as well as lighting education. The CIE considers it important to make digital products including validated calculation tools, apps, databases and machine-readable documents more available for many experts and it takes a step in this direction by provide open access to the individual CIE publications.

Keywords: CIE, Joint Technical Comittee (JTC), colorimetry, International Electrotechnical Vocabulary, weights and measures, human centric lighting, non-visual effects, ganglian cells (ipRGCs)

INTRODUCTION

It is with reverence and humbleness but also with great pleasure that I accept the Presidency of the International Commission on Illumination (CIE), this outstanding and honourable organization founded in 1913 by the lighting societies of several countries.

In recent years, the lighting industry has gone through a turbulent period. This technological but also structural transformation has a direct impact on the work of the CIE. The LED has largely replaced the "classical" light sources. Accordingly, the CIE has adapted many of its guidelines and recommendations. Some of the examples are presented below.

– **CIE S025:2015** [1] *Test Method for LED Lamps, LED Luminaires and LED Modules*: it is the first international agreed standard in respect to the measurement of LED light sources. These standards also include considerations on measurement uncertainties, a concept that not yet fully established in the industry. CIE offered, therefore, several pieces of training and tutorials, including a very successful tutorial in Moscow organized in collaboration with Russian Lighting Research Institute named after Sergey Vavilov (VNISI) in November 2018. A supplement has recently been published dealing with organic LEDs (OLEDs) [2].

– **CIE015:2018** *Colorimetry, 4th Edition* [3], this document collects the fundamental recommendations of the CIE concerning colourimetry. Specifically, it includes the use of the standard colorimetric observers and standard illuminants, the reference

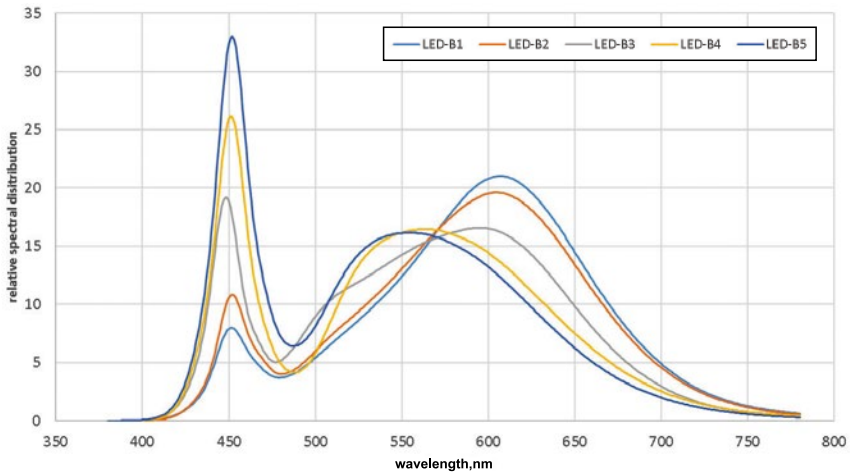

Fig. 1. Relative spectral distribution of LED illuminants as defined in CIE15:2018 [3]

standard for reflectance, chromaticity coordinates, colour space coordinates and colour differences and various other colorimetric practices and formulae. It its latest edition new illuminants for different LED types are introduced (Fig. 1). Furthermore, new findings on cone-fundamental-based tristimulus functions based on CIE170–1 [4] and CIE170–2 [5] are included;

– **CIE232:2019** *Discomfort Caused by Glare from Luminaires with a Non-Uniform Source Luminance* [6]. LEDs allow the design and realisation of aesthetically beautiful, but technically sophisticated luminaires. Among other things, the light distribution, the spectral composition but also the illuminated surface can be adapted practically as desired. However, if this is not done correctly, it can lead to glare. The CIE232 report gives for the first time a recommendation on how to assess the glare of non-uniform illuminated surfaces. The step to evaluate the glare of a non-uniform light source is shown in Fig. 2.

The technological revolution in the field of light and lighting was initially triggered by the increase in luminous efficacy of the light sources. However, for physical reasons, the luminous efficacy of light sources cannot increase indefinitely. An important way to increase energy efficiency is the intelligent control of lighting systems. It includes adaptive light sources as well as smart sensors. In this interconnected world, it is important for the CIE to position itself clearly and address issues such as dynamic or adaptive lighting. CIE has, therefore, set up a new technical committee TC4–62 to analyse needs, specify recommendations, develop methodology and promote the application of adaptive road lighting.

The lighting industry has created the term "Human Centric Lighting" to describe the non-visual effects of light on humans induced or supported by the intrinsically photosensitive retinal ganglion cells (ipRGCs). Personally, I prefer the term "integrative lighting", which is used within the CIE and ISO. It represents the versatility of light and lighting, namely the combination of visual and non-visual effects to produce physiological and/or psychological benefits on humans. With the introduction of the International Standard CIE S026:2018 CIE *System for Metrology of Optical Radiation for ipRGC–Influenced Responses to Light [7]* the CIE has created an important basis for the different stakeholders to use the same terms and metrics. Now it is a matter of establishing these metrics in the research community and, thus, generate results that can be applied for the benefit of the human being.

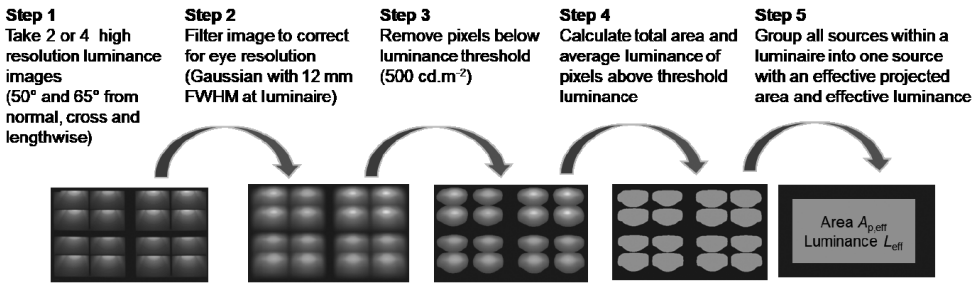

Fig. 2. Overview of the measurement and image processing steps required to obtain the effective projected area and the effective luminance used to predict the glare of a non-uniform light source according to CIE232:2019 [5] (© CIE)

As an important tool, I note the CIE research strategy, which takes a forward-looking approach to the major topics on our field.

But the subject of light and lighting does not end with integrative lighting for humans. Optical radiation is used for horticultural lighting or disinfection applications. In addition to the clever use of optical radiation, it is also about minimizing negative effects, e.g. through light pollution or photobiological damage.

It was with great pleasure that I took note of the initiative of VNISI to promote standardization in the field of horticultural lighting. Based on this proposal, the CIE is in the process of establishing a new joint technical committee, and I hope that many Russian experts will be able to participate in this important activity and contribute their knowledge. I have a fond memory of the first *International Scientific and Technical Greenhouses Lighting Conference*, organized in September 2019 in Moscow.

Triggered by the pandemic outspread of the coronavirus, CIE has recently released a position statement on the use of ultraviolet (UV) radiation to manage the risk of *COVID*-19 transmission. The use of germicidal UV radiation is an important environmental intervention, which can reduce both contact spread and airborne transmission of infectious agents (like bacteria and viruses). However, germicidal UV radiation must be knowledgeably applied with appropriate attention to dose and safety. Inappropriate GUV application can present human health and safety issues and produce insufficient deactivation of infectious agents. Therefore, application in the home is not advisable, and GUV should never be used to disinfect the skin, except when clinically justified. With the help of the different national committees, the CIE position statement was translated into many different languages, including Russian. In addition, CIE has two publications freely available (CIE187:2010 *UV–C Photocarcinogenesis Risks from Germicidal Lamps* [8] and CIE155:2003 *Ultraviolet Air Disinfection* [9]) to support the international community in the fight against the virus. Both publications were translated also in Russian language.

INTERNATIONAL COOPERATION CIE

The CIE is not only a global organisation dealing with the science and technology of light and lighting. It is also a standardization organization since its foundation. Through the cooperation of experts from various national committees, internationally recognised standards are created. The CIE was the first and is still one of the few standards development organisations recognised by the International Organisation for Standardisation (ISO). The cooperation with *ISO*, in particular ISO TC274 Light and Lighting, is defined in a PSDO-Agreement (Partner Standards Developing Organization), which was renewed last year. The *CIE* is responsible for worldwide standardization of the fundamentals, including metrology and vocabulary, while ISO TC274 focuses on standardization in the field of applications. The CIE also works very closely with the International Electrotechnical Committee IEC, in particular IEC TC34 and IEC TC76. The work of the IEC standardization committees focuses on product safety and performance. Examples of the successful cooperation with the IEC is the important lamp and luminaire safety standard IEC62471/CIE S009 [10], which was developed in the CIE and then published as a dual logo standard. Experts are also working together to revise the International Lighting Vocabulary (ILV) [10], which in its latest edition to be published soon, will be fully harmonised with IEC60050–845 (the International Electrotechnical Vocabulary, IEV) [12]. This is very important work, because a common understanding of the meaning of words is needed to eliminate ambiguities and uncertainties. It is therefore important that this comprehensive work is translated into as many languages as possible. The national committees of the CIE also play an important role in this respect. However, language is not something static, but is constantly evolving, especially as new areas are explored. The most recent example is the field of horticulture lighting, which is being worked on together with IEC TC34.

CIE also has a mutual agreement with the Committee for Weights and Measures (CIPM), which recognizes the respective competencies. In particular, CIE recognises the role of CIPM in respect to the definition of units (i.e. the SI-units), whereas the CIPM recognises that CIE is responsible for the definition of quantities and action spectra in the field of photometry, photobiology and photochemistry. Therefore, CIE made a significant contributed to the 9th edition SI-Brochure, in particular, *Annex 3* on photobiological and photochemical quantities [13]. In addition, the joint publication “Principle

Governing Photometry" [14, 15] was updated, reflecting the fundamental changes of the International System of Units of Measurement on May 20, 2019, in which the concept of the seven base units has been replaced by a system based on seven defining constants, including the constant for luminous efficacy of monochromatic radiation of frequency (540×1012) Hz, K_{cd}.

LIGHTING EDUCATION

The field of light and lighting is becoming increasingly interdisciplinary, which is why the CIE has created the possibility of horizontal the technical committees and joint technical committees *(*JTCs*)*. Recently, the number of JTCs has increased significantly. It is a challenge to manage this JTC structure, and the code of procedure may need to be adapted in support of this. The efficient interaction between the different division is not only important at CIE*,* but also within the national committees. Again, good communication between all the concerned experts is relevant. In this context, I would like to highlight the newly created the joint technical committee JTC18 Lighting Education: as we all know, lighting is going through a historical technological change. Therefore, it is very important that these comprehensive changes are also incorporated into the training and education of new experts. The aim of the new JTC is to revise and update the outdated technical report CIE99:1989 Lighting education (1983–1989) [16] and to provide recommendations on curricula for higher education and continuing education. It will propose recommendations for the education of lighting professionals and recommend options to improve and support continuing lighting education throughout the professional working life.

PROGRESS IN COLOUR VISION

But we shouldn't forget the progress in the well established areas of CIE. The present colorimetric concepts are based on the research conducted almost a hundred years ago. In fact, at its eighth session in 1931, the CIE defined the standard illuminants, colour matching functions for standard observers and standard chromaticity diagrams. Since then, research in colour vision has made enormous progress. The colour sensation results from physiological processes, the first of which is the capture of photons by the cones of the retina. The fundamental sensitivities of the cones need to be precisely known to accurately specify a colour stimulus from a given spectral power distribution. Part 1 of CIE170 provides the scientific community with cone fundamentals, which are the relative spectral sensitivities of the long-wave sensitive (LWS), middle-wave sensitive (MWS), and short-wave sensitive (SWS) cones as measured at the entrance of the eye. Part 2 of CIE170 provides the user with practical colorimetric tools in the form of chromaticity diagrams. It includes a link has been established between colorimetry and physiology. Starting from the cone-fundamental based spectral luminous efficiency functions, it is possible redefine new colour spaces including the MacLeod–Boynton LMS tristimulus spaces. Moreover, as the model is based on physiology, it is possible to calculated responsivities for "non-standard" observers, i.e. at different ages, with different field sizes, and even calculated a new, cone-fundamental based spectral luminous efficiency function ($V_F(\lambda)$) or other derivate colour quantities.

PHOTOMETRY

In the field of photometry, the change of the reference spectrum used for the calibration of photometers is discussed in TC2–90, substituting incandescent based reference sources to LEDs. A change of reference spectrum will have a huge impact on many stakeholders of CIE, including the instrument manufacturers, the calibration laboratories, the National Metrological Institutes, and the users. Therefore, it is foreseen to propose a LED spectrum in addition to the existing CIE standard illuminant *A*, and both spectra will be used for calibration purposes.

Increased activity is also observed in the field of the characterization of the appearance of surfaces and materials: the technical committee TC2–85 is preparing a recommendation on the geometrical parameters for the measurement of the bidirectional reflectance distribution function (BRDF), TC*2*–94 deals with the measurement of total transmittance, diffuse transmittance, and transmittance Haze, JTC12 (D2/D1/D8) the measurement of sparkle and graininess, and lastly JTC17 (D1/D2/D8) with a gloss measurement and gloss perception. This latest JTC will prepare a framework for the definition and standardization of visual cues to gloss.

CONCLUSIONS

Finally, in the area of publications, there will be further challenges in the coming years. The call for free access to the publications and proceedings is getting stronger. Certain public research institutions request that the research results, which are financed by public funds, become publicly available. The CIE is taking a step in this direction by making the individual papers of the CIE session in Washington D.C. freely available. In addition to the free access to expertise, digitization is a challenge and an opportunity for the CIE. It will be important to make use of new forms of digital products, including validated calculation tools, apps, databases, machine-readable documents, etc. The digitalization of products, meetings, and events is obviously be pushed by the present extraordinary situation due to the pandemic spread of the coronavirus.

However, the CIE is not only an international forum for the discussion of all questions relating to the science, technology and art of light and lighting, but we should not forget that above all it is the umbrella organization of national associations in the field of light and lighting. The CIE is a fascinating organization. It lives from a high diversity of people and their expertise. I look forward to continuing to work with all the experts spread all over the world, and I hope to meet many experts in person during my term as CIE President.

The Editorial Board of Svetotekhnika / Light & Engineering Journals warmly welcomes member of its Editorial Board Dr. Blattner, the current President of CIE since 2019, and looks forward to fruitful cooperation of CIE with the Russian edition, as well as with the Russian National Committee of CIE

REFERENCES

1. CIE S025:2015 Test Method for LED Lamps, LED Luminaires and LED Modules, Vienna, 2015.

2. CIE S025-SP1:2019 Test Method for OLED Luminaires and OLED Light Sources,, DOI: 10.25039/S025-SP1.2019, Vienna, 2019.

3. CIE015:2018 Colorimetry, 4th Edition, ISBN: 978–3–902842–13–8, DOI: 10.25039/TR.015.2018, Vienna, 2018.

4. CIE170–1: 2006 Fundamental chromaticity diagram with physiological axes – Part 1, ISBN: 978 3901906 46 6, Vienna 2006.

5. CIE170–2::2015 Fundamental Chromaticity Diagram with Physiological Axes – Part 2: Spectral Luminous Efficiency Functions and Chromaticity Diagrams, ISBN: 978–3–902842–05–3, Vienna, 2015.

6. CIE232:2019 Discomfort Caused by Glare from Luminaires with a Non-Uniform Source Luminance, ISBN: 978–3–902842–15–2 DOI: 10.25039/TR.232.2019, Vienna 2019.

7. CIE S026:2018 CIE System for Metrology of Optical Radiation for ipRGC–Influenced Responses to Light, DOI: 10.25039/S026.2018, Vienna, 2018.

8. CIE187:2010 UV–C Photocarcinogenesis Risks from Germicidal Lamps, ISBN: 978 3901906 81 7, Vienna 2010.

9. CIE155:2003 Ultraviolet Air Disinfection [8], ISBN: 978 3901906 25 1, Vienna 2003.

10. IEC62471:2006/CIE S009:2002 Photobiological safety of lamps and lamp systems., Geneva 2006.

11. CIE S017/E:2011 International Lighting Vocabulary (ILV), also available at http://eilv.cie.co.at/, Vienna 2011.

12. IEC60050–845: 1987 (the International Electrotechnical Vocabulary, IEV), Geneva, 1987. Also available at http://www.electropedia.org

13. BIPM, 9th edition SI-Broschure, ISBN978–92–822–2272–0, Sèvres, 2019. Also available at https://www.bipm.org/en/publications/si-brochure/

14. BIPM/CIE, "Principle Governing Photometry" Rapport BIPM-2019/05, Sèvres, 2019.

15. CIE018:2019 The Basis of Physical Photometry, 3rd Edition ISBN978–3–902842–24–4, DOI: 10.25039/TR.018.2019, Vienna 2019.

16. CIE99:1989 Lighting education (1983–1989), ISBN: 978 3900734 36 7, Vienna 1989.

Peter Blattner,
Ph.D. in Physics. He has a Ph.D. in the field of Applied Optics from the University of Neuchâtel, Switzerland. He joined the Swiss Federal Institute of Metrology (METAS) in 2000, where he is currently the Head of the Optics laboratory. Since 2011 he has been the Director of CIE Division 2. In this role he represents CIE at the Consultative Committees for Units (CCU) and for Photometry and Radiometry (CCPR). Furthermore, he is active in several standardization committees (ISO/TC169, IEC/TC34, IEC/TC76, CEN /TC169) and chairs the Swiss Standardization Committee on light and lighting. In 2015 he received the CIE Wyszecki Gold Pin award for outstanding contribution in fundamental research. In October 2017 he was elected CIE President for the period 2019 to 2023

Light & Engineering
Vol. 28, No. 5, pp. 9–24, 2020

https://doi.org/10.33383/2020-018
Svetotekhnika #4 pp.64–76

BRIGHTNESS IN THE PHOTOPIC RANGE: PSYCHOPHYSICAL MODELLING WITH BLUE-SENSITIVE RETINAL SIGNALS

Peter Bodrogi, Xue Guo, and Tran Quoc Khanh

Laboratory of Lighting Technology, Technische Universität Darmstadt, Darmstadt, Germany
Email: bodrogi@lichttechnik.tu-darmstadt.de

ABSTRACT

The brightness perception of a large (41°) uniform visual field was investigated in a visual psychophysical experiment. Subjects assessed the brightness of 20 light source spectra of different chromaticities at two luminance levels, L_v=267.6 cd/m^2 and L_v=24.8 cd/m^2. The resulting mean subjective brightness scale values were modelled by a combination of the signals of retinal mechanisms: *S*-cones, rods, intrinsically photosensitive retinal ganglion cells (*ipRGCs*) and the difference of the *L*-cone signal and the *M*-cone signal. A new quantity, "relative spectral blue content", was also considered for modelling. This quantity was defined as "the spectral radiance of the light stimulus integrated with the range (380–520) nm, relative to luminance". The "relative spectral blue content" model could describe the subjective brightness perception of the observers with reasonable accuracy.

Keywords: subjective brightness, brightness perception, photopic brightness model, retinal mechanisms, spectral blue content

1. INTRODUCTION

1.1. Brightness: Definition and Relevance

Brightness (that is, the subjective brightness impression of a visual stimulus as perceived by human observers) is defined in the International Lighting Vocabulary of the International Commission on Illumination, CIE ILV) as an "attribute of a visual perception according to which an area appears to emit or reflect more or less light" [1]. Although brightness has "at least three aspects" [2], the present article deals only with the so-called "spatial brightness" aspect, the perception of "the overall amount of light reaching the observer's eyes" [2]. The concept of "spatial brightness" is important in many areas of lighting engineering, including the design of a lit interior space, in which brightness should be generally high enough in order "to make seeing easy" [3], that is, for good visual performance. The spatial brightness distributions of interior lighting should be well-balanced for good visual comfort and good (three-dimensional) space perception or perceived spaciousness [3, 4]. With exterior lighting, increasing the perceived spatial brightness of a scene increases the impression of safety [6], which is important for pedestriansy. The concept of spatial brightness refers to the brightness of spatially extended scenes, rather than small light sources or small individual objects [5, 7].

1.2. The Difference Between Brightness and Luminance

In 1933, L.A. Jones was appointed the Chairman of the Optical Society of America Committee on Colourimetry (1922) and asked to update recent work progress. Subsequently, a preliminary report was published, in which the term luminance was introduced [8]. Afterwards, Jones wrote [9] that the Committee recommended that the word 'luminosity' be substituted for 'visibility'. The Committee also decided to reserve the term 'brightness' as the name for the sensory attribute correlated with the

photometric quantity to which the term 'luminance' was assigned. Later it was stated that "photometry was based on an incomplete description of the human visual system's capabilities" [10], because the $V(\lambda)$ function (the basis of photometry) and its derived quantities (luminance, illuminance, etc.) represent the linear combination of only the long- (*L*-) and medium- (*M*-) wavelength sensitive retinal cone photoreceptors and do not include the important signals of the short-wavelength sensitive (*S*-) cones, rod photoreceptors, and intrinsically photosensitive retinal ganglion cells (*ipRGCs*).

The latter (so-called "shorter-wavelength sensitive") photoreceptor signals contribute (depending on the luminance level) to the brightness perception [11–17] together with the signals of the two chromatic (opponent) channels, *(L–M)* and *(L+M-S)* [13]. A saturated colour stimulus looks brighter than its de-saturated counterpart of the same luminance (this is the "brightness-luminance discrepancy" or Helmholtz-Kohlrausch effect) [18, 19]. Thus, the impression of brightness cannot be described by the quantity "luminance" alone. In the above description, the term "signal" is understood mathematically in the sense of weighting the relative spectral power distribution of the light source with the spectral sensitivity of a photoreceptor and integrating in the visible wavelength range.

1.3. Brightness Models

Here, selected brightness models from the literature are summarized and compared with the models used in the present article. Brightness models usually combine the values of the abovementioned retinal signals, including the two opponent channels ((*L–M)* and (*L+M-S*)), or their approximations based on the *XYZ* tristimulus values of standard CIE colourimetry. Brightness models also contain an approximation of the *(L+M)* signal (most often photopic luminance, L_v is used), a representation of the rod signal (most often scotopic luminance is used), and the *ipRGC* signal (the signal of the intrinsically photosensitive retinal ganglion cells) in order to derive a numeric predictor quantity for human brightness impression. In some models, this predictor quantity is only intended to forecast the rank order of the visual stimuli according to their brightness perception, without representing a numeric correlate of the absolute magnitude of perceived brightness. These are the so-called equivalent luminance (or L_{eq}) models. Eq. 1 shows an example of a brightness model according to Fotios and Levermore [20]:

$$L_{eq} = L_v \cdot (S / V)^{0.24}, \tag{1}$$

where the *S*-signal is computed by the Smith and Pokorny cone sensitivity data [21] and the quantity *V* (so-called *V*-signal) is obtained by weighting the relative spectral power distribution of the light source with the *V(λ)* function and integrating in the visible wavelength range.

Another example of a brightness model is "equivalent luminance L_{eq} according to Ware and Cowan" (also called WCCF equation) [22]. This model is based on standard CIE colourimetry and shown below

$$L_{eq} = (B / L) \cdot L_v, \tag{2}$$

where the symbol *(B/L)* represents the so-called "brightness-luminance ratio" to be computed from the CIE *x*, *y* chromaticity coordinates of the stimulus by

$$lg(B / L) = 0.256 - 0.184 \cdot y - 2.527 \cdot x \cdot y + \\ + 4.656 \cdot x^3 \cdot y + 4.657 \cdot x \cdot y^4. \tag{3}$$

Rea et al. (2011) model [15] works with the weighted sum of two signals: the *V*-signal and the *S*-signal. In Fotios and Levermore (1998) model [13], "perceived brightness is considered to be a sum of the total activity in three channels": *(L+M)* (represented by $V(\lambda)$) and the above-mentioned two opponent channels. The Guth model [23] is based on the concept of vector luminance that equals the square root of three squared components, *A* (achromatic component), *T* (first chromatic component) and *D* (second chromatic component). Yaguchi and Ikeda (1983) used a modification of the Guth model to account for the spectral additivity failure that they measured in their visual brightness matching experiments [24]. Kokoschka-Bodmann model [25, 26] computes the value of equivalent luminance for brightness from the 10° tristimulus values (X_{10}, Y_{10}, Z_{10}) and scotopic luminance (*L'*).

In the Yamakawa et al. model [47], obtained as a result of a subjective brightness magnitude estimation experiment, is shown below:

$$R = 0.00484 \cdot G^{1.1} + 2.31 \cdot E^{0.48}, \tag{4}$$

Table 1. Overview of Brightness Models Given in the Literature and Proposed in this Article

The authors of the models	Model type	Signals or quantities
Fotios and Levermore [20] (1)	Equivalent luminance	*S, V,* L_v
Ware and Cowan (*WCCF*) [22] (2, 3)	Equivalent luminance	*x, y,* L_v
Rea et al. [15]	Weighted sum of signals	*S, V*
Fotios and Levermore [13]	Weighted sum of channels	*L+M, L–M, L+M-S*
Guth [23]	Weighted sum of channels	*A, T, D*
Yaguchi and Ikeda [24]	Weighted sum of channels	*A, T, D* (modified)
Kokoschka-Bodmann[25, 26]	Equivalent luminance	X_{10}, Y_{10}, Z_{10}, *L'* (rods)
Besenecker and Bullough's "B_2"[14]	Weighted sum of signals	*S, V, ipRGC*
Yamakawa et al. [47] (4)	Weighted sum of channels	*E*, *ipRGC*
Present article, Eq. (13)	Relative spectral blue content	L_v, $\Phi_{rel,\,blue}$

where the *ipRGC* signal (this was called melanopsin signal on the retina, denoted by *G*) was combined with retinal illuminance (denoted by *E*) to predict the perceived brightness (denoted by *R*) of metameric white stimuli (at the fixed chromaticity of x=0.328 and y=0.367) with different amounts of the ipRGC signal and at different luminance levels (between 22 cd/m^2 and 112 cd/m^2).

Besenecker and Bullough's (2016) so-called "B_2 brightness model" [14] contains the weighted sum of three signals, the *V*-signal, the *S*-signal and the *ipRGC* signal, reflecting the fact that "short-wavelength (<500 nm) output of light sources enhances spatial brightness perception in the low-to-moderate photopic range". Inspired by this idea, in the present article the so-called relative spectral blue content will be considered as a new modelling quantity, and its definition is shown below:

$$\Phi_{rel,blue} = [267.6 / L_v] \cdot \int_{380}^{520} L_e(\lambda) d\lambda, \qquad (5)$$

where $\Phi_{rel,\,blue}$ is relative spectral blue content. It is defined as the spectral radiance *Le(λ)* of the stimulus integrated between 380 nm and 520 nm, relative to its luminance L_v. This definition uses 267.6 cd/m^2 for re-scaling because this was one of the two luminance levels in the experimental method of the present article.

As mentioned above, the quantity of $\Phi_{rel,\,blue}$ is similar to Besenecker and Bullough's [14] concept of short-wavelength (<500 nm) output, but we use 520 nm as the upper limit in (5) in order to overlap slightly more with rod photoreceptor spectral sensitivity (to be able to better account for possible rod contribution). Table 1 shows a classification of the abovementioned brightness models according to the type of brightness model.

1.4. Objectives of the Present Article

In the present article, a visual brightness experiment will be described. The experiment was conducted at two fixed luminance levels (L_v=267.6 cd/m^2 and 24.8 cd/m^2) with 20 different chromaticities (different photoreceptor signal contents) of the visual stimulus at each level. The result will be modelled:

1. With a combination of the abovementioned signals of the retinal mechanisms;

2. With *relative spectral blue content* (5), as a proxy of the signals of the three shorter-wavelength sensitive mechanisms, *S*-cones, *ipRGCs,* and rods.

The research questions of the present article are:

1. Are the contributions of three shorter-wavelength mechanisms (*S*-cones, *ipRGCs* and, rods) to evoke human brightness perception distinguishable from each other (and from the relative spectral blue content) based on the results of the visual brightness experiment?

2. Is there significant rod contribution to perceived brightness at the two luminance levels of the experiment (L_v=267.6 cd/m^2 and 24.8 cd/m^2)?

3. Does the opponent signal (*L–M*) have an effect (the difference of the *L*-cone signal and the *M*-cone signal)?

4. Can we use the quantity of "relative spectral blue content*"* (5) to model the perceived brightness in a new, practicable model?

We will use a combination of the photoreceptor signals and relative spectral blue content for mod-

elling brightness, i.e. to explain the subjective visual brightness scales (*VBS*) of the observers resulting from the experiment of the present article. These two hypotheses are formulated below:

$$VBS \sim lg(L_v)\cdot[A_S(S_{rel})^{\gamma} + A_{ipRGC}(ipRGC_{rel})^{\gamma} + A_R(R_{rel})^{\gamma} + A_{L-M}(|L_{rel} - M_{rel}|)^{\gamma}], \quad (6)$$

$$VBS \sim lg(L_v)\cdot[(\Phi_{rel,blue})^{\gamma}]. \quad (7)$$

Eq. 6 represents signal combination formula, and eq. 7 is relative spectral blue content formula. Optimum model parameters (the signal weighting factors A_S, A_{ipRGC}, A_R, $A_{L–M}$ and the exponent γ) will be calculated based on the mean brightness scales of the observers. The quantity $lg(L_v)$ is included to account for the effect of the changing overall luminance level of the visual stimulus. Here the "~" symbol means that the quantity on the left shall be explained by the quantity on the right. The quantity $|L_{rel}\text{-}M_{rel}|$ is a so-called opponent signal: the difference of the relative *L*-cone signal and the relative *M*-cone signal.

The so-called relative signal values L_{rel}, M_{rel}, S_{rel}, R_{rel} and $ipRGC_{rel}$ in (6) were computed as follows:

1. The spectral power distribution (SPD) of the stimulus was normalized so that its luminance equalled 267.6 cd/m^2;

2. This normalized SPD was weighted by the relative spectral sensitivity of a certain retinal mechanism;

3. This weighted SPD was integrated in the wavelength range (380–780) nm.

This computation is shown below in (8) – (12):

$$L_{rel} = [267.6 / L_v] \cdot \int_{380}^{780} L_e(\lambda)L(\lambda)d\lambda, \quad (8)$$

$$M_{rel} = [267.6 / L_v] \cdot \int_{380}^{780} L_e(\lambda)M(\lambda)d\lambda, \quad (9)$$

$$S_{rel} = [267.6 / L_v] \cdot \int_{380}^{780} L_e(\lambda)S(\lambda)d\lambda, \quad (10)$$

$$R_{rel} = [267.6 / L_v] \cdot \int_{380}^{780} L_e(\lambda)V'(\lambda)d\lambda, \quad (11)$$

$$ipRGC_{rel} = [267.6 / L_v] \cdot \int_{380}^{780} L_e(\lambda)ipRGC(\lambda)d\lambda, \quad (12)$$

where the so-called "Stockman and Sharpe (2000) 2° fundamentals" [27, 28] were taken as the spectral sensitivities of the *L*-, *M*- and *S*-cones, $L(\lambda)$, $M(\lambda)$ and $S(\lambda)$. The spectral sensitivity of the intrinsically photosensitive retinal ganglion cells mechanism, $ipRGC(\lambda)$, was computed according to [29, 30], while the $V'(\lambda)$ function (the CIE scotopic spectral luminous efficiency function) was applied to represent the contribution of the rod photoreceptors to brightness perception.

Another purpose of the present article is to compare the optimum values of the exponent γ in (6) – (7) in case of the two luminance levels, 267.6 cd/m^2 and 24.8 cd/m^2, and to compare these optimum exponent values with the exponent value in Fotios and Levermore model (1) (γ =0.24). Another question is whether the two exponents at the two luminance levels of the present brightness experiment are significantly different. In summary, the objective of the present article is the modelling of the dataset of the new visual brightness experiment (see section 2) using hypothetical (6) and (7).

2. EXPERIMENTAL METHOD

The so-called brightness discrimination procedure [31] was used, during which the subjects were instructed to report which chamber of a two-chamber viewing booth appeared brighter, see Fig. 1. The subjects also had to tell how much brighter it was. To do this, they used the following ordinal scale: 0- almost equally bright, with almost no visible brightness difference; 1- somewhat brighter with a very small difference; 2- somewhat brighter; 3- explicitly brighter; and 4- explicitly brighter with a big difference. Then the subjects were instructed as follows: "if you say, for example, 'right 2', this means that the right chamber is somewhat brighter than the left chamber. If you say, 'left 4', this means that the left chamber is explicitly brighter than the right chamber and a big difference is visible." The investigator recorded every spoken answer immediately to a computer spreadsheet.

The subjects had a controlled sitting position in front of the viewing booth. This was checked by the experimenter. They had to sit in the middle so that the distance between the eyes and the viewing booth equalled 20 cm, and the distance between the eyes and the middle of the bottom of each chamber equalled 80 cm (see Fig. 1). The width of each chamber was 60 cm (corresponding to 41°), their height was 53 cm and their depth was 67 cm. The width of the separating wall between the two chambers equalled 6 cm (corresponding to 4°). The two light sources were positioned on the top of the viewing booth at a height of 72 cm above the top cov-

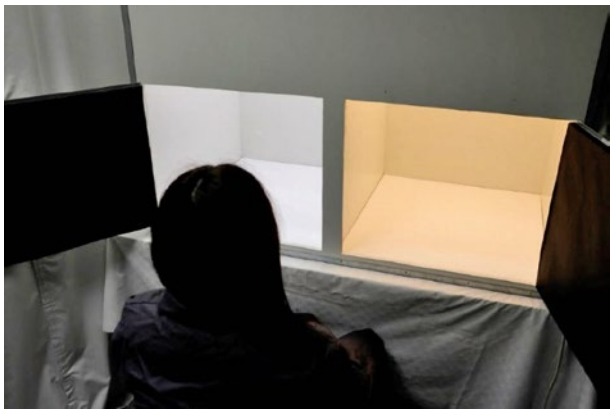

Fig. 1. The subject compared the brightness of the two chambers when the luminance of the two chambers was the same, i.e. at equi-luminance, either at 267.6 cd/m^2 or at 24.8 cd/m^2; here, the reference stimulus appears on the left ("2nd series")

ers of the two chambers. This provided ample space to mix the rays from the light sources for a uniform illumination at the bottom of the chambers. The uniformity was increased by two diffuser plates (one below the light sources and another one at the top covers of the chambers), so that the percentage of luminance differences on the bottom of the chambers was less than 3 %.

In the experiment, there was a reference stimulus: a phosphor-converted LED light source with a fixed relative spectral power distribution at 3991 K. This reference appeared either on the right (this is the definition of the "1st series") or on the left (this is the definition of the "2nd series") to counterbalance for possible "position bias" [31]. Each one of the two series was carried out twice at two separate occasions (called sessions): first with all stimuli at 267.6 cd/m^2 and second with all stimuli at 24.8 cd/m^2, so that there were four sessions in total. One observer carried out only one session on a given day, and one observer completed only one session (there were no repetitions). Subjects were always told whether the reference was on the left or on the right. They were also told that the reference would be the same during the whole session of comparisons with twenty test stimuli.

Before each session, a training phase was conducted in which each of the twenty test stimuli was shown in random order (10 s each) compared to the constant reference stimulus. The subjects did not have to answer in the training phase, they just had to consider a possible answer. During the training phase, in addition to the twenty test stimuli, two anchor stimuli were also shown in combination with the reference stimulus three times. One of the anchors was explicitly brighter (330 cd/m^2 and 33 cd/m^2 in case of the two luminance levels, respectively, with the relative spectrum No. 20 in Table 2) and the other one was explicitly darker (49 cd/m^2 and 5 cd/m^2, with the relative spectrum No. 6 in Table 2) than the reference stimulus (with a clearly visible brightness difference), and the subject was informed about this. The two anchors were shown first at the beginning, then after the 10th test stimulus, and finally at the end.

In the main part of each session, after 15 minutes of initial adaptation to the reference stimulus, the subject viewed the two chambers (reference and test) for 40 s. Then an automatic computer sound said: "please assess". Subsequently, the subject had to answer within 20 s. Before the next test stimulus appeared, the neutral white dark anchor stimulus was always displayed for 40 s, and the automatic sound informed the subject about this. During each 40 s interval, subjects were instructed to compare the brightness of the two stimuli as follows:

1. Consider the two bottoms only, and not the vertical walls;

2. Move your head slowly between the two chambers, looking at the two bottoms at least for 2 s each.

Stimuli with strong chromatic content (for example, the yellowish one in the right chamber in Fig. 1) evoked afterimages, but this effect was mitigated by the neutral white dark anchor stimulus displayed for 40 s between any subsequent test stimulus. The role of this recurrent dark anchor stimulus was not only to clear the afterimages, but also to restart the brightness discrimination procedure of the subject from the "explicitly darker" anchor.

Twenty test stimuli were always shown in random order to avoid the so-called "order effect" [31]. They were generated by an 11-channel LED light engine at two luminance levels: either at 267.6 (mean) ± 0.8 (STD) cd/m^2 or at 24.8 (mean) ± 0.07 (STD) cd/m^2. The 20 test stimuli had the same relative spectral power distributions at both luminance levels. This was ensured by an achromatically transmitting hole pattern positioned below the light engine. One of the test stimuli (No. 16 null condition stimulus) was optimized to have a similar relative $|L–M|$, S, rod and *ipRGC* signal values to the reference stimulus (see Table 2). Other test stimuli were designed (by optimizing the driving values of the 11 channels) to have different combinations of $|L–M|$,

Table 2. Signal Values of the 20 Test Stimulus and the Reference Stimulus

No.	L_v(cd/m^2)	$\|L_{rel}$-$M_{rel}\|$	L_{rel}	M_{rel}	S_{rel}	R_{rel}	$ipRGC_{rel}$	$\Phi_{rel,\ blue}$	Intent of optimization
1	268.2	0.001	0.386	0.387	0.024	0.345	0.211	0.188	rods high
2	267.4	0.168	0.453	0.285	0.015	0.155	0.080	0.058	$\|L–M\|$ high
3	268.3	0.108	0.431	0.322	0.034	0.269	0.171	0.158	rods high
4	267.7	0.088	0.440	0.352	0.331	0.525	0.586	0.740	rods and *ipRGC* high
5	268.1	0.083	0.431	0.348	0.436	0.327	0.426	0.703	*S* high
6	266.8	0.168	0.454	0.286	0.048	0.167	0.109	0.100	warm white
7	266.8	0.033	0.413	0.380	0.343	0.476	0.512	0.652	cool white
8	268.9	0.099	0.431	0.332	0.166	0.322	0.289	0.409	neutral white
9	268.4	0.101	0.433	0.332	0.144	0.292	0.268	0.307	balanced signals with higher *ipRGC*
10	268.0	0.167	0.452	0.285	0.018	0.157	0.083	0.062	$\|L–M\|$ high
11	266.7	0.037	0.415	0.377	0.380	0.477	0.530	0.793	cool white with higher local maxima
12	267.6	0.101	0.429	0.328	0.122	0.294	0.226	0.233	balanced signals with higher rods
13	267.1	0.042	0.426	0.384	0.831	0.538	0.767	1.164	very high *S*
14	268.0	0.095	0.427	0.332	0.150	0.274	0.223	0.238	balanced signals with higher *S*
15	267.4	0.097	0.430	0.333	0.134	0.293	0.253	0.274	neutral white
16	268.0	**0.101**	0.431	0.330	**0.131**	**0.281**	**0.237**	**0.250**	**null condition stimulus**
17	267.9	0.030	0.412	0.382	0.351	0.483	0.514	0.626	*ipRGC* high
18	267.1	0.168	0.455	0.287	0.051	0.206	0.143	0.142	warm white with higher local maxima
19	267.3	0.159	0.459	0.300	0.327	0.300	0.338	0.414	balanced signals with higher *S*
20	266.8	0.069	0.422	0.352	0.194	0.362	0.338	0.381	cool white
Ref.	270.3	**0.100**	0.431	0.331	**0.133**	**0.282**	**0.239**	**0.252**	neutral white (no optimization)

Note to Table 2: test stimulus No. 16 is the null condition stimulus. The reference light source was a phosphor-converted LED light source with a fixed relative spectral power distribution, see Fig. 2.

S, rod and *ipRGC* signal values, while maintaining the luminance level constant. Fig. 2 shows the relative spectral power distributions of the stimuli. Table 2 shows their L_{rel}, M_{rel}, S_{rel}, $|L_{rel}$-$M_{rel}|$, S_{rel}, R_{rel} (rod) and *ipRGC* signal values computed according to (8) – (12) and the optimization intent as a comment. Their relative spectral blue content value (5) is also shown in Table 2.

As for the reproducibility of the LED light engine's twenty SPDs, the change of luminance within the 40 days' experimental period was less than 1 %. The change of luminance of the reference light source was less than 1.5 %. The change of the L_{rel}, M_{rel}, R_{rel} (rod) and $ipRGC_{rel}$ signals was less than 1.5 % (for both the test stimuli and the reference). The change of the S_{rel} signal was less than 2.3 % (for both the test stimuli and the reference).

There were 25 participants in the 1st series (aged between 21 and 47 years, mean: 26.9; 10 Chinese, 1 Taiwanese, 9 Europeans, 2 Vietnamese, and 3 from the Middle East) and 21 participants in the 2nd series (aged between 21 and 47 years, mean: 27.4; 10 Chinese, 1 Taiwanese, 7 Europeans, 1 Vietnamese, and 2 from the Middle East), partially overlapping between the 1st and the 2nd series. All subjects had normal colour vision tested by the *Standard Pseudoisochromatic Plates for Acquired Colour Vision Defects*, Part II [32] and the *Desaturated Panel d-15* [33].

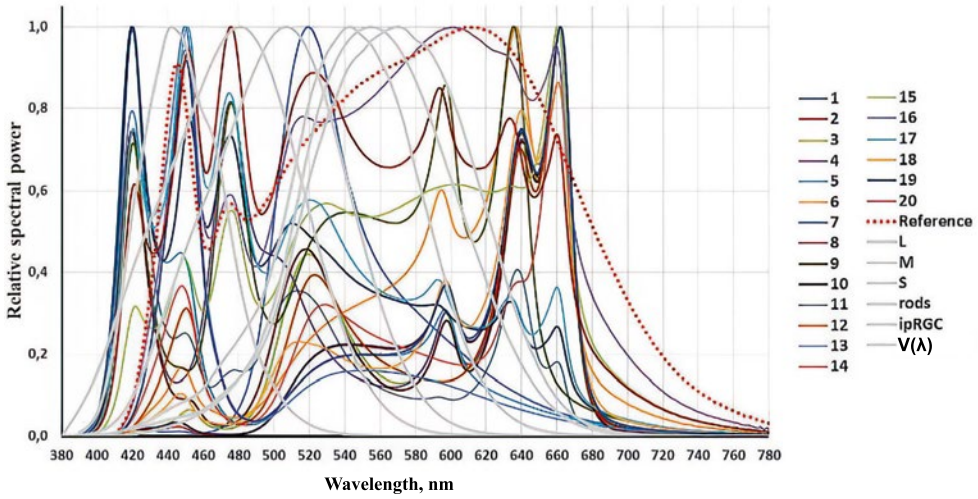

Fig. 2. Relative spectral power distributions of the 20 test stimuli, the reference stimulus, and relative spectral sensitivities of the *L, M, S,* rod, *ipRGC* mechanisms

3. RESULTS, MODELLING, AND DISCUSSION

In each session, the ordinal scale rating of every observer (i.e. an integer number between 0 and 4) was recorded for every one of the 20 test stimuli. If the reference was found to be darker (brighter) than the test stimulus, then the rating of that test stimulus was assigned a positive (negative) sign. Table 3 contains the average values and the average absolute deviation values (a measure of scatter among the observers) for the brightness ratings of all observers. The 20 test stimuli (see Table 2 and Fig. 2) are re-sorted in Table 3 according to their relative blue spectral content ($\Phi_{rel,\ blue}$) in descending order.

As can be seen from the last row of Table 3, the average value of the average absolute deviation value for all participating observers of all test stimuli equals to 1 rating unit in each series (1 and 2) and each luminance level (267.6 cd/m^2 and 24.8 cd/m^2). This (i.e. 1 rating unit of evaluation) is a characteristic value for the inter-observer variability of the result. Fig. 3 shows the average brightness scale values of Table 3.

As can be seen from Fig. 3, the average brightness ratings of all observers participating in each series show a downward trend with a decrease in the relative spectral content of blue. The test stimulus No. 13 with the highest relative spectral blue content value, $\Phi_{rel,\ blue}$ = 1.164, was the brightest. Overall, the last five test stimuli in Table 3 (No. 3, 18, 6, 10, and 2), having the lowest relative spectral blue content ($\Phi_{rel,\ blue}$ < 0.16), were the darkest. Spearman's correlation coefficient between the average brightness difference rating values of the two luminance levels equalled 0.944 for the first series and 0.916 for the second series. Both correlation coefficient values were significant (*T*-test, p<0.0001). This means that the two luminance levels exhibit similar brightness rating tendencies across all 20 test stimuli. The correlation between the brightness ratings of the two series was also high: Spearman's correlation coefficient equalled 0.911 (at 267.6 cd/m^2) and 0.838 (at 24.8 cd/m^2), and both coefficients being significant (*T*-test, p<0.0001). This conclusion involves combining the results of the two series.

To build a brightness model, it is very important to analyse the response tendencies of the individual observers to exclude observers with contradicting response tendencies before modelling. To do so, Spearman's rank correlation coefficient was calculated between the signal values of the test stimuli (Table 2) and the brightness rating values of every observer separately. The minimum, maximum, and average values of these rank correlation coefficients among all participating observers are shown in Table 4.

As can be seen from Table 4, there is positive correlation at average between the brightness ratings and the signals of all three shorter-wavelength mechanisms (*ipRGC, S, R*) as well as $\Phi_{rel,\ blue}$, but the correlation with the |*L–M*| signal is at average negative. Considering the maximum and minimum values of the correlation coefficients, some of the observers contradict the main trend of perception of greater brightness with an increased spectral content of blue at equal luminance. In the framework of the present article, we decided to model only those observers (the majority) who follow the main trend. Similar findings of individual differences of brightness perception have also been found in liter-

Table 3. Average Values and Average Absolute Deviation Values of the Brightness Difference Ratings of All Observers (Fig. 3)

		Average brightness difference rating				Average absolute deviation among all observers			
	Series	**1st**	**2nd**	**1st**	**2nd**	**1st**	**2nd**	**1st**	**2nd**
No.	$\Phi_{rel,\ blue}$	267.6 cd/m^2	267.6 cd/m^2	24.8 cd/m^2	24.8 cd/m^2	267.6 cd/m^2	267.6 cd/m^2	24.8 cd/m^2	24.8 cd/m^2
13	1.164	3.0	3.5	3.0	2.5	1.0	0.5	1.0	1.5
11	0.793	2.0	2.0	3.0	2.0	1.0	1.0	1.0	1.5
4	0.74	3.0	3.0	3.0	2.0	1.0	1.0	1.0	1.0
5	0.703	3.0	2.0	2.0	1.0	1.0	2.0	1.0	1.0
7	0.652	2.0	2.0	2.0	2.0	1.0	1.5	1.0	1.0
17	0.626	2.0	2.0	2.0	3.0	1.0	1.0	1.0	1.0
19	0.414	3.0	2.0	2.0	1.0	1.0	2.0	1.0	2.5
8	0.409	1.0	1.0	1.0	1.0	1.0	0.5	1.0	0.0
20	0.381	2.0	1.0	2.0	2.0	1.0	1.5	1.0	1.0
9	0.307	0.0	0.0	0.0	0.0	0.0	0.0	0.0	0.0
15	0.274	–1.0	–1.0	0.0	0.0	0.0	0.5	0.0	0.5
16	**0.25**	**0.0**	**0.0**	**0.0**	**0.0**	**0.0**	**0.0**	**0.0**	**0.0**
14	0.238	1.0	1.0	1.0	1.0	1.0	0.0	0.0	1.0
12	0.233	–1.0	–1.0	0.0	0.0	0.0	0.0	0.0	0.0
1	0.188	2.0	0.0	2.0	–2.0	1.0	3.0	1.0	2.0
3	0.158	–1.0	–2.0	–1.0	–1.5	2.0	1.0	1.0	1.0
18	0.142	–1.0	–2.0	–1.0	–3.0	3.0	2.0	2.0	1.0
6	0.1	–2.0	–2.5	–1.0	–2.5	2.0	1.5	1.0	1.0
10	0.062	–1.0	–3.0	–1.0	–3.0	3.0	1.0	3.0	1.0
2	0.058	–2.0	–2.0	–1.0	–2.0	2.0	2.0	2.0	1.0
					Average	1.0	1.0	1.0	1.0

Note to Table 3: the 20 test stimuli (see Table 2 and Fig. 2) here are re-sorted according to their relative blue spectral content (5) in descending order. No. 16: null condition stimulus (this stimulus obtained zero average subjective brightness ratings).

ature, see the general discussion below. We use the following mathematical criterion to include the result of this observer in the brightness modelling of the present article: the value of the rank correlation coefficient with the relative spectral blue content $\Phi_{rel,\ blue}$ of this observer should have been greater than 0.2 in each of the four sessions.

Eighteen of 25 observers (72 %) were included in the modelling of the 1st series and fourteen out of 21 observers (67 %) were included in the modelling of the 2nd series. The brightness ratings of the last observers (18 observers + 14 observers = 32 cases) were unified according to the following reasons. The null stimulus condition gave zero average ratings for both series and both luminance levels in the case of the last observers. At 267.6 cd/m^2, there were exclusively zero ratings in case of the null condition stimulus (i.e. same brightness as the reference) in the first series, and there was only one (–1) rating, and all others equalled 0 in the second series. At 24.8 cd/m^2, there were only two (–1) ratings, and one (+1) rating in the first series and three (–1) ratings, and one (+1) rating. Mann-Whitney's *U*-test showed no significant difference of the tendency of any one of the four null condition datasets from zero (p<0.01). We compared the data sets of the 1st series and the 2nd series also for the other 19 stimuli (Table 2, one by one separately) in addition to the null condition stimulus for both luminance levels. Mann-Whitney's *U*-test did not reveal a significant difference between the trends of the 1st series and the 2nd series for any stimulus (p<0.05), which confirms that there is no significant "position bias" (i.e. differences only because observing

Table 4. Spearman's Rank Correlation Coefficients Between the Receptor Signal Values of the Test Stimuli and the Brightness Rating Values for Each Observer and Each Experimental Session

Session							
Series	**Luminance level, cd/m²**		$ipRGC_{rel}$	S_{rel}	R_{rel}	$\lvert L_{rel}\text{-}M_{rel}\rvert$	$\Phi_{rel,\,blue}$
1	267.6	Min.	–0.10	–0.06	–0.05	–0.78	–0.11
1	267.6	Max.	0.94	0.90	0.91	0.22	0.95
1	267.6	Av.	0.49	0.49	0.50	–0.43	0.50
1	24.8	Min.	–0.16	–0.19	–0.04	–0.85	–0.19
1	24.8	Max.	0.95	0.91	0.92	0.09	0.94
1	24.8	Av.	0.56	0.53	0.59	–0.52	0.56
2	267.6	Min.	–0.50	–0.36	–0.40	–0.85	–0.45
2	267.6	Max.	0.87	0.89	0.88	0.24	0.88
2	267.6	Av.	0.50	0.50	0.48	–0.42	0.50
2	24.8	Min.	–0.20	–0.17	–0.22	–0.76	–0.21
2	24.8	Max.	0.89	0.87	0.87	0.34	0.88
2	24.8	Av.	0.59	0.57	0.57	–0.50	0.58

Note to Table 4: this shows the minimum, maximum and average values of these rank correlation coefficients among all participating observers.

the reference stimulus either on the left side or on the right side).

The resulting unified data sets (at the two luminance levels) consisted of 18+14 = 32 (cases) · 20 (test stimuli) = 640 brightness ratings (integers between – 4 and 4) per luminance level. From these two data sets, two continuous brightness scales (so-called Thurstone scales [34]) were computed for the 20 light source spectra (see Table 2 and Fig. 2) at the two luminance levels. These (2×20) Thurstone scale values, i.e. visual brightness scale (*VBS*), are depicted in Fig. 4 as a function of the quantity $\Phi_{rel,\,blue}$ with modelling data points according to (7) with different values of the exponent γ.

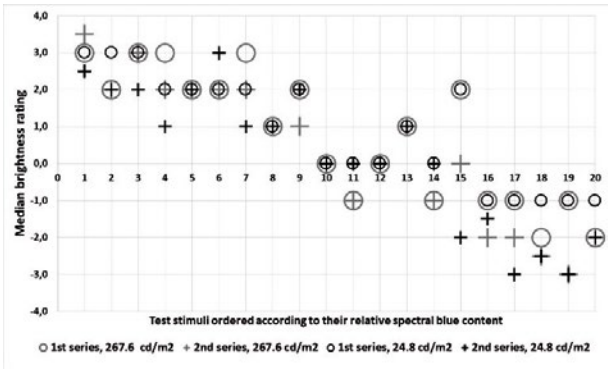

Fig. 3. The average rating on the brightness scale depending on the test stimuli, which are ordered according to their relative spectral blue content in descending order by abscissa

As can be seen from Fig. 4, the optimal values of the exponents γ according to (7) are equal 0.194 (at 24.8 cd/m²) and 0.668 (at 267.6 cd/m²), respectively. With these two optimal exponents, the value of Pearson's correlation coefficient (r) between the model equation (7) and the visual brightness scale was 0.925 (r^2 = 0.856) and 0.924 (r^2 = 0.853), respectively. Optimizing the exponent for the unified data set at both luminance levels, the average exponent value of γ = 0.399 came out with the following correlation coefficient values: r = 0.921 (r^2 =

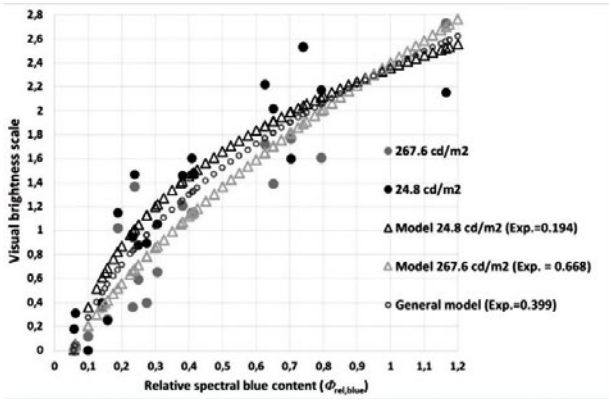

Fig. 4. Values of the visual brightness rating scale (Thurston scale) for 20 light sources at two considered luminance levels (267.6 cd/m² and 24.8 cd/m²) depending on the relative spectral content of the blue colour ($\Phi_{rel,\,blue}$) of the light source, model data points are indicated according to (7) with optimum exponent values for both luminance levels and general model

Table 5. Optimum Parameter Values in Eq. (6) and Pearson's Correlation Coefficients Between the Visual Brightness Scale (*VBS*) Values and the Prediction Formula After Optimisation

Lum. level (cd/m²)		*S, ipRGC,* rods, γ	*S, ipRGC,* γ	*ipRGC,* γ	*S,* γ	*rods,* γ	*S, rods,* γ	*ipRGC,* rods, γ
267.6	γ	0.869	0.845	0.848	0.644	1.337	0.875	0.856
267.6	A_S	0.342	0.003	0	1.000	0	0.652	0
267.6	A_{ipRGC}	1.876	0.376	1.000	0	0	0	1.790
267.6	A_R	0.728	0	0	0	1.000	1.333	0.066
267.6	r	0.932	0.931	0.931	0.880	0.893	0.930	0.931
267.6	r^2	0.868	0.867	0.867	0.775	0.797	0.865	0.867
24.8	γ	0.314	0.259	0.259	0.246	0.560	0.314	0.352
24.8	A_S	0.634	0	0	1.000	0	0.285	0
24.8	A_{ipRGC}	0.000*	2.000	1.000	0	0	0	0.920
24.8	A_R	3.430	0	0	0	1.000	1.543	1.084
24.8	r	0.947	0.939	0.939	0.863	0.934	0.947	0.945
24.8	r^2	0.897	0.882	0.882	0.745	0.873	0.897	0.894

Note to Table 5: optimisation was carried out for the two luminance levels separately. Only the parameters shown in the first line were optimized; the rest were set to zero. *the value of 0.000 resulted from the optimization.

0.848) for 24.8 cd/m² and r=0.918 (r^2 = 0.843) for 267.6 cd/m², respectively. With the exponent of the Fotios and Levermore [20] model (γ = 0.24), we obtain r = 0.925 for 24.8 cd/m² and r = 0.909 for 267.6 cd/m². These correlation coefficients are not significantly different [35] from the previously mentioned values, neither in case of the optimum exponent values nor in case of the average value of γ = 0.399 (p > 0.78). If we use (B/L) from eqs. (2) and (3), we obtain r = 0.711 for 24.8 cd/m² (p = 0.04, significantly less than with (7) with γ = 0.399) and r = 0.815 for 267.6 cd/m² (p = 0.21, not significantly less than with (7) with γ = 0.399). Fig. 5 shows the dependence of the value of r^2 on the value of the exponent γ.

As can be seen from Fig. 5, the dependence of r^2 on γ is rather flat. The difference between the correlation coefficients corresponding to the average exponent value (γ = 0.399) and a specific exponent value (0.194 at 24.8 cd/m² or 0.668 at 267.6 cd/m²) was not significant (p > 0.9) [35]. Therefore, it seemed reasonable to use the average exponent value (γ = 0.399) for both luminance levels in (7).

Regarding the formula for the combination of (6) first, the coefficient A_{L-M} was set to zero because the correlation coefficient with the $|L–M|$ signal was negative, at least within the above mentioned main group of observers that were considered for modelling in the present article. The role of the $|L–M|$ signal is further analysed in section 4. The correlation coefficient between the visual brightness scale values and the prediction formula of (6) was maximized by optimizing the values of γ, A_S, A_{ipRGC} and A_R for the two luminance levels separately. Optimization was also performed by setting some of the parameters from the set $\{A_S, A_{ipRGC}, A_R\}$ to zero and optimizing only the remaining parameters. Results are shown in Table 5.

As can be seen from Table 5, the obtained values of the correlation coefficient do not differ much. The significance test [35] showed no significant difference among the correlation coefficients (p>0.14 at 24.8 cd/m² and p > 0.38 at 267.6 cd/m²). At the next step, the standalone *ipRGC* signal with an average exponent value (γ = 0.399) of the relative spectral blue content ($\Phi_{rel,\ blue}$) model of eq. (7) was considered for predicting the results with the simplest possible model. The correlation coefficients with γ = 0.399 were not significantly less (p > 0.85) than those resulting from the optimum exponent values in the 5th column of Table 5 (r = 0.922 instead of r = 0.931 at 267.6 cd/m² and r = 0.938 instead of r = 0.939 at 24.8 cd/m²). These correlation coefficients are also not significantly greater than those of the $\Phi_{rel,\ blue}$ model with γ = 0.399. This means that based on the present visual brightness scale results, we cannot distinguish between the three shorter-wavelength mechanisms, and we cannot tell whether rod contribution can be neglected. Anyway, the optimal rod coefficients were greater

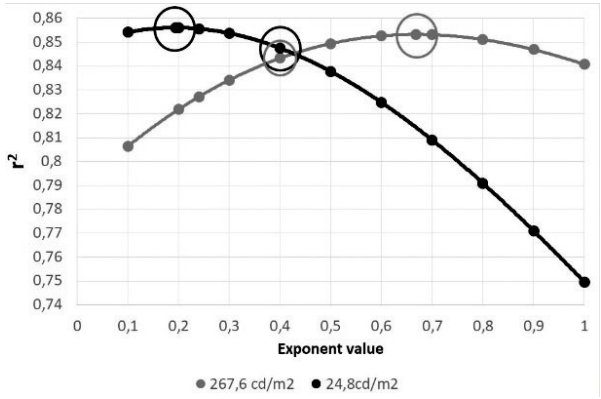

Fig. 5. Dependence of the value of Pearson's correlation coefficient squared (r^2) between visually scaled brightness *VBS* (at 24.8 cd/m^2 and at 267.6 cd/m^2) and the predicting quantity of (7) on the value of the exponent γ in (7), circles indicate optimum value pairs of r^2 and γ

at 24.8 cd/m^2 than at 267.6 cd/m^2 compared to the magnitude of the *S*-cone and *ipRGC* coefficients. This points towards the direction of rod influence at 24.8 cd/m^2. Consider that the chambers were large enough (2×41°) to cover a large retinal area, including the area of highest rod density.

According to the above analysis, the quantity *M* is proposed as the resulting brightness model of the present article that contains the average exponent value $\gamma = 0.399$:

$$M = lg\left(L_v\right) \cdot \Phi_{rel,blue}{}^{0.399}. \qquad (13)$$

4. GENERAL DISCUSSION

The average model (13) that contains the relative spectral blue content and the log-luminance of the stimulus was found to be able to predict the visual brightness result with reasonable accuracy, i.e. with r=0.921 and r=0.918 at 24.8 cd/m^2 and at 267.6 cd/m^2, respectively. In the experiment, the stimulus was the light of the light sources (Table 2) reflected from the white uniform bottom of the viewing chambers (Fig. 1), and the modelling was based on this stimulus. This white stimulus can be considered as the "working point" of the visual system at the time of the brightness assessment. This white point determined the efficacy of each neural mechanism that contributes to perceived brightness.

An important limitation of the present study is that the description of the luminance dependence of brightness by $\lg(L_v)$ in eq. (13) remains a hypothesis because the two luminance levels were fixed in the present brightness experiment. Several brightness models, (1) and (2), assume a linear dependence on luminance and claim (according to the concept of equivalent luminance) to predict only whether one stimulus is brighter than another, and do not claim to predict the absolute perceived magnitude of brightness. The $\lg(L_v)$ term (instead of L_v) represents one possible way of describing luminance signal compression in the human visual system with the aim of predicting the absolute magnitude of brightness perception, and not just the order of different stimuli according to their brightness.

Another limitation of the present results is that only a part of the responses was modelled. Although this part includes the majority of the observers (about 70 %), the remaining observers did not follow the trend modelled by (13): either they had no correlation with any one of the signals, or they had low correlation with the $|L–M|$ signal. Indeed, in a study on brightness perception, observers could be clustered into groups depending on whether their impression of brightness affects their relative spectrum at equal luminance or not [16]. Other authors also found substantial inter-observer variability of brightness perception [36–39] and pointed out that there are at least two main types of observers according to their brightness perception: a mainly chromatic type (having greater chromatic sensitivity in the entire visible wavelength range) and a mainly achromatic type (having approximately the sensitivity of the luminance channel predicted by $V(\lambda)$).

Fig. 5 in the work of Ikeda et al. [36] shows that the variation of the observers between these two main types is continuous, i.e. there are "strong", "medium" and "weak" chromatic types. Figs. 3 and 4 in the work of Ikeda et al. [36] reveal two further variants: a chromatic variant with less blue sensitivity than the main chromatic type, and an achromatic variant with even less sensitivity to blue and red than predicted by the luminance channel. The physiological reason may be that the chromatic observer has greater contribution to perceived brightness from the chromatic channels of the visual system than the achromatic observer. Another reason of the large inter-observer variability of brightness perception may be the difference in the psychological attitude of the subjects the course of the brightness discrimination experiment: achromatic observers tend to isolate the chromatic component of brightness mentally and do not respond to it.

A further question is whether the results of the present experiment is applicable to a real scene because only uniform fields were compared. Previous research indicated that" the presence of coloured objects or surfaces in the target field does not significantly affect the outcome of brightness matching trials" [40]. If, however, there was a spatially extended highly chromatic Mondrian array in the field of view, brightness evaluation was different from achromatic environments [41]. Possibly, highly chromatic images with very saturated red and orange surfaces evoke very strong red-green opponent (*L–M*) signals that contribute to their brightness and this cannot be described by such spatial brightness models that do not contain a dependence on the (*L–M)* signal. In eq. (6), with a non-zero value of the coefficient A_{L-M} and also in Fotios and Levermore model [13], both chromatic channels (|*L–M*| and |*L*+*M*-*S*|) are active so that, increasing the signals of both channels, brightness increases. If there are (several spatially extended) red and/or orange objects in the scene then we shall get higher values of the |*L–M*| signals in the field of view and then, in turn, the contribution of the |*L–M*| channel to the overall spatial brightness perception of the scene might become more explicit.

When combining the signals of the retinal mechanisms to predict spatial brightness in terms of retinal mechanisms, we used the standalone *S* signal instead of |(*L*+*M*)-*S*| for the following mathematical reason. The spectral sensitivity function of the |(*L*+*M*)-*S*| signal spectrally overlaps with the spectral sensitivities of both |*L–M*| and luminance (*L*+*M*), and in general this counteracts successful parameter optimization in eq. (6). Note that in the present brightness experiment, the value of (*L*+*M*) was approximately constant, because luminance was constant. When optimizing 20 multi-LED spectra, the luminance signal (*L*+*M*) was represented by the quantity of conventional 2° photopic luminance (in cd/m^2 units) for modern applications (since this is the conventional luminance definition is most widely used today). We did not consider the alternative representations [42] of the signal of the luminance channel.

As for the adaptation time in the brightness experiment, subjects first adapted 15 minutes to the reference at the current luminance level (267.6 cd/m^2 or 24.8 cd/m^2). After this, the luminance level did not change during a session, and the subject had 40 s, during which the mixed adaptation between a test chromaticity and the reference chromaticity was established by looking slowly (i.e. for at least 2 s at each chamber) back and forth between the test and the reference chambers. The *L*-, *M*-, *S*-cone photoreceptor component of chromatic adaptation has a half-life of only (40–70) ms [43], so that a stay in each chamber for 2 s provided ample time for the chromatic cone signals to stabilize and, subsequently, for the subject to get an impression about the brightness change between the two chambers. The *ipRGC* channel, however, is much slower (with typical light adaptation times of about (100–200) s, see Fig. 3 in [44]), so we surely need a longer observation period than in the present experiment to obtain a significant *ipRGC* contribution to perceived brightness. In the practice of lighting, subjects usually spend several hours in the same visual environment, such as an office or living room. Therefore, as a validation, we need to study the brightness field in realistic viewing conditions.

The model equations (6) and (7) of this article multiply the hypothetical dependence of brightness on luminance lg(L_v) depending on a shorter-wavelength sensitive signal, the relative spectral blue content ($\Phi_{rel,\ blue}$ for ≤520 nm), or a combination of S_{rel}, $ipRGC_{rel}$ and R_{rel} signals. The dependence of modelling accuracy on the exponent γ was rather low (see Fig. 5), with the most probable exponent values ranging (0.15–0.50) (in accordance with previous models), and a representative exponent value of 0.399 was adopted in the model of eq. (13). An alternative modelling hypothesis might be that the dependence of the visual brightness scale (*VBS*) on luminance should not be multiplicatively re-scaled, but additively modified by compressed and combined relative signals of *S*, *ipRGC,* and rod mechanisms:

$$VBS = lg\left(L_v\right) + A{\cdot}lg[A_S\left(S_{rel}\right)^{\gamma} + \\ + A_{ipRGC}\left(ipRGC_{rel}\right)^{\gamma} + A_R\left(R_{rel}\right)^{\gamma}]. \qquad (14)$$

The model (14) compresses the combination of the signals a second time by the aid of the second lg function. Neither the additive concept, nor the double-compression in eq. (14) turned out to be useful during the modelling of the present results. Therefore, we suggest the model (13) to describe the present visual data also for further validation studies. An advantage of eq. (13) is that it is easy to use in modern lighting engineering practice according to the following. For a representative set of 302

light source spectra of widely used light sources today (including LED lamps and luminaires, compact and tubular fluorescent lamps, and incandescent lamps), the relative spectral blue content ($\Phi_{rel,\,blue}$) could be approximated with reasonable accuracy ($r^2 = 0.91$) from the standard 2 ° CIE y chromaticity coordinate like

$$\Phi_{rel,blue} = -2.4174 \cdot y + 1.1405. \qquad (15)$$

The practical significance of the present brightness model is that the spatial brightness impression of real scenes (e.g. a street or a built interior) is very important in interior and outdoor lighting applications. In outdoor lighting, a higher brightness impression is associated with a better feeling of safety [6] and better obstacle detection performance. In interior lighting, a higher brightness impression of a room is associated with better work performance [45]. For architectural and lighting engineering applications, it is important to note that we cannot describe spatial brightness impression only by standard photometry, i.e. by the quantity of luminance (L_v, cd/m^2) [11–17]. Hence, we must offer a practical way to describe brightness based on basic psychophysical research. In the most typical everyday situation, a lighting specialist has a tool, and this tool can measure the luminance and chromaticity coordinates of CIE1931 (x, y). Equations (13) and (15) provide a usable brightness approximation based on the present experimental data set.

Indeed, if the lighting practitioner measures some characteristic values of the luminance (L_v) and the chromaticity coordinate y in the field of view (e.g. in the middle of a wall in a room), it will be possible to obtain a characteristic value of brightness that now depends not only on the luminance, but also on the shorter wavelength content of the spectrum, according to the present experimental results. Thus, the practical significance of the present research is that we provide lighting engineers, practitioners, and designers with the easy-to-use equation (13) by substituting eq. (15). This is ready for a real app to predict the spatial brightness of the scene. To do this, we do not need difficult apparatus. We just need a hand-held colorimetric device to read the values of L_v and y at a characteristic point to get a characteristic value of the spatial brightness prevailing in a given scene. We can also use illuminance (E_v in lx) instead of luminance (i.e. substitute L_v by E_v) and compute an illuminance-based descriptor. To measure E_v and y, we just need a hand-held illuminance-type colourimeter with a well-characterized sensor head.

Finally, we would like to further discuss in what sense the term "spatial brightness" is used, and distinguish this term from another concept. Our goal is to obtain a descriptor of the spatial brightness impression of a scene for the better visibility of small structures, textures and colour shadings on object surfaces and a better acceptance of the appearance of a built environment (e.g. a room) for interior lighting. These are important design goals in the practice of light engineer and light designer. If we increase the average luminance level of a scene (e.g. from 0.3 cd/m^2 to 3.0 cd/m^2 in street lighting or from 30 cd/m^2 to 300 cd/m^2 in interior lighting), then, regardless of the spatial structure of the scene, the overall impression of brightness of the spatially expanded scene (the so-called "spatial brightness") will increase. As mentioned in the introduction, brightness in this sense depends not only on luminance, but also on chromaticity, especially on the "shorter wavelength content" of the light source spectrum. And the lighting of a spatially extended scene with a higher correlated colour temperature (higher shorter wavelength content) results in higher perceived spatial brightness [5, 12, 13, 17, 20, 41].

This article is devoted only to this so-called spatial brightness. We are not concerned with predicting the impression of lightness of certain spatially restricted objects within a scene. To elucidate this, look at a sheet of white paper (with a several small, complicated symbols written with very thin lines and e.g. a small red strawberry image printed on it) in a well-illuminated room under the luminaire. The paper will look white. If we take this sheet in the same room into the shadow of a cupboard, the paper continues to look white, although its luminance becomes much lower. But it will be more difficult to figure out the symbols, and the red strawberry will become less brilliant, because the visual system obtains a less absolute amount of light and it does no more operate at an ideal "working point". If, in turn, we decrease the electric power of all luminaires in the room, the impression of the entire room will become dim and unacceptable, because the overall spatial brightness in the room will become low, independent of the lightness of the individual objects. Subjects entering this room will not like its appearance, because the spatial (colour)

structures on the object surfaces tend to vanish, for example, the detailed structure of the faces and hair of subjects sitting in the room usually becomes less noticeable. The spatial brightness experienced in the room decreases. This effect does not depend on the structure of the scene and does not depend on the perceived lightness [46] of the individual objects in the room, as well as the simultaneous contrasts between these objects. The present article deals only with spatial brightness in the above sense.

5. CONCLUSIONS

In a visual experiment, the perception of the brightness of a large (41°) uniform field was studied. One chamber of a double-chamber viewing booth was illuminated by 20 different light source spectra at 2 different luminance levels. The other chamber contained a reference light source. The subjects had to compare the perceived brightness of the test stimuli with the perceived brightness of the reference spectrum at equal luminance. To model the mean subjective visual scale of brightness, the signal values of different retinal mechanisms (*S*-cones, rods, *ipRGCs* and the |*L–M*| mechanism, eq. 6) plus the so-called relative spectral blue content ($\Phi_{rel,\ blue}$, the spectral radiance of the stimulus integrated for ≤ 520 nm; relative to its luminance, eq. 7) were used. Our hypothesis was that brightness depends on the logarithm of luminance, which is multiplied by either $(\Phi_{rel,\ blue})^{\gamma}$ (7) or a combination of the weighted and compressed signals of the retinal mechanisms (6).

Based on the psychophysical results, the opponent signal (*L–M*) was excluded from the model ($A_{L-M} = 0$). Accuracy of modelling of the standalone signals of the *S*-cones, rods and *ipRGCs,* as well as their combinations according to different weights in eq. (6) did not differ significantly from each other, nor did they differ significantly from the accuracy of modelling the relative spectral content of the blue colour (7). Consequently, it was not possible to decide whether rod contribution in the two experiments based on the present result could be ignored. It should be noted that in the brightness experiment, optimal rod coefficients were greater at 24.8 cd/m^2 than at 267.6 cd/m^2 compared to the magnitude of the *S*-cone and *ipRGC* coefficients. This implies the possible rod influence in case of the large uniform field of view of the brightness experiment at 24.8 cd/m^2.

Modelling quantity *M* (13) may describe the average trend of the visual brightness scale with reasonable accuracy. Eq. (13) it is easy to implement in modern lighting engineering practice, because, in addition to luminance, only the quantity relative spectral blue content ($\Phi_{rel,\ blue}$) is used, and this can be easily approximated from the *y* chromaticity coordinate according to eq. (15).

REFERENCES

1. Commission Internationale de l'Éclairage. e-ILV. Available from http://eilv.cie.co.at/, 2014.

2. Rea M.S. The what and the where of vision lighting research. Lighting Research and Technology, 2018. V50, #1, pp. 14–37.

3. Stiles WS. The Eye, Brightness and Illuminating Engineering. Transactions of the Illuminating Engineering Society, 1952. V17, pp. 241–264.

4. Robinson W. Brightness Engineering. A.M.I.E.E. Transactions of the Illuminating Engineering Society, 1951. V16, pp. 61–85.

5. Fotios SA, Cheal C. Predicting lamp spectrum effects at mesopic levels. Part 1: Spatial brightness. Lighting Research and Technology, 2011. V43, #2, pp. 43–157.

6. Rea MS, Bullough JD, Brons JA. Parking lot lighting based upon predictions of scene brightness and personal safety. Lighting Research and Technology, 2015. V49, #3, pp. 293–304.

7. Fotios S, Atli D. Comparing Judgments of Visual Clarity and Spatial, Brightness through an Analysis of Studies Using the Category Rating Procedure. LEUKOS, 2012. V8, #4, pp. 261–281.

8. Jones LA. Colourimetry: Preliminary Draft of a Report on Nomenclature and Definitions. Journal of the Optical Society of America, 1937. V27, #6, pp. 207–211.

9. Optical Society of America, Committee on Colourimetry, The Science of Colour, New York, USA: Crowell, 1953.

10. Boyce P. Editorial: The paradox of photometry. Lighting Research and Technology, 2015. V47, #7, p. 767.

11. Berman SM, Jewett DL, Fein G, Saika G, Ashford F. Photopic luminance does not always predict perceived room brightness. Lighting Research and Technology, 1990. V22, #1, pp. 37–41.

12. Fotios SA. Lamp colour properties and apparent brightness: a review. Transactions of the Illuminating Engineering Society 2001. V33, #3, pp. 163–178.

13. Fotios SA, Levermore GJ. Chromatic effect on apparent brightness in interior spaces III: Chromatic brightness model. International Journal of

Lighting Research and Technology, 1998. V30, #3, pp. 107–110.

14. Besenecker UC, Bullough JD. Investigating visual mechanisms underlying scene brightness. Lighting Research and Technology, 2016. V49, #1, pp. 16–32.

15. Rea MS, Radetsky LC. Toward a model of outdoor lighting scene brightness. Lighting Research and Technology, 2011. V43, #1, pp. 7–30.

16. Vidovszky-Németh A, Schanda J. White light brightness–luminance relationship. Lighting Research and Technology, 2012. V44, #1, pp. 55–68.

17. Fotios S, Levermore GJ. Perception of electric light sources of different colour properties. International Journal of Lighting Research and Technology, 1997. V29, #3, pp. 161–171.

18. Nayatani Y. A colourimetric explanation of the Helmholtz–Kohlrausch effect. Colour Research and Application, 1998. V23, #6, pp. 374–378.

19. Burns SA, Smith VC, Pokorny J, Elsner AE. Brightness of equal-luminance lights. Journal of the Optical Society of America, 1982. V72, #9, pp. 1225–1231.

20. Fotios SA, Levermore GJ. Chromatic effect on apparent brightness in interior spaces, II: SWS lumens model. Lighting Research and Technology, 1998. V30, #3, pp. 103–106.

21. Smith VC, J. Pokorny J. Spectral sensitivity of the foveal cone photopigments between 400 and 500 nm. Vision Research, 1975. V15, #2, pp. 161–171.

22. Commission Internationale de l'Éclairage. Models of heterochromatic brightness matching. Publ. CIE118–1995. CIE Collection in Colour and Vision, 1995. V118, #2.

23. Guth SL, Massof RW, Benzschawel T. Vector model for normal and dichromatic colour vision. Journal of the Optical Society of America, 1980. V70, #2, pp. 197–212.

24. Yaguchi H, Ikeda M. Subadditivity and superadditivity in heterochromatic brightness matching. Vision Research, 1983. V23, #12, pp. 1711–1718.

25. Kokoschka S, Bodmann HW. Ein konsistentes System zur photometrischen Stralungsbewertung im gesamten Adaptationsbereich. In: Proceedings of the CIE18th Session, London, 1975.

26. Kokoschka S: Advantage of 4-components system and its application to photometer, Proc.1994 Annual Conference and International Symp of IEI Japan, Ohmiya, 1994. Pp. 55–62.

27. Stockman A, Sharpe LT. Spectral sensitivities of the middle- and long-wavelength sensitive cones derived from measurements in observers of known genotype. Vision Research, 2000. V40, #13, pp. 1711–1737.

28. Stockman A, Sharpe LT, Fach CC. The spectral sensitivity of the human short-wavelength cones. Vision Research, 1999. V39, #17, pp. 2901–2927.

29. Rea MS, Figueiro MG, Bierman A, Bullough JD. Circadian light. Journal of Circadian Rhythms 2010. V8, #1, pp. 1–10.

30. Dacey DM, Liao HW, Peterson BB, Robinson FR, Smith VC, Pokorny J, Yau KW, Gamlin PD. Melanopsin-expressing ganglion cells in primate retina signal colour and irradiance and project to the LGN. Nature, 2005. V433, #7027, pp. 749–754.

31. Commission Internationale de l'Éclairage. Publ. CIE212–2014. Guidance towards Best Practice in Psychophysical Procedures Used when Measuring Relative Spatial Brightness, 2014.

32. Ichikawa H, Tanabe S, Hukami K. Standard Pseudoisochromatic Plates for Acquired Colour Vision Defects, Part II. Tokyo, Japan: Igaku-Shoin Medical Publishers, 1983.

33. Lanthony P. The desaturated panel d-15. Documenta Ophthalmologica, 1978. V46, #1, pp. 185–189.

34. Costa M, Gaddi C. Colour Name Distances Scaled by Thurstone's Ranking Order Psychophysical Method. Journal of Vision, 2016. V16, #12, p. 824.

35. Fisher RA. On the Probable Error of a Coefficient of Correlation Deduced from a Small Sample. Metron, 1921. V1, pp. 3–32.

36. Ikeda M, Ikeda J, Ayama M. Specification of individual variation in luminous efficiency for brightness. Colour Research and Application, 1992. V17, pp. 31–44.

37. Kimura-Minoda T, Kojima Sh, Fujita Y, Ayama M. Study on Glare of LED lamp and Individual Variations of Brightness Perception. In: Proceedings of the ISAL 7th International Symposium on Automotive Lighting, 2007.

38. Nayatani Y, Sobagaki H. Causes of individual differences on brightness/luminance (B/L) ratios. Journal of Light and Visual Environment, 2003. V27, pp. 30–34.

39. Yaguchi H, Kawada A, Shioiri S, Miyake Y. Individual differences of the contribution of chromatic channels to brightness. Journal of the Optical Society of America, 1993. V10, pp. 1373–1379.

40. Fotios SA, Cheal C. Brightness matching with visual fields of different types. Lighting Research and Technology, 2010. V43, pp. 73–85.

41. Fotios S, Atli D, Cheal C, Hara N. Lamp spectrum and spatial brightness at photopic levels: Investigating prediction using S/P ratio and gamut area. Lighting Research and Technology, 2014. V47, #5, pp. 595–612.

42. Sharpe LT, Stockman A, Jagla W, Jägle H. A luminous efficiency function, V*(λ), for daylight adaptation. Journal of Vision, 2005. V5, #11, pp. 948–968.

43. Rinner O, Gegenfurtner KR. Time course of chromatic adaptation for colour appearance and discrimination. Vision Research, 2000. V40, #14, pp. 1813–1826.

44. Wong KY, Dunn FA, Berson DM. Photoreceptor Adaptation in Intrinsically Photosensitive Retinal Ganglion Cells. Neuron, 2005. V48, #/6, pp. 1001–1010.

45. Rea MS. The Trotter Paterson Lecture 2012: Whatever happened to visual performance. Lighting Research and Technology, 2012. V44, #2, pp. 95–108.

46. Land EH, McCann JJ. Lightness and Retinex Theory. Journal of the Optical Society of America, 1971. V61, #1, pp. 1–11.

47. Yamakawa M, Tsujimura S, Okajima K. A quantitative analysis of the contribution of melanopsin to brightness perception. Scientific Reports, 2019. V9, p. 7568, https://doi.org/10.1038/s41598–019–44035–3.

Xue Guo,
M. Sc., worked as a research fellow from May 2016 until June 2018 at the Laboratory of Lighting Technology of the Technische Universitaet Darmstadt, Germany. Currently (from July 2018 on) she works for the TÜV SÜD Product Service GmbH as a product specialist for luminaires and light measurement

Peter Bodrogi,
Ph.D., studied physics at the Eotvos Lorand University in Budapest, Hungary. He obtained his Ph.D. degree from the University of Pannonia in Veszprém, Hungary and his lecture qualification thesis (habilitation) from the Technical University Darmstadt in Darmstadt, Germany. He is a research fellow at the Technical University Darmstadt. His research interests concern lighting engineering, mesopic (twilight) lighting, colorimetry, colour science, visual optimisation of displays and LED lighting systems

Tran Quoc Khanh,
Prof., Ph.D. He studied from 1980 to 1985 machine engineering and technical optics before he finished his Ph.D. thesis on the spectroscopy of UV–VIS radiation sources in 1989. Between 1990–1997 and 1997–1999, he was laboratory leader and project manager for photometry, radiometry and colorimetry at PRC Krochmann and Gigahertz Optik. Between 2000 and 2006, he was technical manager for optical imaging systems at ARRI, developed a digital CMOS camera, a film scanner and a laser recorder and optimized colour image processing for cinematography and TV signal processing. In 2005, he completed his Lecture Qualified Thesis (habilitation) on colour appearance and visual performance and started his current work as a Professor for lighting technology and solid-state lighting at the Technical University Darmstadt. He is conducting research and development projects on LED lighting technology. He is also the Chairman of the International Symposium for Automotive Lighting (ISAL). He is the author of several books and scientific articles and inventor of patents on lighting technology and related subjects. He is currently Dean of the Department of Electrical Engineering and Information Technology at the Technical University Darmstadt

Light & Engineering
Vol. 28, No. 5, pp. 25–30, 2020

https://doi.org/10.33383/2020-021
Svetotekhnika #4, 2020, pp. 55–59

FRAUNHOFER DIFFRACTION DESCRIPTION IN THE APPROXIMATION OF THE LIGHT FIELD THEORY

Vladimir P. Budak[1], Dmitry S. Efremenko[2], and Pavel A. Smirnov[1]

[1]Department of Lighting Engineering, NRU MPEI, Moscow, Russia
[2]Deutsches Zentrum fur Luft- und Raumfahrt (DLR), Institut fur Methodik der Fernerkundung (IMF), Oberpfaffenhofen, Germany
E-mail: budakvp@gmail.com

ABSTRACT

The wavelength is that natural scale that determines the applicability domains of the ray approximation and the wave approximation of light. If the change of the radiation power spatial density is significant at the wavelength scale, then we deal with the light diffraction phenomenon, which is a subject to the wave optics. Consider the diffraction phenomenon at the diaphragm. It is possible to distinguish the near zone with significant wave inhomogeneities (i.e. the Fresnel zone) and the far Fraunhofer diffraction zone, in which the wave becomes close to homogeneous (the so-called quasi-homogeneous) and the ray approximation is possible. The problem is that there is no explicit relationship between the radiance of the rays before and after diaphragm. Method for determining the boundary conditions for the radiance in the Fraunhofer zone through the radiance of the incident radiation is proposed in the paper. This approach for computing the radiance field in the Fraunhofer zone can be generalized to other problems of optics, thereby providing the possibility of using computationally efficient ray-approximation-based methods to determine the light fields.

Keywords: diffraction, geometrical optics, wave optics, photometry, quasi-heterogeneity

1. INTRODUCTION

Diffraction is considered as one of the main manifestations of the wave nature of light [1]. However, nowadays, this is most likely related to the school physics course, where it is customary to antagonize the wave representation of light against the ray approximation, which is a consequence of the methodology of classical science in physics. We study any physical phenomenon or object using a specific probe, tester, or test receiver. Still, in classical physics it has always been assumed that the latter can always be made negligible, and thus the properties of the object itself can be formulated. Using the quantum mechanics concepts, it became obvious that we cannot go beyond the description of the tester-object interaction, and in any physical phenomenon there is some probe scale (related to the critical size), such that any attempt to further reduce the receiver's size violates the established physical description of the object.

A feature of optics is that two types of receivers can be distinguished, namely, quadratic and linear receivers. A quadratic receiver responds to the energy it absorbs, while a linear one is a sort of antenna, the reaction of which is proportional to the field strength. Accordingly, each of the measurement processes generates its field: the quadratic receiver generates the light or radiation field, while the linear receiver generates the wavefield [2]. Essentially, the light field is the rays propagating in various directions along which power flows with spatial density

$L\left(\mathbf{r},\hat{\mathbf{I}},t\right)$, i.e. the radiance of the light field at point **r**, time *t*, in the direction $\hat{\mathbf{I}}$. The wave field characterizes the spatial-temporal distribution of the electric field intensity **E**(**r**, *t*). Its structure can be represented as a superposition of random waves in space.

As the energy is a quadratic quantity concerning the electric field, then all the properties of the light field can be expressed in terms of the properties of the wave field. However, only quadratic receivers exist in the optical spectral range. A linear receiver can be set up by placing an optical device, such as an aperture, in front of the quadratic receiver. If the diaphragm dimensions are smaller than a specific size parameter λ, then the field after the diaphragm will be a wave one, however, we can still measure its characteristics only with a quadratic receiver. In the simplest case of a homogeneous monochromatic wave λ is the wavelength.

If the amplitude (i.e. intensity) of the wavefield and the energy density (i.e. power) of the light field does not change in space, then the field is called homogeneous, and both description models are essentially equivalent to each other: at each point in space, the ray is perpendicular to the wave front. The wave front acts as a function, which describes all possible ray paths. If the field is inhomogeneous, especially when the spatial scale of the field change becomes of the order or less than λ, then the ray approximation is not valid anymore. In the narrow sense of the word, this phenomenon is commonly called diffraction.

The field of the diffracted wave right after the diaphragm can be represented as a superposition [1] of a strongly inhomogeneous component, decreasing with distance *r* from the diaphragm faster than 1/*r*, and a quasi-homogeneous component, slowly changing over the scale of λ and decreasing as 1/*r*. Therefore, the field at the diaphragm is strongly inhomogeneous (that is the Fresnel zone), but at a certain distance, the Fraunhofer zone can be distinguished, where the wave is again quasi-homogeneous and can be treated in the framework of the ray approximation. In a general case, the field pattern after diffraction at a circular aperture of radius *a* can be represented as shown in Fig. 1.

The analysis is based on the idea that diffraction generates at each point of the diaphragm a divergent beam with a divergence angle $\alpha_m \sim \lambda / a$, corresponding to the size of the Airy disk [1]. If the overlapping of spots of beams at the distance *z* from the diaphragm aperture is $z \cdot \alpha_m \approx z\lambda / a \ll a$, then the impact of diffraction is negligible, and the field can be described in term of the ray approximation, wherein the radiance of the rays passing through the diaphragm is equal to the radiance of the incident radiation. If the overlapping of the spots is significant (i.e. $z\lambda / a \approx a$), which corresponds to the Fresnel zone, the field is determined by the interference of the beams generated at each point of the diaphragm. It becomes substantially inhomogeneous, and the ray approximation cannot be applied. In the Fraunhofer zone we have $z\lambda / a \ll a$, and the beams generated at all diaphragm points are strongly mixed, the field becomes quasi-homogeneous, and the ray approximation comes into play. However, the radiance of the rays is no longer determined by the radiance of the incident, but rather by the laws of diffraction.

The problem is that the connection between the rays before and after the diaphragm is not apparent. It can only be determined through the properties of the wavefield right after the diaphragm [3]. The goal of this paper is to derive a relationship of the spatial-angular radiance distributions $L(\mathbf{r},\hat{\mathbf{I}})$ of stationary light fields before and after the diaphragm.

2. WAVE DIFFRACTION AT THE EXIT PUPIL OF THE OPTICAL SYSTEM

According to the Abbe principle (Abbe Ernst, 1840–1905) [5], the structure of the optical image can be studied in the geometric optics approximation, considering the wave diffraction at the exit pupil. Let us consider a sharp image from a point lying on the optical axis. As we must have a spherical wave focusing on the image point in the plane of analysis, the wave in the plane of analysis is quasi-homogeneous.

Let the complex amplitude of the wave passing through the optical system (OS) in the plane of the

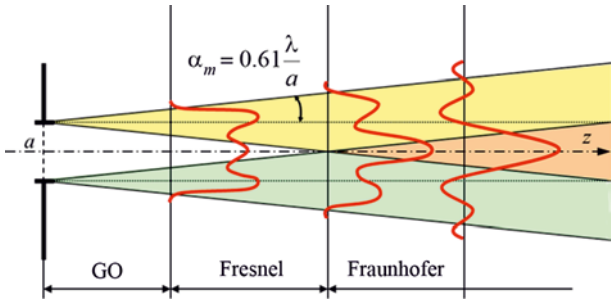

Fig. 1. Distribution of the irradiance (red line) as a function of the distance to the diaphragm aperture *z*

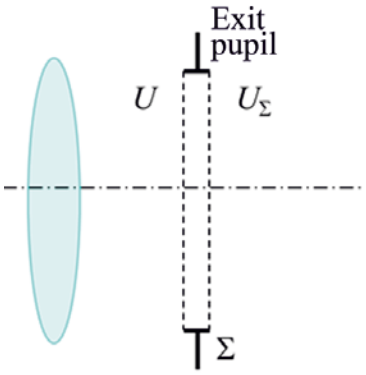

Fig. 2. The exit pupil of the optical system

exit pupil be $U(\mathbf{r})$, where $\mathbf{r}$ is the radius-vector in the plane of exit pupil Σ (as shown in Fig. 2). Then the field immediately after the pupil is expressed through the pupil function $\Theta(\mathbf{r})$:

$$U_\Sigma(\mathbf{r}) = \Theta(\mathbf{r})U(\mathbf{r}), \tag{1}$$

where the pupil function is $\Theta(\mathbf{r}) = \begin{cases} 1, & \mathbf{r} \in \Sigma, \\ 0, & \mathbf{r} \notin \Sigma. \end{cases}$

In the view of eq. (1), the expression for the correlation function of the field right after the exit pupil reads:

$$\begin{aligned} \Gamma_\Sigma(\mathbf{r}_1,\mathbf{r}_2) &= \left\langle U_\Sigma(\mathbf{r}_1)U_\Sigma^*(\mathbf{r}_2)\right\rangle = \\ &= \Theta(\mathbf{r}_1)\Theta(\mathbf{r}_2)\left\langle U(\mathbf{r}_1)U^*(\mathbf{r}_2)\right\rangle = \\ &= \Theta(\mathbf{r}_1)\Theta(\mathbf{r}_2)\Gamma_o(\mathbf{r}_1,\mathbf{r}_2), \end{aligned} \tag{2}$$

where $\Gamma_o(\mathbf{r}_1,\mathbf{r}_2)$ is the correlation function of radiation passing though the OS on the plane of exit pupil.

Introducing the local coordinates in the plane of the exit pupil Σ, i.e.

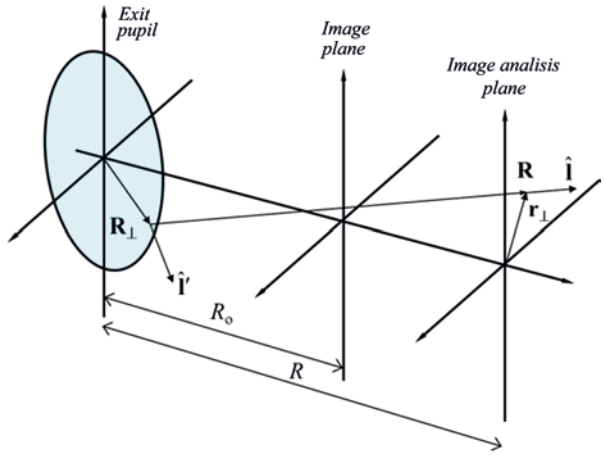

Fig. 3. The scheme of image formation in the optical system bounded by diffraction

$$\mathbf{R} = \frac{\mathbf{r}_1+\mathbf{r}_2}{2},\ \boldsymbol{\rho} = \mathbf{r}_1 - \mathbf{r}_2,\ \mathbf{r}_1 = \mathbf{R} + \frac{\boldsymbol{\rho}}{2},\ \mathbf{r}_2 = \mathbf{R} - \frac{\boldsymbol{\rho}}{2}, \tag{3}$$

yields

$$\Gamma_\Sigma(\mathbf{R},\boldsymbol{\rho}) = \Gamma_o(\mathbf{R},\boldsymbol{\rho})\Theta\left(\mathbf{R}+\frac{\boldsymbol{\rho}}{2}\right)\Theta\left(\mathbf{R}-\frac{\boldsymbol{\rho}}{2}\right). \tag{4}$$

Using our assumption that the field before the exit pupil can be computed in the ray approximation (which is equivalent to the quasi-homogeneous field assumption), we can express $\Gamma_o(\mathbf{R},\boldsymbol{\rho})$ through the generalized radiance in the Wigner spectrum form [3, 4]:

$$\Gamma_o(\mathbf{R},\boldsymbol{\rho}) = \oint L_o(\mathbf{R},\hat{\mathbf{l}})e^{-ik\hat{\mathbf{l}}\boldsymbol{\rho}}d\hat{\mathbf{l}}, \tag{5}$$

where $L_o(\mathbf{R},\hat{\mathbf{l}})$ is the radiance of the radiation passing through the OS in the plane of the exit pupil.

Then the radiance of the quasi-homogeneous part after the exit pupil, which forms the image in the plane of analysis, reads as follows [3]:

$$L(\mathbf{R},\mathbf{l}'_\perp) = \left(\frac{k}{2\pi}\right)^2 l_z \int \Gamma_\Sigma(\mathbf{R},\boldsymbol{\rho})\,\mathrm{e}^{ik\mathbf{l}'_\perp\boldsymbol{\rho}}\,d^2\rho, \tag{6}$$

where $\mathbf{l}'_\perp$ is the vector of projection $\mathbf{l}$ onto the normal to the image plane, while $\hat{\mathbf{l}}$ is defined according to Fig. 3 as follows:

$$\hat{\mathbf{l}} = \frac{\mathbf{r}_\perp - (\mathbf{R}_\perp + R\hat{\mathbf{z}})}{\sqrt{(\mathbf{r}_\perp - \mathbf{R}_\perp)^2 + R^2}}. \tag{7}$$

Substituting eq. (4) in eq. (6) gives

$$\begin{aligned} L(\mathbf{R},\mathbf{l}'_\perp) = \left(-\frac{k}{2\pi}\right)^2 l_z \oint L_o(\mathbf{R},\hat{\mathbf{l}}) \int \Theta\left(\mathbf{R}+\frac{\boldsymbol{\rho}}{2}\right)\Theta \times \\ \times\left(\mathbf{R}-\frac{\boldsymbol{\rho}}{2}\right)\exp\left(-ik(\mathbf{l}'_\perp - \mathbf{l}_\perp)\boldsymbol{\rho}_\perp\right)d^2\rho d\hat{\mathbf{l}}. \end{aligned} \tag{8}$$

Introducing

$$h(\mathbf{l}'_\perp - \mathbf{l}_\perp) = \left(\frac{k}{2\pi}\right)^2\left(\frac{l_z}{l'_z}\right)\times$$

$$\times\int\Theta(\mathbf{R}+\frac{\boldsymbol{\rho}}{2})\Theta(\mathbf{R}-\frac{\boldsymbol{\rho}}{2})\exp\left(-ik\boldsymbol{\rho}(\mathbf{l}'_\perp - \mathbf{l}_\perp)\right)d^2\rho, \tag{9}$$

eq. (8) can be written as a convolution:

$$L(\mathbf{R},\mathbf{l}'_\perp) = \int L_o(\mathbf{R},\mathbf{l}_\perp)h(\mathbf{l}'_\perp - \mathbf{l}_\perp)d^2 l_\perp. \tag{10}$$

Thus, the wave diffraction at the exit pupil acquires a clear ray interpretation of light scattering, while $h(\mathbf{l}'_\perp - \mathbf{l}_\perp)$ is a function of light scattering.

3. OPTICAL TRANSFER FUNCTION OF AN IDEAL OPTICAL SYSTEM

To validate the derived relations, let us consider the optical transfer function (OTF) of a non-aberrational thin lens, the frame of which also serves as the exit pupil in the presence of defocusing. The technique of computing the OTF of such a system is well known from wave optics [1]. For this, we consider an isotropic point source with a luminous intensity I_o on the optical axis having a stigmatic image in the analysis plane at a distance R_o along the optical axis from the plane of the exit pupil (as shown in Fig. 3). The irradiation distribution from it will be the point scattering function (PSF), the Fourier transform of which provides the desired OTF. The radiance of the beam in this case on the plane of the diaphragm can be expressed as follows:

$$L_{\text{o}}(\mathbf{R}_\perp,\mathbf{l}'_\perp)=I_{\text{o}}\delta\left(\mathbf{l}'_\perp+\frac{\mathbf{R}_\perp}{R_{\text{o}}}\right). \tag{11}$$

Substituting eq. (11) into eq. (8) and expressing the result using coordinates $\mathbf{R}_\perp$, $\mathbf{l}_\perp$, we obtain

$$L_\Sigma(\mathbf{R}_\perp,\mathbf{l}_\perp)=I_{\text{o}}\left(\frac{k}{2\pi}\right)^2\left(\frac{l_z}{l'_z}\right)\int\Theta\left(\mathbf{R}_\perp+\frac{\boldsymbol{\rho}}{2}\right)\Theta$$
$$\left(\mathbf{R}_\perp-\frac{\boldsymbol{\rho}}{2}\right)\exp\left\{ik\boldsymbol{\rho}\left(\mathbf{l}_\perp+\frac{\mathbf{R}_\perp}{R_{\text{o}}}\right)\right\}d^2\rho\,. \tag{12}$$

Here we made use the following geometrical properties (see Fig. 3):

$$\mathbf{l}_\perp\simeq\frac{\mathbf{r}_\perp-\mathbf{R}_\perp}{R},\quad \mathbf{l}_\perp+\frac{\mathbf{R}_\perp}{R_{\text{o}}}=\frac{\mathbf{r}_\perp}{R}+\beta\frac{\mathbf{R}_\perp}{R},$$
$$\beta=\frac{R-R_{\text{o}}}{R_{\text{o}}},\quad d^2l_\perp\simeq\frac{d^2R}{R^2}. \qquad . \tag{13}$$

The expression for the irradiance on the plane of analysis reads as

$$E(\mathbf{r}_\perp)=\int\limits_{(\Omega_+)}L_\Sigma(\mathbf{r}_\perp,\mathbf{l}_\perp)l_z d\hat{\mathbf{l}}=\int\limits_{(\Omega_+)}L_\Sigma(\mathbf{r}_\perp,\mathbf{l}_\perp)l_z d^2l, \tag{14}$$

or, making use of eq. (12):

$$E(\mathbf{r}_\perp)=\frac{I_{\text{o}}}{R^2}\left(\frac{k}{2\pi}\right)^2\int\Theta\left(\mathbf{R}_\perp+\frac{\boldsymbol{\rho}}{2}\right)\Theta\left(\mathbf{R}_\perp-\frac{\boldsymbol{\rho}}{2}\right)\times$$
$$\times\exp\left\{ik\boldsymbol{\rho}\left(\frac{\mathbf{r}_\perp}{R}+\beta\frac{\mathbf{R}_\perp}{R}\right)\right\}d^2\rho d^2R_\perp, \tag{15}$$

here it is taken into account that $l_z/l'\approx 1$ under paraxial optics conditions.

OTF OS is the Fourier transform of irradiance distribution:

$$H(\boldsymbol{\nu})=\int E(\mathbf{r}_\perp)\,\mathrm{e}^{-i\boldsymbol{\nu}\mathbf{r}_\perp}\,d^2r_\perp, \tag{16}$$

and using eq. (15), we obtain

$$H(\boldsymbol{\nu})=\frac{I_{\text{o}}}{R^2}\left(\frac{k}{2\pi}\right)^2\int\Theta\left(\mathbf{R}_\perp+\frac{\boldsymbol{\rho}}{2}\right)\Theta\left(\mathbf{R}_\perp-\frac{\boldsymbol{\rho}}{2}\right)\times$$
$$\times\exp\left\{ik\boldsymbol{\rho}\left(\frac{\mathbf{r}_\perp}{R}+\beta\frac{\mathbf{R}_\perp}{R}\right)-i\boldsymbol{\nu}\mathbf{r}_\perp\right\}d^2r_\perp\,d^2\rho d^2R_\perp. \tag{17}$$

Note one obvious formula:

$$\delta\left(\frac{k\boldsymbol{\rho}}{R}-\boldsymbol{\nu}\right)=\int\exp\left\{i\mathbf{r}_\perp\left(\frac{k\boldsymbol{\rho}}{R}-\boldsymbol{\nu}\right)\right\}d^2r_\perp, \tag{18}$$

which can transform eq. (17) to the following form:

$$H(\boldsymbol{\nu})=I_{\text{o}}\int\Theta\left(\mathbf{R}_\perp+\frac{\alpha\boldsymbol{\nu}}{2}\right)\Theta$$
$$\left(\mathbf{R}_\perp-\frac{\alpha\boldsymbol{\nu}}{2}\right)\exp\left(i\beta\boldsymbol{\nu}\mathbf{R}_\perp\right)d^2R_\perp, \tag{19}$$

where, with (18), the constant is defined

$$\alpha=\frac{R}{k}=\frac{\lambda R}{2\pi}. \tag{20}$$

Let us compute OTF of the optical system for zero spatial frequency:

$$H(0)=I_{\text{o}}\int\Theta(\mathbf{R}_\perp)d^2R_\perp=\pi a^2I_{\text{o}}. \tag{21}$$

Note that $H(0)$ corresponds to the transmittance of the optical system.

Then we can express relative OTF (i.e. the modulation transmission function) as follows:

$$T(\boldsymbol{\nu})=\frac{H(\boldsymbol{\nu})}{H(0)}=\frac{1}{\pi a^2}\int\Theta\left(\mathbf{R}_\perp+\frac{\alpha\boldsymbol{\nu}}{2}\right)\Theta\times$$
$$\times\left(\mathbf{R}_\perp-\frac{\alpha\boldsymbol{\nu}}{2}\right)\exp\left(i\beta\boldsymbol{\nu}\mathbf{R}_\perp\right)d^2R_\perp. \tag{22}$$

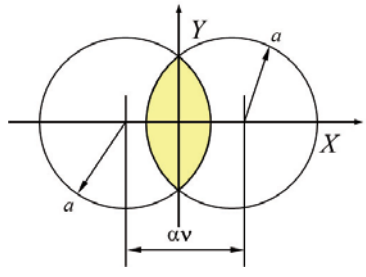

Fig. 4. To definition of the limits of integration in eq. (22)

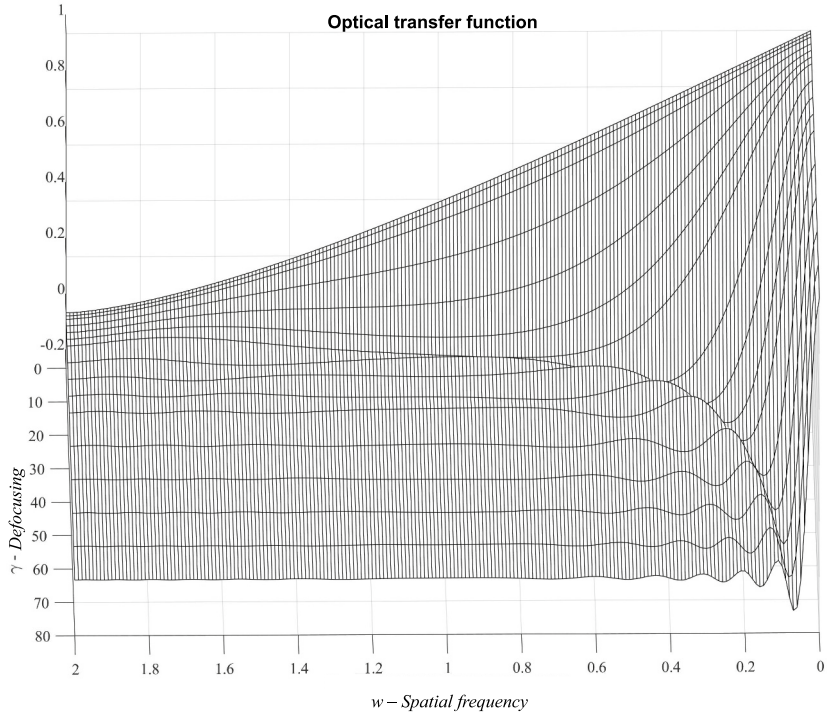

Fig. 5. Influence of defocusing on OTF of the ideal optical system, bounded by diffraction

Let us consider the impact of defocusing on the OTF of the optical system. From Fig. 4, it follows that

$$\left(x-\frac{\alpha\boldsymbol{\nu}}{2}\right)^2+y^2=a^2, \tag{23}$$

and this allows to define the integration limits in eq. (22):

$$x_1=\frac{\alpha\boldsymbol{\nu}}{2}-\sqrt{a^2-y^2},\ x_2=-\frac{\alpha\boldsymbol{\nu}}{2}+\sqrt{a^2-y^2},$$
$$y_{12}=\pm\sqrt{a^2-\frac{\alpha^2\nu^2}{4}}, \tag{24}$$

and express the integral as

$$T(\boldsymbol{\nu})=\frac{2}{\pi a^2}\int_0^{\sqrt{a^2-\left(\frac{\alpha\nu}{2}\right)^2}}\ \int_{\frac{\alpha\nu}{2}-\sqrt{a^2-y^2}}^{-\frac{\alpha\nu}{2}+\sqrt{a^2-y^2}} \mathrm{e}^{i\beta\nu x}\,dx\,dy. \tag{25}$$

Note that the integration over *dx* can be easily computed:

$$T(\boldsymbol{\nu})=\frac{2}{\pi a^2}\int_0^{\sqrt{a^2-\left(\frac{\alpha\nu}{2}\right)^2}}\sin\left[\beta\nu\left(\sqrt{a^2-y^2}-\frac{\alpha\nu}{2}\right)\right]dy. \tag{26}$$

The integral takes a simpler form for further analysis

$$T(w)=\frac{4}{\pi\gamma w}\int_0^{\sqrt{1-\left(\frac{w}{2}\right)^2}}\sin\left[\gamma w\left(\sqrt{1-t^2}-\frac{w}{2}\right)\right]dt, \tag{27}$$

if we switch to the following dimensionless variables:

$$w=\frac{\alpha\nu}{a}=\frac{R\nu}{ak}=\frac{R\nu}{\zeta},\ t=\frac{y}{a},\ \gamma=\frac{\beta a^2}{\alpha}=$$
$$=\frac{\beta k a^2}{R}=\beta\zeta\frac{a}{R},\quad \zeta=ka=\frac{2\pi a}{\lambda}. \tag{28}$$

Fig. 5 shows the OTFs for several values of relative defocusing parameters γ.

Note that if there is no defocusing, which is equivalent to $\beta\to 0$ and, hence, $\gamma\to 0$, we have

$$\lim_{\gamma\to 0}\frac{1}{\gamma w}\sin\left[\gamma w\left(\sqrt{1-t^2}-\frac{w}{2}\right)\right]=\sqrt{1-t^2}-\frac{w}{2}, \tag{29}$$

and eq. (27) is reduced to the expression for the *OTF* for the OS with diffraction at the exit pupil:

$$T(w)=\frac{4}{\pi}\int_0^{\sqrt{1-\left(\frac{w}{2}\right)^2}}\left(\sqrt{1-t^2}-\frac{w}{2}\right)dt=$$
$$=\frac{2}{\pi}\left[\arccos\frac{w}{2}-\frac{w}{2}\sqrt{1-\frac{w^2}{4}}\right],\quad , \tag{30}$$

which completely corresponds to the formula derived in the framework of the diffraction theory [6–8].

In [7], eq. (30) is expressed in terms of Bessel functions, which allows one to obtain the asymptotic formula for *T*(*w*) for large values of γ. It

is straightforward to see that the impact of diffraction blurring becomes negligible when the defocusing parameter increases. At the same time, the blur function for a point is defined by the geometrical optics, and the blur spot turns into a uniformly illuminated disk. In this case, the OTF as a Fourier transform from a uniformly luminous disk is given by a first-order Bessel function for its argument.

4. CONCLUSION

We have proposed a method for determining the relationship between the radiance of the light fields before the diaphragm and in the Fraunhofer zone after the diaphragm. This method can describe all phenomena related to image formation in an ideal optical system. Therefore, the computationally efficient ray approximation can be applied to the image analysis in the optical system, where the diaphragms are treated as scattering elements with the corresponding point spread functions (PSFs) according to eq. (9). Moreover, since the Fraunhofer zone is of considerable practical interest, this approach can be generalized and developed for other problems. For example, nowadays, scattering by particles of complex shape is treated not according to Mie theory [9], but rather based on geometrical optics, in which the wave effects (for example, diffraction, surface wave, and edge effect) are neglected. By imposing new boundary conditions for the scattered rays in the Fraunhofer zone, it is possible to include these effects in the ray optics models.

REFERENCES

1. Born M., Wolf E. Principles of optics. Cambridge: Cambridge University Press, 1999. P. 720.

2. Budak V.P. Theory of the light field, Section 2.1. in the Reference Book on Lighting Engineering, Ed. Yu.B. Eisenberg and G.V. Boos. Editorial Board of the journal "Lighting Engineering", 2020. P. 829.

3. Apresyan L.A., Kravtsov Yu.A. Radiation Transport Theory: Statistical and Wave Effects. Amsterdam: OPA, 1996. P. 456.

4. Wigner E. On quantum corrections for thermodynamic equilibrium. Phys. Rev., 1932. V40, #6, pp. 749–759.

5. Abbe E. Beitraege zur Theorie des Mikroskops und der mikroskopischen Wahrnehmung. Archiv f. Mikroskopische Anat., 1873. B.9. S.413.

6. Hopkins H.H. On the Diffraction Theory of Optical Images. Proc. R. Soc. Lond. A, 1953. V217, pp. 408–432.

7. Hopkins H.H. The Frequency Response of a Defocused Optical System. Proc. R. Soc. Lond. A, 1955. V231, pp. 91–103.

8. Steel W.H. The Defocused Image of Sinusoidal Gratings. Optica Acta: International Journal of Optics, 1956. V3, #2, pp. 65–74.

9. Mie G. Beiträge zur Optik trüber Medien, speziell kolloidaler Metallösungen, Annalen der Physik, 1908. B.330. S.377–445.

Vladimir P. Budak,
Professor, Doctor of Technical Sciences. In 1981, he graduated from the Moscow Power Engineering Institute (MPEI). At present, he is the Editor-in-chief of the Svetotekhnika / Light & Engineering journal, Professor of the Light Engineering sub-department of NRU MPEI. Corresponding member of the Academy of Electrotechnical Sciences of Russia

Dmitry S. Efremenko
graduated from the Moscow Power Engineering institute (MPEI) in 2009. He received his Ph.D. degree from the Moscow State University in 2011 and the habilitation degree from MPEI in 2017. Since 2011 he works as a research scientist at the German Aerospace Centre (DLR). His scientific interests include radiate transfer, remote sensing, and Big Data analysis

Pavel A. Smirnov,
Ph.D. He is graduated from the Moscow Power Institute (Technical University) in 2001. Senior lecturer of the Chair "Svetotekhnika" of the Moscow Power Institute Scientific-and-Research Organization

Light & Engineering
Vol. 28, No. 5, pp. 31–38, 2020

https://doi.org/10.33383/2020-026
Svetotekhnika, #4 , 2020, pp. 45–50

APPLICATION OF THE SAH-NOYCE-SHOCKLEY RECOMBINATION MECHANISM TO THE MODEL OF THE VOLTAGE-CURRENT RELATIONSHIP OF LED STRUCTURES WITH QUANTUM WELLS

Fedor I. Manyakhin*, Arthur B. Vattana, and Lyudmila O. Mokretsova

National University of Science and Technology (MISIS), Moscow
** E-mail: zaomisis@yandex.ru*

ABSTRACT

The Sah-Noyce-Shockley (SNS) space charge region recombination theory is applied to build the mathematic model of the voltage-current relationships (VCR) of light emitting diodes with quantum wells. Unlike the mathematic model of VCR, for SNS in the proposed model, non-uniformity of recombination centres distribution over the space charge region and dependence of their mean concentration on voltage are assumed as well as the fact that the nonideality factor of forward current dependence on bias voltage may have a continuous series of values from 1 to 5 and is defined by the dependence on bias voltage of both saturation current and exponent of the VCR mathematical model.

Keywords: light emitting diodes with quantum wells, voltage-current relationship, nonideality factor, recombination mechanism

1. INTRODUCTION

Thanks to their remarkable properties, light emitting diodes (LED) based on quantum well (QW) heterostructures have reached the leading positions as light sources and elements of full-colour screens. However, the paradox is that no mathematical model of their voltage-current relationship (VCR) has been created over the 25 years since the start of their serial production. To describe experimentally observed VCRs of QW LEDs, models developed for homogeneous *p-n* junctions are used. This leads to difficulties in interpretation of both behaviour of the dependence of current on bias voltage and quantum efficiency of LED.

The VCR model of a diffusion current mechanism was proposed by Shockley [1]:

$$J_{dif} = q\left(\frac{p_n L_p}{\tau_p} + \frac{n_p L_n}{\tau_n}\right)\cdot\left[\exp\left(\frac{qU}{kT}\right)-1\right] = J_0\left[\exp\left(\frac{qU}{kT}\right)-1\right], \quad (1)$$

where J_{dif} is the current density, q is the charge of the electron, p_{n} and n_{p} are the concentrations of minor carriers in *n*- and *p*- areas respectively, L_{n} and L_{p} are the diffusion lengths, τ_{n} and τ_{p} are the electron and hole lifetimes, U is the bias voltage, k is the Boltzmann constant, T is the absolute temperature of *p-n* junction, $J_0\left[\exp\left(\frac{qU}{kT}\right)-1\right]$ is the diffusion current of saturation.

The formula (1) was further amended with the n parameter acquired experimentally and called the nonideality factor (NF) (in other works, it is called the ideality factor):

$$J_{dif} = J_0\left[\exp\left(\frac{qU}{nkT}\right)-1\right]. \quad (2)$$

The physical nature of NF for homogeneous *p-n* structures was described in the work by Sah, Noyce and Shockley (SNS) [2]. It presents the VCR model based on the recombination mechanism of charge

carriers (CC) in the space charge region (SCR) of symmetrical *p-n* junction through uniformly distributed defect levels:

$$J_{rec} = q\frac{\sigma_t N_t W}{2} n_t V_T \exp\left(\frac{qU}{2kT}\right) = J_s \exp\left(\frac{qU}{2kT}\right), \quad (3)$$

where W is the width of SCR, σ is the capture cross-section of recombination centres, V_T is the thermal velocity, N_t is the concentration of recombination centres in SCR, n_i is the intrinsic concentration of CC, $J_s = q\frac{\sigma_t N_t W}{2} n_t V_T$ is the saturation current; NF is taken equal to 2 in (3).

Later, this model was developed [3] for asymmetrical *p-n* junctions keeping the assumption on uniform distribution of defect concentration in SCR.

Experimentally observed VCRs with NF varying between 1 and 2 are attributed to competition of particular recombination mechanisms [4], and it is claimed that NF may vary between 1 and 2 due to equality of total forward current to the sum of diffusion and recombination currents.

In 1994–1996, first blue and green QW LEDs were created based on *AlGaN/InGaN*/*GaN* heterostructures [5, 6] as well as a red LED based on *AlInGaP* heterostructures. Since that, intensive studies of the properties of these LEDs have been carried out [7–12]. Their electric and physical characteristics, in particular VCR, significantly differ from characteristics of previously developed LEDs. For instance, NF of QW LEDs varies significantly over the entire region of current-voltage relationship [13, 14] and its values may be equal to 1.2 to 5 or even higher. With relatively low values of current density (approx. 1 A/cm^2), deviations from the exponential dependence and the trend to saturation of current are observed in semi-logarithmic coordinate VCRs of any and all *GaN* and *AlInGaP* based LEDs. Different models are proposed to explain these facts, with assumptions made on high resistance of contacts and competition between different recombination mechanisms. At the same time, formation of the charge of free CCs in the contact area of wide band gap semiconductors is not taken into account [15, p. 156].

The phenomenological model of the *ABC* recombination rate based on the models of Shockley–Read–Hall (SRH), radiative and Auger recombination mechanisms [16–19] was developed. The *ABC* model rather rationally explains the behaviour of quantum efficiency of QW LEDs with changes of forward current density but is still not used for building the VCR mathematical model.

Researchers still keep on using the (2) and (3) formulae to describe VCR of QW LEDs, which is not correct given that recombination in the SCR layer of WQ LEDs occurs in narrow local regions, QW layers with width of several nanometres. This fact is taken into account in [20, 21].

Analysis of current formation in QW LEDs is one of the focuses in [13, 22]. These works aspire to explain the fall of efficiency at relatively low values of current density, but no expressions to describe VCR were obtained.

All works analysing experimental VCRs of LEDs, both based on homogeneous junctions and on heterogeneous *p-n* structures with QW, provide a formula that defines NF by differentiating the logarithm of current to voltage:

$$n = \left[kT\left(\frac{d}{dU}\ln(J)\right)\right]^{-1}. \quad (4)$$

It is obviously incorrect since experimental VCRs are not analytical functions but discrete tables of concordance between current and bias voltage. Therefore, the following formula is more appropriate for application

$$n = \left[kT\left(\frac{\Delta\ln(J)}{\Delta U}\right)\right]^{-1}, \quad (5)$$

Here $\Delta\ln(J)$ is the increment of the current density logarithm with bias voltage increment by ΔU. However, no work contains information on the values of these increments for calculations, while the result significantly depends on it.

In the majority of the experimental materials, the NF itself and the pre-exponential factor of the formula of VCR of QW LED distinctly change with changes in bias voltage [14], while the formulae (4) and (5) imply that they are constant.

Given the above, it is necessary to define what parameter is calculated by (5) for the entire range of VCR: kT-fold reciprocal of the ratio of increment of the $\Delta\ln(J)$ function to increment of the argument ΔU or the coefficient characterising non-concordance between the exponential factor exp [$qU/(n^*{\cdot}kT)$] and the ideal form exp [$qU/(kT)$]? Obviously, it is the kT-fold reciprocal of the ratio $\Delta\ln(J)/\Delta U$. n^* here is the factor of deviation of the exponential factor from the one given in [1]. The exponent in (2) includes the factor of deviation from the Shockley's ideal VCR model based on the Boltzmann distribu-

tion. Therefore, we will hereinafter identify the NF defined by (5) as n and the factor included in the exponent as n^* (asterisked n).

The review of the works allows us to draw conclusions that:

– When analysing experimental data concerning QW LEDs, they use the Shockley's and SNS mathematical models of VCR, which do not take the distinctions of their technological structure into account;

– The cases of non-uniform distribution of recombination centres [23, 24] common for LED structures are not considered.

These conclusions allowed us to formulate the goal and the objectives of this work:

– The goal is to develop the mathematical model of VCR of *p-n* structures with QW with consideration of their parameters and location in SCR;

– The objectives are to experimentally define VCR properties common for all types of *p-n* LED structures, to substantiate the necessity of development of the mathematical model of VCR of *p-n* structures with non-uniform distribution of recombination centres in SCR, to define the dependence of the n^* factor and NF n on technological parameters of the *p-n* structure[1].

It was initially assumed that *p-n* structures of the LEDs under consideration are uniformly doped both in *p* and *n* regions, have a barrier layer with sharp boundaries, the Boltzmann distribution is true in the barrier region for free CCs, the levels of the recombination centres are located in the vicinity of the middle of the forbidden region and the capture cross-sections of electrons and holes are similar.

2. METHODOLOGY AND THE RESULTS OF THE EXPERIMENT

VCRs of blue and green QW LEDs based on *p-n* structures of *AlGaN/InGaN*/*GaN* manufactured by *Cree*, blue, green and red LEDs (*AlInGaP*-based) manufactured by *Lumileds* as well as white LEDs manufactured in China were obtained (these LEDs are identified in the experimental results below as A1, A3, CC and CW respectively). Each lot contained at least 10 LEDs and was selected from the same technological group. The experimental results

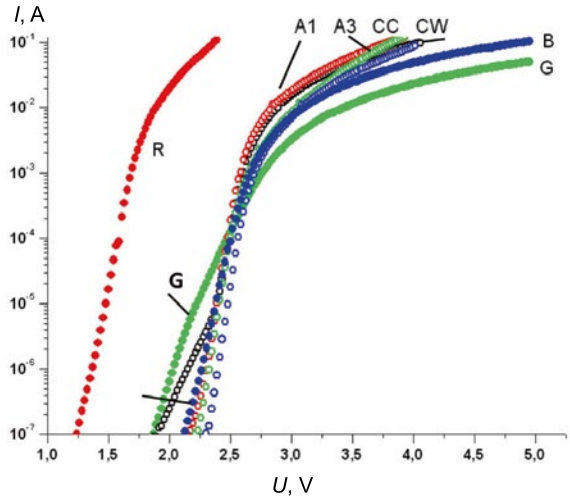

Fig. 1. VCRs of *Lumiled*'s red (*AlInGaP*-based) (*R*), green (*G*) and blue (*B*) LEDs as well as of the white LED with *AlGaN/InGaN/GaN* crystal structure (A1, A3, CC, CW) manufactured in China

presented in the Figs. (1–3) are not for all studied LEDs due to large volume of information, but the main characteristics conform to those presented in the work.

The LEDs used in the experiments had rather long exponential regions of VCRs within the current density range of (10^{-4}–10^{-2}) A/cm^2. Different characteristics if these LEDs, including VCRs, are studied in, for instance, [25, 26]. Measurements at lower values of current density were not conducted since probability of occurrence of creeping currents is high in this case: they would have provided a background addition to the classic generation-recombination mechanism of forward current of the LEDs under consideration.

VCRs of LEDs (Fig. 1) were measured by means of a computerised installation with stabilised bias voltage. Forward current varied within the range of (10^{-7}–10^{-1}) A and current density of (10^{-4}–10^{2}) A/cm^2. Voltage increment was equal to (20±0.01) mV. With such values of forward current density, the high injection level mode is not generated and a rather long exponential region is observed.

Moreover, in order to define the relationship between the form of VCR and distinctions of doping of *p-n* junction, doping profiles (Fig. 2) were measured for some types of LEDs using the technique and the installation described in [27]. Doping distri-

[1] The objectives of the work did not include determination of the relation between NF n with creeping currents or loss currents through inner bridges of diode structures, consideration of series ohmic resistance of quasi-neutral regions and contacts and analysis of the high injection level mode; the work considered only the forward bias condition mode, the main mode of LED.

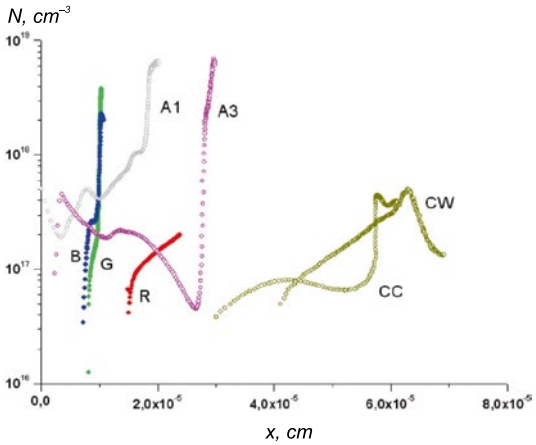

Fig. 2. Doping profiles of the lightly doped region of QW structures of *AlInGaP*-based red (*R*), green (*G*) and blue (*B*) LEDs manufactured by *Lumiled* as well as the white LED with *AlGaN/InGaN/GaN* crystal structure (A1, A3, CC, CW) manufactured in China

bution is measured starting from the metallurgical border in a relatively lightly doped region.

All measurements were made at room temperature of (23–25) °C. Thermal potential kT was taken equal to 0.0259 eV for measurements and modelling.

Processing of the experimental data and modelling of VCR were conducted using *MathCad-14* and *Origin-8* software.

Fig. 2 shows that the doping profiles in the lightly doped region of *p-n* structures are very variable while VCR forms of similar LEDs have almost no differences. In semi-log coordinates, it is possible to identify the long and almost linear regions of 2–4

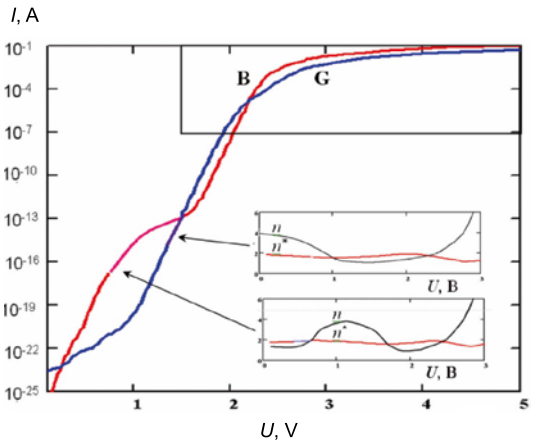

Fig. 3. Model VCRs of blue (*B*) and green (*G*) LEDs based on *AlGaN/InGaNGaN* heterostructures with five QWs. The contour shows the regions of VCR corresponding to the experimental VCRs in Fig. 1, the inserts demonstrate corresponding dependences of NF n and factors n^* on bias voltage

magnitude orders of current with further significant deviation from exponential dependence at current density values higher than (1–2) A/cm^2. The formula (5) was used for calculation of n.

Increase in NF of the presented VCRs at current values exceeding the ones corresponding to the exponential region occurs due to different causes considered, for instance, in [28] as well as due to special phenomena, e.g. generation of a *p-n* junction of an accelerating electric field within the SCR, but these effects will not be reviewed in this article. The measurements have shown that exponential regions of different VCRs have significant variations of NF n and saturation current even within the same groups of LEDs.

3. RESULTS

The energy model of an asymmetrical structure, e.g. p-n^+ (with the n region heavily doped) may be presented in the form of a potential barrier with infinite length and height of φ_k. The front potential forming the SCR of the p–n^+- junction in the lightly doped p layer rises in accordance with a certain law. In the direction of this barrier, a flow of electrons with a broad energy range moves from the quasi-neutral n^+- region with thermal velocity V_T. The electrons with energy exceeding $(\varphi_k - qU)$ cross the SCR and move to the adjacent quasi-neutral p-type region. There they form diffusion current of minor CCs with its density at $qU > 3kT$ expressed as

$$J_{dif} = q\frac{L_n}{\tau_n}N_d \exp\left(-\frac{\varphi_k - qU}{kT}\right). \qquad (6)$$

Dividing and multiplying the right part by V_T and identifying $\frac{L_n}{\tau_n V_T}$ as r_d, let us write down the expression of the forward current of the diffusion mechanism in the form

$$J_{dif} = qr_d V_T N_d \exp\left(-\frac{\varphi_k - qU}{kT}\right) =$$

$$= qr_d V_T N_d \exp\left(-\frac{\varphi_k}{kT}\right)\exp\left(\frac{qU}{kT}\right) =$$

$$= J_0 \exp\left(\frac{qU}{kT}\right). \qquad (7)$$

It is Shockley's ideal VCR form with $n = n^* = 1$ over the entire voltage (current) range. With the ide-

$$F(U)=\int_{-x_n}^{x_p}\frac{1}{W(U)}\cdot\frac{f(x,U)\cdot\exp\left(-\frac{\varphi_k}{kT}\right)\left(\exp\left(\frac{qU}{kT}\right)-1\right)}{b\cdot\exp\left(-\frac{(\varphi_k-qU)}{W(U)\cdot kT}(x-x_n)\right)+\exp\left(-\left(\frac{(\varphi_k-qU)-\frac{(\varphi_k-qU)}{W(U)}(x-x_n)}{kT}\right)\right)+g}dx=$$

$$=\exp\left(\frac{-\varphi_k}{n^*\cdot kT}\right)\cdot\exp\left(\frac{qU}{n^*kT}-1\right), \qquad (10)$$

al VCR, the multiplier J_o does not depend on bias voltage, therefore $n = n^*$.

The physical meaning of the factor r_d is the ratio of CC diffusion current velocity at the level of $(\varphi_k - qU)$ to thermal velocity; $J_0 = qr_dV_TN_d\exp\left(-\frac{\varphi_k}{kT}\right)$ is the density of saturation current. After reaching the front of the barrier, CCs with energy lower than $(\varphi_k - qU)$ will recombine in accordance with the SNS model via the local recombination centres with holes moved to the SCR from the *p*-region. Total current will be equal to the sum of diffusion and recombination currents.

The SNS theory is applicable also to *p-n* structures with QW if the latter are presented in the form of recombination planes. Such idea was proposed in [20, 21].

In this work, we propose to assume that a thin QW located in any place of SCR serves as a single recombination centre with capture cross-section σ. Positions of QW in VCR and distribution of recombination centres of point defects in the barriers may be described by some function $N(x)$:

$$N(x)=N_t(x)+\sum_i\begin{vmatrix}0\mapsto x<a_i\\ \frac{1}{H}\mapsto a_i\ge x\ge(a_i+H)\\ 0\mapsto x>(a_i+H)\end{vmatrix}, \qquad (8)$$

where $N_t(x)$ is the concentration distribution of point defects, i is the QW number, H is the QW width, a is the location of the left edge of QW relative to the metallurgical border of the *p-n* structure.

Using the ideas of the SNS model, current density may be expressed by the formulae

$$J_{rec}=qb\sigma N_{tmd}(U)W(U)V_TN_dF(U), \qquad (9)$$

where $N_{tmd}(U)$ is the mean concentration of recombination centres of point defects and QW of the SCR which depends on bias voltage due to change of the SCR width and the number of QWs and point defects located in it:

$$N_{tmd}(U)=\frac{1}{W(U)}\int_{x_n}^{x_p}[N(x)]dx;\ f(x,U)=\frac{N(x)}{N_{tmd}(U)};$$

$$x_n=-\frac{W(U)\cdot N_a}{N_d+N_a},\ x_p=\frac{W(U)\cdot N_d}{N_d+N_a},$$

$$W(U)=\sqrt{\frac{2\varepsilon\varepsilon_0(N_a+N_d)\cdot\left(\frac{\varphi_k}{q}-U\right)}{qN_aN_d}},$$ (for uniform doping distribution), N_a and N_d are the concentrations of acceptor and donor dopants, $b = N_d/N_a$, $g = 2n_i/N_a$.

Using the factor $r_r(U)=\sigma N_{tmd}(U)\cdot W(U)$, the formula (9) is written as

$$J_{rec}=qr_r(U)V_TN_d\exp\left(\frac{\varphi_k}{n^*(U)\cdot kT}\right)\times$$

$$\times\left(\exp\left(\frac{qU}{n^*(U)\cdot kT}\right)-1\right)=$$

$$=J_S(U)\left[\exp\left(\frac{qU}{n^*(U)\cdot kT}\right)-1\right]. \qquad (11)$$

In the formula (10), there is an assumption that the front of the potential barrier increases linearly, therefore, it is identified as $\varphi(x)=\frac{(\varphi_k-qU)}{W(U)}(x_n-x)$, $J_S(U)=qr_r(U)V_TN_d\exp\left(-\frac{\varphi_k}{n^*(U)\cdot kT}\right)$ in it. The physical meaning of the factor $r_r(U)$ is ratio of CC recombinant current at the level of $(\varphi_k - qU)/n^*$ to thermal velocity.

The factor n^* is defined using the formula

$$n^*(U) = -\frac{(\varphi_k - qU)}{kT}\left[\ln(F(U))\right]^{-1}.$$

Obviously, differentiation of (11) will provide the values of NF n higher than those of n^*. It is rather difficult to define n^* experimentally.

The function $f(x, U)$ in (10) leads to variations of n^* from 1 to 2 and dependence of the pre-exponential factor on voltage leads to high values of NF n.

High values of NF, from 3.3 to 5, are common for *p-i-n* structures and with dependence of doping concentration at edges of SCR on variation of bias voltage, i.e. when N_a and N_d in the pre-exponential factor are the functions of bias voltage $N_a(U)$ and $N_d(U)$. This situation is real, since the doping concentration both in n^+ and p layers declines towards the metallurgical border virtually exponentially forming the compensated region in the vicinity of it (Fig. 2).

Unlike the cases with homogeneous *p-n* structures and uniform distribution of recombination centres, where recombination rate keeps its value after changes of SCR width, the situation is more difficult in structures with QWs. QWs keep their positions and the edge of SCR moves towards the metallurgical border with rise of voltage. The position of maximum recombination rate changes relative to QWs. This is related to variation of the growth rate of forward current with change in voltage, i.e. variations of NF n and n^* factor, as it can be seen from the figures in [13, 14].

In structures with multiple QWs, with $U = 0$, all QWs are located in the SCR. As forward voltage rises, part of QWs located closer to the edge of the SCR of the lightly doped layer leave the SCR and band-to-band recombination occurs in them due to diffusion current flowing in the quasi-neutral region where QWs are located. Therefore total current will be equal to the sum of these currents.

4. CONCLUSION

Based on the obtained mathematical models (9) and (10), using *Mathcad 14* VCR graphs were synthesised for different LEDs. The modelled VCRs of blue (B) and green (G) LEDs as well as dependences of NF n and factors n^* on voltage U for them are shown in Fig. 3. The width of QW is 4 nm; during their movement, it is equal to 15 nm and 16 nm for blue and green LEDs respectively. Doping level of the relatively lightly doped region was taken equal to $7 \cdot 10^{18}$ cm^{-3} and that of the heavily doped region (injector) was taken equal to $2 \cdot 10^{19}$ cm^{-3}. The semiconductor parameters were taken from [29]. For modelling of VCR in the current limitation region within the range exceeding $1 \cdot 10^{-4}$ A, series resistance $R = 10$ Ω.

5. RESULTS

1. The physical and mathematical model of VCR of LED *p-n* structures with QW was developed. It is different from the SNS model in that it includes the function of non-uniform distribution of QWs and point defects in the SCR of the *p-n* structure $f(x, U)$.

2. In LED structures, QWs may be presented as single recombination centres distributed over the SCR, with capture cross-section σ. Recombination rate in QW is defined by the position of maximum distribution of recombination rate as per SNS relative to QW, and quantum efficiency is defined by the relation of rates of radiant and non-radiant components as per the *ABC* model.

3. The factor n^* in the VCR exponent and the derivative of the logarithm of current to voltage n (NF) are different terms. The former parameter reflects the difference of the exponential factor from the Shockley model and the latter characterises behaviour of the functional dependence of forward current on voltage.

4. The physical meaning of the factor n^* is ratio of the value of contact potential φ_k to the efficient level of energy of charge carriers flow to the recombination region in the SCR.

5. The NF values exceeding 2 are attributed to dependence of both the exponent and the pre-exponential factor on bias voltage.

ACKNOWLEDGMENT

The work is conducted under the state grant provided within the Programme of Competitive Growth of NITU MISIS among the World's Leading Research Centres for 2013–2020.

REFERENCES

1. Shockley W. The Theory of p – n Junctions in Semiconductors and p – n Junction Transistors // Belt Syst. Tec. J. 1949, Vol. 28, pp. 435–489.

2. Sah C. T., Noyce R.N., Shockley W. Carrier Generation and Recombination in P-N Junctions and P-N

Junction Characteristics // Proc. IRE. 1957, Vol. 45, pp. 1228–1243.

3. Choo, S.C. Carrier generation-recombination in the space-charge region of an assymmetrical p-n junction // Solid State Electron. 1968, Vol. 11, pp. 1069–1077.

4. Sze S.M. Physics of Semiconductor Devices. Translated from English into Russian under the editorship of R.A. Suris. In 2 books. Book 1, 2nd edition, revised and supplemented. Moscow, Mir, 1984, 456 p.

5. Nakamura S., Iwasa M.S. Method of manufacturing p-tipe compound semicondoctors/ Patent N5, 306,662. Apr.1994. Japan.

6. Amano H., Akasaki I. et.al. Method for producing a luminous element of III-group nitride / Patent N5, 496,766. Mar. 1996. Japan.

7. Kong H-S., Leonard M., Bulman G., Negley G., Edmond J. AlGaN/GaN/AlGaN double-heterojunction blue LEDs on 6H-SiC substrates// Mat. Res. Soc. Proc. 1996, Vol. 395, pp. 903–907.

8. Nakamura, S. InGaN light-emitting diodes with quantum-well structures // Mat. Res. Soc. Pros. 1996, Vol. 395, pp. 979–887.

9. Kudryashov V.E., Turkin A.N., Yunovich A.E., Kovalyov A.N., Manyakhin F.I. Electroluminescence Properties of InGaN/AlGaN/GaN Light Emitting Diodes With Multiple Quantum Wells [Lyuminestsentnyye i elektricheskiye svoystva svetodiodov InGaN/AlGaN/GaN s mnozhestvennymi kvantovymi yamami] // FTP. 1999, Vol. 33, issue 4, pp. 445–450.

10. Yunovich A.E., Kudryashov V.E., Turkin A.N., Kovalev A.N., Manyakhin F.I.. Electroluminescence Properties of InGaN/AlGaN/GaN Light Emitting Diodes with Multiple Quantum Wells // MRS Intern. J. Nitride Semicond. Res. 1999, 4S1, G6, p. 29.

11. Yunovich, A.E., Kudryashov, V.E., Mamakin, S.S., Turkin, A.N., Kovalev, A.N., Manyakhin, F.I. Spectra and quantum efficiency of light emitting diodes based on GaN-heterostructures with quantum wells // Physica Status Solidi (A). 1999, Vol. 176, No. 1, pp. 125–130.

12. Manyakhin, F.I. Kovalev, A.N., Kudryashov, V.E., Mamakin, S.S., Yunovich, A.E. Change of charge centers distribution in AlGaN/InGaN/GaN heterostructures with multiple quantum wells during LED's aging at high currents" // The Fourth European GaN Workshop. Nottingham, Abstract, 2000, 2D.

13. Bochkaryova N.I., Rebane Yu.T. Shreter Yu.G. Growth of Shockley-Reed-Hall Recombination Rate in InGaN/GaN Quantum Wells as the Major Mechanism of Loss of LED Efficiency at High Injection Levels [Rost skorosti rekombinatsii Shokli-Rida-Holla v kvantovykh yamakh InGaN/GaN kak osnovnoy mekhanizm padeniya effektivnosti svetodiodov pri vysokikh urovnyakh inzhektsii] // FTP, 2015, Vol. 49, issue 12, pp. 1714–1719.

14. Risovanyy V.D., Svetukhin V.V., Vostretsov D. Ya., Vostretsova L.N., Ambrozevich A.S., Ermakov M.S. The Effect of Continuous Flow of Forward Current on Electric Characteristics of InGaN-Based LEDs [Vliyaniye dlitelnogo protekaniya pryamogo toka na elektricheskiye kharakteristiki svetodiodov na osnove InGaN] // Successes of Applied Physics [Uspekhi prikladnoy fiziki]. 2013, Vol. 1, issue 1, pp. 92–96.

15. Pikus G.E. Basics of the Theory of Semiconductor Devices [Osnovy teorii poluprovodnikovykh priborov]. Moscow: Nauka, GRFML, 1965, 448 p.

16. Zang M., Bhattacharya P., Singh J., Hinckley J. Direct measurement of auger recombination in $In_{0.1}Ga_{0.9}N$/GaN quantum well and its impact on the efficiency in $In_{0.1}Ga_{0.9}N$/GaN multiply quantum well light emitting diodes // Applied Physics Letters. 2009, Vol. 95, No. 20, pp. 1108.

17. Hopkins M.A., Allsopp, D.W.E., Kappers, M.J. Oliver, R.A., Humpreys, C.J.. The ABC model of recombination reinterpreted: Impact on understanding carrier transport and efficiency droop in InGaN/GaN light emitting diodes // J. Appl. Phys. 2017, Vol. 122, No. 23, p. 4505.

18. David A., Hurni C.A., Young N.G., Craven M.D. Electrical properties of III-nitride LEDs recombination-based injection model and theoretical limits to electrical efficiency and electroluminescent cooling // Appl. Phys. Lett. 2016. Vol. 109, No. 8, pp. 3501.

19. Dai Q., Shan Q., Wang J., Chhajed S., Cho J.M., Shubert E.F., Crauford M.H., Koleske D.D., Kim M.-H., Park Y.. Carrier recombination mechanisms and efficiency droop in GaInN/GaN light-emitting diodes // Appl Phys. Lett. 2010, Vol. 97, No. 13, pp. 3507.

20. Masui H., Nakamura S., DenBaars S.P. Tecnique to evaluate the diode ideality factor of light-emitting diodes // Appl. Phys. Lett. 2010, Vol. 96, No. 7, pp. 3509.

21. Masui H. Diode ideality factor in modern light-emitting diodes // Semicond. Sci. Technol. 2011, Vol. 26, No. 7, pp. 5011–5016.

22. Prudaev I.A., Skakunov M.S., Lelekov M.A., Ryaboshtan Yu.L., Gorlachuk P.V., Marmalyuk A.A. Recombinant Currents in LEDs Based on Multiple Quantum Wells $(Al_xGa_{1-x})_{0.5}In_{0.5}P/(Al_yGa_{1-y})_{0.5}In_{0.5}P$ [Rekombinatsyonnyye toki v svetodiodakh na osnove mnozhestvennykh kvantovykh yam (AlxGa1-x)0.5In0.5P/(AlyGa1-y)0.5In0.5P] // Izvestiya vuzov. Fizika. 2013, Vol. 56, issue 8, pp. 44–47.

23. Torchinskaya T.V., Karabaev A.G., Sheynkman M.K. Injection-Stimulated Transformation of Luminescence Spectra of Green GaP: N LEDs [Inzhektsionno-stimulirovannaya transformatsiya spektrov lyuminestsentsii zelyonykh GaP: N-svetodiodov] // FTP. 1990, Vol. 24, issue 8, pp. 1337–1348.

24. Abdullaev Zh.S., Gusev M. Yu., Zyuganov A.N., Torchinskaya T.V. Parameters of Deep Centres in AlGaAs LEDs Evaluated by Capacity and Injection Spectroscopy Methods [Parametry glubokikh tsentrov v svetodiodakh AlGaAs otsenyonnyye metodami emkostnoy i inzhektsionnoy spektroskopii] // Ukr. Phys. Journal. 1989. Vol. 34, issue 8, pp. 1220–1224.

25. Manyakhin F.I. Mechanism and Pattern of Lowering of Luminous Flux of LEDs Based on AlGaN/InGaN/GaN Structures with Quantum Wells with Continuous Flow of Forward Current of Different Density [Mekhanizm i zakonomernost snizheniya svetovogo potoka svetodiodov na osnove struktur AlGaN/InGaN/GaN s kvantovymi yamami pri dlitelnom protekanii pryamogo toka razlichnoy plotnosti] // FTP. 2018. Vol. 52, issue 3, pp. 378–384.

26. Manyakhin F.I. The Role of the Compensated Layer in Formation of the Voltage-Current Relationship of LEDs Based on Wide Bandgap Semiconductors [Rol kompensirovannogo sloya v formirovanii volt-ampernoy kharakteristiki svetodiodov na osnove shirokozonnykh poluprovodnikov] // Izvestiya vuzov. Materialy elektronnoy tekhniki. 2009, Vol. 3, pp. 51–56.

27. Goryunov N.N., Manyakhin F.I., Klebanov M.P., Lukashev N.V. Impulse Three-Frequency Method of Measurement of Charged Centre Parameters in the Space Charge Region of Semiconductor Structures [Impulsnyy tryokhchastotnyy metod izmereniya parametrov zaryazhennykh tsentrov v oblasti prostranstvennogo zaryada poluprovodnikovykh struktur] // Pribory i sistemy upravleniya. 1999, Vol. 10, pp. 46–49.

28. Manyakhin F.I. The Nature of Resistance of the Compansated Layer and Recombination Mechanisms in LED Structures [Priroda soprotivleniya kompensirovannogo sloya i mekhanizmy rekombinatsii v svetodiodnykh strukturakh] // Izvestiya vuzov. Materialy elektronnoy tekhniki. 2006, Vol. 4, pp. 20–25.

29. NSM Archive. Physical Properties of Semiconductors. URL: http://www.ioffe.rssi.ru/SVA/NSM/Semicond/ (accessed on: 28.02.2020).

Fedor I. Manyakhin, Doctor of Physical and Mathematical Sciences, Professor. In 1973, he graduated from the Moscow Institute of Electronic Engineering (MIEM). At present, he is a Professor of the Automatic Design sub-department of NITU MISIS, author and co-author of more than 150 publications, awarded with the diploma of the Ministry of Education and Science of Russia, prize winner of the Golden Names of Higher Education 2018 contest in nomination of Contribution to Science and Higher Education. His research interests: semiconductor electronics, physics of semiconductor devices

Lyudmila O. Mokretsova, Associate Professor, Ph.D. in Technical Sciences. In 1978, she graduated from the Moscow Institute of Steel and Alloys (MISIS). At resent, she is Associate Professor of the Automatic Design sub-department of NITU MISIS, prize winner of the Golden Names of Higher Education 2018 contest in nomination of Introduction of Innovative Teaching Techniques. Her research interests: 3D modelling in light design

Arthur B. Vattana, engineer. In 1999, graduated from the Microelectronics and Semiconductor Devices sub-department of MISIS. At present, he is a Senior lecturer of the Electric Engineering and Information and Measurement Systems sub-department of NITU MISIS. His research interests: physics of light emitting diodes, experimental studies of LED characteristics

Light & Engineering
Vol. 28, No. 5, pp. 39–47, 2020

https://doi.org/10.33383/2019-103
Svetotekhnika #3, 2020, pp. 64–70

THE METHOD OF QUASI-SPECULAR ELEMENTS TO REDUCE STOCHASTIC NOISE DURING ILLUMINANCE SIMULATION

Sergei V. Ershov[1,1], Dmitry D. Zhdanov[2,2], Alexei G. Voloboy[1,3], and Nikolay B. Deryabin[1,4]

[1]Department of Computer graphics and computational optics of the Keldysh Institute of Applied Mathematics RAS, Moscow, Russia
[2]ITMO University, St. Petersburg, Russia
E-mail: measure@spp.keldysh.ru[1], ddzhdanov@mail.ru[2], voloboy@gin.keldysh.ru[3], dek@gin.keldysh.ru[4]

ABSTRACT

When simulating the propagation of light, luminance/radiance brought by a ray is calculated from the optical properties of the scene objects it interacts with. According to their optical properties, objects can be roughly divided into diffuse and specular. In Monte Carlo ray tracing luminance/radiance is calculated only for diffuse surfaces. When a ray hits a specular a surface, it is reflected (or refracted) until it reaches a diffuse surface, and only then the luminance/radiance is calculated. In the proposed approach, diffuse elements are further divided into genuine diffuse and quasi-specular elements. The most natural criterion for the latter is that it scatters light in a narrow cone about the specular direction. An element of the scene can also be a superposition of both types when its scattering function is a sum of the genuine diffuse and quasi-specular parts. This article shows how different components of illuminance/irradiance interact with quasi-specular objects and describe how this works in the bi-directional stochastic ray tracing. The proposed approach significantly reduces stochastic noise for multiple scenes. This method is also applicable for simulation of volume scattering, treating the phase function of the medium as quasi-specular. In this case, the choice of quasi-specular objects is not based on the nature of the bidirectional scattering distribution function (BSDF): the medium is treated as completely quasi-specular while the surfaces, even if their BSDFs are narrower, remain genuine diffuse. The article shows the advantage of this approach.

Keywords: calculation of illuminance, realistic rendering, bidirectional ray tracing, stochastic ray tracing, noise reduction, BSDF

1. INTRODUCTION

The bidirectional ray tracing using photon maps is an efficient method for calculating the image of a virtual scene [1]. Tracing rays from light sources creates a photon map that allows one to calculate the illuminance of the scene surfaces. Then the ray is traced from the camera, and when it hits a diffuse surface, it takes illuminance from the photon map, "convolves" it with the surface bidirectional scattering distribution function (BSDF) at this point, and adds the result to the accumulated luminance/radiance of the pixel. This idea is implemented in several modifications of the described method [2–5].

An important parameter of this approach is the number of operators (events on the ray path) in the products of integral scattering operators calculated by the backward Monte Carlo ray tracing. Usually only diffuse events are considered, and the maximum allowed number is denoted by backward diffuse depth (*BDD*[1]). The efficiency of the method, that is, its convergence rate (or noise level, which is

[1] A specific parameter of bidirectional ray tracing: the ray from camera terminates after BDD diffuse scattering events.

the same) strongly depends on this *BDD*, and its optimal value differs for each scene.

The best approach would be to use different *BDDs* for different parts of the scene [5], and even mix calculations with different *BDDs* [5], as in "multiple importance sampling". It is often possible to find the optimal *BDD* (automatically or manually), for which calculations become quite efficient. However, this is not always possible, and in some cases, changing the *BDD* does not help, i.e. whatever value is taken, the image is very noisy.

We provide a simple method that helps in such cases. Its idea is that those objects of the scene (surface or volume scattering) that have a diffuse part of BSDF are divided into two groups: genuine diffuse and quasi-specular. Usually, the last ones will be those for which the BSDF is a narrow near-specular cone. Although in principle the criterion can be arbitrary, up to the point that the Lambert surface will be treated as quasi-specular. As a rule, the separation treats the BSDF (for the surface or the phase function for a volume) as a sum of the quasi-specular and genuine diffuse components, which are both non-zero.

Quasi-specular scattering does not increase the diffuse event counter (when it exceeded the *BDD*, the ray is killed). Besides, the quasi-specular part of the BSDF does not convolve with diffuse component of illuminance (that is, those rays from the light source that have been subjected to genuine diffuse scattering). This change in backward ray tracing can be applied to both surface and volume scattering, to reduce noise and the amount of memory used.

An alternative approach is more attractive, in which there is no fixed *BDD*, no a distinction between direct, caustic and diffuse lighting rays. At each intersection of a diffuse surface by the camera ray, all the lighting rays are collected, and the contribution from various points is summed with the weight depending on the full trajectory (joining its parts from the light source and from the camera) and calculated using the multiple importance sampling (MIS) equation [6]. Unfortunately, despite the convincing images in [6], the proposed method does not use photon maps at all, but instead traces one ray from the camera and one ray from the light source, then calculates the contribution from the joining of these paths (it vanishes if they do not meet with the desired accuracy), then forgets this pair and starting a new one. When using photon maps, the same forward ray path is tried to join with each ray from the camera. At first glance, this is all the same since contributions for different forward paths are independent even for the same backward path. In fact, this is not the case [7], and the noise (that is, the variance of the accumulated pixel luminance) is calculated using equations other than those used for the simple Markov chain Monte-Carlo (MCMC). These equations include not only the BSDF along the ray path and the light source goniogram, as in [6], but the geometric factors (distance between surfaces, etc.) as well. Therefore, the method proposed in [6] cannot be used directly without improvement. Meanwhile, it requires that integrating spheres have been installed at all hit points for the camera ray, which increases the memory requirements. And in addition, the photon (the ray from the light source) is checked for intersections with all of them, which slows down the processing process. Therefore, the performance of our proposed method based on a limited *BDD* is higher.

There are variants of the method [6], gradually abandoning photon maps, for example [8], wherein addition to vertex merging, which is much similar to photon maps, the vertex connection is used when the ends of the camera and light paths are not close and connected by an additional segment of finite length. Vertexes for joining can be selected probabilistically [9]. A detailed review can be found in the dissertation [10]. All these methods use MIS, when the merging of the camera and light paths is done at different vertexes and summing the resulting contributions with weights. In addition, in [8] MIS is applied to two possible approaches – vertex connection and vertex merging.

Unfortunately, as in [6], in these studies, the equations for weight calculations are applied to photon maps or their equivalent when the same set of paths from the source is reused for all camera rays.

2. THE RENDERING EQUATION AND CALCULATION OF ITS NEUMANN SERIES BY BIDIRECTIONAL RAY TRACING

The light field in the scene is described by a self-consistent equation that can be written in various forms, such as the equation of global illumination [11], etc. The idea is that there is a light field in the scene, it lights the surfaces that scatter it. This is the transformation of irradiance E (light incident on the surface at a point $\boldsymbol{x}$ in direction $\boldsymbol{v}'$) into lumi-

nance/radiance L (light exiting from a surface point $\boldsymbol{x}$ in direction $\boldsymbol{v}$) by the BSDF of the surface f:

$$L(v;x) = \int f(x;v,v')E(v',x)d^2v'.$$

Then this light emitted from the surface propagates further across the scene and lights its surfaces. This transformation of luminance/radiance (light emitted from the surface) into illuminance (light incident on another point in the scene) is described by the transfer operator. Since the explicit form of the scattering and transport operators is not important for us, we will use compact notation:

$$L = \hat{F} \cdot E, \tag{1}$$

$$E = \hat{T} \cdot L. \tag{2}$$

Note that here $\hat{F}$ includes only diffuse scattering; therefore, the caustic is non-scattered light, that is, part of direct lighting.

Note that L is the luminance/radiance of scene surfaces, while the camera image will be $\hat{S}L$, where $\hat{S}$ describes a purely specular transformation between the scene and the camera (usually it is identity operator). Here and further, we will calculate only L. Then, if necessary, we can apply its conversion to the luminance of the image.

Full illuminance consists of direct and diffuse components:

$$E = E^{(i)} + E^{(0)}. \tag{3}$$

By combining these three equations, we arrive at the self-consistent global illumination equation, used below in the form of the rendering equation introduced by Kajiya [11]:

$$E = \hat{T} \cdot \hat{F} \cdot E + E^{(0)}. \tag{4}$$

In computational optics a combination of forwarding and backward ray tracing is widely used, when the forward part calculates illuminance of diffuse surfaces E and stores it, for example, as a photon map [1], and then the backward tracing converts it into an image visible by the camera. Note that the illuminance obtained by stochastic tracing is noisy, and this noise goes further to the image, its final amplitude strongly depends on how the tracing from the camera works.

The easiest way is to trace the rays from the camera to the first diffuse surface, where the surface luminance/radiance created by all components of the illuminance is calculated ($= \hat{F}E$), which is then added to the accumulated luminance/radiance of the pixel. This provides an estimate of the luminance/radiance of the surface (1), although the result is not ideal, since the illuminance E calculated by the forward ray tracing is usually subjected to a (spatial) filtering to reduce noise. Because of this, small-scale lighting details, such as glare, can be lost.

Instead, one can apply the Nth iteration of (4) to illuminance, which leads to the luminance/radiance equation:

$$L = (\hat{F} \cdot \hat{T})^N \hat{F} \cdot E + \sum_{k=0}^{N-1} (\hat{F} \cdot \hat{T})^k \hat{F} \cdot E^{(0)}. \tag{5}$$

For the exact illuminance E, this naturally gives the same result as the simple $\hat{F}E$ above, however for the actually used noisy E, this second form is often better due to the lower noise level due to the convolution with the power of operator $\hat{F}\hat{T}$. The value N is nothing but the "backward diffuse depth" or *BDD* described in the introduction.

The term $\hat{F}E^{(0)}$ is the luminance/radiance of the surface under direct (including caustic) lighting. The diffuse component of the lighting is considered only at the last hit point of the camera ray: this is the term $\left(\hat{F}\hat{T}\right)^N \hat{F}E$.

Integral operators can be calculated by the Monte Carlo method: we launch rays from the camera through a given pixel of the image, they hit a surface, are scattered (left operator $\hat{F}$), spread across the scene (operator $\hat{T}$; note that in the backward ray tracing the order of events from camera corresponds to the order of operators from left to right, i.e. the leftmost operator corresponds to the transformation in the segment closest to camera), and so on until the Nth diffuse surface is reached, where it terminates. At the kth diffuse hit point (i.e. immediately before the kth diffuse scattering), we calculate the luminance/radiance of the surface under the direct (including caustic!) lighting $\hat{F}E^{(0)}$ if $k < N$, and under the full lighting $\hat{F}E$ for $k = N$. Then the result is scaled to consider the attenuation of light due to specular transformations in $\hat{T}$ and is eventually added to the accumulated luminance/radiance of the pixel. The average value over the ensemble of camera rays converges to L.

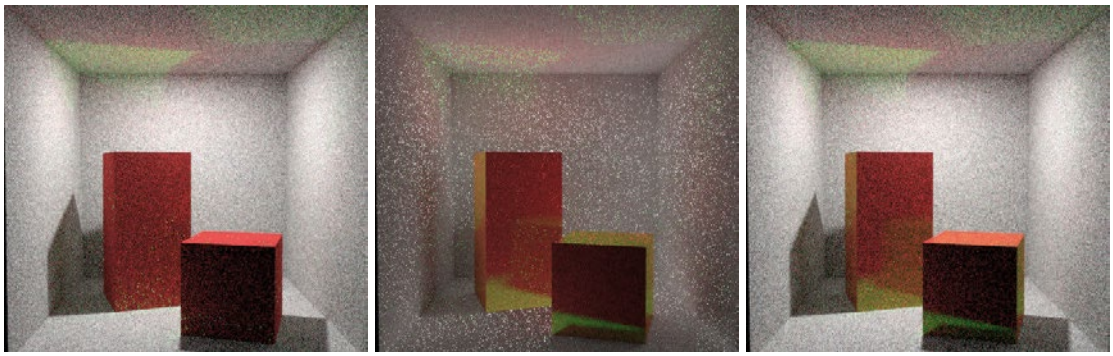

Fig. 1. Camera images for the modified Cornell Box scene calculated during the same time (200 s) for the standard method with *BDD* = 0 (a), the standard method with *BDD* = 1 (b) and for the quasi-specular method with *BDD* = 0 (c)

3. THE IDEA OF THE QUASI-SPECULAR METHOD

Consider a modification of the well-known Cornell Box benchmark scene. It is a box open from the camera side with two parallelepipeds standing on its floor. The light source is a transparent square located very close to the ceiling of the box, which emits upwards. The walls of the box have a Lambertian reflection with an albedo of 50 %, and the parallelepipeds have BSDF, which is a sum of the Lambertian and narrow (almost specular) components. To distinguish their contributions to the image, the Lambert component is pure red (the normalized colour is (1,0,0)), and the sharp component is almost pure green (the normalized colour is (0.1,1,0.1)). The albedo for the maximum colour component is 50 % and 25 %, respectively.

There is practically no direct lighting in the scene (except for a small square of the ceiling above the source).

Consider the case of *BDD* = 0. A ray from the camera that hits any surface of the scene terminates there (since there are no specular BSDFs in the scene) and takes the luminance/radiance of the hit point as a convolution of the BSDF with full lighting. There is a sharp BSDF on the surface of the parallelepipeds, while the lighting is mainly secondary from the walls of the box. The convolution of a sharp BSDF with wide noise lighting from photon maps contains strong noise (green reflection at the bottom of the parallelepipeds in Fig. 1).

In case of *BDD* = 1, only the direct and caustic lighting, which is not present in this scene, except for a small square on the ceiling above the source, is taken at the first hit point of a camera ray. Then the camera ray is reflected and either leaves the scene or hits one of its surfaces, where full lighting collects. In this case, a very small part of the rays hits the square of the ceiling located directly above the source, where the lighting is orders of magnitude higher. Accordingly, the luminance/radiance brought by these rays to the pixel is orders of magnitude higher than the average value. Other rays hit the walls of the box or parallelepipeds, where the lighting is low, and accordingly, their contribution to the pixel luminance/radiance is also small. As a result, the luminance/radiance of the pixel is created mainly by a small fraction of rays, which inevitably leads to a large amount of noise, see Fig. 1. Note that the noise on the parallelepipeds is mostly not green, because the sharp BSDF part sends reflected rays to about the same place in the scene, so either almost all of them hit the bright square on the ceiling or none.

Higher *BDD* values also do not improve the situation.

One could try to use *BDD* = 0 for camera rays reflected by the Lambert part of the BSDF, and *BDD* = 1 for the rays that were first scattered by the sharp BSDF part. This, however, does not work [5], as was proved in [12]. That is when rays scattered in the near- specular direction and off-specular ones collect lighting differently, the accumulated luminance/radiance is incorrect. Thus, a more complex criterion is required to determine at which point to use which lighting rays, and which rays to ignore.

The key idea of the approach remains the same: scattering from the sharp BSDF part is treated not as genuine diffuse, but rather like specular. This sharp BSDF (and the entire method of processing the camera rays scattered by it) is therefore called quasi-specular. The result of the calculation for the same model scene using this method is shown

in Fig. 1 (c), see section 7.1. for a more detailed discussion.

4. OPERATOR SERIES IN PRESENCE OF QUASI-SPECULAR BSDFS

Now let us go to the formal derivation of what to do with the camera ray when the diffuse BSDF is divided into genuine diffuse and quasi-specular parts:

$$\hat{F} = \hat{F}_d + \hat{F}_{qs}. \tag{6}$$

The separation is arbitrary (although some separations are advantageous in terms of noise level and some are not), meaning that for any choice, the image luminance/radiance converges to the exact value.

Considering (6) the luminance at the point of the surface $\boldsymbol{x}$ is

$$L(v,x) = (\hat{F}_d \cdot E)(v,x) + (\hat{F}_{qs})(v,x). \tag{7}$$

Lighting is now also divided into three components: direct (that was not scattered at all or was purely specular BSDF), quasi-caustics (scattered at least once by a quasi-specular BSDF, but never by genuine diffuse BSDF), and diffuse (scattered at least once by genuine diffuse BSDF), i.e.

$$E = E^{(0)} + E^{(qc)} + E^{(i)},$$

so (7) takes the form

$$\begin{aligned} L = \hat{F} \cdot E = \hat{F}_{qs} \cdot (E^{(0)} + E^{(qc)}) + \\ + \hat{F}_{qs} \cdot E^{(i)} + \hat{F}_d \cdot E. \end{aligned} \tag{8}$$

Then, substituting our light separation into the global illumination equation (4), we obtain

$$\begin{aligned} E^{(qc)} + E^{(i)} = \hat{T} \cdot \hat{F}_{qs} \cdot (E^{(0)} + E^{(qc)}) + \\ + \hat{T} \cdot \hat{F}_{qs} \cdot E^{(i)} + \hat{T} \cdot \hat{F}_d \cdot E. \end{aligned}$$

The term $\hat{T} \cdot \hat{F}_{qs} \cdot E^{(i)} + \hat{T} \cdot \hat{F}_d \cdot E$ in its right-hand side describes light that has undergone at least one genuine diffuse scattering, while the term $\hat{T} \cdot \hat{F}_{qs} \cdot (E^{(0)} + E^{(qc)})$ describes the light that has undergone at least one purely specular scattering, but no one diffuse scattering. Considering our splitting of lighting into three components, this means that

$$E^{(i)} = \hat{T} \cdot (\hat{F}_d \cdot E + \hat{F}_{qs} \cdot E^{(i)}), \tag{9}$$

$$E^{(qc)} = \hat{T} \cdot (\hat{F}_{qs} \cdot E^{(qc)} + \hat{F}_{qs} \cdot E^{(0)}), \tag{10}$$

which means that

$$E^{(i)} \big| = (1 - \hat{T} \cdot \hat{F}_{qs})^{-1} \cdot \hat{T} \cdot \hat{F}_d \cdot E, \tag{11}$$

$$E^{(qc)} \big| = (1 - \hat{T} \cdot \hat{F}_{qs})^{-1} \cdot \hat{T} \cdot \hat{F}_{qs} \cdot E^{(0)}. \tag{12}$$

We assume that if the camera ray is subjected to quasi-specular scattering, this does not increase the counter of diffuse events, so the ray does not terminate. Now we will derive which illuminance components should be taken at which hit points of the camera ray so that the mathematical expectation of image luminance/radiance coincides with the exact value.

By combining (8) with (11) and (12), after trivial, though tedious transformations, it can be obtained that the surface luminance/radiance calculated for $BDD = N$ is equal to $L \big| = \hat{F}_{qs} \cdot (E^{(0)} + E^{(qc)}) +$

$$\begin{aligned} \big| + \sum_{k=0}^{N-1} ((1 - \hat{Q})^{-1} \cdot \hat{F}_d \cdot \hat{T})^k \cdot (1 - \hat{Q})^{-1} \times \\ \times \hat{F}_d \cdot (E^{(0)} + E^{(qc)}) + (1 - \hat{Q})^{-1} \times \\ \times \hat{F}_d \cdot \hat{T})^N \cdot (1 - \hat{Q})^{-1} \hat{F}_d \cdot E), \end{aligned} \tag{13}$$

where

$$\hat{Q} \equiv \hat{F}_{qs} \cdot \hat{T}. \tag{14}$$

There is also an alternative form that gives the same result for the exact luminance, while for a real noisy illuminance E may give different (in noise level) result:

$$\begin{aligned} L = (1 - \hat{Q})^{-1} \cdot \hat{F}_{qs} \cdot E^{(0)} \\ \big| + \sum_{k=0}^{N-1} ((1 - \hat{Q})^{-1} \cdot \hat{F}_d \cdot \hat{T})^k \cdot (1 - \hat{Q})^{-1} \cdot \hat{F}_d \times \\ \times (E^{(0)} + E^{(qc)}) + (1 - \hat{Q})^{-1} \times \\ \times \hat{F}_d \cdot \hat{T})^N \cdot (1 - \hat{Q})^{-1} \hat{F}_d \cdot E). \end{aligned} \tag{15}$$

The detailed conclusion is given in [12].

5. INTEGRATION BY CAMERA PATHS

By decomposing $(1 - \hat{Q})^{-1}$ from (13) into the Neumann series, we see that, for example, for $BDD = 2$

$$L = \hat{F} \cdot (E^{(0)} + E^{(qc)}) + \sum_{k=1}^{\infty} \hat{Q}^k \cdot \hat{F}_d \times$$
$$\times (E^{(0)} + E^{(qc)}) + \sum_{k,m=0}^{\infty} \hat{Q}^k \cdot \hat{F}_d \cdot \hat{T} \cdot \hat{Q}^m \times$$
$$\times \hat{F}_d \cdot (E^{(0)} + E^{(qc)}) + \sum_{k,m,n=0}^{\infty} \hat{Q}^k \cdot \hat{F}_d \cdot \hat{T} \times \quad (16)$$
$$\times \hat{Q}^m \cdot \hat{F}_d \cdot \hat{T} \cdot \hat{Q}^n \cdot \hat{F}_d \cdot (E^{(0)} + E^{(qc)}).$$

In this expression, a term of the form $\hat{Q}^k \cdot \hat{F}_d \cdot \hat{T} \cdot \hat{Q}^m \cdot \hat{F}_d \cdot (E^{(0)} + E^{(qc)})$ means that:

1. The final (the last "before" camera) light transformation is k ≥ 0 quasi-specular transformations with the corresponding transfer $\hat{Q}^k = (\hat{F}_{qs} \cdot \hat{T})^k$;

2. Prior to that (i.e. further from the camera), the light undergoes a genuine diffuse transformation with the corresponding transfer $\hat{F}_d \cdot \hat{T}$;

3. Prior to that (i.e. even further from the camera), the light had undergone $m \geq 0$ quasi-specular transformations with the corresponding transfer $\hat{Q}^m = (\hat{F}_{qs} \cdot \hat{T})^m$;

4. And all this affects the convolution of the genuine diffuse BSDF component with direct and quasi-caustic lighting, i.e. on $\hat{F}_d \cdot (E^{(0)} + E^{(qc)})$.

The action of the integral operators $\hat{F}_d$ and $\hat{F}_{qs}$ can be calculated by the Monte Carlo method tracing rays from the camera. Here is the first ray transformation (along the path from the camera) corresponds to the leftmost operator in the product, and the last transformation corresponds to the rightmost operator. Thus, our term $\hat{Q}^k \cdot \hat{F}_d \cdot \hat{T} \cdot \hat{Q}^m \cdot \hat{F}_d \times$ $\times (E^{(0)} + E^{(qc)})$ is estimated from camera rays that first underwent $k \geq 0$ quasi-specular events, then one genuine diffuse, then $m \geq 0$ quasi-specular, and then took the luminance/brightness of the genuine diffuse BSDF part under the direct and quasi-caustic lighting (i.e. diffuse lighting is ignored).

A detailed derivation is given in [12].

The other terms of equation (16) can be similarly calculated by the Monte Carlo ray tracing from the camera. This leads to the algorithm of processing camera rays in which the luminance/radiance of the hit point is calculated as follows:

- Before (and including!) the first non-purely specular event – $\hat{F} \cdot (E^{(0)} + E^{(qc)})$;
- After the first quasi-specular event and until the second genuine diffuse – $\hat{F}_d \cdot (E^{(0)} + E^{(qc)})$;
- After the second genuine diffuse event – $\hat{F}_d \cdot E$;
- And at the third genuine diffuse event the ray terminates.

This relates to *BDD* = 2. Similarly, the case of another *BDD* is considered, as well as the alternative form (13). Trace the rays from camera until they are subjected to *BDD* + 1 genuine diffuse event (or are absorbed earlier); after that, the ray terminates. When the ray hits a surface that has a diffuse or quasi-specular BSDF, it takes a convolution of a part of BSDF with a part of illuminance:

- Diffuse lighting – always only with a diffuse remainder of the BSDF;
- Quasi-caustic lighting: the main variant is before the first quasi-specular event– with a complete BSDF, after it – with the diffuse remainder of the BSDF or the alternative variant is always with the diffuse remainder of the BSDF;
- Direct and caustic lighting: the main variant is before the first quasi-specular event – with a complete BSDF, after it – with the diffuse remainder of the BSDF or the alternative variant is before the first diffuse scattering – with a complete BSDF, after it – with the diffuse remainder of the BSDF.

6. VOLUMETRIC SCATTERING

6.1. Standard Method

It works the same way as for surfaces. For simplicity, suppose that *BDD* = 1 and the camera is inside the scattering medium. Then the camera ray propagates in the medium. When it undergoes the first volume scattering, we collect direct and caustic components of illuminance and convolve it with the phase function. At the point of the second volume scattering, full illuminance is taken. After the second diffuse scattering, the camera ray terminates.

Consider now a model scene in which the camera looks through a layer of scattering medium at an illuminated diffuse surface. Let the medium also be non-absorbing and have a large scattering coefficient, so that the camera ray undergoes many scattering events in it until it reaches this surface. And finally, let the phase function be sharp so that each scattering changes the ray direction only slightly.

In the standard method with a small *BDD,* the camera ray terminates only near its entrance to the medium, so that it does not reach the diffuse surface behind the medium at all. Besides, since the phase function is narrow, its convolution with the illuminance coming from the surface of the scene leads to strong noise, see section 3.

Therefore, to reduce noise, it is necessary to use a large *BDD* so that the camera ray penetrates the medium and reaches the surface behind it, rather than collecting diffuse lighting at the points of volume scattering. However, this requires storing all the volume scattering events along the long ray path (since direct and caustic lighting are collected there), which usually requires too much memory.

6.2. Quasi-Specular Medium

Using a quasi-specular approach can significantly improve the situation for scenes of that kind.

Suppose that the surface of the scene is not quasi-specular (that is, it does not have a quasi-specular component that is processed as described at the end of section 5). Also, let the entire phase function be treated as quasi-specular, i.e. its genuine diffuse part vanishes: $\hat{F}_d = 0$. Then, while the camera ray propagates inside the scattering medium, it only undergoes quasi-specular events that do not increase the counter of diffuse events, and as a result, it propagates in the medium until it leaves it and therefore reaches the surface behind the medium.

Diffuse lighting now consists of the light reflected from the diffuse surface of the scene, quasi-caustics is the light that has undergone at least one diffuse event (and an arbitrary number of specular scattering – but not diffuse surface scattering).

Since $\hat{F}_d = 0$, the "main variant" (see the end of section 5) assumes that at the points of volume scattering:

- Diffuse lighting (from the scene surface) is ignored;
- Direct, caustic, and quasi-caustic lighting is used only at the point of the first volumetric scattering.

As a result, for any *BDD* the camera ray leaves the medium and reaches the surface of the scene. In this case, only one (first) volume scattering is remembered, and the luminance/radiance of the medium is not taken at the subsequent points. There is also no strong noise from the convolution of the sharp phase function in the diffuse component of illuminance (from the surface). However, there is its convolution with the direct, caustic and scattered inside the medium light. But usually, they do not have a wide angular distribution and therefore do not produce much noise.

The "alternative variant" (see the end of section 5) is less good here since the direct and caustic lighting is now taken at all points of the volume scattering. Therefore, it is necessary to store in memory all the points of volume scattering on a long path, so that later it is possible to take a convolution of the phase function with direct and caustic lighting from photon maps in these points. If you first trace the rays from the camera (and only then ray trace from the light sources), forming a backward photon map, and the rays from the source are not stored and processed on the fly, this will require unacceptably large memory.

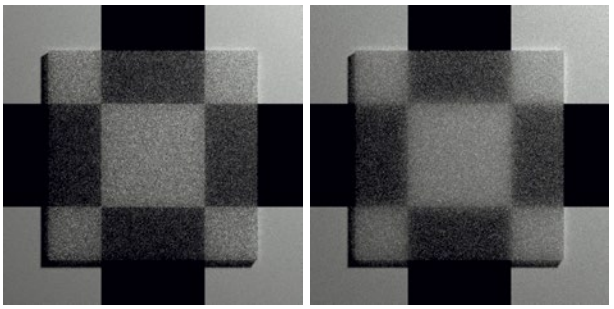

Fig. 2. Camera images for the scene of a turbid medium plate laid upon the paper sheet with a chessboard-like texture. The left panel (a) was calculated in the "standard mode" and the right one (b) was calculated when the volumetric scattering is treated as quasi-specular (in both cases *BDD*=1)

7. RESULTS

7.1. Surface Scattering

Calculations for the modified Cornell Box scene described in section 3 were performed in the quasi-specular mode for *BDD* = 0 and under the same other conditions and for the same time (200 s) as for the standard model. The results for the standard and the quasi-specular methods are shown in Fig. 1.

When applying the proposed method, it was possible to achieve the same low noise of the Cornell Box walls as for the standard method with *BDD* = 0. At the same time, at the bottom of the parallelepipeds, we were able to reduce the noise in about the same way as for the standard method with *BDD* = 1. Thus, in a sense, the best result is obtained.

7.2. For Volume Scattering

The model scene is a 3 mm thick plate laid on a piece of paper with a checkerboard texture, illuminated by a self-luminous sphere above it. The scat-

tering medium inside the plate has a refractive index of 1.5, a scattering coefficient of 7.5 mm^{-1} and a Henyey-Greenstein phase function [13] with parameter $g = 0.9$.

Images calculated the equal time and with the same other parameters are shown in Fig. 2. When using the standard method, the borders of the texture squares are sharp, while they should be blurred. When using the quasi-specular representation of the phase function, these borders are blurred, which corresponds to what one sees.

The left panel (Fig. 2 (a)) was calculated in the "standard model" and the right one (Fig. 2 (b)) was calculated when the volume scattering is treated as quasi-specular. In both cases $BDD = 1$.

REFERENCES

1. H. W. Jensen, Global illumination using photon maps, in Proceedings of the Eurographics Workshop on Rendering Techniques '96, London, UK, Springer-Verlag, 1996. pp. 21–30.

2. H. W. Jensen and P. Christensen, High quality rendering using ray tracing and photon mapping, in ACM SIGGRAPH 2007 Courses, SIGGRAPH '07, (New York, NY, USA), ACM, 2007.

3. T. Hachisuka and H.W. Jensen, Stochastic progressive photon mapping, in ACM SIGGRAPH Asia 2009 Papers, SIGGRAPH Asia '09, New York, NY, USA, ACM, 2009. pp. 141:1–141:8.

4. M. Pharr and G. Humphreys, Physically Based Rendering, Second Edition: From Theory To Implementation. San Francisco, CA, USA: Morgan Kaufmann Publishers Inc., 2nd ed., 2010.

5. Д.Д. Жданов, С.В. Ершов, А.Г. Волобой, Адаптивный выбор глубины трассировки обратного луча в методе двунаправленной стохастической трассировки лучей, in Proceedings of 25-th International Conference on Computer Graphics and Vision, September 22–25, Protvino, 2015. pp. 44–49.

6. J. Vorba, Bidirectional photon mapping, in Proceedings of CESCG 2011: The 15th CentralEuropean Seminar on Computer Graphics, Charles University, Prague, 2011.

7. S. V. Ershov, D.D. Zhdanov, and A.G. Voloboy, Estimation of noise in calculation of scattering medium luminance by MCRT, Mathematica Montisnigri, V14, 2019. pp. 60–73.

8. I. Georgiev, J. Krivanek, T. Davidovic, and P. Slusallek, Light transport simulation with vertex connection and merging, ACM Trans. Graph., Nov. 2012. V31, pp. 192:1–192:10.

9. S. Popov, R. Ramamoorthi, F. Durand, and G. Drettakis, Probabilistic Connections for Bidirectional Path Tracing, Computer Graphics Forum, 2015.

10. N. Dodik, Implementing probabilistic connections for bidirectional path tracing in the Mitsuba Renderer, Sept. 2017.

11. J. T. Kajiya, The rendering equation, in Proceedings of the 13th Annual Conference on Computer Graphics and Interactive Techniques, SIGGRAPH '86, New York, NY, USA, ACM, 1986. pp. 143–150.

12. S. V. Ershov, D.D. Zhdanov, and A.G. Voloboy, Treating diffuse elements as quasi-specular to reduce noise in bi-directional ray tracing, Preprint of the Keldysh Institute of Applied Mathematics, 2018. #122.

13. G. Pomraning, On the Henyey-Greenstein approximation to scattering phase functions, Journal of Quantitative Spectroscopy and Radiative Transfer, 1988. V39, #2, pp. 109–113.

Sergei V. Ershov,
Ph.D. of physical and mathematical sciences. He graduated from the Physics Department of Lomonosov Moscow State University in 1988. He defended his thesis at Keldysh Institute of Applied Mathematics RAS in 1991. Senior Researcher at the Department of Computer graphics and computational optics of Russian Academy of Sciences. Research interests: computer graphics, computational optics, numerical methods of mathematical physics, Monte Carlo methods, ray tracing, diffraction tasks

Dmitry D. Zhdanov,
Ph.D. of physical and mathematical sciences. He graduated from ITMO University in 1984. He defended his thesis at Keldysh Institute of Applied Mathematics RAS in 2006. Currently, he is an Associate Professor at ITMO. Research interests: computer graphics, computational optics, virtual and augmented reality

Alexei G. Voloboy,
Dr. of Phys.-Math. Sciences. He graduated from the Department of mechanics and mathematics of Lomonosov Moscow State University in 1988. He defended his Ph.D. thesis at Keldysh Institute of Applied Mathematics RASin 2005, and his doctoral dissertation in 2012. Leading researcher of the Department of Computer graphics and computational optics of Keldysh Institute of Applied Mathematics RAS. Research interests: computer graphics, computational optics, ray tracing, illuminance simulation

Nikolay B. Deryabin
graduated from the faculty of mechanics and mathematics of Lomonosov Moscow State University in 1977. Research associate of the Department of Computer graphics and computational optics of Keldysh Institute of Applied Mathematics RAS. Research interests: computer graphics, graphic drivers

Light & Engineering
Vol. 28, No. 5, pp. 48–52, 2020

https://doi.org/10.33383/2020-017
Svetotekhnika #4, 2020, pp. 51–54

CONTEMPORARY SYSTEM OF DIRECT BROADBAND OPTICAL MONITORING OF THICKNESS OF SPRAY OPTICAL COATINGS

Oleg F. Prosovsky[1]*, Alexander Yu. Budnev[1], Dmitry G. Denisov[2**], Nikolay V. Baryshnikov[2], Yuri O. Prosovsky[2]

[1] Obninsk Research and Production Enterprise Technologiya named after A.G. Romashin (Romashin ORPE Technologiya), Obninsk
[2] Bauman Moscow State Technical University (BMSTU, NRU), Moscow
*E-mail: * pof@mail.ru, **denisov_dg@mail.ru*

ABSTRACT

In this article, construction schemes direct and indirect control systems were analyzed, and new construction, providing high operating characteristics for optic filters, was introduced. Authors introduce the original decision for creation modern broadband optic control system. Based on the proposed method, approbation of created system was made, and output characteristics control system – spectral transmission dependencies were introduced as a result. Spectral transmission dependencies of interference optical filters, made with different optical control systems were analyzed. Conclusions and prognoses about further developments of direct broadband optic control system for thickness sprayed coatings were made.

Keywords: interference optical filters, straight broadband optic control, thickness of films, vacuum system, spectrum, spectral transmittance factor (reflection factor) curve

1.INTRODUCTION

Nowadays, it is hard to find any optical device manufactured without application of any coating on its surface. For instance, coatings modifying surfaces to increase their resistance against external factors (wear and tear, effects of aggressive substances), to enhance their optical properties (antireflection) and to provide them with new optical properties (polarisation and radiation filtering, etc.) have become widely used.

One of the most important components of spraying equipment is the system for thickness of applied films monitoring, which (primarily) defines process capabilities of spraying equipment in applying multi-layer interference structures. Moreover, monitoring of optical constants is directly linked with quality and repeatability of the process of formation of multi-layer optical coatings [1].

2. CONTEMPORARY METHODS OF OPTICAL COATING THICKNESS MONITORING

Modern spraying equipment is based on the principles of direct and indirect monitoring, and precision of measurement of thickness of the films of applied optical coatings therefore is not always satisfactory for customer's requirements. Today, optical monitoring systems can be divided into 2 major types [2]:

1. Indirect optical monitoring systems, which apply accompanying samples (witnesses) for measurement of spectral transmittance (reflectance) factor of an applied coating (usually placed in the centre of the vacuum jig);

2. Systems of direct optical monitoring, in which measurement of spectral transmittance (reflectance) factor is conducted directly on a product fixed in a rotating vacuum jig.

Fig. 1. Example of an operating broadband optic monitoring system

Only a broadband optical monitoring system may provide the most complete information about the structure of an applied film [3]. It analyses the information on spectral dependence of transmittance factor (SDT) of a coating in the set wavelength range, allows us to define dispersion of optical constants (refractive index and absorption index) and thicknesses of sprayed films right in the course of coating formation on a product in vacuum. Usually contemporary equipment is equipped with ion-assisted sprayers, which in turn provide persistence of optical constants after a coated product is taken out of a vacuum chamber. This fact demonstrates undeniable advantage of modern spraying equipment.

Functioning of the contemporary system of direct broadband optical monitoring implies three cycles of measurement at each rotation of the jig, which is caused by necessity of high precision measurements [4]. Fig. 1 shows the vacuum jig with 3 marked areas which relate to the system of direct optical monitoring:

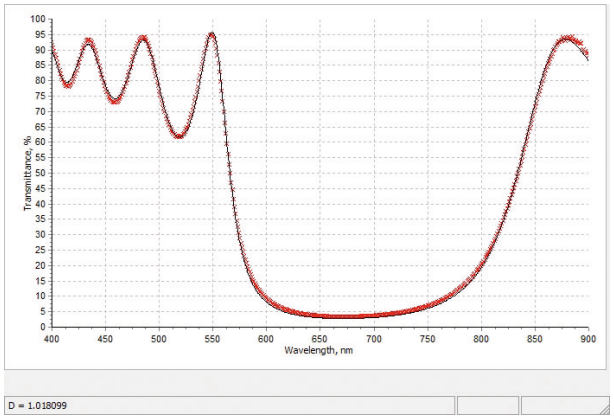

Fig. 3. Example of a design and experimental SDT of multi-layer optic coating

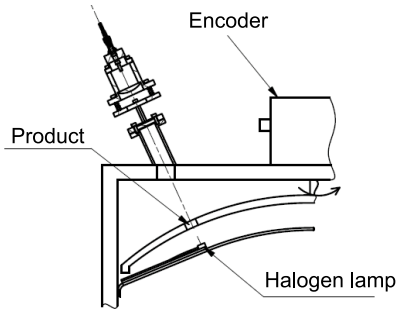

Fig. 2. Structural diagram of the proposed system of direct broadband optic monitoring of thickness of spray coatings

– Area 1 is the product on which SDT of the sprayed coating is measured;

– Area 2 is the section of the jig that does not transmit radiation (0 % transmittance) and used for dark current measurement;

– Area 3 is the hole (100 % transmittance) where transmittance factor has to be measured.

The proposed modern method of direct broadband optical monitoring of layer thicknesses has the following features:

– Transmittance is measured right on a product fixed in a rotating jig;

– To ensure high accuracy of measurement, a digital encoder (Fig. 2) is used, which allows us to make measurements almost at one physical point of a product;

– At each rotation of the jig, measurements are made in 2 major steps: calibration and measurement; calibration consists of transmittance measurements at 100 % and 0 % (areas 2 and 3 in Fig. 1), then the transmittance factor of the product itself is measured (area 1 in Fig. 1);

– Broad wavelength measurement range of (400–1100) nm;

– Application of a mathematical apparatus for processing of information on SDT of applied coatings in a broad spectral range, which allows reanalysis to conduct of the structure of a sprayed coating and to correct errors made during application of previous layers in the course of application of the remaining non-sprayed layers of coating;

– Provision of virtually complete concordance between the acquired design and experimental values of SDT.

Based on the proposed method, the authors conducted testing of the monitoring system they had developed and the result of this test was the system's output characteristics: SDT. Fig. 3 demonstrates the graphs of SDT which characterise precision of the

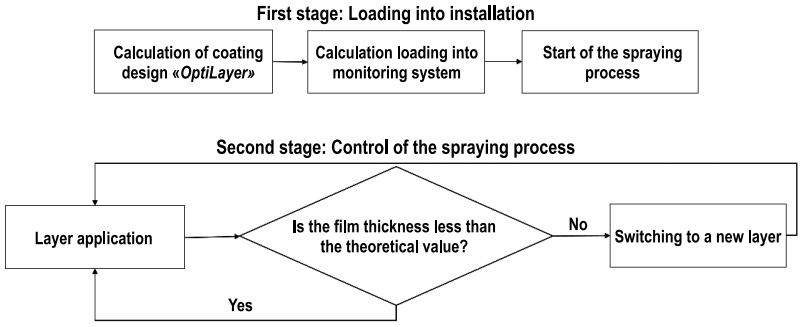

Fig. 4. The process of thickness monitoring of the spray coating

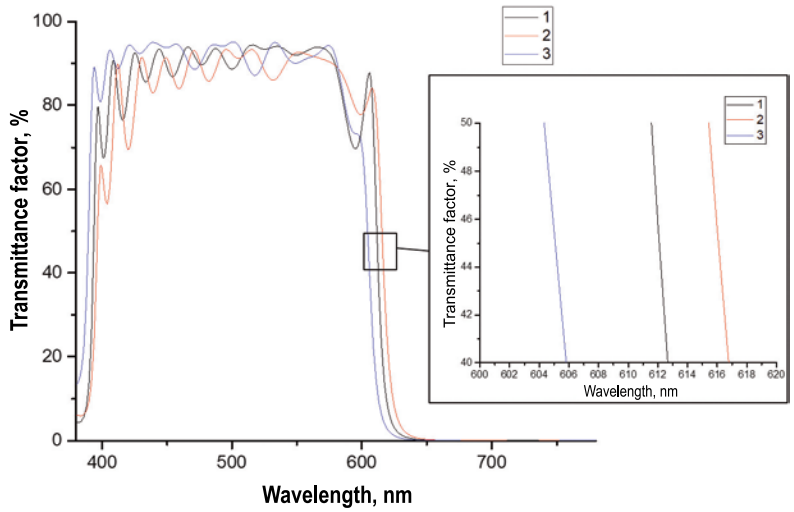

Fig. 5. SDT of a cut-off filter acquired during three processes with use of the monitoring system with an optical witness sample in the centre of the camera

monitoring system by means of which thickness of films sprayed during production of a 9-layer dichroic coating was measured. As the figure shows, SDT of the manufactured filter (the red curve) almost completely corresponds with SDT calculated by means of *OptiLayer*[1] (the black curve).

In the course of manufacturing, monitoring of thickness of an optical coating is conducted by an operator based on analysis of SDT calculated by means of the said software for each layer of the coating.

During spraying, SDT measured on the product shall correspond with the calculated (theoretical) SDT set by the operator. In case of superimposition of the two SDT graphs, the operator stops spraying of the current layer and launches spraying of the following one. Fig. 4 contains the comprehensive algorithm of the developed system of monitoring of thickness of applied coatings and the automated design system *OptiLayer* in the form of a block diagram.

3. COMPARISON OF PRECISION CHARACTERISTICS OF THE DEVELOPED DIRECT MONITORING SYSTEM AND THE SYSTEM OF INDIRECT MONITORING OF THICKNESS OF OPTICAL COATINGS

Fig. 5 demonstrates spectral characteristics of the filters manufactured by means of 3 different processes using the indirect monitoring system with a witness sample in the centre. The insert in this figure shows the variation of $\lambda_{0.5}$ within the spectral region of (605–620) nm equal to 14 nm in more detail. Such variation leads to defects of some of manufactured parts. More detailed analysis of the run of the curves in the insert by means of *OptiRe*[2] shows the

[1] *OptiLayer* is the software for modelling, optimization and calculation of optical coatings and their characteristics. The scope of application is thin-film coatings. It allows the operator to recalculate parameters of coating layers in order to correct errors in previously applied layers [5].

[2] The *OptiRe* software computation module is designed for measurement of parameters of the layers of sprayed optical coatings based on the data of spectral photometry and/or ellipsometry. The results obtained by means of *OptiRe* provide feed-

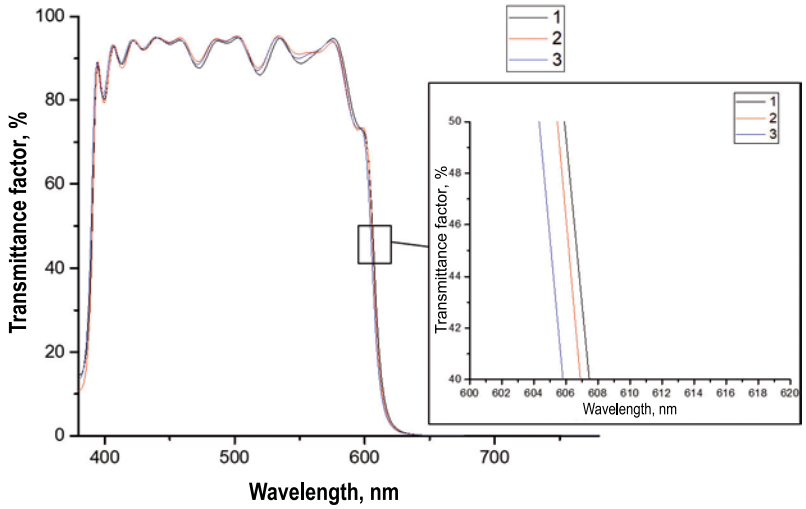

Fig. 6. SDT of a cut-off filter acquired during three processes with use of the direct optic monitoring

values of random deviations of layer thicknesses when repeating the optical structure within the range of (3–5)%. Different runs of the curves in each process confirm availability of a non-systematic error, which significantly complicates automation of the process of application and coating monitoring by an engineer.

It is likely that such high errors of repeating of layer thickness are caused by the change in the solid angle of the flow of vapours of the substance evaporated from the pot due to change in the shape of the substance crater in the pot over the course of the lengthy process which takes (4–5) hours. As a result, the films with different thicknesses are applied on the witness sample and the product. The nature of such errors is non-systematic, they depend on many factors and are very difficult to forecast in most cases.

In order to minimise the errors of the indirect monitoring system, the system of direct broadband optical monitoring was developed and experimentally studied. Its structural elements are shown in Fig. 2 and the results of the experimental studies are shown in Fig. 6, which contains the graphs of spectral dependences of filters obtained in the course of three different processes with use of direct optical monitoring of thickness of applied coatings.

The insert in Fig. 6 demonstrates the variation of $\lambda_{0.5}$ in more detail – it is only equal to 3 nm. With that, the analysis of the run of the curves in this insert makes it possible to conclude that, in the course of application of the optical structure layers, thanks to use of direct optical monitoring, high-precision repeatability of each layer is observed in the series of three processes. The analysis of the achieved results by means of the *OptiRe* modules shows that deviations of actually applied layers from the design ones are less than 0.5 %.

4. DISCUSSION OF THE RESULTS

The system of direct broadband optical monitoring described above is currently being tested by Romashin ORPE Technologiya. It is planned to supplement it with the *OptiReopt* software module (part of the *OptiLayer* software) which is a library for support of optical coatings application monitoring.

Since errors still accumulate in the course of spraying (they are determined by the damper closure time, non-ideality of operation condition, etc.), when a larger (≥30) number of layers is applied, these errors turn out to be significant, which may lead to non-satisfactory quality of a product. Moreover, it is planned to implement a completely automatic spraying process eliminating the human factor.

To conclude, as a result of the conducted studies:

– A prospective optical monitoring system is developed – the system of direct broadband optical monitoring, which has demonstrated high repeatability of thicknesses of dichroic coating layers in production conditions;

– The system of direct broadband optical control is practically implemented on an electron-beam evaporation installation;

back of the spraying process. Using these results, it is possible to adjust the parameters of the spraying process or the process of layer monitoring and thus to increase the quality of the sprayed coatings. The module is a part of *OptiLayer*.

– The system of direct broadband optical control is introduced in the production process of dichroic filters for optical devices (cut-off, narrow-band and other types of filters).

REFERENCES

1. Lequime M., Nadji S., Stojcevski D., Koc C., Grézes-Besset C., Lumeau J. Determination of the optical constants of a dielectric layer by processing in situ spectral transmittance measurements along the time dimension // Appl. Opt., 2017, Vol. 56, pp. C181–C187.

2. Okatov M.A., Antonov E.A., Baygozhin A. Optic Engineer's Handbook [Spravochnik tekhnologa-optika]. St. Petersburg: Politekhnika, 2004, 679 p.

3. Nadji S.L., Lequime M., Begou T., Koc C., Grézes-Besset C., Lumeau J. Use of a broadband monitoring system for the determination of the optical constants of a dielectric bilayer // Appl. Opt. 2018, Vol. 57, pp. 877–883.

4. Zhupanov V.G., Kozlov I.V., Fedoseev V.N., Konotopov P., Trubetskov M.K., Tikhonravov A.V. Production of Brewster angle thin film polarizers using a ZrO2/SiO2 pair of materials // Appl. Opt., 2017, Vol. 56, pp. C30–C34.

5. URL: https://www.optilayer.com/ (accessed on: 20.01.2020).

Oleg F. Prosovsky, an engineer. Head of the Optic Coatings Laboratory of AO ONPP Romashin Tekhnologiya

Alexander Yu. Budnev, an engineer 3rd category, technical engineer of the Optic Coatings Laboratory of Romashin ORPE Technologiya

Dmitry G. Denisov, an engineer. Associate professor of the RL-2 sub-department of Baumann MSTU (NRU)

Nikolay V. Baryshnikov, an engineer. Associate professor of the RL-2 sub-department of Baumann MGTU (NIU)

Yuri O. Prosovsky, student of the 4th year of the RL-2 sub-department of Baumann MGTU (NIU)

Light & Engineering
Vol. 28, No. 5, pp. 53–60, 2020

https://doi.org/10.33383/2020-015
Svetotekhnika #4, 2020, pp. 5–10

MODERN APPROACHES TO NORMALIZING NATURAL LIGHTING OF RESIDENTIAL BUILDINGS: RESEARCH RESULTS

Alexei K. Solovyov

Moscow State University of Civil Engineering (NRU MGSU)
E-mail: kafedraarxitektury@yandex.ru; agpz@mgsu.ru

ABSTRACT

In the premises of residential buildings, there are practically no requirements for the conditions of visual work. The light environment is evaluated by the criterion of the saturation of the premises with natural light. The required time of using natural light and providing natural lighting in space are also of great importance here. The task for residential buildings is to link these criteria to create an integrated method of rationing natural lighting in such rooms. The article discusses the modern trends in development of regulations of natural lighting from traditional, using Daylight Factor (*D*), to the modern ones, connected with dynamic evaluation of day lighting in time and space, necessarily taking into account real statistical brightness distribution on the sky. Evaluation of Daylight Factor method analyses its assessment, energy indicators and provides a comparison with the norms of Germany DIN. The results of research at MGSU on the evaluation of day lighting using the spatial criterion of the light field – cylindrical illuminance, which best describes the saturation of the light of the room are presented. It is noted that the full amount of natural light is not required over the entire area of the living room during the whole daylight hours. In this case, you can find the relationship between *D* and the coefficient of natural cylindrical illuminance (D_{ci}). This provides a link between traditional regulation and regulation on the saturation of rooms with natural light. The final assessment of the standardized parameters of natural lighting in residential premises is carried out using methods of psychophysics, which can connect the main and secondary factors affecting the comfort of the light environment.

Keywords: daylighting, light environment, visual work, light saturation of premises, daylight rationing, cylindrical illuminance, daylight climate, energy efficiency, static rationing, dynamic rationing, psychophysical assessment

1. INTRODUCTION

The twentieth century was the century when the science of daylight of buildings developed and flourished. All developments of this time were an attempt to determine as accurately as possible the conditions of day lighting in the rooms. Methods were developed for calculating the coefficients of daylight illuminance (*D*) [1, 2, 3], which with some degree of accuracy could determine the conditions of day lighting in the rooms. In order for the calculation results to be comparable with each other, we had to make the basic assumption about cloud conditions, which is the most unstable and uncertain characteristic. As a basic assumption, the International Lighting Commission (CIE) adopted the cloudy sky as the worst condition for daylight. Under this condition, the values of *D* in the premises for various purposes began to be compared with the norms. Relative values of *D* were included in the norms. However, these standards were based on the required conditions for visual work in artificial lighting. These conditions were determined by the methods of psychophysics in terms of speed and accuracy of distinguishing observers of conditional objects (Landolt rings test) and in the fatigue of

observers in time. In residential buildings, the tasks of visual work are difficult to determine, therefore, for living rooms, the standardized level of general artificial illuminance is 150 lx, and the notes indicate that this value is recommended. The norms of natural lighting were obtained from the condition that the amount of lighting under artificial lighting for the year is equal to the amount of natural lighting for the year obtained by summing the integrals of the average hourly values of the outdoor daylight for each month during the daylight hours in the area where the building in question is located and multiplying by the number of days in a month. The ratio of the first value to the second as a percentage will be the value of the average *D*. The average *D* should be distinguished from the *D* value in the centre of the room. It is about 1.5 times larger. For example, standardized illuminance for the Moscow City according to conditions of visual work equal to 150 lx during single-shift work for 8 hours and at 226 working days a year, the amount of artificial lighting for the year $A_{artlight/\,year}$ is equal: $A_{artlight/year} = 150 \cdot 8 \cdot 226 = 271200$ lx · h/year.

At the beginning of work, at 9.00 a.m., and the end of work at 18:00 (1 hour lunch break) the amount of natural light in the open air will be the sum of the integrals of the functions of changing the total natural light for Moscow according to SP 367.1325800.2017 "Residential and public buildings: Rules for the design of natural and combined lighting". This value will be 36160000 lx · h/year. The average value of *D* will be: *D* norms. = (271200 / 36160000) · 100 % = 0.75 %. In the centre of the room, this value will be: *D* = 0.75 % / 1.5 = 0.5 %. This value is determined by the existing system of rationing of natural lighting in the Russian Federation. But is it satisfactory for the comfort of the internal light environment in terms of light saturation in the rooms? This was called into question in the article of the graduate student of the Department of Design of Buildings and Structures of the National Research University of Moscow State University Muravyova N.A. [4]. The studies were based on the work of M.M. Epaneshnikov and T.A. Sidorova [5] for artificial lighting of subway stations. It was found that the best characteristic that determines the saturation with room light is the spatial characteristic of the light field – cylindrical illuminance. At the same time, the saturation with light of the underground metro halls turned out to be acceptable for observers even at 200 lx of cylindrical illuminance.

2. THE RELATIONSHIP OF DAYLIGHT FACTOR *D* WITH THE SPATIAL CHARACTERISTIC OF THE LIGHT FIELD – CYLINDRICAL ILLUMINANCE

How to connect the traditional planar characteristic of the light field – *D* with the value, characterizing the cylindrical illuminance $D_{ci,}$ the coefficient of natural cylindrical illuminance. This value is the ratio of the internal cylindrical illuminance E_c to the simultaneous external horizontal illuminance E_n, taken in %. It makes no sense to take the ratio of internal and external cylindrical illumination as D_{ci}, since all data on the light climate around the world are tied to E_n, and data on external natural cylindrical illuminance simply do not exist. At the same time, the external horizontal illuminance characterizes well the change and the amount of natural illumination [6].

Experimental studies were conducted at the NRU MGSU under the guidance of the author, which showed that in rooms with ordinary windows with a windowsill at a height of 1 m from the floor, the *D* and D_{ci} graphs intersect almost exactly in the centre of the characteristic section of the room (*D* at the level of the working surface and D_{ci} at the observer's eye level at a height of 1.5 m from the floor) [4] for any room parameters. Thus, these studies have shown how the existing standardization system can be combined with standardization according to the light saturation of the room. Preliminary studies in the living quarters showed that observers considered acceptable saturation with room light at 120 lx cylindrical illumination. This means that in the centre of the room this value corresponds to a horizontal illumination of 120 lx. If we go to *D*, then with artificial illumination of 120 lx, included for 8 hours a day and at 30 days in a month, the annual amount of artificial lighting will be equal $A_{\,artlight/year} = 120 \times 8 \times 12 \times 30 = 345600$ lx · h/year. The value of the normalized *D* in the centre of the living room at the level of the working surface will be:

E_n = (345600 / 36160000) · 100 % = 0.956 %, i.e. approximately 1.0 %.

If compare the obtained value with the norms of the Federal Republic of Germany (DIN5034–1 Appendix A.1), the norms are indicating that, in rooms for long-term stays of people with windows for sufficient lightness, the value of *D* should be in half of the room depth at a height 0.85 m above the floor and at a distance 1 m from the side walls is not less

than 0.9 % in the middle between these points and not less than 0.75 % in each of both points. Thus, the obtained value is approximately consistent with the norms of the Federal Republic of Germany, and an experimental justification has been obtained for this. Of course, the value obtained at MGSU requires additional verification by additional psychophysical studies, but the principles of rationing set forth in the article can be used.

It should be noted that in the scientific literature there is no justification for both the norms of the Federal Republic of Germany for residential buildings and the norms of the Russian Federation for residential buildings, which require one, two and three bedroom apartments in one of the rooms and four or more room apartments in two rooms apartments D equal to 0.5 % on the floor at a distance of 1 m from the wall opposite the windows. In other rooms, this value should be in the centre of the room.

3. CONSIDERATION OF THE REAL LIGHT CLIMATE OF THE AREA WHEN NORMALIZING DAYLIGHT

In the article of S. Darula [5], it was shown that there are two ways to standardize day lighting:

– Standardization of day lighting according to the simple "static" criterion of D in the sky, completely covered by clouds;

– The second way is based on the dynamic criterion of "autonomy of daylight", which is associated with the absolute values of daylight illuminance.

The last one method is currently being actively implemented by the British Institute for Building Research on Environmental Assessment (BREEAM). According to this method, the natural lighting of the premises should satisfy two indicators:

– The minimum value of the average D should be provided for 80 % of the room area at the height of the conditional working surface;

– The average daylight illuminance should be provided at a level of 200 lx or more for 2650 hours a year and at least 60 lx or more for 2650 hours a year in the worst places in terms of illuminance.

The average value of D in ordinary rooms depends on the latitude of the area, varying from 1.5 % for latitudes less than 40 degrees and up to 2.2 % for latitudes more than 60 degrees north latitude. For residential buildings, such regulatory data are not provided.

We see that, applying normalization according to the dynamic criterion of "autonomy of daylight", we take into account the change in daylight exposure by month and during the day. This can be considered as a higher level of standardization, for which, however, data are needed on the light climate of the area in dynamics by month of the year and time of day. Of course, a simple "static" criterion is easier to use, given the light climate by introducing light-climatic coefficients into the calculation formula. But its accuracy is low. In general, the concept of D is universal. The human eye cannot evaluate the absolute levels of illuminance and evaluates this only in comparison with the illuminance of something. In this case, it is outdoor natural light. Therefore, it is impossible to refuse relative values when evaluating natural lighting, and D or D_{ci} (or other relative spatial characteristics of the light field, referred to as external illuminance) are full-fledged estimated characteristics for natural lighting, which we will operate in the future. Linking the static and dynamic criteria for evaluating natural light is an important task that specialists in the field of daylighting will have to work on. And first of all it concerns the light climate of the area. The light climate depends on many factors such as the latitude of the terrain and, in connection with this, the height of the sun rising above the horizon, the duration of daylight hours, cloud statistics and its prevailing species. R. Kittler and S. Darula proposed in article [6] to classify 15 types of firmament according to the distribution of luminance from clear to cloudy sky, completely covered with 10-point cloud cover. At the same time, D, as a constant value for a given room point, makes sense only with a cloudy sky with a distribution of the luminance of the CIE according to the law of P. Moon and D. Spencer and with an equally bright sky, which is also sometimes found statistically, especially for upper natural lighting systems. In all other cases, the D value depends on the position of the sun in the sky, since an aura of increased brightness forms around the sun, which affects the D value. This halo during the day moves relative to the orientation of the window.

Accordingly, at this point the value of D changes. Therefore, it is necessary to choose a position of the sun relative to the orientation of the window, which is suitable for the purpose of calculating D. For example, comparing natural light in different rooms or determining the energy consumption for daylight devices.

Determining the type of firmament according to R. Kitterler and S. Darule is quite complicated. For this, there is not always enough data on the light climate in a particular area. At MGSU, another possibility was developed to determine the luminance distribution of the real sky by the value of the ratio of the total and diffuse horizontal illuminace by the hours of the day (for example, the 15th day of each month). In the absence of data on illuminance, data on the total and diffuse solar radiation, which are available at numerous actinometric stations in all cities of Russia, can be used. It is possible to construct charts of the hourly stroke of outdoor illuminance for any city using the light equivalent of solar radiation [7, 8, 9]. Thus, in MGSU were obtained graphs of the course of outdoor illuminance in real average sky for cities in Vietnam.

4. DEFINITION OF THE AREA OF LIGHT APERTURES AS A SIMPLIFICATION FOR DESIGNERS OF DAYLIGHTING

Until the end of the first half of the twentieth century, one of the methods of normalizing natural lighting was the normative determination of the ratio of the area of windows in a room to the area of a floor. Now this is called the "opening of the room." This method is simple and convenient for designers, but is not accurate. After that, the norms became more complicated, new indicators were introduced, the main of which was Daylight Factor *D*. Despite this, attempts to simplify calculations and design did not stop. This can be most simply represented by a characteristic expressed in terms of the ratio of the area of windows to the area of the floor. In the norms of SNiP P-4.79 "Daylight and Artificial Lighting" and in the subsequent Code of Rules, it was recommended that the design of daylighting systems has to be carried out in two stages. The first stage involved an approximate determination of the area of light apertures, which was based on formulas for lateral and upper daylight:

$$100 \cdot \frac{S_0}{S_f} = \frac{e_{norm} \cdot \eta_0}{\tau_0 \cdot r_0} \cdot K_{b.sh.} \cdot K_{sfactor}, \quad (1)$$

$$100 \cdot \frac{S_{cl}}{S_f} = \frac{e_{norm} \cdot K_{sfactor} \cdot \eta_w}{\tau_0 \cdot r_2 \cdot K_{cl}}, \quad (2)$$

where So, S_{cl}, and S_f are the areas of windows, daylight ceiling, and floor respectively; e_{norm} – normalized D; τ_0 is the total light transmission coefficient of the openings; r_0 and r_2 are the coefficients that take into account the effect of reflected light from the internal surfaces of the room at the design point in lateral and upper natural light; $K_{b.sh.}$ is the coefficient, taking into account the shading of windows by opposing buildings; $K_{sfactor}$ is the safety factor, taking into account the pollution of openings; K_{cl} is the coefficient, taking into account the type of daylight ceiling; η_0 is the light characteristic of the window, showing the ratio of the windows area So to the floor area S_f in %, providing the value of D = 1 % at the calculated point in the depth of the room on the conditional working surface; η_w is the light characteristic of the daylight ceiling.

For the most common geometric and lighting parameters of the side and top light openings in the later Code of Rules SP 23–102–2003, graphs are given to determine the relative area of daylight openings, somewhat simplifying the calculation by equations (1) and (2). If we consider these graphs, it can be noted that for light apertures of the upper light, there is a direct proportionality between the values of D and the ratio of the openings area to the floor area, S_0/S_f. For light apertures of lateral daylight, the graphs are constructed according to a different principle. Here, as shown in Fig. 1, the aperture is determined depending on the ratio of the room depth d_r to the height of the top of the window above the working plane h_0. At the same time, there is no shading by opposing buildings. The graphs are represented by a series of curves. If we imagine the

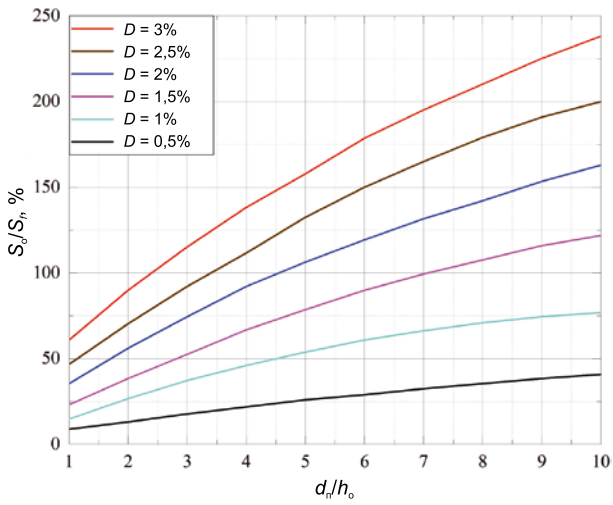

Fig. 1. Dependence of the opening on the ratio of the depth of the room to the height to the top of the window

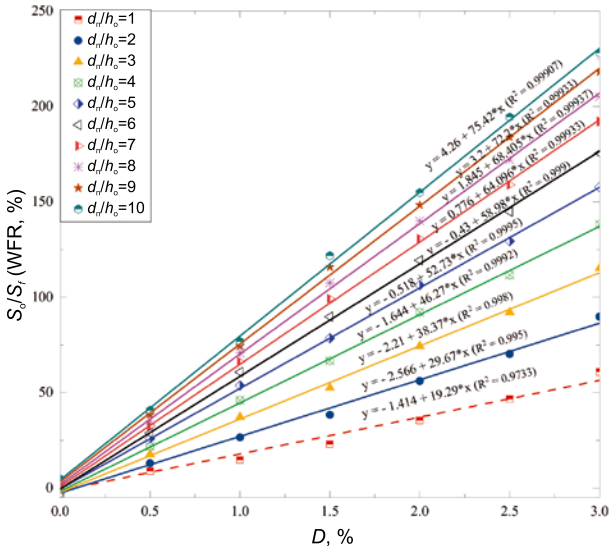

Fig. 2. The dependence of D from the magnitude of the opening

dependences of D on the S_0/S_f, they will also express direct proportionality between these values. To do this, you just need to select the characteristic ratio of the depth of the room to the height of the top of the window and build a series of graphs. In Fig. 2, such graphs constructed at MGSU are shown, for example, for the characteristic parameters of working rooms.

To normalize daylight, perhaps we should return to the definition of the "openness" of the premises, but at a higher level that increases accuracy and is most convenient for designers.

5. ENERGY EFFICIENCY OF WINDOW OPENINGS

The area of windows is closely related to the amount of energy spent on the device of light apertures in the building. There are more apertures for light transmission, the lower the cost of electricity for artificial lighting. This is confirmed by the above that the value of D is proportional to the ratio of the area of the windows to the area of the floor (i.e., the opening). But the larger the area of the windows, the greater the heat loss through them in winter, since the heat transfer resistance of good windows is about three times less than the heat transfer resistance of the blind parts of the walls. Of course, the heat transfer resistance for hygienic reasons in modern windows can reach similar values for walls, but based on the requirements of energy saving, this is not yet possible.

In summer, the larger the area of the windows, the greater the heat input into the premises through the windows of the south, west and south-east orientation. Less heat passes through the east-facing windows into the room, as the sun still does not have time to warm the air after night. However, nevertheless, solar thermal radiation in this case should also be taken into account in the heat balance of the room. Mostly only heat losses and daylighting of the rooms occur through the northern light paths. Therefore, on the north side should be located rooms with reduced requirements for natural lighting and, accordingly, reduced size of window openings.

Thus, energy costs for electric lighting, heating, ventilation and cooling in the summer should be minimal. To do this, you need to find the appropriate area of light apertures. This area may vary depending on the climatic conditions of the construction site. This energy-efficient glazing area should be compared with the required window area according to the lighting conditions from the conditions of saturation of the room with natural light, the conditions of visual work, the necessary time to provide it and the necessary area of the room on which it should be provided at this time.

The methodology for determining the energy costs for the device of light apertures was developed back in 1985 at the Research Institute of Building Physics [10]. It seems very reliable. But at present, it is slightly changed by us in connection with the advent of new air conditioners and is somewhat simplified [11]. We also developed a computer program "ECON", with the help of which the energy-efficient dimensions of daylight ceiling openings in the climatic conditions of Arkhangelsk were determined. It seems that a detailed presentation of this technique in this article would be interesting for designers.

The total energy costs should be calculated with the conversion to equivalent fuel costs, since the production of thermal energy and electric energy requires different costs. Therefore, they should be calculated by the formula:

$$W_{eq.fuel\,cost} = A_1 \cdot w_{hl} + A_2 \cdot (w_{heat} + w_{vent} + w_{coolair} + w_{artlight}), \quad (3)$$

where A_1 = 41.2 kg/GJ and A_2 = 0.33 kg/kW·h are specific consumptions of equivalent fuel in power plants of general use per 1GJ of thermal energy and

1kW·h of electricity; w_{hl} is the energy consumption for replenishing heat losses through light gaps GJ/m^2/year; w_{heat} is the specific annual energy consumption for heating, adopted by the formula:

$$w_{heat} = 7.1 w_{hl}, \tag{4}$$

for air heating systems and equal to zero for other heating systems; w_{vent} is the specific amount of electricity for ventilation kW·h/m^2; $w_{coolair}$ is the amount of electricity per year spent on cooling the supply air kW· h/m^2; $w_{artlight}$ is the energy consumption for artificial lighting per year kW·h/m^2. The determination of energy costs for heating, ventilation, cooling and artificial lighting is carried out according to the formulas given in [10]. Values ω_{hl} determined by the formula:

$$w_{hl} = 10^{-6} \cdot 1.1 \cdot 3.6 \cdot (1.3 + \eta) \cdot \left(\frac{1}{R_{ts}} - \frac{1}{R_{ws}}\right) \times \times (t_{at} - t_{htt}) \cdot Z_{ht} \cdot 24 \cdot \frac{S_{lightopenning}}{S_f}. \tag{5}$$

Here 1.1 is the coefficient taking into account useless heat losses in the heating system; 3.6 is the conversion factor of units kJ/W·h; 1.3 is the coefficient taking into account heat losses due to heating of the outdoor air entering through light apertures by means of infiltration, which can approach 1.0 with high sealing of openings; η is the coefficient taking into account additional heat losses, its value should be taken according to SNiP "Heating and Ventilation "; R_{ts} and R_{ws} – heat transfer resistance of the translucent structure and the wall" on the surface "; t_{at} and t_{htt} are the calculated temperatures of the indoor air and in heating period too; Z_{ht} is the duration of the heating period (days); 24 is the hours in days; $S_{lightopening}$ and S_f are the areas of light apertures and floor indoors (m^2).

The cost of electric energy for cooling with the help of air conditioners is determined if the air conditioners in the house exist. In this case, their value is determined by the formula:

$$w_{ec} = 10^{-3} \cdot (1.3 + \eta) \cdot \left(\frac{1}{R_{ts}} - \frac{1}{R_{ws}}\right) \cdot (t_{o.a.t} - t_{\max}) \times \times T_{28} \cdot \frac{S_{lightopenning}}{S_f} + 0.72 \cdot L_o \cdot N_o \cdot T_{28}, \tag{6}$$

where $t_{o.a.t}$ is the average outdoor temperature during the cooling period, determined by the reference SNiP P-A. 6–72 [12] in accordance with table of temperature repeatability in hours, in descending total hours at a temperature above 28 °C; t_{max} is the maximum permissible temperature of the internal air during the cooling period, taken for hygienic reasons (in Russia, there is no such standardized temperature, however, from the experience of application household air conditioners, it can be accepted as 24° C; T_{28} is the duration of cooling period in the days, taken in the same directory [12]; N_a is the specific consumption of electric energy for cooling, kW·h/m^3; L_o is the performance of the ventilation system in the chilled air distribution devices ("fan coil") and in general in ventilation systems m^3/h per 1 m^2 of flow area, calculated as:

$$L_0 = 3.6 \cdot q_{rad}^{\max} \Big/ c \cdot \rho \cdot (t_{avercool} - t_{\max}), \tag{7}$$

where c = 1 kJ/kg/°C is the specific heat capacity of air; ρ = 1.2 kg /m^3 is the air density; $q_{rad}^{\max}$ is the value of radiation entering the room in W/m^2, the main part of which is determined by the maximum value of the total solar radiation incident on the plane of the light openings of this orientation during the day and determined by the formula:

$$q_{rad}^{\max} = Q_B^{\max} \cdot \tau_e \cdot \tau_2 \cdot MF \cdot \beta_{sp} \cdot \frac{S_{lightopening}}{S_f}, \tag{8}$$

where $Q_B^{\max}$ is the maximum value of solar radiation arriving in a given area on a vertical surface of the most unfavourable – western orientation in July; τ_e is the heat transfer coefficient of windows; τ_2 is the light transmittance, depending on the type of binding (for single-chamber double-glazed windows in plastic binders τ_2 = 0.69, for double-chamber τ_2 = 0.57); MF is the operating factor taking into account pollution; β_{sp} is the heat transfer coefficient of sunscreens (if any), relative units. The corresponding coefficients are determined by SP 367.1325800.2017.

Energy costs for artificial lighting are calculated by the formula:

$$w_{eart} = 10^{-3} \cdot E \cdot K_{safe.art} \cdot Z \cdot \alpha \cdot P_l \times \times (1 + \beta) \cdot \frac{T_{art}}{\Phi_l \cdot K_{ld}}, \tag{9}$$

where E is the normalized value of artificial illumination, Φ_l is the luminous flux of artificial lighting lamps, T_{art} is the time of use of artificial lighting, P_l is the power of the lamps, and K_{ld} is the coefficient of use of the luminous flux of the lighting device [13], α is the coefficient taking into account energy losses in the ballast; β is the same in the network; Z is the coefficient taking into account the illuminance non uniformity (it is taken equal to 1.15 for spot lamps and 1.1 for fluorescent lamps).

To determine the time of use of artificial lighting, you can use the tables [10] or use the analytical method with approximation of the graphs of the course of outdoor natural illumination depending on the sinus of the height of the sun with small corrections for cloudiness.

Thus, using this technique, it is possible to determine the energy efficiency of the "opening" for a given construction site and, if necessary, adjust the size of the windows taking into account their orientation to the cardinal points.

6. CHECKING THE RATIONING OF NATURAL LIGHTING USING METHODS OF PSYCHOPHYSICS

Finally, all methods for determining regulatory requirements for daylighting in residential premises should be checked by the method of psychophysics. Indeed, we can calculate the physical parameters of natural light in a room, determine the requirements for daylight levels based on the conditions of some visual work with the determination of normalized values of D, but only the needs of residents, determined by the method of psychophysics, can give us the final answer.

At the Moscow State University of Psychology, psychophysical research was carried out at the end of the twentieth century in relation to the issues of the movement of human flows and the application of the spatial characteristics of the light field to improve the conditions of visual work with volumetric and relief objects of distinction. These studies were carried out in conjunction with existing at that time laboratory of psychophysics at Moscow State University, in accordance with methods developed in this laboratory and applied to our tasks. Currently, when conducting research, we used the work of the American scientist H. Helson [14], in which he proposes to consider any questions of sensation and perception associated with a subjective assessment by observers, as the sum of the main, secondary and background factors raised to a degree, the indicators of which show the significance of these factors in the assessment. The calculation formula of H. Helson is as follows:

$$A = X^p \cdot B^q \cdot P^r, \quad (10)$$

where X^p is the main factor. If this is the illuminance, then this is the quantity necessary to ensure that the main task. In rooms where the main is visual work, artificial lighting is normalized. In rooms where the basic requirements are imposed on the saturation of the room with natural light, this is cylindrical illuminance, determined according to the results of psychophysical studies conducted by a similar technique [15]. For residential premises, this factor A will be the main factor, and the normalized artificial lighting will be a secondary factor (B^q). Background factor P^r for residential premises may not be present at all. Values of weights coefficients, p, q, and r, may vary depending on the situations being evaluated. Moreover, in residential premises, the main and background factors can be estimated, for example, at $p = 0.7$ and $q = 0.3$. This should be determined by analysing the time of use by residents for different types of activity at home.

CONCLUSION

This article shows the results of scientific developments carried out at NRU MGSU and in many other research organizations of the world, which, with appropriate refinement, can be used as the basis for normalizing the daylighting of residential buildings. Based on these results, possible directions for further research in this field can be formulated. Briefly, for residential buildings these areas are as follows:

- Determination of the required average illuminance in lx, which must be provided in the living room during a certain period of daylight hours during the year, and determination of percentage of the area of the room on which it is necessary to provide the required amount of average illuminance during a certain period of daylight hours during the year;
- Determining the period of the year during which, at a given percentage of the room's area, it is necessary to provide the required average illuminance at time of the daylight hours;

• Determination of the average value of Daylight Factor *D,* which must be provided at a given percentage of the area of the room, and determination of the "openness" of the room;

• Checking the energy efficiency of the obtained glazing area for the equivalent fuel consumption for heating, cooling and artificial lighting per 1sq.m of the room; and it should be noted that the energy consumption for artificial ventilation for residential buildings may not be taken into account, since ventilation during the outdoor temperature period of more than 21 degrees in the housing, as a rule, is carried out by natural ventilation by opening the windows;

• Correct the "opening" according to the orientation of the openings to the cardinal points;

• Calculate the required illuminance according to the Helson's formula, depending on the requirements for the room according to the magnitude of the main factor, for example, the saturation with natural light of the room, and the value of the secondary factor, for example, the requirements for the conditions of visual work;

• Determine the normalized average value of *D* in the room from required luminance value.

Each of the topics can be an independent study, especially if we consider not only residential buildings, but also buildings and premises, where the conditions of visual work are determining. In the case of volumetric and relief objects of distinction, one should use such spatial characteristics of the light field as average spherical illuminance, average hemispherical illuminance, light vector, and their relationships [16]. Using the spatial characteristics of the light field only due to its own shadowing can significantly save energy costs for artificial lighting.

REFERENCES

1. Gusev N.M. Fundamentals of building physics. Textbook for high schools // Textbook for high schools, architecture speciality, M. Stroyizdat,1975, 440p.

2. Gusev N.M., Kireev N.N. Lighting of industrial buildings // M. Stroyizdat,1968, 160 p.

3. SNiP P-A.4–79. Natural and Artificial Lighting // Building Norms and Rules. GOSSTROY of the USSR, M. Stroyizdat, 1979.

4. Muravyova N.A., Solovyov A.K. The system for determining the required parameters of the natural light environment in the premises by the criterion of saturation with natural light // Scientific Review, 2013, № 9, pp. 132–137.

5. Stanislav D. Review of the Current State and Future Development in Standardizing Natural Lighting in Interiors // Light & Engineering, 2018, Vol. 26, # 4, pp. 5–26.

6. Darula Stanislav, Kittler Richard. Classification of Daylight Conditions in Cloudy covered Situations // Light & Engineering, 2015, Vol. 23, # 1, pp. 4–15.

7. Perrez R., Seals R., Michalsky J. All weather for sky luminance distribution – Preliminary configuration and validation.//Solar Energy, 1993, V.13, # 4, pp. 235–245.

8. Littlefair P.J. The luminance distribution of the average sky // Lighting Research and Technology, 1998, V.13, #4, pp. 192–198.

9. Nakamura H., Oki M., Hayashi Y. Luminance distribution of the intermediate sky. // Journal of Light and Visual Environment, 1985, V.9, # 1, pp. 6–13.

10. NIISF Gosstroy of the USSR. A guide to the calculation and design of natural, artificial and combined lighting (to SNiP P-4–79), M. Stroyizdat, 1985.

11. Alexei K. Solovyov and Guofu Bi. Selection of the Area of Window Openings of Residential Buildings in Conditions of Monsoon Climate of the Far East of the Russian Federation and Northern Areas of China// Light & Engineering, 2019, Vol. 27, # 6, pp. 27–33.

12. SNiP P-A .6–72. "Construction climatology and geophysics." Building regulations. GOSSTROY of the USSR, M. Stroyizdat, 1973 (used as a reference).

13. A reference book for the design of electric lighting. Edited by G.M. Knorring. Leningrad, Publishing house "Energy", 1976.

14. Helson H. Adaptation Level Theory. New York: Harper, 1964.

15. Nina A. Muraviova, Alexei K. Soloviev, and Stetsky Sergei V. Comfort Light Environment under Natural and Combined Lighting: Method of Their Characteristics Definition with Subjective Expert Appraisal Using//Light & Engineering, 2018, Vol. 26, # 3, pp. 124–131.

16. Solovev Alexey K. Die Anvendung der Lichtfeldtheorie bei der Proektierung der Beleuchtung von Arbeitstaetten. // Licht, 1996, # 5, pp. 442–446.

Alexei K. Solovyov,
Professor, Dr. of Tech. Sciences. He graduated from Moscow Institute of Fine Arts named by V.V. Kuibyshev in 1965. At present, he is a Professor of the Department of Designing Buildings and Structures at NRU MGSU, Advisor to RAASN, member of the European Academy of Sciences and Arts and the Editorial Board of the Journal "Svetotekhnika/Light & Engineering". He has the title of Honorary Builder of the Russian Federation and Honored Worker of Higher School of the Russian Federation

Light & Engineering
Vol. 28, No. 5, pp. 61–67, 2020

https://doi.org/10.33383/2020-011
Svetotekhnika #5, 2020, pp. 90–95

OPTIMAL TILT ANGLE FOR GETTING MAXIMUM ENERGY PRODUCED BY PV PANEL BY UTILIZING CLEAR SKY AND ARRAY PERFORMANCE MODELS

Muhammad Aleem Zahid [1, 2], Ganesh T. Chavan [1],
Young Hyun Cho [1*], and Junsin Yi [1*]

[1] College of Information and communication, Sungkyunkwan University (SKKU), Suwon, South Korea
[2] Electrical Engineering Department, University of Engineering & Technology, Taxila, Pakistan
E-mail: aleem12394@skku.edu

ABSTRACT

In this paper, we analysed and implement clear sky and array performance models to achieve maximum electrical energy produced from the photovoltaic (PV) panel. The selected models just not only include location dependent parameters but also include environmental factors such as Linke Turbidity (include aerosols, absorption due to assorted gases, Rayleigh scattering), cloud cover, albedo, perceptible water vapour. 250 W PV panel was used as a reference to check the output electrical energy in a given location by inputting the latitude and longitude of a location. It is concluded that 27° facing south is the optimized tilt angle for every locations having latitude at north direction and longitude at east direction. By taking the example of location Nagpur India (21.14° N, 79.08° E), a difference of only 0.35 % is reported when comparing the computed electrical energy with actual electrical energy that have been acquired by using pyranometers, pyrheliometers and illuminance meters installed by the National Renewable Energy Laboratory (NREL). So, a good approximation of electrical energy can be computed by combining clear sky and array performance models.

Keywords: solar radiation, irradiance, beam radiation, diffuse radiation, ground reflected radiation, tilt angle, electrical energy

Quantity designations and abbreviations:

θ_z is the zenith angle;
E_{ext} is the extra-terrestrial solar irradiance;
λ is the latitude of location;
H is the altitude of location in feet's;
δ is the declination angle;
w is the hour angle;
d is the day of the year;
L_{std} is the standard meridian of local time;
L_{oc} is the actual longitude of location;
AM is the air mass;
E_{bh} is the beam component at horizontal surface;
I_b is the beam component at tilted surface;
E_n is the direct normal irradiance;
a is the angle of incidence;
γ_{sun} is the solar azimuth;
θ_{sun} is the solar zenith angle;
γ is the panel azimuth;
β is the panel tilt;
K_n is the direct beam transmittance;
K_{nc} is the maximum clear sky value;
$I_{d,sky}$ is the computed diffuse radiation on tilled surface;
P_{dc} is the DC power.

1. INTRODUCTION

Solar energy is an emerging, clean and safe source of electrical energy. The PV module directly converts light energy into electrical energy. In actu-

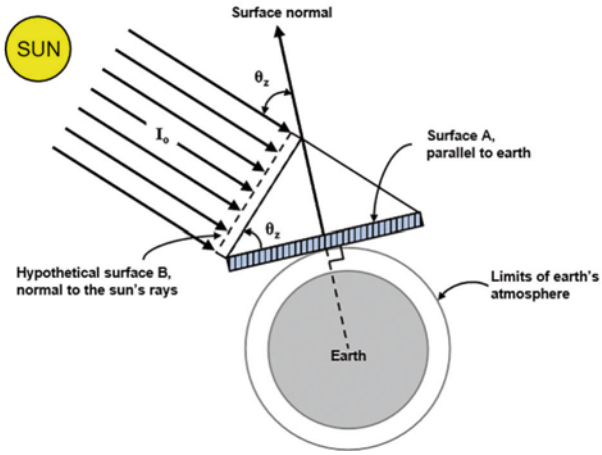

Fig. 1. Extra-terrestrial Radiation on horizontal surface (*Source*: www.powerfromthesun.net/Book)

al, the solar irradiation which exists above the atmosphere of the earth has more intensity than radiations reaches on the earth's surface [1]. The losses are owing to various atmospheric gases, clouds and various ecological effects. The incident solar insolation on earth could generate 1 kW/m^2, if it can convert competently [2]. Solar radiation and sunshine illuminance statistics are necessary for engineers and architects for planning and designing energy-efficient buildings [3]. For extracting maximum electrical outputs from the PV panel, the extent of solar irradiation incident on a particular region and time interval of peak sun shine hours are very important. Solar irradiation at every locality on the earth may depend on different parameters such as attitude, latitude, longitude, geographical location and humidity [4].

We also considered the consequences of several environmental parameters such as air mass, Linke turbidity (include aerosols, Rayleigh scattering and absorption due to assorted gases), cloud cover, albedo, perceptible water vapour and atmospheric turbidity (smoke, dust, water droplets), and location dependent parameters such as zenith angle, solar azimuth angle and elevation on PV panel. As a reference, 250W PV panel is selected for receiving the data of electrical power in a given location. It is valuable to measure the outcome of orientation and tilt of the PV panel to capitalize solar radiations incident on it. Solar irradiance on the tilted surface is a combination of a direct (beam), diffuse and ground reflected radiations [5]. On the other hand, it is quite difficult to purchase and install illuminance meters, sensors and pyranometers at every tilted angle and orientation to gather all of the requisite data. Because the measurement using those equipment is very expensive, therefore a model-based methodology has been adopted to evaluate the electrical energy of PV panel.

Previously, the optimal tilt angle of PV panel was calculated for some specific area [6–9]. The novel idea for this research is proposed by reviewing the various reports on this issue. The purpose of this approach is to combine several clear sky and array performance models to predict different solar irradiation components at an earth's location. The focal aim of this work is to implement optimized clear sky and array performance models of high prediction accuracy in MATLAB to compute electrical energy for locations on hourly, monthly and yearly basis and corresponding outcomes have been presented in the graphical form. A comparison has also been done to relate our results with actual data available in NREL.

2. MODELLING PROCESS

2.1. Extra-terrestrial Solar Irradiance (ESI):

The radiation above the atmospheric surface of earth as shown in Fig. 1 is known as *ESI*. It is the intensity of the sun at the top of the earth's atmosphere. It can be computed as:

$$E_{ext} = E_{SC} \cdot \left(1 + 0.033 \cdot \cos\left(\frac{360\,n}{365}\right)\right), \qquad (1)$$

where $E_{SC} = 1367\,\mathrm{wm}^{-2}$, n is the Julian day.

The ESI on horizontal surface could be computed as:

$$E_{h\_ext} = E_{ext} \cdot \cos\theta_z. \qquad (2)$$

2.2. Global Horizontal Irradiance (*GHI*):

GHI is the complete amount of solar irradiation above the earth's horizontal surface to the ground level. It has a significant impact on PV installation and contains direct normal irradiance (*DNI*) and diffuse horizontal irradiance (*DHI*). Pyranometer is usually used to compute *GHI* which has a hemispherical (180°) view angle. Kasten model could be used for computation of *GHI* [11].

$$GHI = C_{g1} \cdot E_{ext} \cdot \cos\theta_z \times$$
$$\times\, e^{(-C_{g2} \cdot AM \cdot (f_{h1} + f_{h2}(TL-1)))} \cdot e^{(0.01 \cdot AM^{1.8})}, \qquad (3)$$

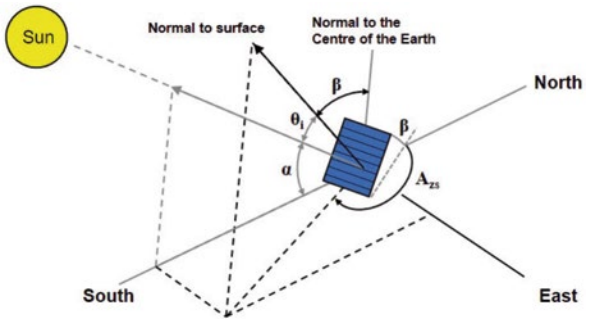

Fig. 2. Elevation, Zenith and Azimuth and incidence angle (*Source:* www.itacanet.org/the-sun-as-a-source-of-energy)

where *TL* is the Linke turbidity, which is equal to 2 in this case,

$$C_{g1} = 5.09e^{-5\cdot}\, h + 0.868, \tag{4}$$

$$C_{g2} = 3.92e^{-5\cdot}\, h + 0.0387, \tag{5}$$

$$f_{h1} = e^{(-h/8000)}, f_{h2} = e^{(-h/1250)},$$

$$\cos\theta_z = \cos\cos\ \cos w + \sin\lambda\sin\delta, \tag{6}$$

where $\delta = \sin^{-1}\left(\sin\left(23.45^o\right)\sin\left(\frac{360}{365}(d-81)\right)\right)$, (7)

$$w[degrees] = 15\left(Solar\,Time[h] - 12\right), \tag{8}$$

$$Solar\,Time = Clock\,Time + \left(\frac{1}{15}\right)\left(L_{std} - L_{oc}\right) + E, \tag{9}$$

$$E = 0.165\sin 2B - 0.126\cos B - 0.025\sin B, \tag{10}$$

$B = \frac{360(n-1)}{364}$, and *n* is the any day of the year.

The optical thickness of the earth's atmosphere can be represented by *AM* which can be derived as follows:

$$AM = \frac{1}{\cos\theta_z},\ AM =$$

= 1 means that the Sun is overhead. (11)

2.3. Beam radiation Model for Horizontal and Tilted Surface

Beam component at horizontal $\left(E_{bh}\right)$ and beam component at tilted surface $\left(I_b\right)$ [12] can be computed as:

$$E_{bh} = E_n.\cos\theta_z, \tag{12}$$

$$I_b = E_n.\cos a, \tag{13}$$

where E_n is the direct normal irradiance, *a* is the angle of incidence and computed as:

$$a = \arccos\left[\begin{matrix}\sin_{sun}\cos\left(\gamma - \gamma_{sun}\right)\sin\beta + \\ +\cos_{sun}\cos\beta\end{matrix}\right], \tag{14}$$

where

$$\gamma_{sun} = \arccos\left(\frac{\sin\cos - \sin\cos cosw}{cos\left(90 - \theta_z\right)}\right). \tag{15}$$

Fig. 2 shows the angular picture of Elevation, Zenith and Azimuth angles.

2.4. Direct Normal Irradiance Model

It is total amount of solar irradiation realized per unit area by the plane surface that is placed perpendicular to the sun rays. Pyrheliometer is usually used for the measurement of *DNI*. It can also be computed by *DISC* Model [13] as:

$$E_n = K_n.E_{ext}, \tag{16}$$

where K_n is the direct beam transmittance,

$$\Delta K_n = K_{nc} - K_n, \tag{17}$$

K_{nc} is the maximum clear sky value, ΔK_n is the disappearance of transmittance value from its corresponding maximum values K_{nc}. Clear Bird model [14] is used to compute K_{nc} value, which is given below:

$$K_{nc} = 0.866 - 0.122\,AM + 0.0121\,AM^2 + \\ +0.000653\,AM^3 + 0.000014\,AM^4. \tag{18}$$

Least square regression analysis is used to compute ΔK_n:

$$\Delta K_n = a + be^{(cAM)}. \tag{19}$$

The coefficients $a, b,$ and c can only be known if we know clearness value K_t [15] and it strongly depends on cloud cover (*CC*).

$$K_t = \frac{GHI}{E_{h\_ext}}. \tag{20}$$

If $K_t < 0.60$ (cloudy conditions), a=0.512–1.56.K_t+ +2.286.K_t^2 – 2.222.K_t^3, $b = 0.370 + 0.962.K_t$, and $c = -0.280 + 0.932.K_t - 2.048.K_t^2$.

If $K_t > 0.60$ (mostly clear conditions), $a = -5.743 + 21.77.K_t - 27.49.K_t^2 + 11.56.K_t^3$, $b = 41.40 - 118.5.K_t + 66.05.K_t^2 + 31.90.K_t^3$, $c = -47.01 + 184.2.K_t - 222.0.K_t^2 + 73.81.K_t^3$.

When ΔK_n and K_{nc} are known, then *DNI* (E_n) and beam radiation incident on tilted surface can be easily computable as: $I_b = E_n \cdot \cos\ \alpha$.

2.5. Diffuse Radiation Model

DHI is the terrestrial diffused or scattered irradiance by the atmosphere received on a horizontal. *DHI* is normally measured with a pyranometer, however, in this case the direct light of the sun is blocked in order to remove the beam component of the radiation.

Diffuse radiations on tilted surface can be categorized into:

- Isotropic diffuse radiation;
- Circumsolar radiation;
- Horizon brightening.

Klucher Model [16] covers all the three parameters as discussed above, so that the computed diffuse radiation on tilled surface as:

$$I_{d,sky} = I_d \left[\begin{array}{l} \left(1 - A_l\right).\left(\dfrac{1+\cos(\beta)}{2}\right)\times \\ \times 1 + F\sin^3\left(\dfrac{\beta}{2}\right) + A_l R_b \end{array} \right], \qquad (21)$$

where I_d is the hourly diffuse horizontal radiation,

$R_b = \dfrac{I_b}{E_{bh}}$, $A_l = \dfrac{E_{bh}}{E_{h\_ext}}$, $F = \dfrac{E_{bh}}{GHI}$.

2.5. Ground Reflected Radiation Model

Lui and Jordan's assumption [17] concluded that the constant coefficient of albedo could be added to GHI to realize ground reflected irradiation on PV panel

$$R_h = 0.2 \cdot G_h. \qquad (22)$$

2.6. Array Incidence Plane Model

A fundamental step in calculating PV performance is determining the irradiance incident on the plane of the array (*POA*) as a function of time. This *POA* irradiance is dependent upon several factors, including array orientation, beam, diffuse and ground reflected radiation. These factors are incorporated through the use of the Perez algorithm [18]

$$I_{poa} = I_b + I_{d,sky} + I_{d,ground}, \qquad (23)$$

where $I_{d,ground} = 0.2$ default value.

2.7. Module Cover Model

Given the total *POA* irradiance incident on the module cover, *PV Watts* applies an *AOI* correction to adjust the direct beam irradiance for incidence angles greater than 50 degrees to account the reflections losses. The correction uses the Sandia PV Array Performance Model polynomial correction, with coefficients for glass.

$$f = b_0 + b_1 a + b_2 a^2 + b_3 a^3 + b_4 a^4 + b_5 a^5. \qquad (24)$$

Coefficients b_0, b_1, b_2, b_3, b_4 *and* b_5 are module cover Polynomial coefficients:

$b_0 = 1.0$, $b_1 = -2.438 \cdot 10^{-3}$, $b_2 = 3.103 \cdot 10^{-4}$, $b_3 = -1.246 \cdot 10^{-5}$, $b_4 = 2.112 \cdot 10^{-7}$, $b_5 = -1.359 \cdot 10^{-9}$,

$$I_{tr} = I_{poa} - (1 - f) E_n \cdot \cos. \qquad (25)$$

2.8. Power Computation Model

PV Watts module has been approached to compute electrical power that is an edition of *PVFORM* version prototypes [19]. DC power through an array can be calculated by providing panel's rated power, *POA* irradiance and cell temperature.

$$P_{dc} = \frac{I_{tr}}{1000} P_{dc0} \left(1 + \gamma \left(T_{cell} - T_{ref}\right)\right),$$

if

$$I_{tr} > 125\ W\mathrm{m}^{-2}. \qquad (26)$$

$$P_{dc} = \frac{0.008 I_{tr}^2}{1000} P_{dc0} \left(1 + \gamma \left(T_{cell} - T_{ref}\right)\right),$$

if

$$I_{tr} < 125\ \mathrm{Wm}^{-2}. \qquad (27)$$

Here γ is the temperature coefficient fixed at –0.5 %/° C which is assumed for crystalline sil-

Table 1. Purpose of Choosing Models

Model	Purpose	Reason
Kasten	GHI	Environmental factors e.g. Air Mass (AM) and Linke Turbidity (include Aerosols, absorption due to assorted gases and Rayleigh scattering) and location dependent parameters like Zenith Angle (z), Elevation (h).
DISC	DNI	Covers air mass, cloud cover, albedo, perceptible water vapour and atmospheric turbidity (dust, smoke and water droplets).
Klucher	Diffuse Radiations	Circumsolar Radiation, Isotropic diffuse radiation and Horizon brightening
Perez algorithm	Module Cover	Merges beam, diffuse and ground reflected radiation
Power Computation	Power output	Include all module parameters

icon PV module, T_{ref} = 25 °C, T_{cell} is the cell temperature, and P_{dc0} is the nominal module power equal to 250 W.

2.9. Block Diagram of Modelling Process

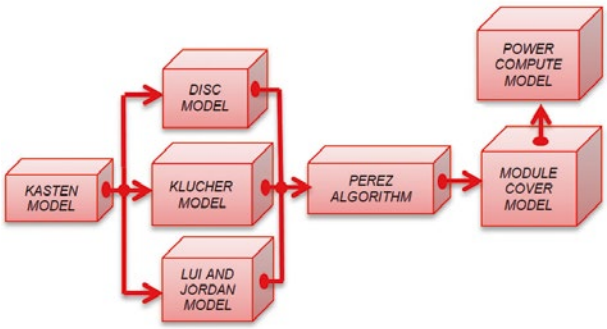

Fig. 3. Block diagram of modelling procedure

3. MODELS SELECTION AND SIMULATION TOOL

Fig. 3 and Table 1 display the modelling process, purpose and reasons for selecting the models for implementation. We have implemented the entire process in MATLAB. A Guided User Interface (*GUI)* of the system is presented in Fig. 4.

4. RESULTS AND DISCUSSIONS

In our process, the result can be computed by keeping the panel azimuth fixed at 180° while the tilt of the panel is varied. Fig. 5 summarizes average energy/month and average energy/year with variable tilt angle of panel and at fixed Panel's azimuth 180° facing south and shows its graphical representation.

4.1. Comparison of Computed Electrical Energy with Actual Energy

In this section, we have made a comparison of the computed results from our software with the actual data (http://pvwatts.nrel.gov/India/pvwatts.php). We have selected the specification given below:

Location: Nagpur India,
Latitude = 21.14° N,
Longitude= 79.08° E,
Tilt of panel = 27°,
Panel Azimuth =180°.

Table 2 compares computed and actual monthly and yearly average energy with the optimal tilt angle of the panel which is 27° and at fixed Panel's azimuth 180° facing south. Fig. 6 displays the graphical comparison between computed and actual yearly average energy.

The difference of Output Electrical Energy between Computed and Actual Energy is little greater in the months of July, August and September. This difference is because of the monsoon season from July to September.

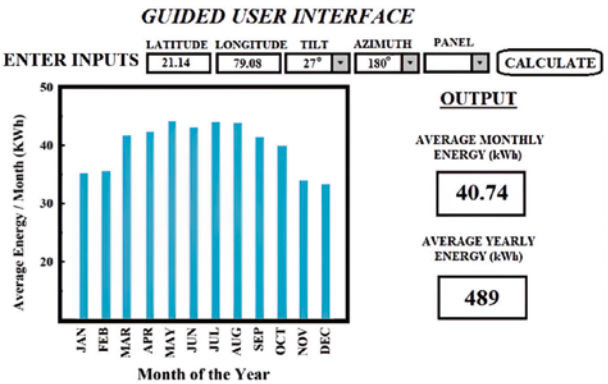

Fig. 4. Guided user interface of the system

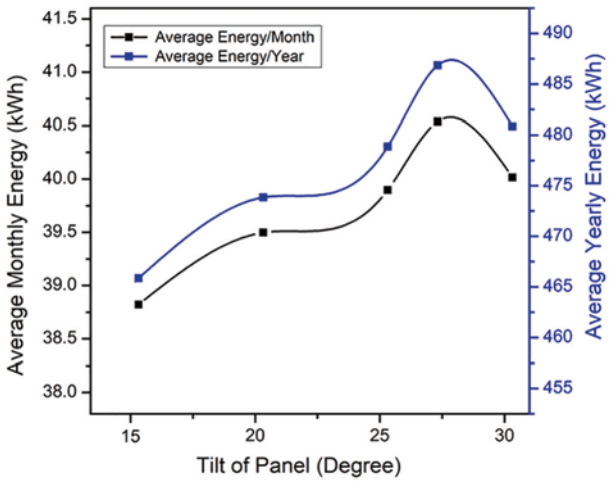

Fig. 5. Average monthly and yearly energy on the variable tilt angle of the panel

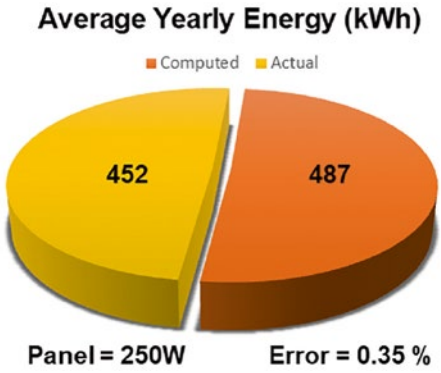

Fig. 6. Computed and actual yearly average energy with an optimal tilt angle of 27°

5. CONCLUSIONS

This work is focusing to compute optimal tilt angle of PV panel for getting maximum amount of energy produce per month and per year for every locations having latitude at north direction and longitude at east direction. The selected clear sky and array performance models include various environmental location and module dependent parameters. Evaluation has been done by comparing actual energy with computed energy for location Nagpur India (21.14° N, 79.08° E) at 27° tilt and we found difference of only 0.35 % has been recorded between actual and computed electrical energy. It is concluded that 27° facing south is the optimal tilt angle for generating maximum electrical energy. We can conclude from current work that the clear sky and array performance models are much known and easy to use without installing expensive sensors like pyranometer and pyrheliometers to get the data of solar irradiance.

Table 2. Computed and Actual Average Energy

Month	Computed Average Energy (kWh)	Actual Average Energy (kWh)
JAN	40.4	41.7
FEB	38.1	38.5
MAR	44.0	43.8
APR	42.2	39.6
MAY	41.3	38
JUN	38.1	32.3
JUL	40.2	30.2
AUG	42	30.2
SEP	42	36.5
OCT	44.1	41.7
NOV	37.4	39.6
DEC	37	39.6

ACKNOWLEDGMENT

The work is supported by Korea Institute of Energy Technology Evaluation and Planning (KETEP) 20193010014850.

REFERENCES

1. Schiermeier Q, Tollefson J, Scully T, Witze A, Morton O. Energy alternatives: Electricity without carbon// Nature News, 2008, Aug 13, Vol. 454 (7206), pp. 816–823.

2. Ulfat I, Javed F, Abbasi FA, Kanwal F, Usman A, Jahangir M, Ahmed F. Estimation of solar energy potential for Islamabad, Pakistan// InTerragreen 2012: Clean Energy Solutions for Sustainable Environment (CESSE), Elsevier, 2012, Vol. 18, pp. 1496–1500.

3. Li D.H., Lam J.C. Measurements of solar radiation and illuminance on vertical surfaces and daylighting implications// Renewable energy, 2000 Aug 1; Vol. 20, #4, pp. 389–404.

4. Xu C.Y., Singh V.P. Dependence of evaporation on meteorological variables at different time-scales and intercomparison of estimation methods// Hydrological processes, 1998, Mar 15, Vol. 12, #3, pp. 429–42.

5. Ineichen P., Guisan O., Perez R. Ground-reflected radiation and albedo// Solar Energy, 1990, Jan.1, Vol. 44, # 4, pp. 207–214.

6. Yu C., Khoo Y.S., Chai J., Han S., Yao J. Optimal orientation and tilt angle for maximizing in-plane solar irradiation for PV applications in Japan// Sustainability, 2019, Jan., Vol. 11, #7, p. 2016.

7. Khoo Y.S., Nobre A., Malhotra R., Yang D., Rüther R., Reindl T., Aberle A.G. Optimal orientation and tilt angle for maximizing in-plane solar irradiation for PV applications in Singapore// IEEE Journal of Photovoltaics, 2013 Dec. 12, Vol. 4, #2, pp. 647–53.

8. Benghanem M. Optimization of tilt angle for solar panel: Case study for Madinah, Saudi Arabia// Applied Energy, 2011 Apr. 1, Vol. 88, #4, pp. 1427–33.

9. Skeiker K. Optimum tilt angle and orientation for solar collectors in Syria// Energy Conversion and Management, 2009 Sep. 1, Vol. 50, #9, pp. 2439–2448.

10. Noia M., Ratto C.F., Festa R. Solar irradiance estimation from geostationary satellite data: I. Statistical models// Solar Energy,1993, Dec. 1, Vol. 51, #6, pp. 449–456.

11. Ineichen P., Perez R. A new air mass independent formulation for the Linke turbidity coefficient// Solar Energy, 2002, Sep. 1, Vol. 73, #3, pp. 151–157.

12. Duffie J.A. and Beckman W.A., Worek W.M. Solar Engineering of Thermal Processes// Wiley: New York, USA, 2003, Vol. 116.

13. Marion B. A model for deriving the direct normal and diffuse horizontal irradiance from the global tilted irradiance// Solar Energy, 2015, Dec. 1, Vol. 122, pp. 1037–1046.

14. Reno M.J., Hansen C.W., Stein J.S. Global horizontal irradiance clear sky models: Implementation and analysis// SANDIA report, SAND2012–2389. 2012 Mar.

15. Mellit A., Kalogirou S.A., Shaari S., Salhi H., Arab A.H. Methodology for predicting sequences of mean monthly clearness index and daily solar radiation data in remote areas: Application for sizing a stand-alone PV system// Renewable Energy, 2008, Jul. 1, Vol. 33, # 7, pp. 1570–1590.

16. Klucher T.M. Evaluation of models to predict insolation on tilted surfaces// Solar energy, 1979, Jan. 1, Vol. 23, # 2, pp. 111–114.

17. Liu B.Y., Jordan R.C. The long-term average performance of flat-plate solar-energy collectors: with design data for the US, its outlying possessions and Canada// Solar energy, 1963, Apr. 1, Vol. 7, # 2, pp. 53–74.

18. Perez R, Ineichen P., Seals R., Michalsky J., Stewart R. Modelling daylight availability and irradiance components from direct and global irradiance// Solar energy, 1990, Vol. 44, # 5, pp. 271–289.

19. Menicucci D.F., Fernandez J.P. Users manual for PVFORM: A photovoltaic system simulation program for stand-alone and grid-interactive applications// Sandia National Labs., Albuquerque, NM (United States); 1989 Oct 1.

Muhammad Aleem Zahid received his Bachelor and Master degrees in Electrical Engineering from UET Taxila, Pakistan in 2012 and 2016. He is doing his Ph.D. in Electrical Engineering from Sungkyunkwan University (SKKU), Suwon, South Korea. Area of his interest is PV modules and Solar cell technology

Ganesh T. Chavan received his M. Sc. degree in 2014 and Ph.D. from Solapur University, Solapur, M.S., India in 2017 with Materials Science as specialization. He is working as postdoc researcher in Sungkyunkwan University (SKKU), Suwon, South Korea. His present research interests include Silicon heterojunction (SHJ), bifacial solar cells, different types of TCO materials for SHJ solar cells, Solar to hydrogen generation and super-capacitor applications

Young Hyun Cho earned B.S. and M.S. degree on Electrical Engineering at Hanyang University and University of New South Wales in 1987 and 1994 respectively, and Ph.D. on Photovoltaic Engineering at University of New South Wales in 2009. He is a Research Professor of Sungkyunkwan University (SKKU), Suwon, South Korea. He is a Vice President of Committee of Korea Photovoltaic Society

Junsin Yi received the B.S. degree in Electronic and Electrical Engineering from Sungkyunkwan University, Korea in 1989. He received the M.S. and Ph. D. degrees in Electronic and Electrical Engineering from The State University of New York, University at Buffalo, U.S.A. in 1991 and 1994 respectively. He is currently working as a Professor at Sungkyunkwan University (SKKU), Suwon, South Korea. His main research interest is solar cells and thin film transistor

Light & Engineering
Vol. 28, No. 5, pp. 68–75, 2020

https://doi.org/10.33383/2020-019
Svetotekhnika #4 , 2020, pp. 17–22

METHODOLOGY FOR LIGHT DESIGN TRAINING IN THE SPHERE OF ARCHITECTURAL ENVIRONMENT DESIGN

Vladimir E. Karpenko

Department of Architectural Environment and Interior Design, School of Engineering,
Far Eastern State Technical University (FESTU), Vladivostok
E-mail: vekarpenko@gmail.com

ABSTRACT

The problem of development of the new profession of light designer primarily resides in development of the training methodology, cooperation of architects, lighting engineers, psychologists, colourists, social scientists in the sphere of education and their common understanding of importance of both artistic and technical design of lighting. Since the beginning of the 2000's, the methodology for light design training has been created in Vladivostok, and the results of this work are presented in student projects and some theoretical projects, methodological and training guidelines and scientific articles. The methodology is based on contemporary examples and theory of light design in Russia and abroad; studying of media facades and light surfaces, lighting installations, light design of architectural ensembles; modelling of light panoramas of the city and areas of esplanades; training in the basics of light composition. The article describes the logic of the training process, which starts with creation of a light composition for modelling of the light panorama and lighting ensemble and forming of night time architectural and environmental spaces of the city, and methodology for light design in the sphere of architectural environment projects and education of light designers.

Keywords: light and colour modelling, light panorama, light ensemble, architectural and lighting environment, light composition, lighting model, education

1. INTRODUCTION

Not so long ago, the discussion of the problems and prospects of light design took place in the Svetotekhnika Journal [1–3, 5]. Nowadays, there are several large educational projects in the field of light design, architecture and art running both in state and private educational institutions. In a large university, where students, the main authors of practical projects, change artistic tastes and styles of their projects almost every year, it is possible to propose new tasks and modelling objects, to develop and test new methodological concepts. The current reality makes it necessary to train skills of quick presentation of main ideas in the form of sketches. It has been largely stimulated by introduction of design software in the training process, which increased technical level of practical projects in the field of light and colour modelling of architectural environment. Publications of many scientific articles, monographs and study guides, implementation of light-design projects by Russian and foreign authors and development of electronics allowed us to formulate new methods of luminous environment development.

2. LIGHT COMPOSITION IN EDUCATION

Development of new creative methods and approaches to lighting, aspiration to enlarge the range of light-composition opportunities in formation of light images of environment objects have re-

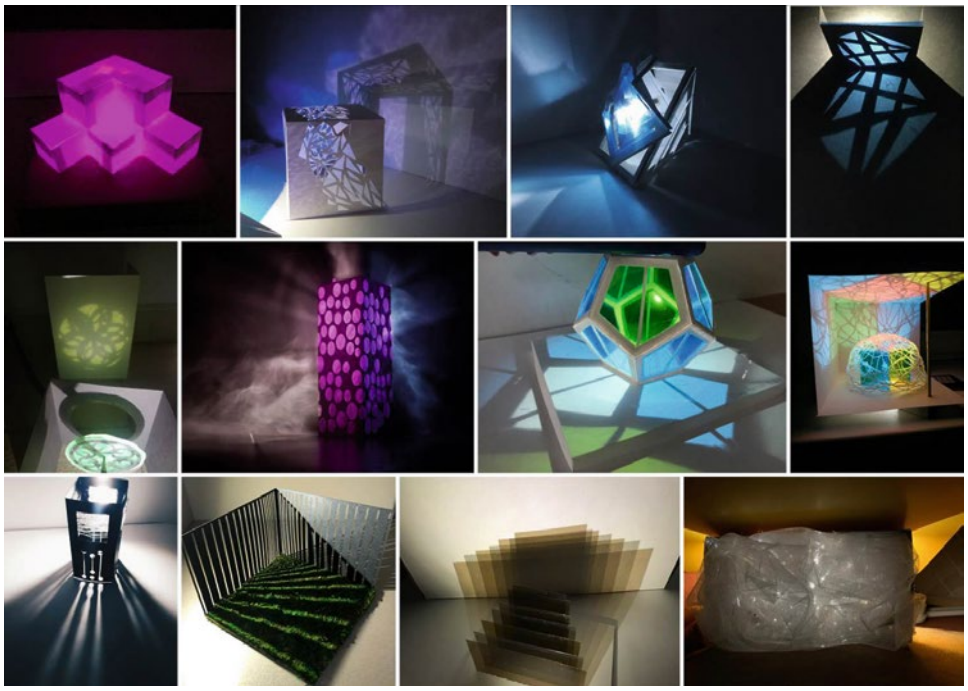

Fig. 1. Training project "Lighting Composition" (students of FEFU, 2019)

quired development of the theory of light composition based on the practice of optic art (op art). Lectures describe development of op art in Italy in the 1960's, review the principles and works by well-known artists who worked in this field of visual art: James Turrell, Thomas Wilfred, Victor Vasarely, etc. [8–11]. According to the practice task, it is necessary to create a spatial or frontal composition using artistic methods of op art such as reflection, refraction, absorption and translucence of natural or artificial light. A composition may involve light kinetics, coloured light with inclusion of reflective, glossy or matte surfaces to reach a psychological effect of depth and other optical illusions (Fig. 1). Technically, numerous artistic methods in light composition are implemented by means of small-size LED-based light sources (LS) of different colours (in particular, LED strips), wireless control devices (dimmers) and control boards [4, 7].

3. LIGHT AND COLOUR MODELLING OF ARCHITECTURAL PANORAMAS OF VLADIVOSTOK IN PRACTICE PROJECTS

Particular landform of the city and many scenery spots on the hills as well as domination of the Zolotoy Rog Bay and the Amur Bay in the central part of Vladivostok allow tourists and local residents to watch its evening and night time light panoramas. By means of light-composition modelling of panoramas, it is possible to change their visual forms and to fill them with new light dominants and accents. In 2008, as part of the practical tasks, the daytime panorama of Vladivostok was studied; architectural monotony of development and lack of land improvement of esplanades were noted. As a result of computer modelling, light and colour dominants were added, landscape was accentuated, facades and the space of the esplanade were illuminated, and light accents on the water were introduced (Fig. 2, *a*). Then in 2009, as part of practice tasks, initial approaches to formation of the light panorama were worked out using a questionnaire and the semantic differential method[1] (Fig. 2, *b*).

In 2010 and 2012, aiming at a detail study of visual perception of the shape of light panorama of Vladivostok and development of its design variant, statistic research (survey) was conducted using the semantic differential method again. Residents and architectural design students participated in the survey. Their opinions on contemporary shape and distinctions of the light panorama were studied. With consideration of the acquired data, the conclusions

[1] Semantic differential is the quantitative methods of studying perception of a studied object by means of a seven-mark grading system ranging from very negative (–3) to neutral (0) and positive (+3) opinion. This method was first introduced by American psychologist Charles E. Osgood in 1952.

Fig. 2. Computer modelling of the lighting panorama of the visual basin of Fyodorov bay of Amur Gulf in Vladivostok: *a* – formation of the lighting rhythm and water lighting in accordance with the concept of night panorama (O.V. Romanenko, student of FESTU, 2008); *b* – formation of light dominants (A. Yu. Balaeva, student of FESTU, 2009)

on aesthetic, artistic, psychological, architectural and town-planning aspects of perception of the daytime and evening time panoramas of Vladivostok from the opposite banks of the Zolotoy Rog Bay were made. The computer models of the light panoramas were created, new light dominants were arranged, the existing architectural verticals were accentuated by means of artificial light, and a new lighting silhouette was formed.

4. ACHITECTURAL LIGHTING OF SVETLANSKAYA AND ADMIRAL FOKIN STREETS, AND OKEANSKY AVENUE IN VLADIVOSTOK

In 2013, the training project "The Concept of the Architectural Lighting of Svetlanskaya street and Okeansky Avenue in Vladivostok" was presented. As part of this work, graphic, light and colour models with use of artistic lighting methods were created for many historical buildings with distinctive architecture located in the central part of the city. The original main idea of light design was to form a uniform evening time lighting facades of the streets. However, later, in 2014, the concept of lighting of the remaining part of Svetlanskaya st. as a notable interior space and modelling of human-scaled lighting effects appeared. In terms of visual content, the space of the street was imagined as a gallery filled with festive light of yellow street lamps. Both initial and final composition forms, light towers and avant-corps, corresponding to architectural elements of the facades of the historical buildings were illuminated. For light design of some vertical dominants and buildings with glass facades, the media facade technology was used with application of coloured LED-based LS [4].

As part of a practice work in the field of light and colour modelling in design of urban environment, when designing art lighting of the Admiral Fokin st., its historical and pedestrian environments, remarkable plastic of buildings and perception of the light composition of facades at a level of human eyes were taken into consideration (Fig. 3). Warm white lighting which highlighted initial colours of the facades was used in design of illumination. Local and contour light draws attention to facade elements. Directed-light luminaires form the light rhythm and differently directed light beams create the effect of a three-dimensional light image. Linear LED-based lighting elements (LE) accentuate the cornices. Further studies of the architectural environment of this street involved its spatial light characteristics (V.E. Karpenko, V.I. Kryuchkova, A.E. Kurkina, O.S. Shlykova, 2017). Values of horizontal and vertical illuminance were measured, levels of semi-cylindrical illuminance, and contrast and uniformity of illuminance were calculated, the light-modelling effect was evaluated, and conclusions were made on the light-composition parameters, light saturation, comfort and safety in the evening pedestrian space of Admiral Fokin st. [4].

Fig. 3. Architectural lighting of Admiral Fokin st. in Vladivostok (A.E. Kurkina, Master Degree student of FEFU, 2017). (The project was presented at the Russian Light Design contest in 2017 as part of the International Exhibition ***Interlight Moscow powered by light + building***, Moscow)

The following training and methodological step conditioned by the town-planning role of the panorama as an active visual background of the coastal city was to develop design of esplanade lighting.

5. LIGHT AND COLOUR MODELLING OF THE ESPLANADES

Some coastal parts in the centre of Vladivostok have never been recreational areas. Nowadays, production and ship-repairing facilities are being partially relocated, which leads to appearing of a uniform pedestrian environment which may become safe, comfortable and aesthetically expressive during evening and night time. The training projects of unique public and residential buildings, museum and landscape facilities were developed for the coasts of the Zolotoy Rog and Amur bays. Design of the new architectural environment in the coastal part of the city includes art lighting with use of innovative technologies and marine semantics. For instance, Elena Kiselyova developed energy saving street lamps with contemporary design which include wind generators and LED-based LS (Fig. 4, *a*). The project by Alexandra Vorontsova presents interactive systems in the form of bionic light compositions, along with original art light effects in small architectural forms of the esplanade and elements of decorative lighting (Fig. 4, *b*) [7].

Later the principles of esplanade lighting modelling were developed in some bachelors' projects in which the visual-art and town-planning role of artificial lighting was identified and the principles of design of night time environment of the esplanades were formulated (students of FEFU, 2016). The projects present different variants of such lighting effects as "flight above the ground" and "hovering above the sea" as well as decorative lighting methods such as "constellation" and "plankton fluorescence" in pedestrian pavements (by means of low-size LEDs). Smooth light graphics resembles shapes of marine animals and contour lighting reproduces symbols of digital technologies. Light is an active component of lighting objects in conjunction with translucent and reflective materials and energy-saving technologies, it accentuates structural joints and serves as a warning at the border of the open pier and water [4].

Two projects in the field of light design of pedestrian spaces on the esplanades were awarded at the Russian Light Design contest in Moscow in 2016. Konstantin Rasulov took first place for the project of architectural lighting of Sportivnaya esplanade in Vladivostok, and in 2017, Oksana Shlykova also took ferst place for the project of architectural lighting of the esplanade of Sportivnaya Harbour and Tsesarevitch esplanade in Vladivostok (Fig. 5). In Shlykova's project, the ideas of lighting of small architectural forms were the project mate-

Fig. 4. Light design of esplanades in practical projects of FEFU students:
a – architectural lighting of Sportivnaya Harbour in Vladivostok (E.S. Kiselyova, student, 2014); *b* – design of architectural lighting of Sportivnaya esplanade ("Sea Bioluminescence") in Vladivostok (A.I. Vorontsova, student, 2014) [4, 7]

rial for her Master Thesis "Problems of Arrangement of Lighting Environment of the Marine Esplanades of Vladivostok" which was successfully defended in 2018. It describes development of comprehensive principles of lighting of the esplanade, the "curtain facades" which surround the esplanade and the surrounding landscape. To create favourable psychological atmosphere, concepts of formation of the lighting environment of Tsesarevich esplanade, Sportivnaya Harbour esplanade (Fig. 5) and the Olimpiets sports centre esplanade were proposed with consideration of the town-planning analysis, discovered flaws and distinctions of the light and colour condition of the existing areas. The light plans of the esplanades identify the compositional axes and dominants, transport and pedestrian links between the light-planning elements of the esplanade environment. In accordance with the lighting space model and the selected concept, the problems of esplanade lighting were solved at three levels: urban planning, ensemble-wide, and object-wide.

6. WORKSHOPS AND LECTURES BY EXPERTS IN LIGHT DESIGN

The modern light design training approach contains the active component which includes in-situ evaluation of luminance distribution and light fields,

Fig. 5. Architectural lighting of Sportivnaya Harbour esplanade and Tsesarevicha esplanade in Vladivostok (O.S. Shlykova, Master Degree student of FEFU, 2017)

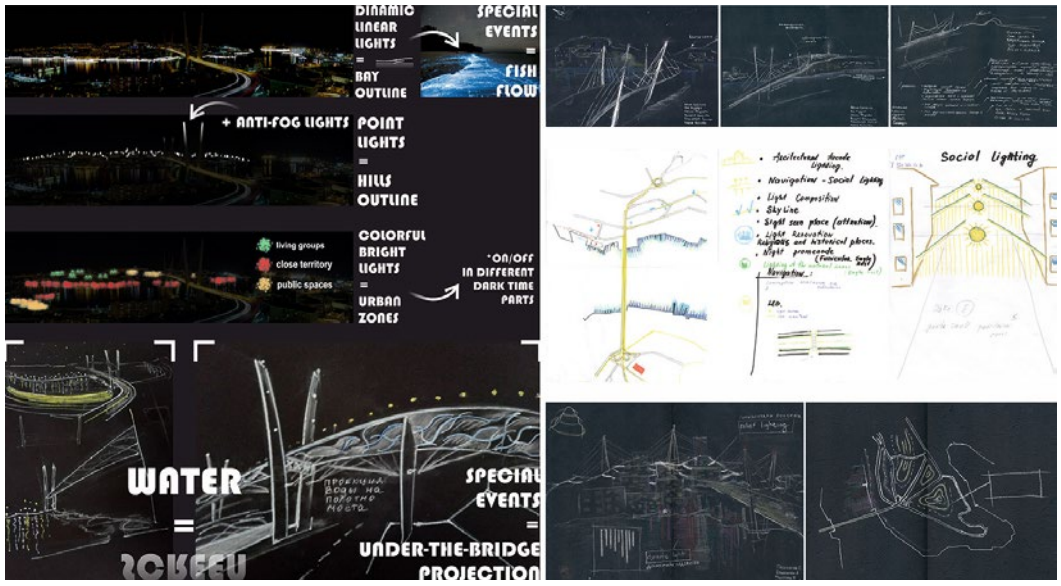

Fig. 6. Concepts of lighting of Vladivostok and the results of the Light Urbanism and Methodology for Lighting Master Plan Design workshop of Roger Narboni in FEFU (FEFU students, 2018)

measurement of light engineering parameters (illuminance and luminance) and then (based on the acquired data) creation of the concept of the city illumination. In 2015, as part of the *Visiting Professors* programme, N.I. Shchepetkov visited FEFU, and this visit included his familiarisation with the architectural and lighting environment of Vladivostok and a cycle of lectures on Urban Light Design covering history, theory, and means of contemporary light design. After the lectures, the workshop on search for the lighting images of historical buildings (through the example of the Vladivostok Central Post Office building) was conducted as well as a consultation for students on light design of objects and selection of their lighting images [4].

In 2018, also as part of the *Visiting Professors* programme, the lectures and the workshop were conducted by Roger Narboni (a globally known French light designer, teacher of professional and training courses on light design in France and other countries). Together with students, he walked around the evening city and visited the city's characteristic scenery spots in the area of the cable tramway and the Opera: on two opposite coasts of the Zolotoy Rog Bay and in the centre of Vladivostok. Dynamics of the architectural and lighting environment, the predominating spectral composition of artificial light and the light-compositional role of the architectural dominants were identified. This was a creative stimulus for consideration, preparation and development of four concepts of the master plan of Vladivostok illumination (Fig. 6) [4].

7. DESIGN OF VLADIVOSTOK TOURIST ROUTES ILLUMINATION

Tourists are very interested in Vladivostok in any time of a day. However, the city streets are not safe during evening and night time and lack of lighting does not allow them to see memorial boards and plates, historical architecture objects and landscape; different monuments, memorials and sculptures are almost not marked out. With that, the historical centre of Vladivostok may be illuminated during night time as a museum environment, its streets with landmarks may form a museum exhibition, artificial light of different colours may direct tourists, form the feeling and intimacy of tourist ways and environments, underline their uniqueness and historical and cultural value. To solve this set of environment problems, it was proposed to create a model of a fragment of the urban space. Five student teams created illumination by means of the model with use of small lamps or decorative light strings powered by the supply network or autonomously. Cuts were made in the models to insert small-size LED-based LE. In other cases, LED-based LE of specific chromaticity produced shadows and shone on model walls, steps, fences, etc. Then photos and videos were made (Fg. 7). In one of the works, patterns are projected on opposite walls by means of lighting devices thus creating a particular general level of light saturation, while in another one, the theme of Japanese symbols is being developed, with the fence pattern containing the motives of sakura, Fujiyama,

Fig. 7. Modelling of lighting of fragments of urban environment in Vladivostok (FEFU students, 2018)

shapes of roofs, red light (the pattern is projected on walls and creates coloured shadows). Modelling of new lighting in the historical environment of the city does not contrast to the surrounding illumination design; the warm shade of light on the adjacent facades is repeated in the new lighting effects. Random graffiti on the walls are accentuated by neutral white light in the evening. Light accentuate facade plastic, fragments of walls and ledges create a lighting rhythm and different optical effects of contraction or expansion of intimate spaces.

8. RESULTS

When forming the methodology for light design training and in the course of training, the logical connection between application of light effects in op art, contemporary visual art and training light compositions was found.

The large-scale visual shape of a light panorama allows us to form new light dominants, accents and background in its space, to accentuate the existing elements and move to detailed design of light ensembles in the urban environment. In this case, a night panorama is a drawing canvas on which a light designer draws light spots, dashes and dots.

The street space is limited by lighted facades of buildings, shop windows, advertising boards, navigation and different types of other light forms which complicate the architectural and lighting environment. Light and volumetric parameters shall be also taken into account. In view of this, the city space and building volume may be divided into elementary illuminated town-planning and composition elements preventing lighting chaos and limiting the amount of artificial light.

In terms of light structure and perception from the water area, the esplanades are enclosed by the urban light panorama with its lighting being possibly built on the basis of light composition methods and principles, and the lighting effects may be based on visions, symbols and semantics of a coastal city and water.

Application of active types of training with visits to the territory and study of the night-time environment by using measurement devices and further discussion and development of the concepts of the city lighting as well as international workshops in Russia and abroad on sites, which lighting installations and design of urban spaces lighting by means of special equipment are created, make a specific educational and methodological contribution, which allows the importance of the practical part of the training process to identify. Such educational and methodological activity allowed us to form new ideas and approaches in modelling of artificial light using sketch models of the existing territory of the city. At the same time, it is possible to capture the moment, the atmosphere and trace translucence of beams through modelled elements of land improvement, small design and street art objects and enclosing surfaces.

9. DISCUSSION AND PROSPECTS OF RESEARCH

Workshops and active training methods in light design may supplement class exercises and accentuate the training process in practical terms, in the real architectural and lighting environment of the city using LS by different manufacturers.

The lighting methodology may include development of light models of urban environment fragments with inclusion of coloured areas, with change of their chromaticity and compositional methods of lighting tested in laboratory conditions under lighting by different test LS. Modelling of lighting by means of small-size LSs in models of urban environment fragments may provide considerable practical and artistic results.

Evaluation and analysis of the measured photometric parameters (illuminance and luminance) in the urban environment may demonstrate the directions towards obtainment of necessary light-modelling effects, uniformity of lighting and light saturation with achievement of visual and artistic expression, visual and psychological comfort and sufficient level of safety.

REFERENCES

1. Discussion on the Problem of Light Design [Diskussiya po probleme svetovogo dizayna] // Svetotekhnika, 2018, # 3, pp. 72–82.

2. Discussion on the Problem of Light Design [Diskussiya po probleme svetovogo dizayna] // Svetotekhnika, 2018, # 4, pp. 80–93.

3. Discussion on the Problem of Light Design [Diskussiya po probleme svetovogo dizaiya] // Svetotekhnika, 2018, # 5, pp. 79–86.

4. Karpenko V.E. Light and Colour Modelling of Urban Environment: study guide for universities [Svetotsvetovoye modelirovaniye gorodskoy sredy: uchebnoye posobiye dlya vuzov] / Engineering School of FEFU, Vladivostok: Far East Federal University, 2019, 153 p. 1 CD, ISBN978–5–7444–4460–0.

5. Karpenko V.E., Lebedkova S.M., Ovcharov A.T., Sanzharov V.B., Silkina M.A., Snetkov V. Yu., Khadzhin A.G., Shchepetkov N.I. On the Subject of the Article by Bysrtyantseva N.V., Lekus E. Yu., Matveev N.V. Russian Light Engineering School: Strategies and Tactics [Po teme statyi Bystryantsevoy N.V., Lekus E. Yu., Matveeva N.V. Shkola otechestvennogo svetodizayna: strategii i taktiki] // Svetotekhnika, 2015, # 4, pp. 65–66.

6. Shlykova O.S. Problems of Arrangement of Lighting Environment of the Marine Esplanades of Vladivostok [Problemy organizatsii svetovoy sredy primorskikh naberezhnykh v g. Vladivostok] / Extended abstract of the Master Degree Thesis in the 07.04.03 Architectural Environment Design Programme, Urban Environment Planning profile. Vladivostok: FEFU, 2018, 31 p.

7. Karpenko V.E. Educational complex of light-coloured modelling of urban environment // SHS Web of Conferences. The 4th International Research-to-Practice Conference Lighting Design, 2017, St. Petersburg, Russia, 12–13 October, 2017, Vol. 43 (2018), 9 p. URL: https://doi.org/10.1051/shsconf/20184301013 (date of reference: 15.02.2020).

8. Govan M., Kim C.Y. Turrell J. A Retrospective. Los Angeles, Country Museum of Art, Munich, London, New York: DelMonico Books. Prestel Verlag, 2013, 304 p.

9. Holzhey M, Vasarely V. 1906–1997. Pure Vision. Kőln: Tashen, 2005, 96 p.

10. ITALIAN ZERO & avantgarde'60s. Cinisello Balsamo, Milano: Silvana Editoriale Spa. 2011, 288 p.

11. Orgeman K. Lumia: Thomas Wilfred and the Art of Light. New Haven: Yale University Art Gallery, 2017, 172 p.

Vladimir E. Karpenko,
Associate Professor, Ph.D. in architecture. In 1999, he graduated from Far Eastern State Technical University (FESTU). At present, he is the Associate Professor of the Architectural Environment and Interior Design sub-department of the Engineering School of FESTU and member of the Union of Architects of Russia

Light & Engineering
Vol. 28, No. 5, pp. 76–83, 2020

https://doi.org/10.33383/2020-006
Svetotekhnika #4, 2020, pp. 11–16

RECOMMENDATIONS FOR RESTORATION OF HISTORICAL TRANSPARENT COATINGS IN PUSHKIN MUSEUM

Alexander V. Spiridonov, Nina P. Umniakova, and Boris L. Valkin

Research Institute of Building Physics of Russian Academy of Architecture and Construction Sciences (NIISF of RAACS), Moscow
E-mail: spiridonov_aleks@list.ru

ABSTRACT

Due to the intensification of historical buildings restoration works that are cultural monuments and related to architectural monuments, numerous questions arise about the possibility of increasing the efficiency of translucent structures, including their energy efficiency, using modern innovative technologies. The cost of competent reconstruction of windows and lanterns with the preservation of historical elements is much higher than the cost of standard modern structures, as a result of which there are numerous examples of barbaric illegal replacement of historical windows with modern ones. This not only spoils the appearance of buildings, but also contradicts federal laws (with all the ensuing consequences).

Earlier, NIISF RAASN carried out multifactorial field studies of historical translucent coverings of a cultural monument of federal significance – the main building of the Pushkin Museum, on the basis of which their inconsistency with modern requirements for such structures was established. According to the technical assignment and the project for the reconstruction of the building, 13 options were proposed for the possible restoration of these coatings. To assess the proposed options, a comprehensive computer simulation and corresponding calculations were carried out in accordance with the certified software package "WINDOW TECT".

On the basis of the conducted examinations and computer calculations, optimal solutions were proposed for the restoration of historical translucent coatings of the main building of the Pushkin Museum, providing for the preservation of the original elements of metal structures and ensuring an increase in the thermal characteristics of the lantern and side lamp.

Keywords: restoration of old buildings, historical translucent coatings, computer modelling, resistance to heat transfer, condensation, lantern, sidelight, recommendations, translucent structures, energy efficiency, micro-climate parameters, museum exhibition premises

1. INTRODUCTION

Recently, work on the preservation of buildings related to the historical and cultural heritage has intensified – practically throughout the Russian Federation and, to a greater extent, in a number of other countries. (In Moscow in 2019 alone, more than 170 historical buildings were restored, and in 2020 even more activity is planned in this direction.) However, the number of unsuccessful decisions, scandals and even court proceedings related to with the restoration of historical buildings, including those with light-transparent structures.

As already noted [1], most of the problems with the unjustified replacement of historical translucent structures of old buildings are observed in St. Petersburg and Moscow. This is absolutely understandable because in these cities is the largest number of surviving buildings belonging to the "objects of cultural and historical heritage" and, accordingly, increased budgets.

However, examples of the barbaric attitude to the "historical heritage" are not only in Moscow [2–5] and St. Petersburg [6–8], but also in Ryazan [9], Omsk [10], Nizhny Novgorod [11], Pereslavl-Zalessky [12] and in many other cities and towns of the immense Russian Federation.

We cannot say that everyone agrees with this practice. For example, there are known court decisions on the restoration of historical windows [11, 13, 14], and a ban on the installation of grilles and air conditioners disfiguring the facades of old buildings [15], and cases of the creation of special commissions designed to monitor the competent restoration of light transmission – transparent structures [16, 17], and thousands of fines for disfiguring building facades [14, 18]. True, there exist some "funny" initiatives. Thus, the new governor of St. Petersburg A.D. Beglov suggested simply paint the illegally installed white PVC-profile windows in a "historical" colour and thus cheaply "fix" these violations [19].

In fairness, it is worth noting successful reconstructions of historical light-transparent structures [20, 21], but, unfortunately, there are not very many of them. The relevance of the topic of preserving the identity of old buildings in cities is also emphasized by the publication in 2019 of the book [22], prepared with the participation of the well-known window companies VEKA and SIEGENIA. Of course, due to the main professional and commercial interest of these companies, the book focuses on the use of modern windows made of PVC profiles, and this is still not a "clean" restoration, but rather "reconstruction" or, fashionable today, "renovation". Nevertheless, the book [22] is certainly interesting and useful.

Specialists in the field of scientific restoration are trying to restore the damaged elements of historical buildings. This is not always possible – many windows are practically lost (wooden ones have rotted, and metal ones have rusted). In this case, they try to replace the frames with exact replicas made of similar materials. Unfortunately, PVC window profiles did not exist until the middle of the 20th century.

Disputes about the possibility of using different methods for the preservation of historical buildings have been going on for a long time – the supporters of different approaches are almost equally divided. Quite interesting considerations on this matter are published in the article [23].

At the same time, increasing the energy efficiency of translucent structures made of metal at the beginning of the 20th century and requiring the preservation of the main elements for the protection of a cultural monument, up to modern requirements using modern technologies is a unique task that has no analogues in practice.

2. METHOD OF INVESTIGATION

As a result of the conducted surveys of historical translucent coatings [24], it became obvious that they do not meet modern requirements either in terms of heat transfer resistance or other indicators. While preserving most of the metal frames (which is a requirement of the Law on the Protection of Cultural Heritage Monuments and the Customer's assignment [25]), it was necessary to carry out large-scale computer calculations to determine the optimal parameters for the restoration of coatings.

In accordance with the reconstruction plan of the Pushkin's Museum is supposed – while maintaining the main historical structures (the author is the outstanding engineer V.G. Shukhov) – to isolate the under-roof space from the exhibition premises and install energy-saving double-glazed windows instead of glass on the window lamp (Fig. 1).

The calculation of the thermal technical characteristics of historical and proposed for reconstruction translucent coatings, as well as the temperature distribution over the inner surfaces of glazing and profiles of metal frames was carried out in accordance with the certified software package "WINDOW TECT" for thermal engineering calculations and the calculation of thermal technical coefficients of translucent structures as part of programs "WINDOW THERM TEMPER", according to [26], under different boundary conditions for each of the applied options for filling translucent structures. The

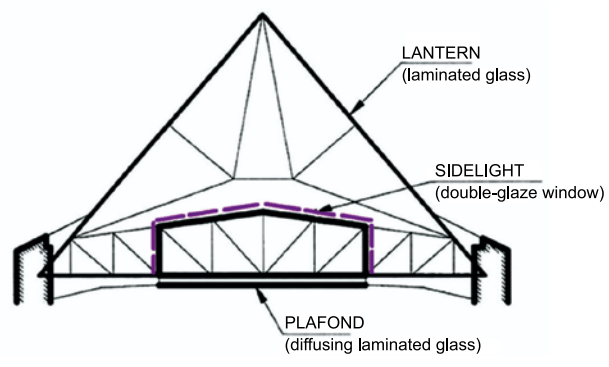

Fig. 1. Reconstruction project of translucent coverings

calculation technique and the area of its application are described in more detail in [27, 28].

3. CALCULATION RESULTS

To carry out these calculations, the following options for the execution of light-transparent structures were proposed, the general diagram of which is shown in Fig. 1:

Skylight:

Option 1 – the existing historical design of the skylight glazing: 4 mm thick glass installed in metal brackets (35×35×3) mm;

Option 2 – instead of glass, laminated glass is installed in the existing historical structure (option 1) in accordance with the strength calculations carried out [28].

Sidelight:

Option 3 – an existing metal frame made of a brand with dimensions of (35×35×3) mm, glazed with 4 mm thick plain glass;

Option 4 – the existing metal frame (option 3), glazed with a two-chamber glass unit 4I-10Ar-4–10Ar-4I (I-glass: "PLANITHERM 4S", emission coefficient 0.013, "warm" distance frame "TGI");

Option 5 – the existing metal frame (option 3), glazed with a two-chamber glass unit 4I-10Ar-4–10Ar-4I (I-glass: "PLANITHERM 4S", emission coefficient 0.013, "warm" spacer "TGI"); on the side of the under-roof space on the T-profile there is a 10 mm thick foam polystyrene pad;

Option 6 – an existing metal frame (option 3), glazed with a two-chamber glass unit 4I-10Kr-4–10Kr-4I (I-glass: PLANITHERM 4S, emission coefficient 0.013, "warm" spacer "TGI");

Option 7 – existing metal frame (option 3), glazed with a two-chamber glass unit 4I-10Kr-4–10Kr-4I (I-glass: "PLANITHERM 4S", emission coefficient 0.013, "warm" spacer "TGI"); on the side of the under-roof space on the T-profile there is a 10 mm thick foam polystyrene pad;

Option 8 – a repetition of the historical design with an exact replica made of fiberglass with glazing with a double-glazed unit 4I-10Ar-4–10Ar-4I (I-glass: PLANITHERM 4S, emission coefficient 0.013, "warm" spacer "TGI");

Option 9 – a repetition of the historical structure with an exact replica made of glass-fiber-reinforced plastic with glazing with a double-glazed unit 4I-10Ar-4–10Ar-4I (I-glass: "PLANITHERM 4S", emission coefficient 0.013, "warm" spacer "TGI"); on the side of the under-roof space on the brand there is a 10 mm thick pad of foam-polystyrene;

Option 10 – a repetition of the historical design with an exact replica made of fiberglass with glazing with a double-glazed unit 4I-10Kr-4–10Kr-4I (I-glass: "PLANITHERM 4S", emission coefficient 0.013, "warm" spacer "TGI");

Option 11 – a repetition of the historical structure with an exact replica made of glass-fiber reinforced plastic with glazing with a double-glazed unit 4I-10Kr-4–10Kr-4I (I-glass: "PLANITHERM 4S", emission coefficient 0.013, "warm" spacer "TGI") from the side of the under-roof space on the T-profile there is a 10 mm thick foam polystyrene pad;

Option 12 – frame – facade system "Raico", made according to the geometry of the existing side lamp using a box-shaped steel profile 50×50 mm with glazing with two-chamber glass unit 4I-10Ar-4–10Ar-4I (I-glass: "PLANITHERM 4S", emission factor 0.013, "warm" spacer "TGI").

Option 13 – frame – facade system "Raico", made according to the geometry of the existing side lamp using a box-shaped steel profile 50×50 mm with glazing with two-chamber glass unit 4I-10Kr-4–10Kr-4I (I-glass: "PLANITHERM 4S", emission factor 0.013, "warm" spacer "TGI").

The options 8–13 calculation are related to the replacement of the existing metal frame, which would be possible if the replacement of the historical design of the side of the restorers was agreed upon.

The internal (in the exhibition halls) microclimatic conditions for calculations were taken in accordance with the project for the reconstruction of the main building of the Pushkin Museum – the temperature of the internal air (20 ± 1) °C, relative humidity (50 ± 5)%.

The calculations for the glazing of the lantern were carried out at an outside air temperature of minus 28 °C (in accordance with the document [29, Table 3.1]).

At the same time, the air temperature in the under-roof space according to the survey results was taken (in the absence of solar irradiation) minus 18 °C.

When calculating the thermo-technical characteristics of the side lamp, the following boundary temperature conditions were taken: air temperature in the under-roof space is the minus18 °C and

air temperature inside the space under the lamp is the + 21 °C.

In accordance with the recommendations [30, 31], it was assumed that the heat transfer coefficients at the inner surface of the glass unit, at the inner surface of the bindings (frames) and at the outer surface of the glass unit are equal to 8.0 W/(m^2·°C), 8.7W/(m^2·°C), and 23W/(m^2·°C) respectively.

Thermal conductivity coefficients [W/(m^2·°C)] of some materials, taken in calculations are equal to 0.25 (EPDM sealant), 160 (aluminium), 58 (steel), and 0.17 (polyurethane).

The following conditions were accepted when calculating the glazing of the lantern: dimensions of the structural element are (1300×435) mm, glass dimensions are (1110×415) mm, and tilt angle to the horizon is the 50°.

When calculating the sidelight glazing, the following conditions were accepted: dimensions of the structural element are (2240×890) mm, glass dimensions are (2200×850) mm, and inclination to the horizon is the 13°.

The results of assessing the resistance to heat transfer, [m^2·°C/W], for different versions of the two circuits (lantern and sidelight) of the translucent coating are as follows:

Skylight: 0.18 (option 1) and 0.16 (option 2);

Sidelight: 0.17 (option 3), 0.68 (option 4), 0.74 (option 5), 0.82 (option 6), 0.92 (option 7), 0.82 (option 8), 0.85 (option 9), 1.03 (option 10), 1.08 (option 11), 0.71 (option 12), and 0.85 (option 13).

Other results of calculations of translucent structures are shown in Fig. 2 for two of the above options.

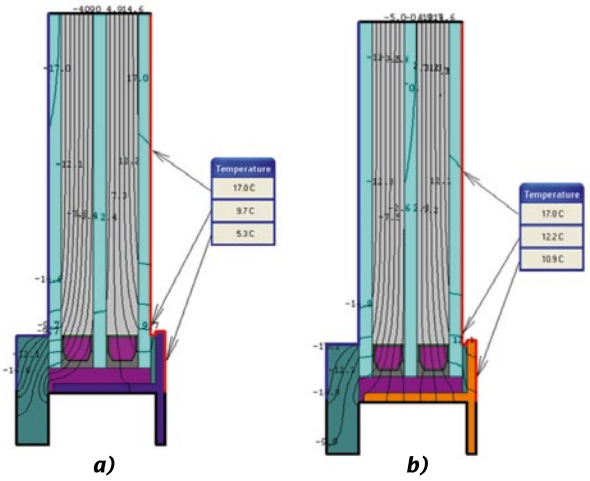

Fig. 2. Temperature distribution on the inner surface of the sidelight glazing for options 7*a* and 11 *b*

The main conclusions based on the results of the calculations are as follows:

– The thermal technical characteristics of the historical translucent structures of the flashlight and side lamp (options 1 and 3) do not correspond to the current regulatory documents [32], including after replacing the glazing of the lantern in accordance with strength calculations (option 2);

– All options for replacing glass in the lamp holder with the proposed double-glazed windows (options 4–13) seem to meet the requirements [32], however, the above calculations were carried out for the vertical arrangement of structures; at the same time, for an inclined structure (13° to the horizon), a reduction factor must be introduced, which is associated with the peculiarities of convection processes in the inter-glass space of glass packets and is recommended by the developers of the software package (Lawrence Berkeley National Laboratory, National Fenestration Rating Council), and confirmed to the testing laboratories of NIISF RAASN; however, only options 7, 10 and 11 meet the regulatory requirements [32];

– In museum premises it is necessary to exclude the possibility of condensation on the surfaces of glazing and frames – condensation is fraught with the danger of damage to works of art; at the same time, within the framework of computer modelling, an assessment of temperatures at critical points of structures was carried out, and it is pointless to assess the likelihood of condensation formation on the inner surfaces of the lantern – their temperature is almost equal to that of the street, and condensation in the under-roof space will be guaranteed; however, in accordance with the project of a comprehensive restoration [25], it is proposed to isolate the under-roof space from the under-lamp and exhibition spaces, and when assessing the possibility of condensation formation on the inner surfaces of the under-lamp contour, the same microclimate parameters were adopted in the under-lamp space, as in the exhibition halls;

– If the historical metal structures of the lantern and side lamp (options 1–7) are preserved during the restoration process, condensation is very likely to fall on them; however, in option 7, this is possible both for a short time and at "especially extreme" negative outside temperatures (below minus 30 ^{0}C);

– Thermal insulation linings made of polystyrene foam do not greatly affect the resistance to heat transfer, but they significantly increase the tempera-

Fig. 3. Amazing "resoration" of translucent structures

tures at critical points of the structure, which reduces the likelihood of condensation on the frames.

4. RECOMMENDATIONS FOR RESTORATION OF HISTORICAL TRANSPARENT COATINGS

Based on the results of the surveys carried out the following recommendations were issued for the restoration of historical translucent coatings of the Pushkin State Museum of Fine Arts aimed at restoring and increasing the efficiency of metal structures of two circuits (skylight and plafond) installed in 1912 according to the project of V.G. Shukhov.

4.1. General results:

1. Despite the fact that the reports [33, 34] made a conclusion about the possibility of further operation of the structures of translucent coatings, the authors strongly recommend an additional assessment of the strength and performance of the load-bearing and other metal structures. This is largely due to both their unsatisfactory condition and the fact that, in accordance with the calculations carried out, it is recommended to use glass for the lantern one and a half times heavier than the existing one, and for the side-lamp – a glass unit three times heavier than the glazing available today.

2. It is necessary to provide for the restoration of the natural ventilation systems of the under-roof space, originally planned by the architect R.I. Klein and muffled, apparently, during repeated subsequent repairs.

3. It is necessary to provide for a high-quality vapour barrier of the exposure area from the under-roof space to exclude the ingress of moist air and the formation of condensation and frost on the inner surfaces of the lantern.

4.2. Skylight:

1. In accordance with the calculations of the strength of the glass, it is recommended to use laminated glass instead of 4 mm thick glass 3.3.1. If it is impossible to use laminated glass due to insufficient strength of the metal structures, it is possible to use sun-protective tempered or heat-strengthened glass with a thickness of 5 mm.

2. Metal structures are affected by large-scale corrosion, and therefore during their restoration it is necessary:

– To disassemble and replace defective structural elements;

– To clean them from traces of numerous paints carried out over the past 100 years;

– Carry out a thorough cleaning of rust, as well as processing with modern anti-corrosion compounds of absolutely all structural elements;

– There is a fear that some structural parts cannot be restored and will require replacement;

– With the possible replacement of historical elements with "remakes" due to the complete impossibility of their restoration, it is necessary to exclude the use of modern materials that can enter into an electrochemical reaction with historical materials;

– New painting of elements of metal structures should be carried out only after carrying out the above measures.

3. When replacing glass, should be noted:

– The glasses in each segment must have such horizontal dimensions that there is a gap of (5–6) mm between the glass and the T-profiles (on both sides); the vertical size of the glass in the segment is considered equal to the distance between the midpoints of the horizontal steel corners minus 10 mm;

– Glass fixing should be done using spacer double-sided self-adhesive gaskets, for example, "Robiflex", which 2 mm thick on one side is glued to the horizontal shelf of the T-profile along its entire length, and the other side to the glass, and Gasket "Robiflex" 5 mm thick on one side is glued to the outer flange of the steel corner along the entire length, and the other side to the glass;

– After the glass is placed in the segments, the formed gaps ((5–6) mm between glass and T-bars,

10 mm between glasses horizontally) must be filled with a structural glazing sealant;

– Work on replacement of glass and restoration of the frame must be carried out in conjunction with roofers to prevent damage to glass after replacing steel sheets at the bottom of the slope and in the ridge of the roof;

– The installation of double-glazed windows or energy-saving glass for this glazing circuit is impractical, because "Puffs" for ventilation of the under-glass space practically "to naught" the heat-saving properties of these glasses;

– Restoration of the translucent cover of the lantern is possible in two main variants: a) reproduction of the existing system developed by V.G. Shukhov, using special clamps to create additional ventilation; b) reproduction of the standard for modern translucent coverings of solid glazing of the lantern. In the first of them, it is necessary to preserve (restore) the additional ventilation system envisaged during the initial construction through the slots in the glazing, which are formed by metal clamps. For this, it is necessary to develop and manufacture new clamps, possibly from modern polymer materials.

4. Due to the unsatisfactory maintenance of this translucent coating, it becomes completely "not translucent". Probably, one should consider the issue of using modern self-cleaning (hydrophobic) glasses, which are produced by all major glass companies, as part of the triplex. The coatings of these glasses allow natural precipitation to wash off a significant part of the dirt on the glasses.

5. It is absolutely imperative that devices are provided to protect the under-roof space from direct sunlight. On clear days, even during the cold season, the temperature in this zone exceeds all permissible limits. In this regard, we recommend motorized curtains made of metallized polymer fabrics, which should be installed on the slopes of lanterns overlooking the solar rumba of the horizon (southern, southeastern, southwestern and western). Such sun protection devices are produced by many companies (for example, one of the leading manufacturers of solar protection systems, Renson, Belgium). These devices can be installed under the ridge and will not disturb the architectural appearance of the building.

4.3. Sidelight

1. The scheme of the restoration of the sidelight contour depends on the decision on whether the historical metal structures will be preserved or replaced. Until the moment this article was submitted to the editors, this decision had not been made.

2. In the first case, option 7 is optimal (see above). In this case, heat-strengthened or tempered outer glasses should be used – in order to minimize the risks of their destruction and the ingress of foreign objects on the glass of the plafond.

3. In the second case, we consider it expedient to use one of the options for effective aluminium profiles with thermal break, for example, option 13 (see above), and change the geometry of the lamp post from trapezoidal to triangular.

4. In any reconstruction option when using double-glazed windows (with the exception of options 12 and 13), heat-insulating linings should be used, which can significantly increase the temperatures at critical points of the structure.

5. When carrying out computer modelling, the thermal characteristics of the side lamp were considered separately from the cover. However, the instrumental examinations carried out showed that when jointly assessing these contours of translucent structures, approximately 0.25 $m^{2\cdot\circ}C/W$ can be added to the calculated heat transfer resistance of the headlamp structure.

4.4. Plafond

1. In the shade, it is advisable to use a laminated glass composed of two tempered or heat-strengthened glasses with a thickness of 4 mm each or tempered glass with a thickness of 6 mm with a protective scattering film, which simultaneously functions as a glass lamination and protection from falling of glass fragments into the exhibition halls.

2. The degree of matting of laminated glass should be discussed with the museum specialists responsible for the lighting of the exhibits. In this case, a film with a maximum light transmission coefficient should be used.

We present these recommendations in such detail precisely because they all work only when they are fully implemented.

5. CONCLUSION

The main purpose of surveys of historical windows and translucent coverings of the main building of the Pushkin Museum [1, 24, 27, this article] were an objective assessment of the current state of these

structures, mounted in 1912, and the development of recommendations for their improvement and energy efficiency with the maximum preservation of the elements that are subject to protection in accordance with the Federal Law of June 25, 2002?73-FZ "On Objects of Cultural Heritage (Monuments of History and Culture) of the Peoples of the Russian Federation." The authors are sure that as a result of numerous examinations and computer assessments, they have developed rational recommendations for the use of modern materials and identified optimal solutions to improve the energy efficiency of historic windows and light-transparent coatings.

The results of these surveys can be useful in the restoration of historic buildings. NIISF RAASN is ready to take part in similar works both in Moscow and in other regions of the Russian Federation.

The authors hope very much not to come across any more "restorations" like the one shown in Fig. 3.

REFERENCES

1. Alexander V. Spiridonov and Nina P. Umnyakova Inspection of the State (General and Instrumental) of Historical Translucent Structures of the Pushkin State Museum of Fine Arts// Light & Engineering, 2019, Vol. 27, # 3, pp. 26–31.

2. URL: https://tybet.ru/content/news/index.php?SECTION_ID=605&ELEMENT_ID=106288&sphrase_id=3536914 (date of the application: 07.06.2019).

3. URL: https://tybet.ru/content/news/index.php?SECTION_ID=605&ELEMENT_ID=99734&sphrase_id=3536942 (date of the application: 07.06.2019).

4. URL: https://tybet.ru/content/news/index.php?SECTION_ID=605&ELEMENT_ID=107525&sphrase_id=3536945 (date of the application: 07.06.2019).

5. URL: https://www.mk.ru/moscow/2018/11/12/v-rossii-raskryta-set-makhinatorovrestavratorov.html (date of the application: 07.06.2019).

6. URL: https://tybet.ru/content/news/index.php?SECTION_ID=609&ELEMENT_ID=91395&sphrase_id=3536934 (date of the application: 07.06.2019).

7. URL: https://tybet.ru/content/news/index.php?SECTION_ID=374&ELEMENT_ID=100297&sphrase_id=3536936 (date of the application: 07.06.2019).

8. URL: https://tybet.ru/content/news/index.php?SECTION_ID=605&ELEMENT_ID=105548&sphrase_id=3536940 (date of the application: 07.06.2019).

9. URL: https://tybet.ru/content/news/index.php?SECTION_ID=605&ELEMENT_ID=105601&sphrase_id=3536939 (date of the application: 07.06.2019).

10. URL: https://tybet.ru/content/news/index.php?SECTION_ID=605&ELEMENT_ID=104754&sphrase_id=3536933 (date of the application: 07.06.2019).

11. URL: https://tybet.ru/content/news/index.php?SECTION_ID=605&ELEMENT_ID=106717&sphrase_id=3536918 (date of the application: 07.06.2019).

12. URL: https://tybet.ru/content/news/index.php?SECTION_ID=605&ELEMENT_ID=105486&sphrase_id=3536946 (date of the application: 07.06.2019).

13. URL: https://tybet.ru/content/news/index.php?SECTION_ID=605&ELEMENT_ID=98994&sphrase_id=3536938 (date of the application: 07.06.2019).

14. URL: https://tybet.ru/content/news/index.php?SECTION_ID=605&ELEMENT_ID=104966&sphrase_id=3536958(date of the application: 07.06.2019).

15. URL: https://tybet.ru/content/news/index.php?SECTION_ID=605&ELEMENT_ID=105915&sphrase_id=3536919 (date of the application: 07.06.2019).

16. URL: https://tybet.ru/content/news/index.php?SECTION_ID=605&ELEMENT_ID=103759&sphrase_id=3536931 (date of the application: 07.06.2019).

17. URL: https://tybet.ru/content/news/index.php?SECTION_ID=605&ELEMENT_ID=104669&sphrase_id=3536947 (date of the application: 07.06.2019).

18. URL: https://tybet.ru/content/news/index.php?SECTION_ID=605&ELEMENT_ID=99820&sphrase_id=3536957 (date of the application: 07.06.2019).

19. URL: https://tybet.ru/content/news/index.php?SECTION_ID=605&ELEMENT_ID=105548&sphrase_id=3536940 (date of the application: 07.06.2019).

20. URL: https://tybet.ru/content/news/index.php?SECTION_ID=606&ELEMENT_ID=99645&sphrase_id=3536920 (date of the application: 07.06.2019).

21. URL: https://tybet.ru/content/news/index.php?SECTION_ID=605&ELEMENT_ID=106122&sphrase_id=3536943 (date of the application: 07.06.2019).

22. Boriskina I.V., Isaikin A.S., Balakina A.E. Modern Windows for Historical Buildings and Architectural Monuments [Sovremennue okna dlya istoricheskikh zdani i pamyatnikov arkhitektyru]//St. Petersburg, 2019, 145 p.

23. Khalil A.M.R. et al. Implementing Sustainability in Retrofiting Heritage Buildings. Case Study: Villa Antoniadis, Alexandria, Egypt // Heritage, 2018, Vol. 1, # 1, pp. 57–87.

24. Alexander V. Spiridonov, Nina P. Umnyakova, and Valkin Boris L. Examination of Condition of Historical Transparent Structures of the Pushkin State Mu-

seum of Fine Arts// Light & Engineering, 2020, Vol. 28, # 1, pp. 63–69.

25. "Comprehensive reconstruction, restoration and adaptation to modern museum technologies of the main building of the State Museum of Fine Arts named after A.S. Pushkin (Moscow, Volkhonka str., 12)" (documentation prepared by the Federal State Unitary Enterprise "Central Scientific and Restoration Design Workshops").

26. User manual for the "WINDOW-TECT" software package as part of the "THERM", "WINDOW" programs. M.: APROK-TEST, 2006, 140 p.

27. Alexander V. Spiridonov and Umnyakova Nina P. Computer Modelling and Recommendations for Restoration of the Historical Translucent Structures of the Pushkin State Museum of Fine Arts// Light & Engineering, Vol. 27, # 6, pp. 58–64.

28. Scientific and technical report of NIISF RAASN on the topic: "Thermal calculations of the zone of the translucent coating of the object" Complex reconstruction, restoration and adaptation to modern museum technologies of the main building of the State Museum of Fine Arts named after A.S. Pushkin ". – M., 2018. – 88 p.

29. SP 131.13330.2012 "Construction climatology. Updated edition of SNiP 23–01–99 ".

30. GOST 26602.1–99 "Window and door blocks. Methods for determining resistance to heat transfer".

31. GOST R54861–2011 "Windows and external doors. Methods for determining resistance to heat transfer".

32. SP 50.13330.2012 "Thermal protection of buildings", Updated edition of SNiP 23–02–2003 (with Amendment No. 1).

33. Scientific and technical report of NIIOSP named by N.M. Gersevanov on the topic "Complex reconstruction, restoration and adaptation to modern museum technologies of the main building of the State Museum of Fine Arts named after A.S. Pushkin (Moscow, Volkhonka st.,12), Vol. 4. Results of inspection of metal skylights of the building", Moscow, 2015, 460 p.

34. Scientific and technical report of the Research Center "Construction" "On the corrosion resistance of existing bearing structures of the coating". Volume 3, 2018, 109 p.

Alexander V. Spiridonov,
Ph.D. in Technical Sciences, graduated from the Moscow Power-Energy Institute (MPEI) in 1975 on specialty "Lighting and Light sources". At present, he is the Fellow in Chief of Research of the NIISF of RAACS, President of the Association of Manufacturers of Energy Efficient Windows (APROK), Laureate of the RF Government Prize in Science and Technology

Nina P. Umnyakova,
Dr. of Technical Sciences, Associate Professor. She graduated from the Moscow Civil Engineering Institute. At present, she is Deputy Director of the NIISF of the RAACS. Her research interests are thermal protection of buildings, energy saving, evaluation of thermal protection qualities of cladding in the presence of reflective thermal insulation

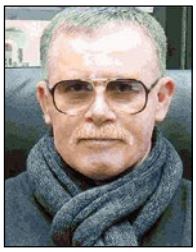

Boris L. Valkin,
Dr. of Architecture. In 1974, he graduated from Moscow architecture institute (MARhi). At present, he is Professor of International Academy of Architecture, Moscow, and Associate Professor of MGSU

Light & Engineering
Vol. 28, No. 5, pp. 84–88, 2020

https://doi.org/10.33383/2020-08
Svetotekhnika #4, 2020, pp. 60–63

NEW RULES OF ACCESS TO LIGHTING TECHNICAL PRODUCTS IN THE EAEU MARKET: COMPLIANCE WITH FOUR TECHNICAL REGULATIONS

Tatiana A. Rozhkova[1] and Eugenia A. Sysoeva[2]

[1] Certification Centre for Electric Lamps and Lighting Products, Saransk
[2] Ogarev Mordova State University, Saransk
E-mail: sysoewa@mail.ru

ABSTRACT

The article discusses the new technical regulations of the Eurasian Economic Union: "On the Requirements for the Energy Efficiency of Energy-consuming Devices" (TR EEU048/2019) and "On the Limitation of the Use of Hazardous Substances in Electrical and Radio Electronics" (TR EEU037/2016), which establish uniform requirements for energy-consuming and containing regulated (hazardous) substances of products, including products for lighting. It is shown that the compliance of lighting products with existing and newly introduced technical regulations during its manufacture and the implementation of conformity assessment procedures will protect the Eurasian market from low-quality, unsafe and energy-inefficient products.

Keywords: lighting products, energy efficiency, resource saving, Eurasian Economic Union, technical regulation, conformity assessment, safety, energy efficiency classes, standards, label, directives and regulations of the European Union

1. INTRODUCTION

The prerequisite for product access to the market of the countries of the Eurasian Economic Union (EEU) is the compliance of the delivered products with the requirements of the EEU technical legislation, guided by which the products are put into circulation on the territory of the Union only if it meets the requirements of the EEU technical regulations (TR of the Customs Union). Product compliance with the TR requirements is carried out through the conformity assessment procedure of technical TR requirements, the effect of which extends to it in order to obtain permits established in the EEU: certificates of conformity and declarations of conformity, which have equal legal force and the right to apply the conformity mark – EEU marking. Products that have not passed the conformity assessment procedure of the TR requirements, which apply to it, should not be marked with a single sign of circulation on the Union market and shall not be allowed on its territory to be put into circulation. Such a system of technical regulation in the EEU not only helps protect the internal market of the Union from low-quality, unsafe and energy-inefficient products, but also contributes to the development of export potential and promotion of products to the markets of other countries.

2. NEW TECHNICAL REGULATIONS: ENERGY EFFICIENCY REQUIREMENTS AND THE CONTENT OF HAZARDOUS SUBSTANCES IN LIGHTING PRODUCTS

The process of establishing common requirements and rules for access of lighting products to the Russian market began with the bring into force on February 15, 2013 of two TRs [1, 2], used in the form of certification with an assessment of electrical and fire safety, as well as electromagnetic compatibility. Starting from 2016, in assessing the

conformity of lighting products with these TRs, requirements for photo-biological safety and for restrictions related to the exposure of a person to electromagnetic fields are additionally included.

In March 2018, TP [3] was put into action, establishing new requirements for products of electrical engineering and radio electronics in terms of limiting the use of harmful substances in their composition during development and manufacture. According to this TR, the list of products covered by it includes "Light Sources and Light Equipment, Including Equipment Built into Furniture", for which special requirements have been established to limit the use of hazardous substances – mercury and lead. The content of this TR is maximally harmonized with international standards and rules, including the legislation of the European Union (EU) on the restriction of the use of hazardous substances in electrical and electronic equipment, according to the EU directive [4].

Considering the need for a lot of preparatory work in connection with the implementation of the TR [3], the decision of the Board of the Eurasian Economic Commission (EEC) dated February 28, 2017 No. 24 approved the transitional provisions of this TP, according to which production was allowed until March 1, 2020 and the release into circulation of products of electrical and radio electronics, including lighting, without a conformity assessment and documents on conformity assessment requirements of the regulations. Such an approach with a delay in the implementation of the TP [3] in terms of assessing the conformity of products to the requirements of this TP was necessary for preparatory work for the fulfilment of TP requirements by certification bodies, accredited testing laboratories and importers of products. Thus, starting from March 1, 2020, for access to the EEU market, lighting products, the list of which is given in the TR [3], must undergo a conformity assessment procedure and be released to the Union market only if they comply with the standards of this TR, as well as the requirements of the TR [1, 2].

In order to ensure energy efficiency and resource conservation within the framework of the EEU, as well as to prevent actions that mislead consumers about the energy efficiency of energy-consuming devices, on August 8, 2019, the EEC Council adopted the TR [5], which establishes requirements for energy efficiency and resource conservation of energy-consuming devices, which include lighting products. TR [5] will enter into force on September 1, 2021. The new TR will be able to prevent the actions of unscrupulous entrepreneurs who mislead consumers about the energy efficiency of energy-consuming devices. The new TR sets the energy efficiency classes of energy-consuming devices, and for better informing customers, such devices will be equipped with special labels and technical sheets containing information about their energy efficiency. Energy-consuming devices will be released to the Union's market only if they comply with the TP [5] standards and the requirements of other TPs that apply to them and pass the conformity assessment procedure. Such products receive the right to be marked with a single sign of product circulation on the EEU market. In accordance with the decision of the EEC Council, a phased implementation of the individual requirements of the EEU TR048/2019 is planned, which will ensure a smooth transition of manufacturers of energy-consuming devices to uniform mandatory requirements.

Requirements for energy efficiency of specific types of energy-consuming devices are formulated in 19 appendices to TR [5], of which three relate to lighting products:

– Electric lamps;

– Fluorescent lamps without built-in ballasts, gas discharge lamps HP, ballasts and luminaires for such lamps;

– Directional light bulbs, LED bulbs and related equipment.

The annexes to TR [5] for lamps, ballasts and luminaires with such lamps contain the necessary terms and definitions, requirements for product identification, labelling, operational documents, conformity assessment and energy efficiency, contain information on permissible deviations of the energy efficiency parameters for electric, fluorescent lamps, without built-in ballasts lamps, HP gas-discharge lamps, ballasts and luminaires with such lamps, directional lamps, LED lamps and related equipment for testing (measurements) after they are put into circulation, including requirements for the content of labels and technical sheets as well as classes of lamps energy efficiency establishing.

According to TR [5], the requirement to contain information on the energy efficiency class in the technical documentation attached to these devices, in their labelling and on their labels, applies to the following lamps put into circulation in the customs territory of the EEU:

– Electric lamps of non-directional light for domestic and similar purposes, which can also be used for other purposes in addition to lighting or built into other electrical energy-consuming devices;

– Fluorescent lamps without built-in ballasts, gas discharge lamps HP, ballasts and luminaires for such lamps, also if they are built into other energy-consuming products;

– Both individual and built-in other products directional lamps, LED lamps, as well as related equipment intended for installation between the power supply network and lamps, including ballasts, control devices and luminaires.

To designate lamps with the highest energy efficiency, the energy efficiency classes "A +" and "A ++" are used, the class "E" is given as the least efficient, and the previously used classes with the lowest energy efficiency of the lamps "F" and "G" in TR are absent.

The Table shows, as an example, the energy efficiency classes of electric lamps, determined in accordance with the energy efficiency index (*EEI)*, which is calculated by the method described in TP [5].

TR [5] defines new requirements for energy efficiency and operational characteristics of lamps and luminaires, which, depending on their type, will be introduced in stages, starting from September 1, 2021, and then annually, with a delay in the introduction of the final stage until September 1, 2024. Such a phased introduction of requirements for the characteristics of products will allow manufacturers of lighting products to conduct a comparative analysis of the actual values of energy efficiency parameters and operational characteristics achieved in production and established in the normative and technical documentation (ND) with parameters regulated by TR [5]. According to the results of the analysis, enterprises will need to carry out a range of works to introduce appropriate changes in the normative documents if the indicators achieved in production are not lower than the standardized TR, or bring the product characteristics to the level established by the TR [5], with subsequent updating of the normative documents in order to bring it in accordance with the requirements of this TR.

Until the date of entry into force of the TR [5], that is Until September 1, 2021, the EEC Council must approve a list of standards containing the rules and methods for research (testing) and measurements, including the rules for sampling, necessary for the application and implementation of the requirements of this TR and the implementation of conformity assessment. Currently, there is a public discussion of the draft list of standards with the participation of interested parties (the protection of the interests of which the development of this list is aimed at), including product manufacturers, certification bodies, testing laboratories, state control and supervision bodies, consumers of products and other interested parties. In terms of lighting products in the draft, a list of standards is given for electric lamps; fluorescent lamps without built-in ballasts, gas discharge lamps HP, ballasts and luminaires for such lamps; on directional light bulbs, LED bulbs and related equipment, and is grouped in accordance with the TR [5] Annexes 9, 13, 14.

It should be emphasized that according to the provisions of the EEU agreement [6] for the objects of technical regulation, in respect of which the TR of the Union comes into force, these requirements become mandatory, and the previously existing laws of the Member States become invalid. Thus, after the entry into force of the TP [5], all are previously existing national regulations regarding the requirements for lighting devices and electric lamps used in AC circuits, as well as their energy efficiency classes, which should be contained in the technical documentation attached to these products in the marking and on their labels, will lose their force.

In TR [5], certification is established for evaluating the conformity of all types of lighting products as a single form of conformity assessment. After the TR [5] is put into action, the applicant will have the opportunity to obtain one certificate of compliance with the requirements of four TRs immediately [1–3, 5] to carry out certification of lighting products. Moreover, the analysis of the state of production, which is mandatory for certification of mass-produced products, can be carried out once, which will significantly save the applicant's money. If there is an act of analysis of production carried out earlier by the certification body in the framework of certification of lighting products for compliance with the requirements of TR [1], and (or) TR [2] and (or) TR [3], when certifying products for compliance with the requirements of TR [5] additional analysis of the state of production is not required if no more than three years have passed from the date of analysis. We emphasize that obtaining a certificate of compliance with four TRs in one certification body will be possible subject to accreditation by the Federal Accreditation Service and inclusion in the unified reg-

Table. 1. Energy Efficiency Classes for Electric Lamps (EEU TR048/2019, sect. VI, Table. 1 of Appendix No. 14)

Energy efficiency class	Energy efficiency index	
	For lamps (light sources) of non-directional light	For lamps (light sources) of directional light
A ++	*EEI* <= 0.11	*EEI* <= 0.13
A +	0.11 < *EEI* <= 0.17	0.13 < *EEI* <= 0.18
A	0.17 < *EEI* <= 0.24	0.18 < *EEI* <= 0.4
B	0.24 < *EEI* <= 0.60	0.4 < *EEI* <= 0.95
C	0.60 < *EEI* <= 0.80	0.95 < *EEI* <= 1.20
D	0.80 < *EEI* <= 0.95	1.20 < *EEI* <= 1.75
E (least effective)	*EEI* > 0.95	*EEI* > 1.75

ister of certification bodies and testing laboratories (centres) of the EEU (Customs Union). Moreover, the certification body must have in the field of accreditation all four TR and experts in lighting products with certificates of competence in this field.

TR [5] establishes the obligation of sellers to inform buyers about the energy efficiency class of energy-consuming devices and about other energy efficiency parameters when selling, including remotely. The energy efficiency label for electric lamps should contain the following information: name or trademark (if any) of the manufacturer; model designation; energy efficiency class; estimated energy consumption in kWh per 1000 hours of lamp operation. The label for energy efficiency of luminaires should contain the following information: name or trademark (if any) of the manufacturer; model designation; information about the lamp (type, design, compatibility); energy efficiency class; information in accordance with one of the options specified in the technical regulations.

The TR [5] does not provide label forms for energy-consuming devices; therefore, the EEC Council established that this TR will not enter into force without approving the labels of energy-consuming devices of different types and the rules for their design, which the EEC should develop before March 1, 2021. In this regard, TR [5] will begin to operate no earlier than September 1, 2021 after the requirements establishing the label forms of energy-consuming devices of various types and the rules for their design come into force.

In order to prepare the business community for the transition to the requirements of the TR [5], it is assumed that until September 1, 2023, the production and circulation of products in the territories of the EEU Member States will be allowed:

– A mandatory assessment of compliance with the mandatory requirements for energy efficiency established by acts that are part of Union law or the legislation of the EEU Member State, without documents on a mandatory assessment of compliance and without marking with a national conformity mark (a market circulation mark);

– If there are documents on the assessment of the conformity of products with the mandatory requirements for energy efficiency, previously established by acts that are part of Union law or the legislation of the EEU Member State issued or adopted before the TR entry into force. The draft decision of the EEC Board also provides that the circulation of such products is allowed during its service life, established in accordance with the legislation of the EEU Member State.

It is important to note that the requirements of TR [5] are based on the European approach and are largely harmonized with the requirements of directives and regulations of the European Union. Currently, in the EU, in accordance with the regulation [7], the system of energy efficiency classes is being reviewed, which are reflected on the label of energy efficiency of products. A new product labelling will be established with an updated system of energy efficiency classes in comparison with the directive [8], which was repealed on August 1, 2017 by the regulation [7]. Changes in labelling and energy efficiency class systems will also affect lighting products, as delegated regulation [9], supplementing directive [8] regarding energy efficiency labelling of electric lamps and luminaires and described in detail in article [10], will continue to be applied in the EU until the relevant changes, the introduction of which according to regulation [7], is planned to be completed by 2030.

3. CONCLUSION

Energy-consuming devices, including lighting products, are widely used products that have a significant share in the energy balance of the Russian Federation and thus have a significant impact on the total consumption of fuel and energy resources, greenhouse gas emissions and energy security of the state, and the state of the environment. The adoption of TR [5] is a necessary and relevant solution to ensure the energy and environmental safety of the Russian economy. The introduction of requirements for energy efficiency and the phased tightening of the criteria for classifying lighting products as more energy efficient are based on scientific and technical prerequisites, structural reserves and fundamental possibilities for increasing the energy efficiency of products.

The compliance of lighting products with their assessment of the requirements of the newly introduced TR [3, 5], as well as the requirements of the existing TR [1, 2], will serve as a guarantee of safe, high-quality and energy- efficient products entering the Eurasian market.

REFERENCES

1. Technical regulation of the Customs Union "On the safety of low-voltage equipment" (TR CU004/2011) (as amended on December 9, 2011). URL: http://www.docs.cntd.ru/document/902299536 (accessed: 01/10/2020).

2. Technical regulations of the Customs Union "Electromagnetic compatibility of technical means" (TR TS020/2011). URL: http://www.docs.cntd.ru/document/902320551 (accessed: 01/10/2020).

3. Technical regulation of the Eurasian Economic Union "On the restriction of the use of hazardous substances in electrical products and radio electronics" (TR EEU037/2016). URL: http://docs.cntd.ru/document/420387089 (accessed: 01/10/2020).

4. Directive 2011/65 / EU RoHS of the European Parliament and of the Council of June 8, 2011 on the restriction of the use of certain hazardous substances in electrical and electronic equipment (EU Directive 2011/65 / EU RoHS of the European Parliament and of the Council of the EU dated June 8, 2011 to limit the content of harmful substances in electrical and electronic equipment). URL: http://www.schmidt-export.ru/sites/default/files/pdf/ce_cert/2011–65_rohs-en.pdf (accessed: 01.10.2020).

5. Technical regulation of the Eurasian Economic Union "On requirements for the energy efficiency of energy-consuming devices" (TR EAEU048/2019). URL: http://docs.cntd.ru/document/564066230 (accessed: 01/10/2020).

6. Treaty on the Eurasian Economic Union (Astana, May 29, 2014) with comparisons and additions. URL: https://base.garant.ru/70670880/ (accessed 03.03.2020).

7. Regulation (EU) 2017/1369 of the European Parliament and of the Council of 4 July 2017 setting a framework for energy labelling and repealing Directive 2010/30 / EU (Regulation (EU) 2017/1369 of the European Parliament and of the Council of 4 July 2017, setting the framework for energy labelling and repealing Directive 2010/30 / EU) // Official Journal of the European Union, 07.28.2017, L 198, pp. 1–24.

8. Directive 2010/30 / EU of the European Parliament and of the Council of 19 May 2010 on the indication by labelling and standard product information of the consumption of energy and other resources by energy-related products (the indication Directive labeling and in standard product information, information on energy consumption of energy-consuming products and other resources) // Official Journal of the European Union, 06.18.2010, L 153, pp. 1–12.

9. Commission Delegated Regulation (EU) No 874/2012 of 12 July 2012 supplementing Directive 2010/30 / EU of the European Parliament and of the Council with regard to energy labelling of electrical lamps and luminaires (Delegated Regulation supplementing Directive 2010/30 / EU regarding the energy labeling of electric lamps and luminaires) // Official Journal of the European Union, 09.26.2012, L 258, pp. 1–20.

10. Abrashkina M.L., Sysoeva E.A. Requirements for Energy Efficiency, Labelling and Eco-Design of Lighting Products: European Experience // Light & Engineering, 2017, Vol. 25, # 4, pp. 130–133.

Tatiana A Rozhkova, engineer. In 1976, she graduated from Ogarev Mordovia State University. At present, she is leading specialist of the Centre for certification of electric lamps and lighting products. Her research interests: organization and conduct of work on the assessment (confirmation) of compliance of lighting products

Eugenia A. Sysoeva, Doctor of Economy Siences, Associate Professor. In 1998, she graduated from Ogarev Mordova State University. At present, she is a Head of the Department of Statistics, Econometrics and Information Technology in Management, National Research Mordovian State University named after N.P. Ogarev. Her research interests: study of the problems of quality and competitiveness of lighting products

Light & Engineering
Vol. 28, No. 5, pp. 89–96, 2020

https://doi.org/10.33383/2020-025
Svetotekhnika #4, 2020, pp. 66–70

THE INFLUENCE OF THE LED LUMINAIRES ELECTRICAL PARAMETERS ON THEIR CORRELATED COLOUR TEMPERATURE DURING OPERATION MODE

Sergei S. Kapitonov[1,2], Alexei S. Vinokurov[2], Sergei V. Prytkov[1,2], Sergei Yu. Grigorovich[1], Anastasia V. Kapitonova[1], Dmitry V. Gushchin[2], Sergei A. Medvedev[1], and Dmitry V. Wilhelm[1]

[1] Ogarev Mordovia State University, Saransk
[2] Lodygin NIIIS, Saransk
E-mail: kapitonov_ss@vniiis.su

ABSTRACT

The article describes the results of comprehensive study aiming at increase of quality of LED luminaires and definition of the nature of changes in their correlated colour temperature (CCT) in the course of operation. Dependences of CCT of LED luminaires with remote and close location of phosphor for 10 thousand hours of operation in different electric modes were obtained; the results of comparison between the initial and final radiation spectra of the luminaires are presented; using mathematical statistics methods, variation of luminaire CCT over the service period claimed by the manufacturer is forecast; the least favourable electric operation modes with the highest CCT variation observed are defined.

The obtained results have confirmed availability of the problem of variation of CCT of LED luminaires during their operation. Possible way of its resolution is application of more qualitative and therefore expensive LEDs with close proximity of phosphor or LEDs with remote phosphor.

The article may be interesting both for manufacturers and consumers of LED light sources and lighting devices using them.

Keywords: LED luminaire, electric mode of operation, supply current, radiation spectrum, radiant flux, correlated colour temperature

1. INTRODUCTION

The problems of LED lighting development in Russia are primarily caused by lack of relevant regulatory framework, which allows unfair manufacturers create lighting products of poor quality and confuse consumers by claiming, for instance, insubstantially long service life for LED lighting devices (LD), about (70–100) thousand hours [1, 2].

In 2018, the standard of the Association of LED and LED-Based Systems Manufacturers became effective [3]. It united general requirements to LDs, requirements to their photometric, colorimetric, and electric parameters, electromagnetic compatibility, safety, reliability and warranty liabilities. According to the standard, one of the standardised colorimetric parameters of LDs is correlated colour temperature (CCT) which is calculated based on a LD radiation spectrum [4].

The value of CCT should comply with the range of permissible deviations from the corresponding rated value of CCT [5] which shall be declared by manufacturers in technical specifications and operational documentation with specification of the size of areas of possible deviations in MacAdam Ellipses [3].

At present, manufacturers of LED-based luminaires have no information on the nature of changes of CCT of these devices in the course of their operation due to degrading of LEDs with consideration

Table 1. Technical Specifications of the Tested Luminaires

№	Parameter	Manufacturer 1	Manufacturer 2
1	Rated power, W	24	19
2	Rated luminous flux, lm	3750	2580
3	Rated LED current as per the data sheet, mA	350	350
4	Rated current of LEDs in the luminaire, mA	350	260
5	CCT (K)	3000	4000
6	Service life, thousand hours	> 70	90

of their electric and thermal operation modes [6, 7]. Therefore, it is impossible to precisely evaluate service life of LED-based luminaires as manufacturers do not know in what time CCT of a luminaire will go beyond the specified limits even in the nominal operation mode [8]. With that, LEDs in luminaires often operate in electric and thermal modes which are different from the nominal one, therefore studies of their radiation spectra and their temporary changes in different operation modes remain a relevant problem.

In view of this, the goal of the work was to increase quality of LED-based luminaires by defining the nature of changes of CCT during their operation with consideration of the electric operation mode. To reach this goal, the following objectives were set:

– To obtain time dependences of luminaire CCT over 10 thousand hours of operation in different electric modes of operation;

– To compare radiation spectra of luminaires in the beginning with that after 10 thousand hours of operation;

– To forecast variation of luminaire CCT over the service life claimed by manufacturers using methods of mathematical statistics;

– To define electric modes of operation which are the least favourable for luminaires and demonstrate the highest variation of CCT over the course of operation.

It was assumed that the results of the study would allow manufacturers of LEDs and LED-based luminaires to understand the causes of variation of radiation spectra and CCT of these products in the course of operation and to take relevant measures in order to increase their service life [9].

2. METHODS

The study of time dependence of radiation spectrum and CCT was conducted using a series of LED-based luminaires by two Russian manufacturers in different electric modes of their operation. For ethical reasons, the names of manufacturers are not mentioned in the article. The luminaires by Manufacturer 1 are based on LED with remote phosphor, which, according to the manufacturer's data, allows them to keep its characteristics and parameter values close to rated ones over the entire service life. In the luminaires by the Manufacturer 2, LEDs with close location of phosphor (the most common type of LEDs) are used. Table 1 contains major technical specifications of the said luminaires.

The photo-colorimetric installation (approval certificate of measuring instruments No. RU.E.37.003.A NG 64752) was designed to measure luminous flux, CCT, and chromaticity coordinates in *x, y, z* (1931), *u, v* (1960) and *u,'v'* (1976) systems and used for measurements of radiation spectra and CCT. The operation principle of the installation is based on definition of the values of radiometric, photometric and colorimetric values by measuring absolute spectral radiant flux within the wavelength range of (360–1100) nm. CCT was defined automatically using software supplied with the installation. The latter consists of the integrating sphere *OL IS-7600*, the multi-channel spectrometer *OL 770 VIS/NIR* and the auxiliary lamp *A180* with the power supply source *OL 410–200*. The aluminium integrating sphere has diameter of 1950 mm and consists of two separate hemispheres, two output ports, lamp port (auxiliary) and the internal fixture of the lamp holder. Both hemispheres can be easily disconnected (for simplification of installation and replacement of the lamp or fixture parts). The sphere diameter allows us to measure luminaires with length of up to 1800 mm and maximum luminous flux of 200 klm. One of the output ports is connected with the entrance slit of the spectrometer using a fibre-optic cable. The light incident on the inner wall of the sphere gets into this slit via the

Table 2. Results of Measurements of CCT of the Luminaires in the Nominal Operation Mode

	Luminaire No. 1	Luminaire No. 2	Luminaire No. 3	Luminaire No. 4
CCT, K (Manufacturer 1)	3084	3066	3082	3100
CCT, K (Manufacturer 2)	4195	4230	4235	4198

Table 3. Ranges of Maximum Deviation of CCT Values for Corresponding Nominal Values

Nominal value of CCT, K	Central value of CCT and range of permissible deviations for 7-step MacAdam Ellipse, K	Central value of CCT and range of permissible deviations for 4-step MacAdam Ellipse, K
3000	3045 ± 175	3045 ± 100
4000	3985 ± 275	3985 ± 154

fibre-optic cable. Then it falls on the concave diffraction grid, which separates the light into monochromatic components and focuses it on the CCD matrix. After the light is reflected from the grid, each its monochromatic component falls on the section of the CCD matrix allocated for it. In front of the output hole of the sphere and in front of the auxiliary lamp inside the installation, protective screens are installed, which prevent escape of any direct radiation.

The following operating modes of the luminaires were selected for the study.

Mode 1

Nominal mode with LED current in the luminaire equal to the nominal one: 350 mA (Manufacturer 1) or 260 mA (Manufacturer 2) claimed by the manufacturer, and current ripple factor does not exceed 1 %.

Mode 2

Overload current mode with LED current in the luminaire, exceeding the nominal one. In luminaires by the Manufacturer 1, this current was 10 % lower than nominal one and equal to 390 mA (Table 1). Since nominal LED current in the luminaire by the Manufacturer 2 (260 mA) is less than rated (nominal) current for these LEDs (350 mA), it was decided to select the specified rated current as current overload of LED in the luminaire (Table 1). Current ripple factor of the luminaires by both manufacturers does not exceed 1 %.

Mode 3

The mode in which LED current in the luminaire is equal to nominal LED current and the current ripple factor is equal to 10 %. Ripple frequency in the modes 3 and 4 is 50 kHz.

Mode 4

The mode in which LED current in the luminaire is equal to nominal LED current and the current ripple factor is equal to 40 %.

The required supply currents of LED matrix of the luminaires were set by means of adjustable control devices (drivers) manufactured by the Argos-Trade company (Saint Petersburg) which allow to adjust output current from 240 mA to 390 mA [10] and necessary current ripple factors by changing and selecting output inductance of CD using the time dependence of current on the screen of the digital oscilloscope.

3. RESULTS

For the experiment, two lots each consisting of four luminaires by each manufacturer were selected. First, luminaire CCT values were measured in the nominal operation mode, Table 2.

The ranges of maximum deviation of CCT values from its corresponding nominal value as per the standard [3] are shown in Table 3. Tables 2 and 3 demonstrate that for the new luminaires (by the Manufacturer 1) the CCT variations comply with the requirements of the standard [3]. The deviation of CCT values of new luminaires (by the Manufacturer 2) is much higher and goes beyond permissible deviations for 4-step zones as per Table 3 (the upper limit of 4139 K).

The variations of radiation spectrum and CCT of the said luminaires over 10 thousand hours of operation were measured each 2 thousand hours. Time spent for measurements was not included in calculation of total operation time of the luminaires. Us-

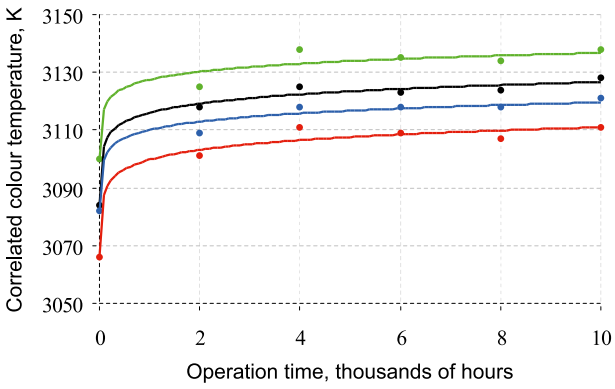

Fig. 1. Time dependences of CCT of the luminaires by the Manufacturer 1 in different operation modes: mode 1 (black); mode 2 (red); mode 3 (blue); mode 4 (green)

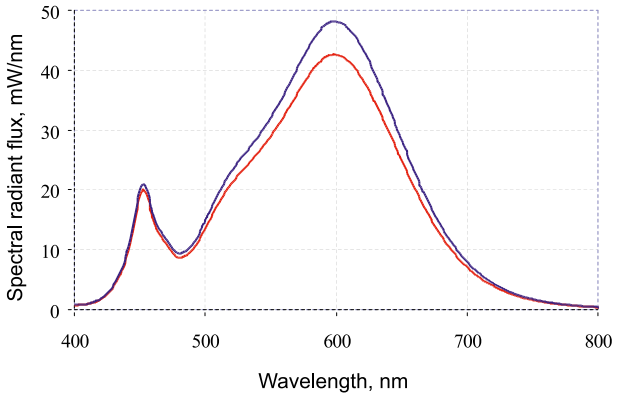

Fig. 2. Radiation spectra of the luminaire by the Manufacturer 1: initial (blue) and after 10 thousand hours of operation in mode 2 (red)

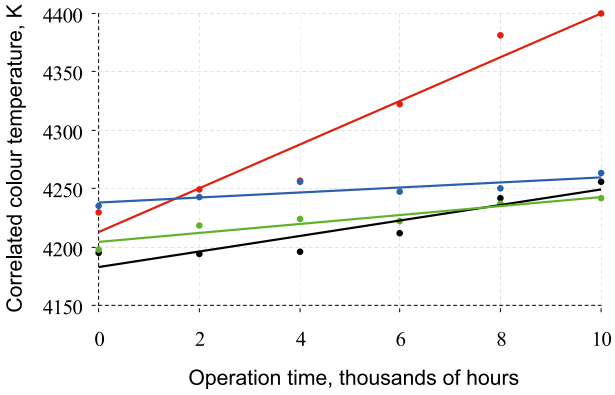

Fig. 3. Time dependences of CCT of the luminaires by the Manufacturer 2 in different operation modes: mode 1 (black); mode 2 (red); mode 3 (blue); mode 4 (green)

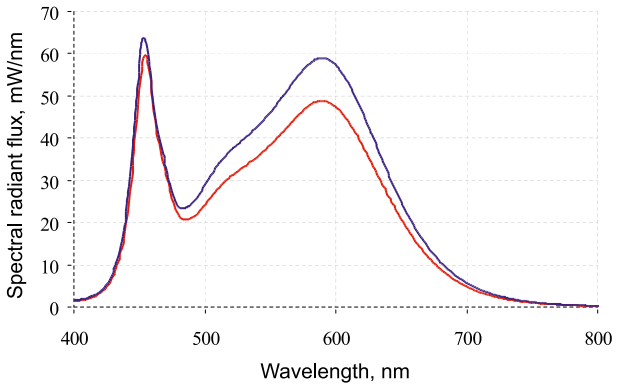

Fig. 4. Radiation spectra of the luminaire by the Manufacturer 2: initial (blue) and after 10 thousand hours of operation in mode 2 (red)

ing Table 2, corresponding operation mode was set for each luminaire.

Fig. 1 shows time dependences of CCT of the luminaires by the Manufacturer 1 in different operation modes. Optimal approximations (logarithmic) of these dependences, CCT, K on operation time t (thousand hours) obtained using *MS Excel* are as follows:

CCT = 4.5998·ln(t) + 3115.9 (mode 1); CCT = 4.8382·ln(t) + 3099.7 (mode 2);

CCT = 4.1064·ln(t) + 3110 (mode 3); CCT = 4.0043·ln(t) + 3127.4 (mode 4).

Fig. 1 shows that the rate of increase in CCT of the luminaires by the Manufacturer 1 is roughly the same in different modes of operation. After 10 thousand hours of operation, the values of CCT did not go beyond the ranges of permissible deviations for 4-step and 7-step zones (Table 3), the upper limits of which are equal to 3145 K and 3220 K respectively.

The highest variation of CCT was observed in a luminaire by the Manufacturer 2 operating in the Mode 2 (current overload) and the change of its radiation spectrum after 10 thousand hours of operation is shown in Fig. 2. The figure shows that peak spectral radiant flux at wavelength of about 600 nm corresponding to orange-red light has lowered by 6 mW/nm over this period, while the peak at wavelength of about 450 nm (blue light) has not changed much. This pattern explains that increase in CCT over time is related to increase in the share of the blue component in the radiation spectrum of the luminaire.

The results of tests of the luminaires by the Manufacturer 2 in different modes of their operation are shown in Fig. 3. Optimal approximations (linear) of these dependences also obtained using *MS Excel* are as follows:

CCT = 6.0359·t + 4184 (mode 1); CCT = 16.978·t + 4216.9 (mode 2);

CCT = 1.807·t + 4239.5 (mode 3); CCT = 3.4238·t + 4205.4 (mode 4).

The nature of variation of CCT over 10 thousand hours of operation of the luminaires by the Manu-

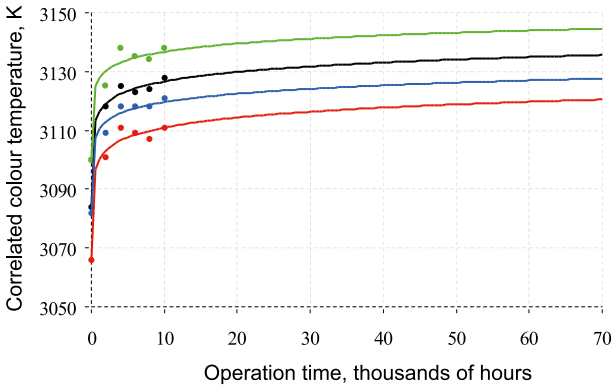

Fig. 5. Time dependence of CCT of the luminaires by the Manufacturer 1 over 70 thousand hours of their operation: mode 1 (black); mode 2 (red); mode 3 (blue); mode 4 (green)

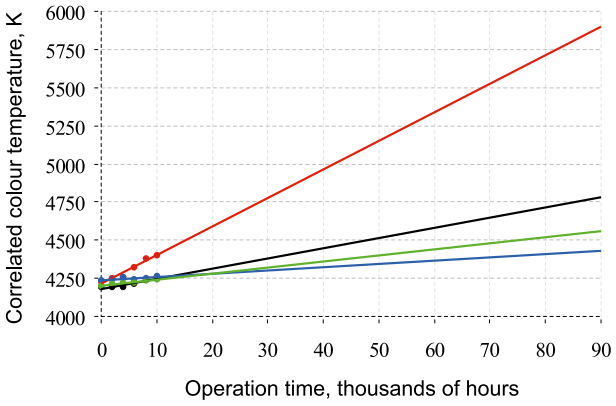

Fig. 6. Time dependence of CCT of the luminaires by the Manufacturer 2 over 90 thousand hours of their operation: mode 1 (black); mode 2 (red); mode 3 (blue); mode 4 (green)

facturer 2 is the same for all operation modes. The highest CCT increase rate was observed in mode 2.

CCT in this mode increased by 170 K and reached 4400 K, which is much higher than the upper limits of the permissible deviations for the 4-step and 7-step MacAdam Ellipses (Table 3).

The change of radiation spectrum of this luminaire operated in the mode 2 after 10 thousand hours of operation is shown in Fig. 4. In the peak area at wavelength of 590 nm, the decrease in spectral radiant flux was equal to value 10 mW/nm, while in the peak region at wavelength of 450 nm this value decreased by 4 mW/nm. Like in the case of the luminaire by the Manufacturer 1, this explains the increase in CCT in that case.

It was interesting to evaluate the limits of CCT variation of the said luminaires over the service life claimed by their manufacturers (Table 1). Given the duration of these periods, the methods of mathematical forecasting were applied based on the results of luminaire tests over 10 thousand hours. Possibility to forecast based on a rather short period of time is conditioned by the fact that, after 10 thousand hours of continuous operation, parameters and characteristics of LED start changing significantly due to degradation processes in the phosphor and the crystal, which is usually mentioned in data sheets of any LED or LED-based LD. Therefore, while forecasting on the basis of the first 10 thousand hours of operation of the luminaires, we consider the most favourable option, and if the luminaires do not comply with the specified requirements [3] in these conditions, then it is obvious that the claimed service life of the luminaires (Table 1) will not be real.

One of the most popular types of graphic forecasting (implemented in *MS Excel*) was used: extrapolation by building a trend line. This type of forecasting is based on building of a graph of the considered dependence using tabular data consisting of arguments and values of the function, superimposition of the trend line, and selection of one of the six types of approximation.

The results of forecasting of the time dependence of CCT of the luminaires by the Manufacturer 1 are presented in Fig. 5, which shows that "final" CCT values of the luminaires did not go beyond the ranges of permissible deviations specified in Table 3 for the 4-step and 7-step MacAdam Ellipses (the upper limits are equal to 3145 K and 3220 K respectively). Maximum CCT of 3143 K is shown by the luminaire operating in mode 4. The highest CCT variation, 50 K, is observed for the luminaire operating in mode 2.

The results of forecasting the time dependence of CCT of the luminaires by the manufacturer 2 are presented in Fig. 6, which shows that CCT values of each test mode goes significantly beyond the ranges of permissible deviations specified in Table 3 for the 4-step and 7-step MacAdam Ellipses (the upper limits are equal to 4139 K and 4260 K respectively). The maximum CCT variation of 1650 K, with which it reached 5880 K, is found in test mode 2.

4. CONCLUSION

Based on the conducted studies, the following conclusions may be drawn.

1. CCT of the luminaires by the Manufacturer 1 based on LEDs with remote phosphor did not ex-

ceed the ranges of permissible deviations as per the standard [3] in any test mode [3]. CCT of the luminaires by the Manufacturer 2 based on LEDs with close location of the phosphor significantly exceeds the upper limits of the ranges of permissible deviations [3] in each test mode. The reason of it is that in the LED with close location of phosphor, the latter, together with the crystal, suffers bigger thermal effect than the remote phosphor with corresponding crystal, and, therefore, they degrade and change CCT faster. The remote phosphor technology allowed us to solve this problem partially.

2. Resulting from degradation of phosphor and LED crystal, predominant decrease in the level of spectral radiant flux of LED-based luminaires over their operation within the wavelength range of (500–700) nm changes (increases) CCT of these products.

3. The highest variations of CCT of the luminaires by both manufacturers were observed in mode 2 (current overload), in which LEDs suffered thermal overloads that accelerated the degradation processes in the crystal and phosphor. However, in the luminaires by the Manufacturer 1, this mode did not causes fatal changes of CCT, while in the luminaires by the Manufacturer 2, CCT exceeded the limits of the ranges of permissible deviations already after 10 thousand hours of their operation. Therefore, the mode with supply current of LED higher than nominal current, which is often used by manufacturers to increase luminous flux of luminaires, is highly undesirable.

4. In terms of CCT variation rate of the luminaires by both manufacturers, modes 3 and 4 (with supply current ripple factors significantly higher than permissible values) are just slightly different from mode 1 (nominal).

5. A possible way to increase stability of CCT of luminaires in the course of operation is to use more qualitative (and hence expensive) LEDs with close location of phosphor or LEDs with remote phosphor.

REFERENCES

1. Chervinsky M. Failures of LED Luminaires: Causes and Prevention Methods [Otkazy svetodiodnykh svetilnikov: prichiny i sposoby preduprezhdeniya] // Sovremennaya svetotekhnika, 2015, # 4, pp. 42–52.

2. Nikiforov S.G. Relevance of Study and Necessity of Development of the Methods of Studying Degradation of Parameters of LED Based on Solid Solutions of AlGaInP and AlGaInN [Aktualnost izucheniya i neobkhodimost sovershenstvovaniya metodik issledovaniya degradatsii parametrov svetodiodov na osnove tvyordykh rastvorov AlGaInP i AlGaInN] // Poluprovodnikovaya svetotekhnika, 2012, # 15, pp. 36–37.

3. STO 69159079–01–2018 LED Luminaires.Technical and operational specifications: Requirements.

4. Nikiforov S.G. Development of Measurement Means and Methods of Control of Parameters of Semiconductor Emitters Based on AIIIBV Compounds Applied in High-Reliability Instruments [Razrabotka sredstv izmereniy i metodov kontrolya parametrov poluprovodnikovykh izluchateley na osnove soyedineniy AIIIBV, ispolzuemykh v vysokonadyozhnykh priborakh] / Extended abstract of Dr. Tech. Sci. (Eng.) Dissertation. Moscow, 2015, 39 p.

5. ANSI C78.377–2017 “American National Standard for Electric Lamps – Specifications for the Chromaticity of Solid State Lighting (SSL) Products”.

6. Liu Z., Yang B., Zhang C.E., Li Y., Zou J., Shi M., Qian X., Zheng F. Model prediction on the correlated color temperature of white LED based on chromaticity coordinate // Journal of Luminescence, 2019, Vol. 216, № 116652.

7. Lin D., Zheng P., He G. Color temperature tunable white LED cluster with color rendering index above 98 // EEE Photonics Technology Letters, 2017, Vol. 29, #12, pp. 1050–1053.

8. Kapitonov S.S., Prytkov S.V., Grigorovich S. Yu., Kapitonova A.V., Medvedev S.A., Slugina N.P. The Study of Variation of Colour Temperature and Radiation Spectrum of LED Luminaires over the Course of their Operation [Issledovaniye izmeneniya tsvetovoy temperatury i spektra izlucheniya svetodiodnykh svetilnikov v protsesse ikh ekspluatatsii] // Nauchno-tekhnicheskiy vestnik Povolzhya, 2019, Vol. 1, pp. 84–87.

9. Huang Y.-S., Luo W.-C., Wang H.-C., Feng S.-W., Kuo C.-T., Lu C.-M. How smart LEDs lighting benefit color temperature & luminosity transformation // Energies, 2017, Vol. 10, # 4, p. 518.

10. Bespalov N.N., Ilyin M.V., Kapitonov S.S. Testing equipment for LED luminaire control devices and fluorescent lamp electron ballasts [Oborudovaniye dlya ispytaniy upravlyayushchikh ustroystv dlya svetilnikov so svetodiodami i EPRA dlya lyuminestsentnykh lamp] // Svetotekhnika, 2017, # 4, pp. 42–46.

11. Bespalov N.N., Ilyin M.V., Kapitonov S.S. Testing equipment for LED luminaire control devices and fluorescent lamp electron ballasts // Light & Engineering, 2017, Vol. 25, #4, pp. 86–91.

Sergei S. Kapitonov,
Ph.D. In 2010, he graduated from the Ogarev Mordovia State University. At present, he is an Associate Professor of the Electronics and Nano-electronics sub-department of the Ogarev Mordovia State University and the Director for Scientific and Technical Development with Lodygin NIIIS. His research interests are: agricultural photonics, research and development of LED light sources and control devices for them, development and research of low-pressure discharge lamps

Alexei S. Vinokurov,
engineer. In 2008, he graduated from the Ogarev Mordovia State University. At present, he is the Director General of Lodygin NIIIS. His research interests**:** research and development of LED light sources and control devices for them, development and research of low-pressure discharge lamps

Sergei V. Prytkov,
Ph.D. In 2010, he graduated from the Ogarev Mordovia State University. At present, he is Associate Professor of the Lighting Engineering sub-department of the Ogarev Mordovia State University. His research interests: photometry, research and development of LED light sources and control devices for them, development and research of low-pressure discharge lamps

Sergei Yu. Grigorovich,
an engineer. In 2010, he graduated from the Ogarev Mordovia State University. Currently he is postgraduate student of the Electronics and Electric Engineering sub-department of the Ogarev Mordovia State University. His research interests: research and development of LED light sources and control devices for them

Anastasia V. Kapitonova,
engineer. In 2013, she graduated from the Ogarev Mordovia State University. At present, she is postgraduate student of the Light Sources sub-department of the Ogarev Mordovia State University. Her research interests: research and development of LED light sources and control devices for them

Dmitry V. Gushchin,
engineer. In 2020, he graduated from the Ogarev Mordovia State University. Currently he is the radio-electronic engineer with the Lodygin NIIIS. His research interests: research and development of LED light sources and control devices for them

Sergei A. Medvedev
graduated from the Bachelor's Programme of the Electronics and Nano-electronics sub-department of the Ogarev Mordovia State University in 2019. His research interests: research and development of LED light sources and control devices for them

Dmitry V. Wilhelm
graduated from the Bachelor's Programme of the Electronics and Nano-electronics sub-department of the Ogarev Mordovia State University in 2019. His research interests: research and development of LED light sources and control devices for them

Light & Engineering
Vol. 28, No. 5, pp. 97–105, 2020

https://doi.org/10.33383/2019-107
Svetotekhnika #3, 2020, pp. 44–50

A NOVEL STRATEGY FOR TRANSFORMATION OF CONVENTIONAL ROAD LIGHTING TO SMART ROAD LIGHTING

Mustafa Eyyup Gursoy[1], Burak Dindar[2], and Omer Gul[3]

Istanbul Technical University, Electrical Engineering Department, Istanbul, Turkey
E-mails: [1]mustafaeyyupgursoy@gmail.com,
[2]burakdindar@itu.edu.tr, [3]gulomer@itu.edu.tr

ABSTRACT

In recent years, smart road lighting (SRL) design and application researches has been increasing rapidly. However, SRL applications remain pilot project and cannot become widespread sufficiently. Main reason for this is that, although the cost of production of LED luminaires is reduced, when existing road lighting systems are transformed to LED road lighting, existing electrical installations and lighting poles cannot be used. Increased investment costs due to electrical installation and poles renovation, decrease interest in SRL transformation. In this study, an innovative solution is developed to decrease the costs of the SRL. First, a new LED luminaire is designed, which can work without changing the installations and poles of the existing projects. Then a test road is created using *DIALux* software, and the newly designed lighting installation is compared with completely redesigned one and conventional road lighting. Thus, contributions are provided for spreading of the SRL transformation, using low cost SRL approach.

Keywords: energy efficiency, LED luminaires, lighting, road lighting design, smart road lighting

1. INTRODUCTION

Nowadays, the communication possibilities of the devices increase with the developing technology. In this regard, many studies are performed and various concepts are developed. *Industry 4.0* is one of the concepts developed in this purpose. With the advent *Industry 4.0*, it has been possible to establish a faster network of objects, referred to as the Internet of Things, in which physical objects are coordinated with each other or larger systems [1]. Thus, objects that were formerly controlled by humans can now interact with each other through software and hardware mechanisms, such as algorithms, artificial intelligence, and wireless communication. In addition, they decide how the system works.

Variables that people may overlook due to carelessness are efficiently considered because there are no people in the decision-making mechanism of the Internet of Things [2]. All these technological developments have been utilized also in road lighting. In SRL systems, cameras and sensors measure external variables. The measured results are processed using algorithms to produce the desired data [3]. The data is transmitted to the network via wireless communication. The control mechanism is created by processing the data in the central control units. Thus, SRL systems are created that do not require human intervention, and efficiency is increased significantly.

In order to transform existing conventional road lighting systems to the SRL, it is necessary to add sensors to the existing system and establish communication networks, as well as to replace existing luminaires with controllable luminaires. High-pressure sodium (HPS) lamps used in conventional road lighting are difficult to dim, and the dimming steps are low. The lifetime of HPS lamps is shortened by frequent luminance changes. The closing and opening times are also long. LED luminaires have short

dimming time, easy and precise luminance adjustment. The lifetime of the LED luminaires does not change with frequent changes of luminance. The closing and opening times are very short [4]. LED luminaires also produce less harmonics than luminaires with HPS lamps [5]. Thanks to this information, LEDs are preferred instead of HPS lamps in the SRL.

Conventional road lighting systems do not provide appropriate lighting for changing situations [6]. Many important parameters for road lighting, such as traffic flow and vehicle speed change momentarily. Thus, driver safety, driving comfort and energy efficiency of the system are not ideal. Well-designed road lighting saves energy, time, labour and costs [7]. The investment costs are high due to the additional equipment needed for the SRL [8]. Another important factor that increases the investment costs is need to change the distance between poles and their length in the existing road lighting, because LED luminaires to be used instead of luminaires with HPS lamps cannot efficiently provide lighting in this conditions. When changing the distance between poles in road lighting, all electrical installations must be replaced. Furthermore, if the height of the pole is changed, new poles must be used. This situation significantly increases the cost of the SRL. Therefore, it is difficult to expect that the SRL will become widespread and preferred by decision makers, especially in developing countries like Turkey, where investments are made with limited resources. In contrast to increased investment costs, operating costs are expected to be decreased due to the high energy efficiency of the SRL. Two important parameters affect energy efficiency in the SRL. First, it is the use of LEDs instead of HPS lamps. LEDs have a much higher efficiency factor than HPS lamps used in conventional road lighting, so their energy consumption is considerably low. Secondly, when using LED luminaires in the SRL, sensitive dimming can be made. Another positive effect of this is reduction of CO_2 emissions. In a study performed in Saudi Arabia, it was observed that the CO_2 emissions were 900 % higher with the use of petroleum and petroleum products instead of renewable energy in the production of consumed energy for lighting [9].

When considering the benefits such as reduced energy consumption and CO_2 emissions, as well as improved driver comfort, the SRL is needed to be expanded rapidly. In this study, cost reducing solutions are proposed to accelerate the process of transformation to the SRL. Smart road lighting is created by replacing the luminaires with HPS lamps to LED luminaires without changing existing electrical installation and lighting poles. This reduces the cost of installation. In this respect, an appropriate LED luminaire is designed to be installed on existing poles. The relationship between the lighting pole geometries and the light distribution curves of the designed luminaires is examined. A test road is created in *DIALux* software, and the developed solutions are examined in the test road. The proposed solution is compared with the conventional road lighting and the situation that the whole system is renewed.

2. SMART ROAD LIGHTING

There are two important criteria in designing the SRL. The first is that road lighting conforms to guidelines and standards accepted and used around the world. The second is to enable the hardware in the road lighting installation to interact with each other. This study examines the guidelines used by International Commission on Illumination (CIE) and *Zigbee* wireless communication protocol for the design of road lighting project [10, 11].

In international standards and guidelines, the most important criteria for the SRL is luminance. Luminance is a measure of how bright a surface looks. The technical report CIE140–2000 describes in detail all the necessary parameters to achieve appropriate luminance [10]. In cases where the road lighting classes are changed due to dimming, these parameters must be adjusted appropriately for each road class. In this study, investigations are performed between *M*1 and *M*5 road classes, and all of these parameters are considered to achieve successful road lighting.

In addition, wireless communication is one of the most important elements of the SRL. Thanks to the wireless communication, the system becomes manageable from a single point. In this way, by putting the control in one place, controls made by people can be fully autonomous with a good algorithm. Thus, many variables can be calculated for very complex road lighting and dynamic, efficient lighting can be provided.

The SRL uses *Zigbee* wireless communication network. A fast and simple network structure can be established with *Zigbee* [11].The *Zigbee* protocol communicates with radio waves. Radio waves prop-

Table 1. Technical Data of Luminaires and Poles in Scenarios

	Classical road lighting	Only luminaires are replaced	Completely redesigned system
Power of luminaire	447 W	305 W	243 W
Luminous flux of luminaire	45866 lm	45192 lm	28862 lm
Pole heights	14 m	14 m	10 m
Pole distance	40 m	40 m	35 m
Pole numbers	25 pc.	25 pc.	29 pc.
Pole boom lengths	2.5 m	2.5 m	3 m
Pole boom angles	0˚	0˚	0˚
Arrangement type	Single row from the right	Single row from the right	Single row from the right

agate in the space at the speed of light. The speed of the radio waves should be considered, as it will cause a delay in calculating the speed of the vehicles that pass on the road.

3. CASE STUDY

When making the roads smart, that is actually to answer the questions:

– How the topology of the network will be;

– How the system will follow a strategy in case of a possible failure;

– How dynamic lighting of the roads will have an impact on the drivers.

Before doing this, it should be analysed using questionnaires and tests to make a decision about optimum design. In this study, a test road is created in the computer environment to determine why it is necessary to get road lighting smart and which method of transforming the SRL is more appropriate.

3.1. Creating the Test Road

In this part of the study, a test road is created according to the LED lighting regulation prepared by *Turkish Electricity Distribution Corporation (TEDAŞ)* [12]. The test road has three lanes, each lane is 3.5 m wide and the test road is 1000 m long. When positioning poles along the test road, the first pole is positioned at half the selected pole distance from the starting point. Accordingly, the number of poles is determined.

The test road is created according to three different scenarios. The first is the conventional road lighting. In the second scenario, only luminaires with HPS lamps in conventional road lighting are replaced with LED luminaires. In this case, only the luminaires are modified and other parameters, such as pole distance and pole heights are the same as conventional road lighting. In the third scenario, all the electrical instalments such as pole distance, pole heights, luminaires etc. are designed from the beginning by changing all these parameters. Thus, the SRL is created. The details of designs for these three scenarios are shown in Table 1.

In the third scenario, the parameters are selected in order to minimize energy consumption. Thus, each scenario can be compared with high accuracy, considering energy efficiency. In all scenarios, lighting classes are designed to ensure luminance values between *M*1 and *M*5 road lighting classes, according to varying traffic intensities.

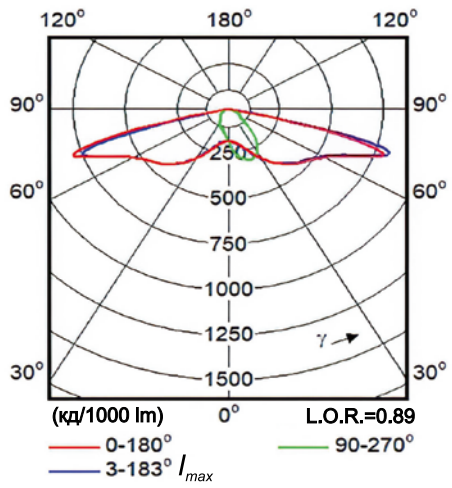

Fig. 1. The distribution curve of luminous intensity of the LED luminaire used in the second scenario

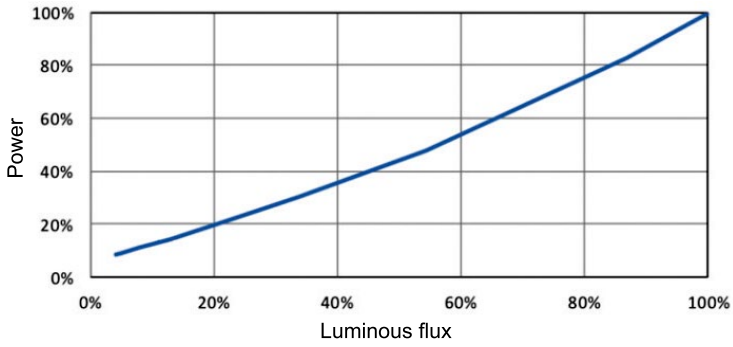

Fig. 2. LED luminaire dimming example relative luminous flux vs power [13]

3.2. Investigation of the Effect of Pole Geometry

Pole geometries are very important in road lighting. The lighting pole geometry and luminaire distribution curve of luminous intensity directly affect each other. In order to obtain a good lighting design, either the pole geometry should be determined according to selected luminaire geometry, or a suitable luminaire should be chosen according to the specific pole geometry.

The distribution curves of luminous intensity published by many manufacturers were examined for luminaires with HPS lamps used in conventional road lighting. As a result of the examinations, it was observed that distribution curve of luminous intensity *C* and γ planes of luminaires with HPS lamps have a circular shape. In LED luminaires, the distribution curves of luminous intensity have no specific shape. Thanks to the arrangement of the lenses and LED luminaires, the distribution curves of luminous intensity can be changed. However, as the height of the pole increases in the road lighting, the distribution curves of luminous intensity should be extended horizontally in parallel with the road using the *C* and γ planes for uniform light distribution. Fig. 1 shows the distribution curves of luminous intensity of the LED luminaire used in the second scenario.

Since existing pole distance used in the study are longer than normal for LED luminaires, the distribution curves of luminous intensity is determined horizontally in parallel with the road. Pole geometry depends on pole height, boom lengths of poles, boom angle of poles and pole-road distance. The dependence between pole geometry and distribution curves of luminous intensity is examined for luminaires with HPS lamps in *DIALux*. If the height of the pole is 14 m, and the pole-road distance is taken as 0.5 m, then the examination is considered sufficient in three cases:

– Assuming the boom angle of poles is 0°, increasing the boom lengths of poles by 0.1 m;

– Assuming the boom lengths of poles is 2.5 m, increasing the boom angle of poles by 0.1°;

– Increasing the boom angle of poles and the boom lengths of poles by different combinations.

According to these three cases, it is observed that the average pole geometry should be either the boom lengths of poles of (3.5 – 6) m and the boom angle of poles of (0° – 10°) or the boom lengths of poles of (2.5 – 3.5) m and the boom angle of poles of (5° – 15°).

Since LED luminaires do not have specific distribution curves of luminous intensity, a standard pole geometry could not be found for LED luminaires in the examinations performed with *DIALux*. Therefore, when designing a SRL project, a suitable LED luminaire can be selected by referring to the pole geometry used in the projects. Thus, replacing existing luminaires with LED luminaires simultaneously ensures appropriate illumination and makes the system smart without changing the pole geometry of conventional road lighting.

3.3. Control Strategy and Luminaire Structure for Smart Road Lighting

The change in dimming-related energy consumption of LED luminaires for the SRL has an approximate linear relation. Fig. 2 shows this relation. Therefore, the study assumes that LED luminaires consume energy in a linearly changing manner by dimming.

Sensors and communication modules must be installed in luminaires to make the road lighting smart by changing luminaires without changing the existing pole structure. Thus, the luminaires can transfer variable traffic and weather conditions from the real environment to the virtual environment. In this study, a luminaire, which is currently used in con-

Table 2. The Average Monthly Sunset and Sunrise Hours in Istanbul and Total Operating Time of a Luminaire [14]

Months	Jan.	Feb.	Mar.	Apr.	May	Jun.
Average sunset and sunrise hours	18:01	18:37	19:08	19:44	20:15	20:37
	–	–	–	–	–	–
	08:25	07:58	07:19	06:25	05:46	05:32
Total operating time of a luminaire (h)	446.4	373.8	377.68	320.5	295.02	267.5
Months	Jul.	Aug.	Sept.	Oct.	Nov.	Dec.
Average sunset and sunrise hours	20:33	20:00	19:12	18:25	17:46	17:38
	–	–	–	–	–	–
	05:46	06:14	06:44	07:15	07:51	08:21
Total operating time of a luminaire (h)	285.7	317.23	346	397.83	422.5	456.22

ventional lighting, is redesigned without changing its pole structure for the second scenario. In order to get rid of the cables inside the luminaire, use an equipment that has a socket and can be fixed to the outer cover of the luminaire. The communication module, the sensor module, the driver and the LED luminaire each have a slot. In this way, it is expected to reduce solution time and labour costs in case of hardware failures of the luminaire. Fig. 3 shows bottom view, top view, and side view of the luminaire in a millimetre scale.

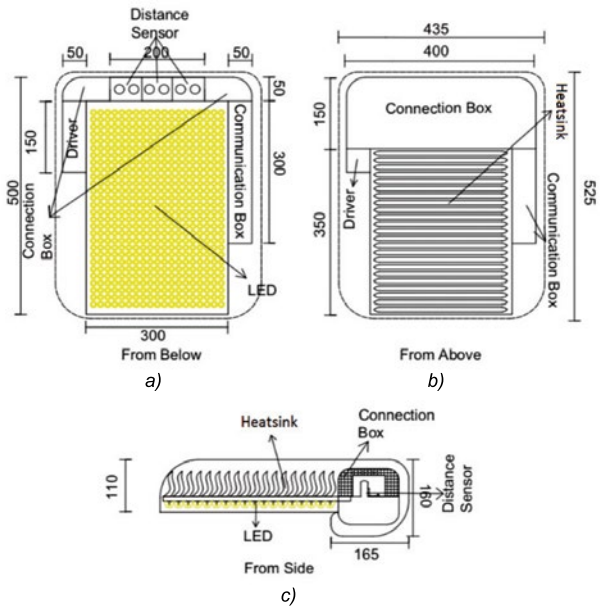

Fig. 3. Demonstrations of the designed luminaire: bottom view (a), top view (b), side view (c)

Determining vehicle speed and traffic intensity in the SRL system is critical. This information is used for dimming LED luminaires, thus very high-energy efficiency levels can be achieved compared to conventional lighting. The SRL system tracks vehicles using height information of vehicles. In Fig. 4, distances between luminaires and the test road lane are shown in meter scale while a vehicle not passing, and while a vehicle passing.

The luminaires are equipped with laser distance measuring sensors. These sensors recalculate the speed of the vehicle at each pole it passes. Therefore, the control system identifies the vehicle by matching the height information of the vehicle with the luminaires it passes through. The traffic flow is determined by the number of vehicles passing in front of a pole during a determined period according to vehicle speed. The speed of a vehicle is determined by the time it takes to cross the poles. The

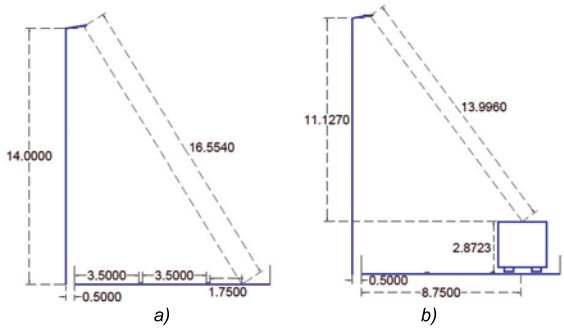

Fig. 4. The distance between the luminaire and the test road when the vehicle does not pass (a) and the vehicle passes (b)

Table 3. Annual Energy Consumption and Achieved Energy Saving For Each Scenario

Relative luminous flux of luminaires	100 %	75 %	50 %	25 %	Total	Energy saving (E_s^i)
1. Conventional road lighting	4306.4 h 48124 kW·h	–	–	–	4306.4 h 48124 kW·h	Reference
2.1. Only luminaires are replaced, without dimming	4306.4 h 32836 kW·h	–	–	–	4306.4 h 32836 kW·h	31.77 %
2.2. Only luminaires are replaced, with dimming	66.43 h 2454.26 kW·h	324 h 1920.47 kWh	1389.43 h 5595.68 kW·h	2526.53 h 4174.68 kW·h	4306.4 h 12472.85 kW·h	74.08 %
3. Completely redesigned system	66.43 h 2204.79 kW·h	324 h 1774.89 kWh	1389.43 h 5171.44 kW·h	2526.53 h 3858.23 kW·h	4306.4 h 1157.37 kW·h	76.04 %

speed of a vehicle is calculated as follows: when the vehicle has crossed a certain pole, the next pole receives the signal, which is the vehicle is coming, with a specific delay, and the time that takes to reach the next pole is measured with this delay. The time it takes for the radio wave that locate in Eq. 1 to cross the same pole is calculated. Then these two calculated times are added up. Thus, the speed of the vehicle is determined by dividing the distance by the time obtained.

3.4. Comparison of Different Scenarios

This part of the study provides a one-year energy consumption analyses for designed three scenarios on the test road created in computer environment. In the analyses, firstly operating time of luminaires are determined by considering the average monthly time of sunset and sunrise in Istanbul. Table 2 shows the average monthly sunset and sunrise times in Istanbul and the total operating time of a luminaire.

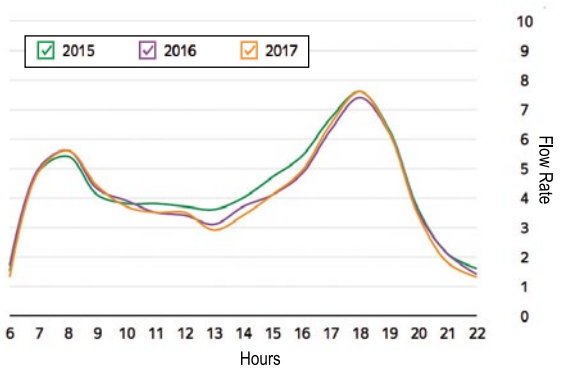

Fig. 5. Hourly traffic flow in Istanbul [15]

After determining operating time of luminaires on a monthly basis, as one of the basic principles of the SRL, it should be decided to what extent the luminaires are dimmed according to condition of the road. Thus, continuous monitoring of the road with the help of sensors should ensure the appropriate dimming. For this purpose according to the CIE recommendations, road dimming rates should be determined by selecting class of the road according to structure of the road, flow, and speed of vehicles. Accordingly, real traffic flow data of in Istanbul is used to determine these dimming rates. Fig. 5 shows hourly traffic flow in Istanbul.

In this study, to compare scenarios with each other, luminous flux of the luminaire depending on dimming rates is determined according to the actual traffic flow data obtained from Fig. 5 in Istanbul in accordance with regulations. Fig. 6 shows determined relative luminous flux of the luminaire according time intervals in a day.

When Fig. 6 is examined, it is observed that the relative luminous flux is coherent with hourly traffic flow in İstanbul shown in Fig. 5. When the traffic flow falls below 10 %, luminous flux of the luminaire is kept at 25 % for safety reasons. In the calculations, instantaneous luminous flux changes are not considered due to the lack of data. In this study, 2.6 cd/m^2 is chosen for *M*1 road class instead of 2 cd/m^2, which is the lower limit for luminance level. Because to make an appropriate comparison between smart and conventional road lighting. In

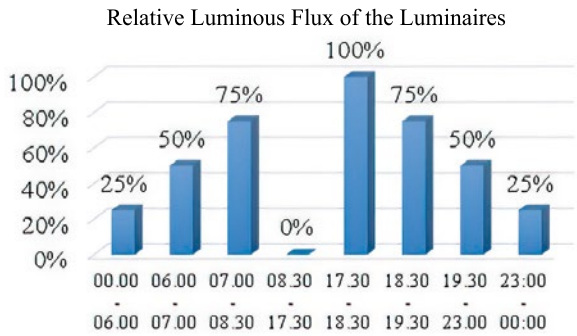

Fig. 6. Relative luminous flux of luminaires in Istanbul (luminaires do not active during the daytime)

addition, luminance levels are preferred above the minimum luminance level, considering the maintenance factor of the luminaires. According to the relative luminous flux in Fig. 6, 100 %, 75 %, 50 %, 25 % luminous fluxes correspond to the luminance values of road lighting classes *M*1, *M*2, *M*3, and *M*5, respectively. After determining the luminous flux of the luminaires depending on hours, in order to find total energy consumption, it is determined by how long the luminaires work in case at each luminous flux level considering the average time of sunset and sunrise in Istanbul. In Fig. 7, the operating time of the luminaires at variable luminous flux levels is set monthly.

Using Fig. 7, annual operating times of luminous flux levels for each scenario are calculated. Then, the annual energy consumption and energy saving for each scenario are calculated as follows:

$$P_t^{i,j} = P_l^i \cdot P_r^{i,j} \cdot NP^i, \tag{1}$$

$$E_y^{i,j} = P_t^{i,j} \cdot OT^{i,j}, \tag{2}$$

$$E_y^i = \sum_{j \in \mathcal{J}^i} E_y^{i,j}, \tag{3}$$

where $P_t^{i,j}$ is total power of the system, P_l^i is power of a luminaire, $P_r^{i,j} \in \{0.25, 0.5, 0.75, 1\}$ is power ratio dependent on variable luminous flux, NP^i is number of pole, $E_y^{i,j}$ is yearly total energy consumption, $OT^{i,j}$ is operating time, $\mathcal{I} = \{1, 2.1, 2.2, 3\}$ is the set of scenarios, $i \in \mathcal{I}$ is the scenario number, $\mathcal{I}^i$ is the set of luminous flux levels for scenario i, and $j \in \mathcal{J}^i$ is the luminous flux level. The data associated with these variables are given in the relevant sections of Table 1, Fig. 6, and Fig. 7.

Conventional road lighting is chosen as reference to achieve the energy saving in the other scenarios. The energy savings relative to conventional road lighting (E_s^i) are calculated as follows:

$$E_s^i = \frac{E_y^1 - E_y^i}{E_y^1} \cdot 100 . \tag{4}$$

After the calculations, the annual energy consumption and achieved energy saving for each scenario are shown in Table 3, together with operating times of luminaires at different luminous flux level.

Energy consumption is high in conventional road lighting, since dimming is not performed and HPS lamps are used. The scenario 2, where only the luminaires are replaced without changing the electrical installation and poles, is examined in two different cases to determine the energy savings achieved by dimming and changing HPS lamps with LEDs, respectively. The achieved energy savings in the first case is 31.77 % due to the replacement HPS lamps with LEDs without dimming. In the second case, energy saving is 74.08 % with dimming. So in case of dimming, the energy savings are highly increased. However, the cost increases slightly com-

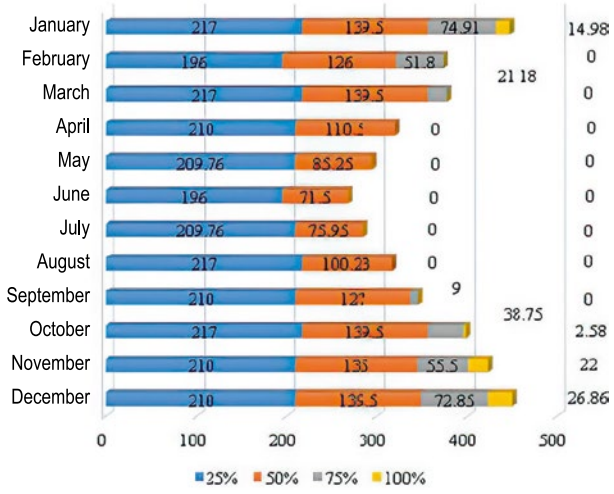

Fig. 7. Monthly operating time of the luminaire at variable luminous flux levels

pared to the first case due to equipment required for dimming. In the third scenario, which is the case where poles, electrical installations and luminaires are completely replaced to achieve maximum energy savings, the energy savings are 76.04 %. When the results are examined, it is observed that obtained energy saving only by replacing the luminaires is very close to the one achieved by replacing the whole system.

4. CONCLUSIONS

High costs lead to the fact that the SRL cannot be widespread. In this study, an appropriate LED luminaire is designed and the SRL transformation is proposed without changing the electrical installation and poles. It is observed that the SRL created only by replacing the luminaires provides very high energy saving. Even if it is found that the scenario of changing the whole structure is the highest energy saving scenario, in this case the investment cost is quite high. In the proposed solution, high costs are reduced, since only the luminaires are replaced. Thus, it is shown that the SRL can be performed with low costs. Reducing high costs will make a significant contribution to spread of the SRL, especially in developing countries where the SRL cannot become widespread.

In this study, the costs of the scenarios are not examined in detail due to the lack of data. However, if a cost comparison is performed, it would already appear that proposed solution has a relatively low cost compared to the third scenario, since the proposed solution does not replace the poles and electrical installations. When the proposed solution is compared with conventional road lighting, only the luminaires are replaced. This cost can be paid back in a short time with the high energy saving.

Nevertheless, it will be more useful for decision makers to determine the break-even time of the options with detailed cost/benefit analyses using the net present value method.

In addition, changing the road class by dimming for energy saving can cause safety problems. In fact, for the *M*1 road class, the luminance level is allowed to reduce to maximum of *M*3 road class. In this study, when no vehicle passes, the luminance level is reduced to *M*5 road class. For safety reasons, the luminaires are not turn off completely. If a vehicle passes through the road, sensors detect this vehicle, and the luminance level at the location where the vehicle passes is increased to *M*3 road class. In countries with high acceptable level of risk and difficulties in energy supply, it may be an appropriate option to reduce the luminance level to the *M*5 road class.

In this study, only technical analysis of the SRL is performed. Thus, potential energy savings of the SRLs are shown. However, it is up to the decision makers to determine the luminance level of road class by considering the energy saving and safety criteria.

5. REFERENCES

1. L. Atzori, A. Iera, G. Morabito, The internet of things: A survey. Computer networks, Computer Networks, 2010. V54, #15, pp. 2787–2805.

2. A. Adriansyah, A.W. Dani, G.I. Nugraha Automation control and monitoring of public street lighting system based on internet of things, In 2017 International Conference on Electrical Engineering and Computer Science, Palembang, 2017, pp. 231–236.

3. T. H. Do, M. Yoo An in-depth survey of visible light communication based positioning systems, Sensors, 2016. V16, #5, p. 678.

4. L. Tähkämö, R.S. Räsänen, L. Halonen Life cycle cost comparison of high-pressure sodium and light-emitting diode luminaires in street lighting, International journal of life cycle assessment, 2016. V21, #2, pp. 137–145.

5. A. Gil-de-Castro, A. Moreno-Munoz, A. Larsson, J. J.G. De La Rosa, M. H.J. Bollen LED street lighting: a power quality comparison among street light technologies, Lighting Research & Technology, 2013. V45, # 6, pp. 710–728.

6. G. Shahzad, H. Yang, A.W. Ahmad, C. Lee Energy-efficient intelligent street lighting system using traffic-adaptive control, IEEE Sensors Journal, 2016. V16, #13, pp. 5397–5405.

7. J. F. De Paz, J. Bajo, S. Rodríguez, G. Villarrubia, J.M. Corchado Intelligent system for lighting control in smart cities, Information Sciences, 2016. V372, pp. 241–255.

8. Ö. Gül, Ö. Sen, Technical and Economical Evaluation of LED Road Lighting in Turkey, Light & Engineering, 2010. V18, #4, pp. 29–36.

9. C.C.D. Fonseca, R.P. Pantoni, D. Brandão Public street lighting remote operation and supervision system, Computer Standards & Interfaces, 2015. V38, pp. 25–34.

10. Road Lighting Calculations, CIE140–2000, 2000.

11. P. T. Daely, H.T. Reda, G.B. Satrya, J.W. Kim, S.Y. Shin Design of smart LED streetlight system for

smart city with Web-based management system, IEEE Sensors Journal, 2017. V17, #18, pp. 6100–6110.

12. TEDAŞ. (2019, March). LED'li Yol Aydınlatma Tasarımına İlişkin Usul ve Esaslar [Online]. Available: http://www.tedas.gov.tr/uploads/LEDliYolAydinlatma%20TasariminaIliskinUsulveEsaslar%20(Taslak).pdf

13. National Electrical Manufacturers Association. (2014, July). Energy Savings with Fluorescent and LED Dimming [Online]. Available: https://www.nema.org/Standards/SecureDocuments/NEMALSD%2073–2015 %20WATERMARKED.pdf

14. Time and Date. (2019). World Clock [Online]. Available: http://www.timeanddate.com/worldclock/astronomy.html

15. Yandex. (April, 2018). İstanbul Trafik Analizi [Online]. Available: https://yandex.com.tr/company/press_center/infographics/istanbul_traffic

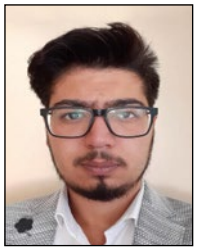

Mustafa Eyyup Gursoy
received B. Sc. degree at Electrical Engineering Department from Istanbul Technical University in 2019. He is an M. Sc. student. His research areas include smart road lighting and energy saving

Burak Dindar
received his B. Sc. degree at Electrical Engineering Department from Kocaeli University in 2016. He works at the Electrical Engineering Department of Istanbul Technical University as a research assistant and he is an M. Sc. student in same department. His main research interests include smart grid, electricity distribution system and power quality

Omer Gul
received B. Sc., the M. Sc. and Ph.D. degrees at Electrical Engineering Department from Istanbul Technical University, Istanbul, Turkey in 1991, 1995, and 2001, respectively. He had been at UMIST, Manchester, UK, as a visitor researcher for six months during 1999 – 2000. He is recipient Award 2001 Siemens excellence researcher. His research areas include smart distribution system, electricity market, power quality and efficiency, electrical safety and lighting, electrical project management. He is presently working at Istanbul Technical University as an Associate Prof

Light & Engineering
Vol. 28, No. 4, pp. 106–115, 2020

https://doi.org/10.33383/2019-101
Svetotekhnika #3, 2020, pp. 63–70

RESEARCH INTO THE JUNCTION TEMPERATURE AND POWER OF NEW LED MODULES GENERATION IN DEPENDENCE ON VARIABLE PARAMETERS

Kemal Furkan Sokmen and Osman Bedrettin Karatas

Bursa Technical University, Bursa, Turkey
E-mail: furkan.sokmen@btu.edu.tr

ABSTRACT

In this research, the change in the junction temperature and luminous flux of a new generation LED module depending on variables such as radiation, lens piece, ambient temperatures, currents, and quantity of elements had been studied. Commercial software *FloEFD2019* was used in the finite volume analysis made during the study. The analyses were verified by experiments. On basis of the analysis, a solution was obtained that does not depend on the number of elements. The force of gravity was taken into account. While the ambient temperatures were taken as *Ta* = 23 °C and 40 °C, and the radiation value as 1009 W/m^2, currents as 140 mA, 160 mA, 180 mA, 200 mA, 220 mA and 240 mA, meanwhile, samples numbers on PCB were taken as 101 and 202. In order to determine the effect of the lens piece located on the LED module, the analysis was repeated with and without using the lens. As a result of the study, it was found that the increase in ambient temperature and radiation has an adverse effect on the temperature T_j and luminous flux. It has been observed that changing samples number has a negligible effect on luminous flux and temperature *Tj*. It was found that the use of radiation and lenses are the most important factors affecting the luminous flux of the module.

Keywords: LED automotive lamp, laminar natural convection, Monte Carlo method of radiation, computational fluid dynamics (CFD), junction temperature

1. INTRODUCTION

LED (Light Emitting Diode) systems have recently become widely used in lighting systems. The LED provides a lifetime of up to 100 000 hours depending on usage. The temperature below 110 °C helps the energy distribute more efficiently at 3000 °C in halogen bulbs, and 700 °C in xenon bulbs. The basic studies of the thermal management of LEDs were carried out by Karim et.al. [1]. Another study on the thermal behaviours of LEDs was carried out by Poppe and Lasance [2]. Besides, in other studies [3] regarding the determination of the junction temperature (*Tj*), an attempt was made to determine both the optical features and the lifetime of the thermal conductivity resistances of LEDs [4]. Some technical articles regarding the calculation and formulation of *Tj* have been published by LED manufacturers [5–7]. In 2009, Bider investigated the effect of ambient temperature on LEDs and their lifetime [8]. Another basic study was conducted by Bielecki and et.al.in 2007 [9]. While the study by Kikuchi et.al aimed to determine the values of *Tj* using a three-dimensional model, Monte Carlo random radiation method was used for the radiation model [3]. Rubenstein and Kroese also studied the Monte Carlo method for the simulation [10]. The increase in thermal conductivity and a decrease in *Tj* temperature to 20 °C due to increase of copper plating on the printed circuit were reported in another study by Vora and Vijaykumar on LED [11]. Sheu et.al. [12] conducted a study of thermal conductiv-

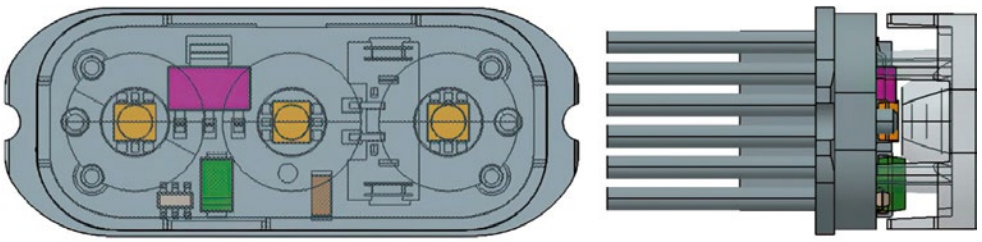

Fig. 1. Geometry and location of LEDs and electronic devices

ity and thermal resistance based on the determination of the temperature *Tj*.

LEDs that consume a large amount of power in the direction of increasing demands are intended for use in smaller volumes, which makes the thermal design of LEDs more difficult [13]. Arık et al. investigated the effects of local thermal points available on LEDs using finite elements method in order to define the thermal problems arising in LEDs [14]. Petroski et al. developed a spot module with LED equipped with heat distributor. In this study, where cooling is provided by natural convection, the positioning problem of LED was resolved using a heat distributor with vertical wings located throughout a cylindrical pipe [15]. Yung et al. investigated the effect of printed circuit board (PCB) positioning at different angles on heat transfer in a system with LED, where cooling is provided with natural convection. Yung et al. investigated how the availability of PCB at different angles affects heat transfer in a system with LED, where cooling is provided by natural convection [16]. Some researchers have investigated the design of led cooling systems using a thermoelectric cooler. Zhong et al. compared the system with thermoelectric cooler, with cooling system with heat distributor and fun. As a result of the comparison, it was found that a system with a thermoelectric cooler is more efficient than that with heat distributor and fun, in the case that when the air speed is 3.6 m/s and the LED power is less than 35 W [17]. Computational fluid dynamics method is often used in thermal designing of the system with LED. Cheng et al. in their study, done using the finite element method, investigated the change in heat distribution at different heat convection coefficients in the system, where there are 10 LEDs, a closed volume existing behind PCB, and vertical winglets are available. It was seen that LED temperature could be decreased using a fan to increase heat convection coefficient [18]. In another study, which used the finite elements method, the effect of the number, widths and lengths of winglets available in a heat distributor on thermal design was investigated. Weng investigated the thermal performances of the systems with LED using the finite elements method [19]. There are also various studies in the literature, which describe the use liquid instead of air in the cooling system. Lai et al. developed a liquid cooling system in their study. They showed that air cooling could be insufficient compared to a liquid cooling system [20].

This study, which differs from other studies, took into account variables such as thermal analysis of LED module, ambient temperature, radiation, current, and samples number. The study analysed the interaction of the junction temperature and luminous flux of LED module.

2. MATERIAL AND METHOD

2.1. Geometry and Model

The new generation LED module used in this study is shown in Fig. 1. 3 LEDs are used in the module. These produced LED modules are mounted to any intended design.

Each LED consumes power of 0.1 W in response to a current of 0.4 A. One of the drivers operates

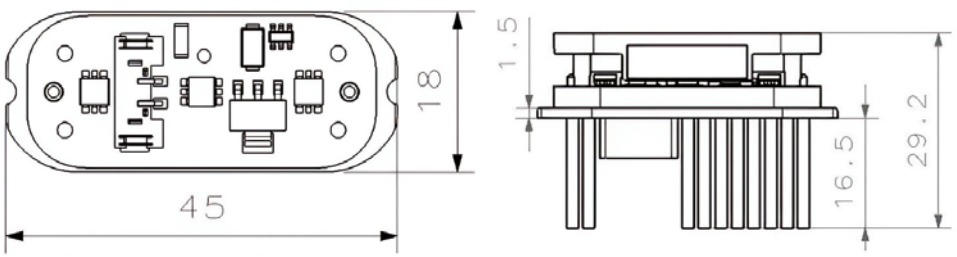

Fig. 2. Dimensions of the LED module

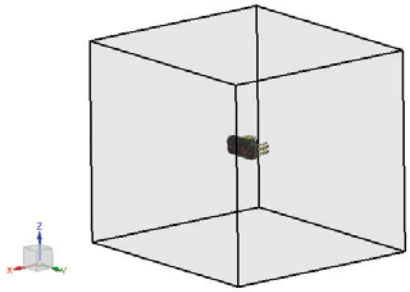

Fig. 3. Modelling of computational domain and solar radiation

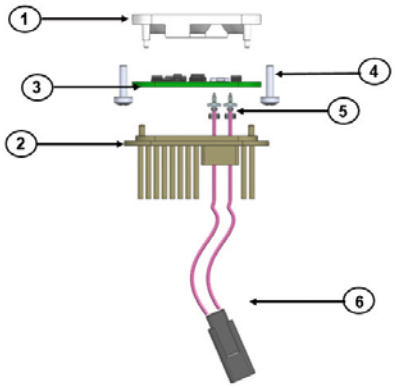

Fig. 4. LED module consists of six blocks: 1 – lens *PC Lexan LS2,* 2 – heatsink *AL 6063,* 3 – PCB *FR4 PCB, 4-*vida *Ejot Delta,* 5 – crimp *CuZn33,* 6 – cable *FLY-R Cable* 200 mm

with a voltage of 0.13 A and 1.8 V. One of the diodes draws 0.15 A and operates under 0.7 V. Transıstor operates with 0.3 A and under 1.4 V. The geometrical model and measurements of PCB used are shown in Fig. 2.

2.2. Numerical Simulations

The temperature estimations of electronic parts were calculated using computational fluid dynamics (CFD) method. *FloEFD2019*, *Mentor Graphics* software, was used to make the thermal analysis of electronic cooling. *FloEFD* can work with different CAD software, but this study *CATIA V5 R19*. With the direct integration of the simulation software in *CATIA V5*, a CAD program; the simplification and analysis process will be quite simple and rapid. The geometry of PCB and electronics were simplified for thermal analysis and imported from CAD data. Later on, a computational influence area was formed considering the sizes of PCB. The computational domain should comprise all parts of PCB to get correct results. Afterwards, the analysis conditions and solution methods are defined (Fig. 3).

Table 1. Number of Mesh and Junction Temperature of LED

Mesh number	T_j, °C
550986	95.2
687250	98.3
765687	105.4
863547	116.4
954376	117.1
1025468	117.0

Having created the computational domain, the boundary conditions were applied. The ambient temperature was set to 23 °C, and external analysis was selected as the analysis type for this study. The Monte Carlo radiation model and natural convection were selected. Photon radiation is applied with random access in Monte Carlo method. This process is repeated for *N* times, depending on the maximum of photons defined at the beginning of the analysis. The selection of proper N the repetition number of random access (previous number), is important in this method. In addition, the force of gravity is taken into account, and weight direction is (g = 9.81 m/s^2) is the -*z* direction. The thermodynamics parameters of computational domain are given for the pressure of 101325 Pa, and ambient temperature equal to 23 °C. Besides, the solar radiation model was located in the direction of x = –0.568562, y = 0 and z = –0.8226405, and solar density was defined as 1009 W/m^2.

All LEDs and electronic parts were mounted on *FR*4 PCB containing a double-sided layer of copper. The thickness of each copper layer is 35 µm, and that of PCB is 1.5 mm in total.

The types of material and electronic component should be selected properly to avoid of thermal risks. The list of materials and electronic components are shown in Fig. 4.

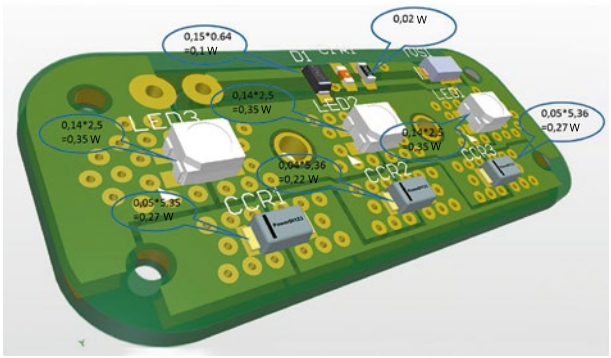

Fig. 5. Power of all electronics

Initially, the analysis verification study was conducted to see whether analyses yield correct results. In the verification study, the powers applied to components on PCB are shown in Fig. 5. All components were driven with the current of 140 mA.

In order to get a solution independent of the element number, the analyses were made with different element numbers, and the results of the analyses are shown in Table 1. It was seen that the results did not change after a certain number of elements, and the number of elements was defined in the analyses on condition that it should not be less than 954376.

FloEFD solves Navier-Stokes equations, the formulation of mass, momentum, and energy conservation for fluid flows. The obtained equations are confirmed by the fluency equations that define the structure of the fluid, and with fluid density, viscosity and empirical dependences of thermal conductivity. The time spend on heat distribution is very short, and heat convection time from LED and electronics to the other parts is not so long, because of that temporal behaviours can be taken into consideration. That is why in this study, preference was given to stationary conditions. The equations for stationary conditions are mass conservation equation, momentum equation, and the thermal energy conservation equation [21]. Eq. 1 determined the temperature of LED junction. The normalized luminous flux graphics associated with *Tj* and current value of *Samsung* LED used in the study are shown in Fig. 6 and Fig. 7.

$$T_J = T_{LED} + P_{LED} \cdot R_{jc} \quad , \tag{1}$$

where T_j is the junction temperature, T_{LED} is the LED temperature, R_{jc} is the thermal resistance, P_{LED} is the LED power.

The normalized luminous flux values corresponding to *Tj* and the current value obtained from luminous flux catalogues of LEDs are calculated using (2), (3), and (4) by multiplying 32.4 lm, which is the maximum luminous flux at 140 mA included in the catalogue:

$$Luminous\ flux = 32.4 \cdot \beta \cdot \alpha \, , \tag{2}$$

$$\alpha = 0.0068 \cdot I + 0.037 \, , \tag{3}$$

$$\beta = -0,0014 \cdot T_j + 1.0237 \, , \tag{4}$$

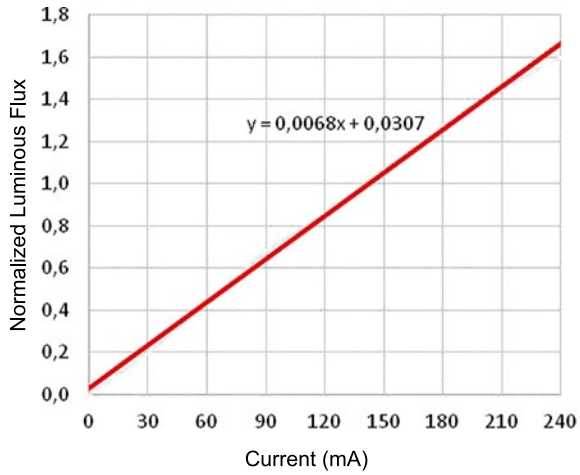

Fig. 6. Normalized luminous flux according to current

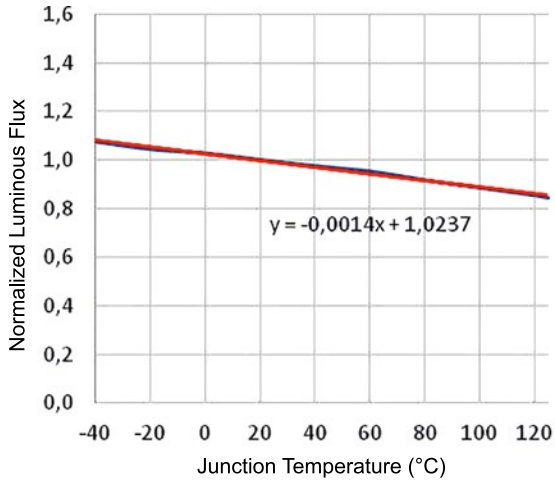

Fig. 7. Normalized luminous flux according to T_j

where α is the normalized luminous flux value corresponding to the current value is calculated using the function shown in Fig. 6, and β is the normalized luminous flux value according to junction temperature in Fig. 7, *I* is the current, *Tj* is the junction temperature.

2.3. Experimental Study

The thermal analysis should be verified using the laboratory experiment. Test equipment and their specification are shown in Table 2.

The test was performed in an air-conditioned room in a controlled environment, see Fig. 8. PCB was placed almost in the middle of the room.

The room air speed was kept at the minimum level to ensure natural convection conditions, as in numerical simulations. The thermal measurement system consists of thermocouples associated with data acquisition system by company *National In-*

Table 2. Test Equipment

Equipment	Trademark	Working range	Inaccuracy
Climatic oven	Angelantoni CST 157 2T	–80/+220 °C	+/-0.1 °C
Thermometer	APPA-50	–40/204 °C	+/-2.2 °C
Thermocouples	Standard (K type)		

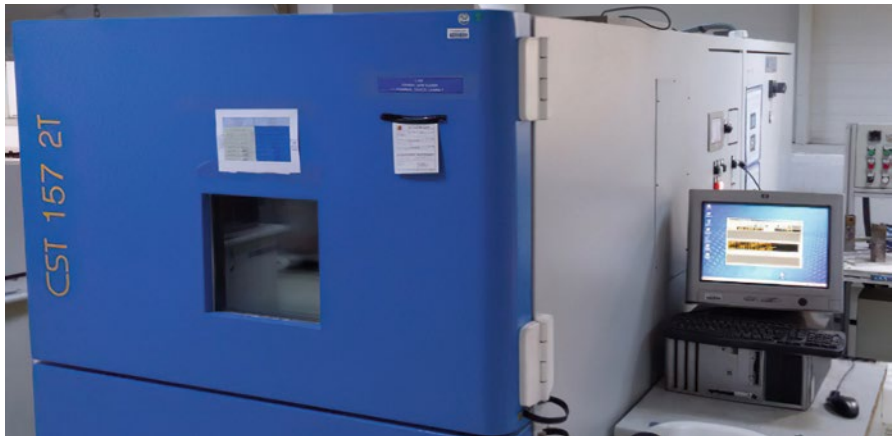

Fig. 8. The climate chamber

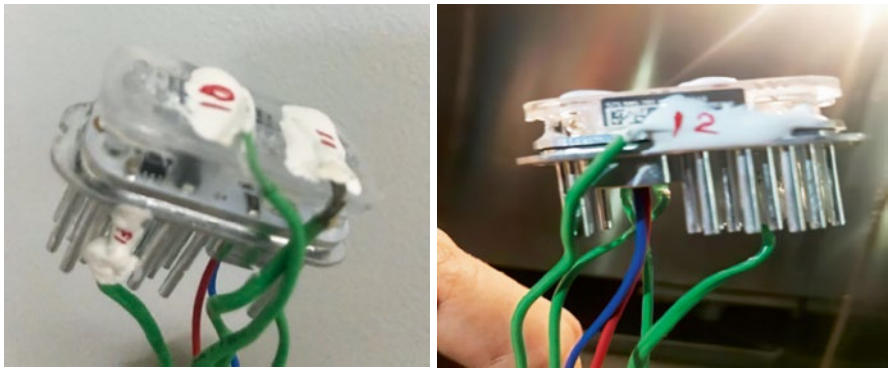

Fig. 9. Schematic demonstration of electronics measurement point

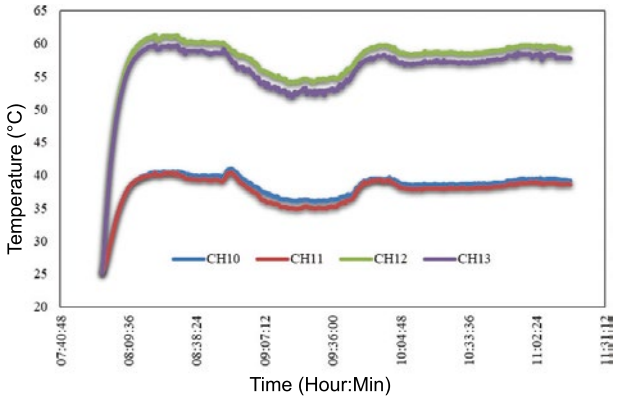

Fig. 10. Test results

strument. The temperature of the parts and electronics was monitored by software. The stable state data was collected after thermal stabilization had been ensured in a conditioned division.

Thermocouples were located on four LED modules, including two of them on lens, one on winglets, and one on PCB (Fig. 9).

The test measurements were performed three times depending on the time, and test results were shown in Fig. 10. It was determined that LEDs reached the maximum temperature in a short time and kept to maintain this temperature. As can be seen from Fig. 10, a decrease in temperature between 09:07 and 09:36 hours was found due to a decrease in current. Later, it was noticed that the temperature kept the same value with such small fluctuations. For this reason, permanent regime practice was carried out in the analyses. No time-dependent analysis was made. The results of the analysis are shown in Figs. 11.(a) – 11.(c), from the locations where thermocouples were connected. The comparison of the analysis and experiments are shown in Table 3.

After confirming the correctness of the calculation's analysis, the analyses were made with *Samsung PLCC4* LEDs, Table 4.

Table 3. Comparison of Tests and Analyses

LED module	CH10 (°C)	CH11 (°C)	CH12 (°C)	CH13 (°C)
Test-1	38.44	36.85	61.30	61.18
Test-2	38.26	37.73	62.59	62.07
Test-3	38.70	37.53	62.85	61.92
Analysis results	38.25	36.46	63.16	62.20

Note to Table 3: CH10 – CH13 – channels of the measuring device, to which the appropriate thermocouples are connected.

Table 4. Analysis' Conditions

Samsung PLCC4	Ambient temperature (°C)	Current (A)	Samples number (pc.)
Analysis-1	23 °C	0.14	101
Analysis-2	40 °C + rad	0.14	101
Analysis-3	23 °C	0.18	101
Analysis-4	40 °C + rad	0.18	101
Analysis-5	23 °C	0.18	202
Analysis-6 (with lens)	40 °C + rad	0.18	202
Analysis-7 (with lens)	23 °C	0.18	202

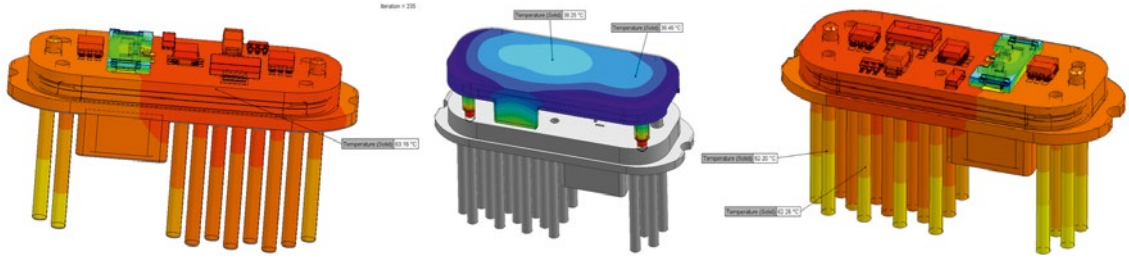

a) b) c)

Fig. 11. Experimental result of driver 1 with locations where thermocouples were connected for test-1 (a), test-2 (b), test-3 (c)

3. RESULTS AND DISCUSSION

After checking the results of the analysis, seven different analyses were performed (Table 4), and the effects of the factors, such as ambient temperature, radiation, samples number, lens effect, and the change of the current value that LED is driven with, on temperature *Tj* was investigated. The results are shown in Figs. 12 (a) – 12 (g). According to the analysis results, since the resistance temperatures of electronic parts except LED is 150 °C, they are not found to be at risk in terms of temperature.

As a result of seven analyses made during the study, the maximum *Tj* values calculated for LEDs are shown in Table 5.

In our study, because of seven analyses results of the new generation LED module, *Tj* values were found to be less than permitted junction temperature value. In analyses made at the current value of 0,14 A, and *Ta* = 40 °C radiation, and under two different weather conditions (analysis-1, analysis-2); an increase of 27.45 °C was seen in *Tj* and a decrease of 1.2 lm at luminous flux, with the increase of ambient temperature and radiation.

In the analyses made at the same ambient conditions by increasing LED driving current in order to increase the luminous flux (analysis-3, analysis-4); it was found that *Tj* increased 26.68 °C and luminous flux decreased 1.6 lm, with the increase of ambient temperature and radiation. While the increase in ambient temperature causes an increase in *Tj*, it also leads to a decrease in luminous flux. In order to better understanding the effect of radiation on the junction temperature, the increase in ambient air temperature was subtracted from temperature difference *Tj*, as in (5) and in (6):

Table 5. Junction Temperature and Luminous Flux for Seven Analyses

Samsung PLCC4	Junction temperature, °C	Luminous flux, lm
Analysis-1	87.10	28.7
Analysis-2	114.55	27.5
Analysis-3	102.86	35.8
Analysis-4	129.54	34.2
Analysis-5	102.64	35.8
Analysis-6 (with lens)	121.00	34.7
Analysis-7 (with lens)	94.74	36.2

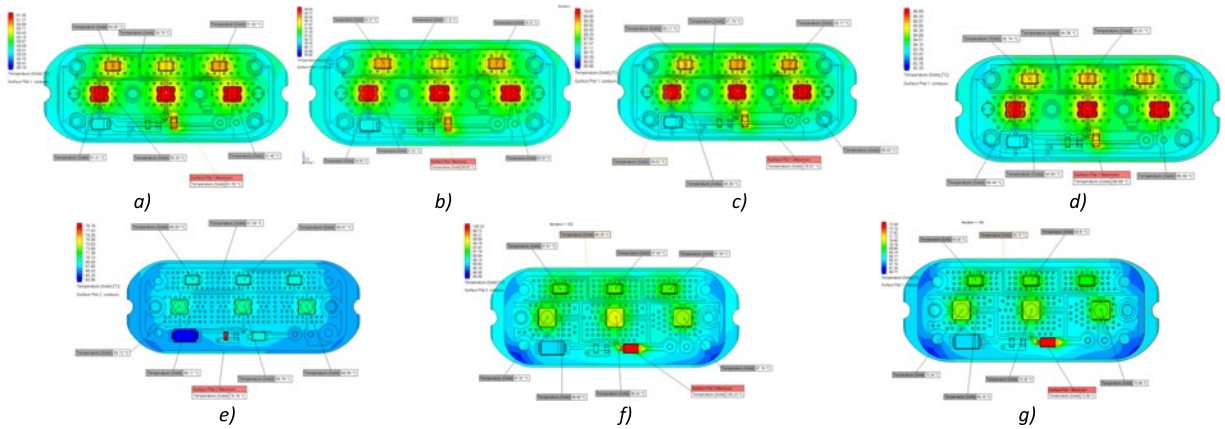

Fig. 12. Analysis results of LED module: result of analysis-1 (a), result of analysis-2 (b), result of analysis-3 (c), result of analysis-4 (d), result of analysis-5 (e), result of analysis-6 (f), result of analysis-7 (g)

$$T_{jdif\,(2-1)} = \left(T_{j\,analyse-2} - T_{j\,analyse-1}\right) - 17\ ^{o}C\,, \quad (5)$$

$$T_{j\ dif\,(4-3)} = \left(T_{j\,analyse-4} - T_{j\,analyse-3}\right) - 17\ ^{o}C\,, \quad (6)$$

where $T_{j\,dif}$ is the temperature difference, $T_{j\,analyse\text{-}1}$ is the junction temperature analyse-1, $T_{j\,analyse\text{-}2}$ is the junction temperature analyse-2, $T_{j\,analyse\text{-}3}$ is the junction temperature analyse-3, $T_{j\,analyse\text{-}4}$ is the junction temperature analyse-4.

When the increase of 17 °C in ambient air was subtracted from *Tj* temperature differences, as in the above equations, the values such as 10.45 °C and 9.68 °C were obtained. It is thought that these temperature values obtained came to exist by the effect of radiation. It was calculated that radiation caused an increase of 10 °C in temperature, which caused an increase of *Tj* in the range of (36–38)%. Since an increase of *Tj* decreased the radiant flux, as seen in Fig. 7, it also caused a decrease of 1.2 and 1.6 lm in the luminous flux for both ambient conditions. This is a negative effect for lighting. Samples number, which is 101 on PCB was rose up 202 so that the junction temperature would drop; analysis-5 was performed under the ambient condition was 0.18 mA and 23 °C. Although samples number doubled, when analysis-5 was compared to analysis 3, it was seen that there was only a *Tj* decrease of 0.22 °C, and that samples number was not so effective at the decrease of temperature, which is thought to be because of that the size of PCB is small. Analysis-3, analysis-5 were found to have the same value in terms of luminous flux. For this reason, samples number was neglected in analysis comparisons. In analysis (5–7), which was made in two different ambient environments, under 0.18 mA, and at 23 °C, by mounting lens on LED module, so as to examine the effect of lens on luminous flux, it was determined that lens caused a decrease of 7.9 °C at *Tj* temperature. It was determined that a 7.9 °C of *Tj* decrease caused 0.4 lm of increase in luminous flux. In analyses 4 and 6, which were made at 40 °C and +radiation, it was found that the lens causes a temperature drop of 8.54 °C. It was found that a decrease in temperature by 8.54 °C causes an increase in luminous flux by 0.5 lm. When comparing the results of analyses 5 and 6, it was seen that *Tj* increased by 18.36 °C, while there is an effect of increasing the ambient air by 17 °C and a radiation effect. It was calculated that this increase caused a decrease in lu-

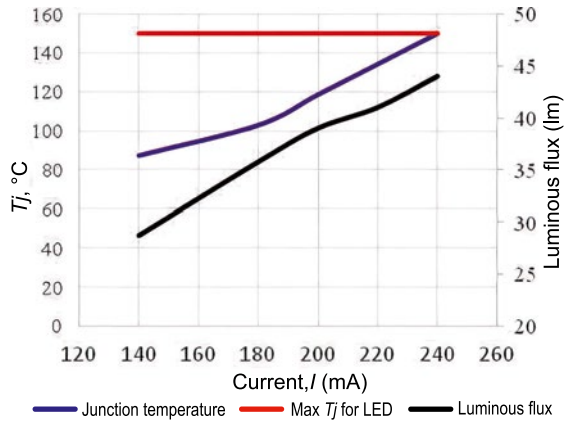

Fig. 13. *Tj* and luminous flux according to the current at the ambient temperature of 23 °C without lens

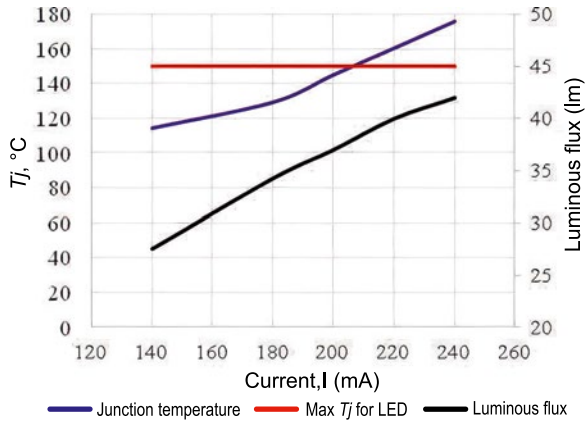

Fig. 14. *Tj* and luminous flux according to the current at the ambient temperature of 40 °C and radiation without lens

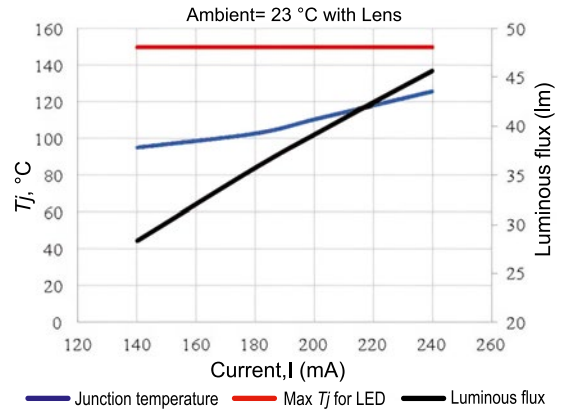

Fig. 15. *Tj* and luminous flux according to the current at the ambient temperature of 23 °C with lens

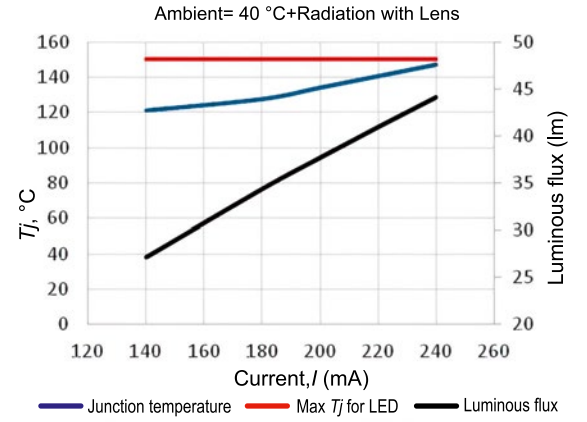

Fig. 16. *Tj* and luminous flux according to the current at the ambient temperature of 40 °C and radiation with lens

minous flux by 1.1 lm. Considering that 17 °C of the increase of 18.36 °C is the result of an increase in the ambient temperature, it is seen that 1.36 °C of this temperature is the result of radiation with lens. It was determined that lens usage seriously reduces radiation effect. Because of the study, it was found that an increase in temperature due to radiation, which will occur due to heat transfer, causes an increase in luminous flux. However, since the *Tj* value increased with increasing ambient temperature, luminous flux also decreased. In order to make the study more detailed, according to Fig. 6, the analyses were made to increase the current value from 0.14 A to 0.24 A in order to obtain the highest luminous flux from LEDs. In the analyses, the ambient air was assumed as 23 °C and 40 °C, and + radiation, the LED module was assumed both with and without lens. The results are shown in Figs. 13–16.

The effect of the lens piece is clearly seen when Fig. 13 and 15 are compared. According to Fig. 13, if the LED module offering the best lighting at 240 mA current value is without lens piece, whether *Tj* value is exceeded is determined from Fig. 13. In that case, the LED module will fail to perform lighting duty because *Tj* value has been exceeded. According to the analysis made with the lens piece, when Fig. 15 is examined at a current of 240 mA, it is seen that *Tj* value is below the permitted value, and highest lighting value is 44 lm.

This was also determined in a scenario where the ambient temperature was assumed as 40 °C and radiation was available. It was seen in Fig. 14 that the permitted *Tj* value was exceeded after 200 mA in the module without lens, that LED module failed in performing lighting duty, compared to Fig. 16. It was determined that the module with lens didn't exceed *Tj* value even at 240 mA, that luminous flux was 46 lm, and that module performed its duty, in the same ambient conditions. The effect of the changing the ambient air is striking in this part of the study. The ambient air in 40 °C and radiation clearly affect the module design without a lens; the permitted *Tj* value is exceeded after the current value of 200 mA,

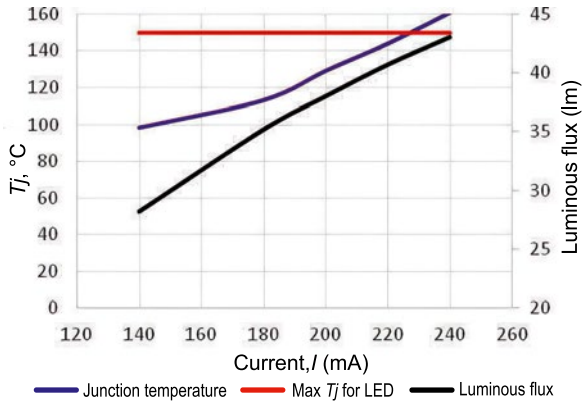

Fig. 17. *Tj* and luminous flux according to the current at the ambient temperature of 23 °C + radiation without lens

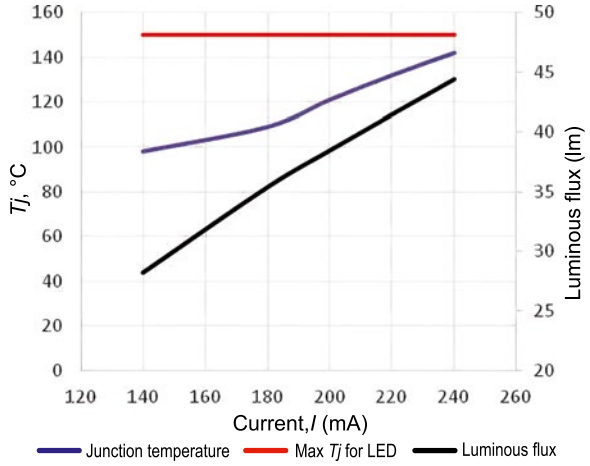

Fig. 18. *Tj* and luminous flux according to the current at the ambient temperature of 23 °C + radiation with lens

and at the ambient temperature is 23 °C and eliminating the radiation effect, then *Tj* value is exceeded at 240 mA, according to Fig. 14 (Fig. 13).

It was found that the boundary *Tj* value wasn't exceeded at 240 mA in both ambient conditions, while the lens was mounted at the LED module, and that the LED module would perform the lighting duty. This is shown in Fig. 15 and Fig. 16, which the module with the lens could operate in both ambient conditions.

To see how the lens piece would affect the radiation effect, the analyses with and without radiation lens were repeated only at ambient air of 23 °C. The results are shown in Figs. 17–18.

It was determined that the permitted *Tj* value was exceeded, reaching the value of 220 mA when exposed to radiation (Fig. 17). Fig. 18 showed that *Tj* value was not exceeded even at the current value of 240 mA, and an analysis performed under the same ambient conditions produced a luminous flux of 44 lm.

4. CONCLUSION

It was revealed in this study that convenient ambient conditions should be provided so that new generation LED modules could have catalogue lighting values. In particular, it was found that the effect of radiation on luminous flux was greater than expected. It was found that *Tj* value increased by 10 °C with the effect of radiation in LED module used in the study, and reached above the permitted *Tj* value. It was determined that the value of *Tj* increases by (2–2.5) °C when exposed to radiation in the module in which the lens piece was used, and that LEDs could perform lighting duty. According to these results, it was confirmed that the lens piece used in LED modules directly affects the module lifetime and lighting duty. As a result of the study, it was determined that LED modules should be placed in locations where the radiation effect is minimal, and that lens piece definitely should be used. The study results should be evaluated in detailed to get the desired performance from the new generation of LED modules. The study also found that computational fluid dynamics software should be widely used to determine the behaviours of LED modules in ambient conditions and to eliminate risks.

REFERENCES

1. Rosenberg E., Fidje A., Espegren K.A., Stiller C., Svensson A.M., Moller-Holst S. Market penetration analysis of hydrogen vehicles in Norwegian passenger transport towards 2050. International Journal of Hydrogen Energy. 2010. V35, #14, pp. 7267–7279. doi:10.1016/j.ijhydene.2010.04.153

2. Poppe A., Lasance CJM. On the standardization of thermal characterization of LEDs. Annual IEEE Semiconductor Thermal Measurement Management Symposium, 2009. #2, pp. 151–158. doi:10.1109/STHERM.2009.4810757

3. Kikuchi K., Hamashiam Y., Kobayashi Y. Prediction of LED junction temperatures with CFD for headlamp application. In: ISAL Symposium Proceeding, 2005.

4. Senawiratne J., Zhao W., Detchprohm T., et al. Junction temperature analysis in green light emitting diode dies on sapphire and GaN substrates. Physica status solidi (c), 2008. V5, #6, pp. 2247–2249. doi:10.1002/pssc.200778648

5. Weber R. Calculating an LED's Junction Temperature, 2015.

6. Application Guide, 2010.

7. Thermal Management of SMT LED Application Note, 2014.

8. Bider C. Effect of thermal environment on LED light emission and lifetime. LED Prof Rev May/June 2009, 2009.

9. Bielecki J., Jwania A.S., Khatib F. El., Poorman T. Thermal Considerations for LED Components in an Automotive Lamp. 23rd IEEE SEMI-THERM Symposium, 2007.

10. Rubenstein R.Y., Kroese D.P. Simulation and the Monte Carlo method, 2011.

11. Vora A.K., Vijaykumar P. Basic Thermal Guidelines for using PowerPSoC ®, 2009. #001, pp. 1–12.

12. Sheu G.-J. The heat dissipation performance of LED applied a MHP, 2005. p. 5941, 594113–594118. doi:10.1117/12.616355

13. Jen-Hau Cheng, Chun-Kai Liu, Yu-Lin Chao, Ra-Min Tain. Cooling performance of silicon-based thermoelectric device on high power LED. In: ICT 2005. 24th International Conference on Thermoelectrics, 2005. IEEE; 2005. pp. 53–56. doi:10.1109/ICT.2005.1519885

14. Arik M., Becker C.A., Weaver S.E., Petroski J. Thermal management of LEDs: package to system. Third Int Conf Solid State Light, 2004, 5187 (July 2014), 64. doi:10.1117/12.512731

15. Petroski J. Understanding longitudinal fin heat sink orientation sensitivity for Light Emitting Diode (LED) lighting applications. In: Advances in Electronic Packaging, 2003.

16. Yung K.C., Liem H., Choy H.S., Lun W.K. Thermal performance of high brightness LED array package on PCB. International Communications in Heat and Mass Transfer, 2010. doi:10.1016/j.icheatmasstransfer.2010.07.023

17. Zhong D., Qin H., Wang C., Xiao Z. Thermal performance of heatsink and thermoelectric cooler packaging designs in LED. In: Proceedings – 2010 11th International Conference on Electronic Packaging Technology and High Density Packaging, ICEPT-HDP 2010, 2010. doi:10.1109/ICEPT.2010.5582819

18. Cheng H.H., Huang D.S., Lin M.T. Heat dissipation design and analysis of high power LED array using the finite element method. Microelectron Reliab, 2012. doi:10.1016/j.microrel.2011.05.009

19. Weng C.J. Advanced thermal enhancement and management of LED packages. International Communications in Heat and Mass Transfer, 2009. doi:10.1016/j.icheatmasstransfer.2008.11.015

20. Lai Y., Cordero N., Barthel F., et al. Liquid cooling of bright LEDs for automotive applications. Applied Thermal Engineering, 2009. doi:10.1016/j.applthermaleng.2008.06.023

21. Raypah M.E., M.k. D, Devarajan M, Sulaiman F. Investigation on thermal characterization of low power SMD LED mounted on different substrate packages. Applied Thermal Engineering, 2016. doi:10.1016/j.applthermaleng.2016.02.092

Kemal Furkan Sokmen
is an assistant professor at the Department of Mechanical Engineering, Faculty of Engineering and Natural Science, Bursa Technical University, Bursa, Turkey. He received his Ph.D. in Mechanical Engineering from Bursa Uludag University. His research interests include heat transfer, computational fluid mechanics, electronic cooling, and thermal comfort

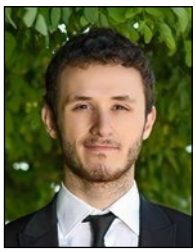

Osman Bedrettin Karatas
is a research assistant at the Department of Mechanical Engineering, Faculty of Engineering and Natural Science, Bursa Technical University, Bursa, Turkey. He received his M.Sc. degree in Mechanical Engineering from Hitit University. His research interests include heat transfer, fluid mechanics and electronic cooling

Light & Engineering
Vol. 28, No. 4, pp. 116–126, 2020

https://doi.org/10.33383/2019-096
Svetotekhnika #3, 2020, pp. 80–88

ANALYSIS ON THERMAL BEHAVIOUR OF THE SINK AND DIE AREA WITH DIFFERENT THERMAL INTERFACE MATERIAL FOR HIGH POWER LIGHT EMITTING DIODES

Debashis Raul and Kamalika Ghosh

School of Illumination Science Engineering and Design, Jadavpur University, Kolkata, India
E-mails: debashis.raul@gmail.com, kamalikaghosh4@gmail.com

ABSTRACT

Its self-heating process directly affects the optical performance and reliability of light – emitting diodes (LEDs). It is important to disperse the generated heat from LED to surrounding atmosphere and keep the LED light performances same as declared by the manufacturer. Thermal interface material (TIM) is applied in between sink and source to reduce contact resistance at the junction between substrate and heat sink interface of the LED modules. This paper provides an assessment on 'thermal interface materials'. Here different TIM materials used and the performance and problems of these commercial interface materials are discussed. From this study, one can calculate the temperature distribution in the sink area for different types of TIM materials under thermal conductivity perspective and be able to find the capability of dissipation of heat at the end surfaces of heat sinks, and design their system as well. In another process, TIMs with different thickness and input drive currents for the COB-based LED are investigated by using *COMSOL* simulation software. The results show that the junction temperature of the LED luminaire increases and reduce the lifetime when the input drive current and thickness of the TIM layers increase.

Keywords: heat dissipation capability, heat sink, junction temperature, luminous flux, thermal interface material (TIM), thermal pad

1. INTRODUCTION

The solid state lighting device like light emitting diode (LED) is the most prospective solution for lighting issue in the today's world considering its low power consumption, long lifetime, eco-friendly behaviour and instant-start-up characteristics over the other conventional lighting sources. In this case, the LED luminaires do not provide the rated light output according to the data provided by the manufacturers in actual use. As a solution, many manufacturers are overload the LEDs at high power to provide more light output. Therefore, an experimental study was conducted to investigate the photometric results of white LED as a function of time with different drive currents [1]. As per the feedback from field, it is reported that improper heat dissipation leads to failure of LEDs. Thus, thermal management [2, 3] is essential for the design of LED based luminaires because of its higher junction temperature, which reduces the light output, luminous efficacy, and of course its reliability too [4, 5, 6, 7].

When a higher driving current is applied to LEDs, although light output increases [8] but it is associated with increase in heat generation, energy consumption etc. Light output again decreases with temperature rise at the junction of the LEDs, which is termed as junction temperature. Daren Alfred Lock et al. [9] described the technique for determining the junction temperature using generated photocurrent within the device. Quan Chen et al. [10] proposed a system for measuring the dynamic junction temperature for LEDs with the calibration includ-

ing instrument calibration and factor *K* calibration. They analysed influence of the fast time switching in dynamic junction temperature test and quantified measurement errors caused by sampling delay. They also conducted a comparative experiment to prove the accuracy of the present system, which shows a good agreement between the experimental data and reference value. Chi-Yuan Lee et al. [11] fabricated a flexible micro resistive temperature sensor to measure the junction temperature of LED, and the junction temperature of the LED can be measured from the linear relationship between the temperature and the resistance. Minseok Ha et al. [12] implemented an analytical thermal resistance model for high-power LED packages of chip-on-board (COB) architecture combined with a power electronic substrate and validated by comparing it with finite element analysis (FEA) results, which allows us to understand the impact of design parameters (e.g., material properties, LED spacing, substrate thickness, etc.) on the packaging thermal resistance. A.E. Chernyakov et al. [13] studied of the current crowding effect on the LED thermal resistance and its variation with the driving current. They had been studied current spreading in a high-power flip-chip LED and its effect on the chip thermal resistance both theoretically and experimentally. Kai Han et al. [14] used different measurement currents to estimate the junction temperature of high-brightness LED at a sampling rate of 1 MHz.

In this study, temperature distributions at the package level and the high power LED- array system had been investigated using numerical models of heat flows and a network model of thermal resistors in combination with a 3D finite element sub model of an LED structure for predicting the system and die level temperatures. This makes it easier to calculate the effect of the LED array density, LED power density, and the method of active and passive cooling during operation of the device [15]. Direct measurements of LED junction temperature are difficult. An alternative method had been developed using current-voltage characteristics of commercial high power LEDs. The same has been used for measurement at six different temperatures in the range from 295 K to 400 K [16]. Comparison of the thermal parameters of various substrates, such as standard glass epoxy substrate (*FR*4) and insulated metal substrate (IMS) for high power LEDs, has been made with an emphasis on cost and size [17]. A deeper understanding of the thermal behaviour of an LED module could be gained by in-depth analysis of the thermal path during operation of the device [18]. LED failure factors are one of the big issues, which are the challenge to find out and solve the said problems. The main failure modes, such as bonding defects, die attaching defects, and other defects caused by poor packaging process, are investigated using some failure analysis cases [19]. Using experiments and numerical analysis, high power LED modules encapsulated with different lens shapes and size after thermal-aging test were studied [20].

Although the claimed lifetime of LEDs is very high, but in tropical countries their lifetime appears very short. Thus, experimentation were conducted using various types of commercially available high power LEDs and in various major locations, e.g. die and sink areas, the test results have been presented here after [21]. Humidity and high temperature are used as accelerating variables, especially for destruction mechanisms associated with optical degradation [22]. In this paper, three different types of thermal interface materials (TIM) with different thermal conductivity were used for the experiment. The main role of TIM materials is to eliminate air gaps or spaces (which act as thermal insulator) from the interface area in order to maximize heat transfer. End surface temperature of the heat sink were measured at intervals up to one-hour and the results were analysed. Another simulation was performed of the COB-based LEDs with different drive currents, as well as thickness of the TIM layer, and the simulation results were investigated.

This paper presents a method for conducting experiments and analysing test data (the temperature of the end surface of the heat sink), as well as a new formula for calculating the junction temperature of LEDs, which could not be measured directly. In addition, an empirical formula has been developed, by which the area of trailing surface of the heat sink can be estimated or calculated based on different operating time. The driver current and the thickness of the LED's TIM layer increase, which raises the junction temperature and reduces its lifetime.

2. LUMINAIRES AND THERMAL INTERFACE MATERIALS SELECTION

This experiment involves ten luminaires, each of which is a commercial downlight type luminaire based on modules SMD (a) and COB (b) with the

Table 1. Luminaires Specifications

LED luminaire	Power	Input current (DC)	Input voltage (DC)	CCT	Dimensions (D×H)	Material
COB-based Cool White	5 W	300 mA	18 V	6500 K	D=75 mm H=22 mm	aluminium alloy
SMD-based Cool White	5 W	300 mA	18 V	6500 K	D=90 mm H=55 mm	aluminium alloy

Table 2. Thermal Interface Materials Specifications

Material name	Thermal conductivity (W/mK)	Typical thickness (mm)
Type 1: thermal paste	0.50	0.0825
Type 2: non-silicone thermal pastes	0.72	0.0825
Type 3: thermal insulator pads	0.90	0.1

same structures as shown in Fig. 1. Two different types of thermal interface materials (TIM) are imported in a different way than provided by the manufacturer. The list of LED modules and material specifications are given below in Table 1 and Table 2, respectively. The heat sink is made of aluminium alloy and surrounds the back of the LED luminaire housing. The typical driver is an external part to LED luminaires**.**

3. METHODOLOGY ADOPTED

3.1. Luminous Flux and Sink Area Temperature Measurement Process of LEDs

In this part of the experiment, selected commercial led lights (both SMD and COB modules) provided by the manufacturer are placed inside the integrating sphere one by one to measure photometric and electrical parameters. The temperature around the luminaire in the integrating sphere is set at room temperature (25 °C). Each LED luminaire is allowed to keep in thermal equilibrium at this temperature, which takes about 45 minutes, and then the luminaire turns on in the nominal mode. Then the stabilization time of a LED luminaire at power-ON condition in the sphere was taken 30 minutes for each case. Then photometric parameters, i.e. luminous flux of the luminaire, are measured according to Indian standards (IS:16106,2012). Electrical and photometric measurements of the luminaires were carried out according to recommended method of IESNA LM-79, designed for electrical and photometric measurements of *SSL* (LED) products. The next step is to measure the surface temperature of the end position of the LED heat sink. For this measurement, an enclosure box made by plywood with a dimension of (350 mm×350 mm×350 mm) was used, and the temperature inside the box was set at (25–27) °C as determined by Joint Electron Device Engineering Council (JEDEC) [23]. Then each LED module was mounted horizontally in the geometric centre of the box, and a non-contact calibrated infrared (IR) camera (Fluke make *Ti* 400) was fixed at a distance of half a meter from the end surface of the heat sink. The temperature measurement of end surface of the sink is recoded at initial condition of the luminaires power-ON condition and carried forward it after every five minutes interval up to one hour. For these cases, TIM materials of all LEDs match the thermal paste provided by the manufacturer (type 1, thermal conductivity of 0.50 W/mK). During IR thermographic measurements, the humidity inside the box was 45 %.

Fig. 1. The selected LED luminaires with external drivers

Then the TIM material normally provided by the manufacturer was removed, and after that a new non-silicone TIM material, such as thermal paste (type 2), whose thermal conductivity is higher (0.72 W/mK), is placed between the substrate and the heat sink. The above experimental procedures were repeated for each LED module. After that, similarly, the higher heat conducting, i.e. non-sili-

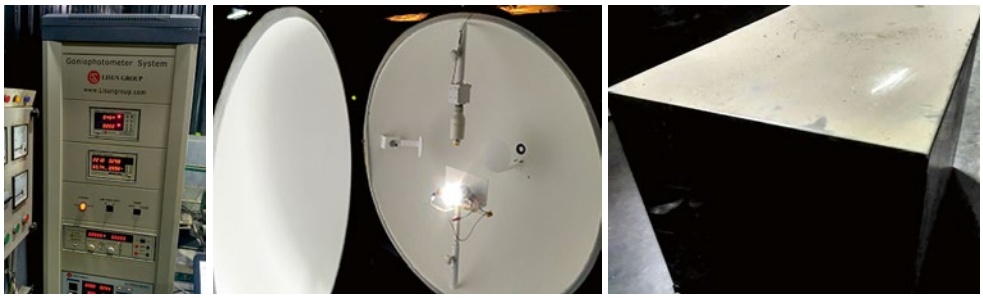

Fig. 2. Experimental setup

cone TIM material was replaced with a thermal insulation pad (type 3), taking the appropriate cleaning process. Then the corresponding measurements of photometric and thermal parameters were made.

All of the above measurements were repeated for 10 times for all the methods, and average values were used in all calculations and graphical plots presented below.

Photometric parameters, such as the luminous flux of both types of COB and SMD-based LED luminaires, were measured using goniophotometric system (photometric integrator, diameter of 1.0 m). Colorimeter type Konic Minolta, model CL 200A, was used as a photodetector. The temperature around the luminaires at the time of measurements should be kept almost at 25 °C. An additional thermometer was used for this condition in the sphere. The Fluke make infrared thermal imager (*Ti* 400) was used to measure temperature using a thermal imager on the surface of the heat sink area. The thermal sensitivity of the *Ti* 400 was ≤ 0.05 °C at 30 °C. The driver output in DC voltage and current were measured at the point where the driver was connected to the LED module. In this study, all the LED luminaires were powered by a current of 300 mA. The experimental setup is shown in Fig. 2.

3.2. Simulated Model of COB-based LED Module

According to the selected COB, a 5 W LED was selected. The overall dimensions of the radiator board are 75 mm in diameter and 22 mm in height, and the material of the sink is aluminium. The chip becomes a heat source during the thermal simulation and has a diameter of 2 mm and height of 0.1 mm. The 3-D model of the LED luminaire is established by *COMSOL* software. The LED chip was connected with the heat sink by type 1 (thermal paste conventionally used by manufacturer – 0.50 W/mK), type 2 (proposed thermal paste – 0.72 W/mK) and type 3 (proposed thermal pad – 0.90 W/mK) TIM materials, one by one. The initial thickness of the type 1 and type 2 TIM materials are 0.0825 mm. However, the thickness of the type 3 TIM material is 0.1 mm. The mesh is applied in the COB-based LED model with all TIM condition. Now the drive current of the LED luminaires are selected as 80 mA, 130 mA, 180 mA, 230 mA, 300 mA, respectively, where the input voltage of the diode is 18 V (DC). Accordingly, the input power of the LED for said drive current is set as 1.44 W, 2.34 W, 3.24 W, 4.14 W, and 5.4 W, respectively. Now in terms of the efficiency of the LED, it is assumed that 80 % of the input power is equal to the thermal power. Therefore, the heat generation rates at *COMSOL* platform are set as follows: (0.92×10^9) W/m^3, (1.49×10^9) W/m^3, (2×10^9) W/m^3, (2.63×10^9) W/m^3, and (3.4×10^9) W/m^3, respectively. For these simulations boundary heating conditions were met on all surfaces of the designed LED module at a given ambient temperature of 27 °C, i.e. 300 K.

Now, type 2 and type 3 materials are selected for further modelling. The thickness of each material is set to double, i.e. 0.165 mm (type 2) and 0.2 mm (type 3). After that, all the condition of the *COMSOL* platform are kept the same as the above process, and simulations are performed to find the required parameters.

4. RESULTS AND ANALYSIS

4.1. Temperature Distribution at Sink Area of the LED Luminaires with Different Types of TIMs

Optical parameters were measured by placing various TIM materials between substrate and sink for two types of LED modules. Here in this experiment, three types of thermal interface material (TIM) were used between substrate and sink with different thermal conductivity, which is shown in Table 2. In each of the cases, the lumen outputs of

Table 3. Luminous Flux for Various TIM Materials between LED Substrate and Heat Sink

TIM materials –’	**Type 1: thermal paste**	**Type 2: thermal paste**	**Type 3: thermal pad**
Thermal conductivity –’	0.50 W/mK	0.72 W/mK	0.90 W/mK
Luminaire types ↓	**Average luminous flux (lm) ↓**		
COB-based 5 W LED	493.90	513.70	521.25
SMD-based 5 W LED	392.00	412.40	435.76

Table 4. Average Temperature at the End Surface of the Sink Area for Three Types of TIM

LED type	**COB-based 5 W LED luminaire**			**SMD-based 5 W LED luminaire**		
TIM material	Type 1: thermal paste	Type 2: thermal paste	Type 3: thermal pad	Type 1: thermal paste	Type 2: thermal paste	Type 3: thermal pad
Thermal conductivity	0.50 W/mK	0.72 W/mK	0.90 W/mK	0.50 W/mK	0.72 W/mK	0.90 W/mK
Time (min)↓	Average Temperature (°C)			Average Temperature (°C)		
Initial	38.4	39.2	39.8	37.1	39.3	39.7
1	39.6	43.3	43.7	37.3	39.6	44.8
10	41.7	46.8	50.6	39.2	45.2	59.2
15	41.6	47.1	51.5	38.4	44.8	59.4
20	42.3	47.5	51.3	39.6	46.7	61.6
25	42.8	47.7	51.5	39.3	46.8	66.4
30	42.5	47.2	51.9	40.3	46.7	70.7
35	42.7	47.2	51.8	41.8	48.0	70.8
40	43.1	47.3	52.0	40.5	48.9	69.8
45	43.8	47.6	51.8	41.9	48.6	68.8
50	44.0	47.3	51.7	42.6	47.0	69.4
55	44.9	47.4	51.8	43.5	48.6	70.3
60	45.2	47.8	51.7	43.3	49.0	69.7

each of the LED luminaires were observed. These optical parameters were recorded after ten measurements rounds, and their average results are shown in the Table 3.

The rated luminous flux of 5 W COB-based LED luminaire is higher than that of 5 W SMD-based LED luminaire. In this study, it is clearly shown that the lumen output is directly affected by the value of thermal conductivity of the LED TIM. When the thermal conductivity of TIM increases, the lumen output of the LED increases. Due to the poor thermal conductivity of the thermal paste, heat accumulates in the interface between the LED substrate and heat sink, so the temperature of the LED chip increases and reaches a high level, which reduces the generation of photons as a result of a lower lumen output. Therefore, heat dissipation from the LED chip is one of the important factors to get the rated lumen output of these types of LED luminaires, which is improved by using higher thermal conductivity of the thermal interface materials.

The temperature of the end surface of the attached heat sink was measured and recoded for both types of LED luminaires when luminaires were at power on conditions. The sink area temperature were taken at the initial moment when the luminaires were switched on and the measurements were continued at intervals of five minutes for one hour. Table 4 shows the average temperatures in sink area as a function of time for both types of LED luminaires with three types of TIM used with different thermal conductivity. The experimental results are shown in Fig. 3, showing the established relationship between operating time (t_b) of LED luminaires

Table 5. Projected Initial Constant Values for Predicting the Temperature of the Sink with Consideration for Operating Time [Ref: Fig. 3]

LED type	COB-based 5 W LED luminaire			SMD-based 5 W LED luminaire		
TIM material	Type 1: thermal paste	Type 2: thermal paste	Type 3: thermal pad	Type 1: thermal paste	Type 2: thermal paste	Type 3: thermal pad
Initial constant value	Projected initial constant value			Projected initial constant value		
p	39.903	44.902	48.976	37.708	41.442	50.861
q	0.0021	0.0013	0.0013	0.0024	0.0034	0.007

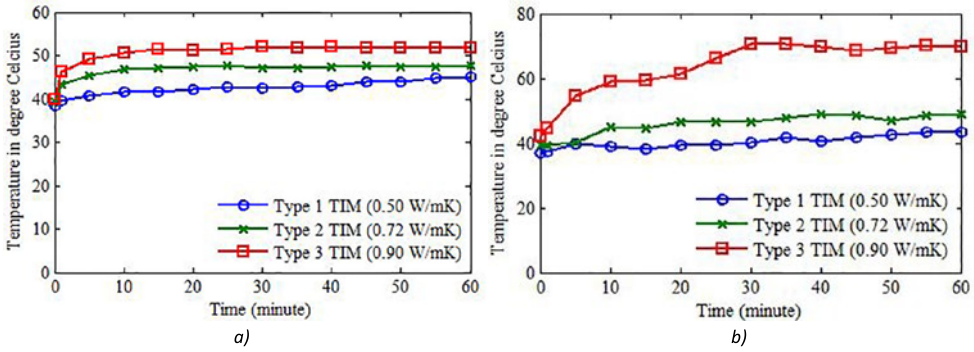

Fig. 3. Temperature at end surface area of the heat sink for a 5 W COB-based LED module (a) and an SMD-based LED module (b) as a function of operating time at room temperature (25 °C) using three types of TIM material

and the temperature of their sink area (T) for three different types of thermal interface materials. The application of the basic curve fitting method to obtain the dependence between the temperature of the sink area (T) or $f(t_b)$ and the operating time of the LED t_b is exponential and can be obtained empirically as an Eq. 1,

$$T = f\left(t_b\right) = p \cdot e^{q \cdot t_b}, \tag{1}$$

where p and q are the projected initial constant values for all two types of LEDs with different TIM materials (Table 5).

The temperature of the LED junction area due to the applied electrical power to the device usually increased during testing, and gradually heat was dissipated from the LED to the surface of the heat sink. This heat release usually depends on the thermal conductivity of the LED packaging materials used. Due to the low thermal conductivity of the TIM material, smooth heat dissipation to the environment is difficult. As can be seen from Fig. 3, the heat release temperature of the sink area is higher when using a higher thermal conductive TIM material for both COB and SMD-based LED luminaires. Therefore, generated junction temperature is more dissipated from LED chip area to its sink area, which gives to chip the ability to reduce excess heat generation. This keeps the health of the LED very good and maintains proper luminous flux as well as reliability.

Measuring the junction temperature of LEDs is very critical and not accurate under normal environmental conditions using an IR sensor or a thermocouple. The applied electrical power of the LED is only converted to light by (20–30)%, and the rest of the power is converted to heat, which caused damage to the LED devices. Therefore, it is very important that the excess heat of the LED junction area is dissipated from the LED into the environment. Currently, there are LED luminaires on the market that usually do not have proper thermal management due to the lack of information about the junction temperature of the LED chip. Therefore, designers of led devices need an easy method for predicting the junction temperature of LED luminaires, which will help them estimate the junction temperature and design LED luminaires with an ideal heat dissipation system. Here, the LED chip manufacturer provides the thermal characterization parameter (ψ_{JH}) to the LED luminaires manufacturer. Now it is possible for a LED luminaires designer to measure the temperature at the end position of the outer surface of LED heat sink. Thus, the junction temperature is calculated using the thermal characterization parameter (ψ_{JH}) from the LED junction

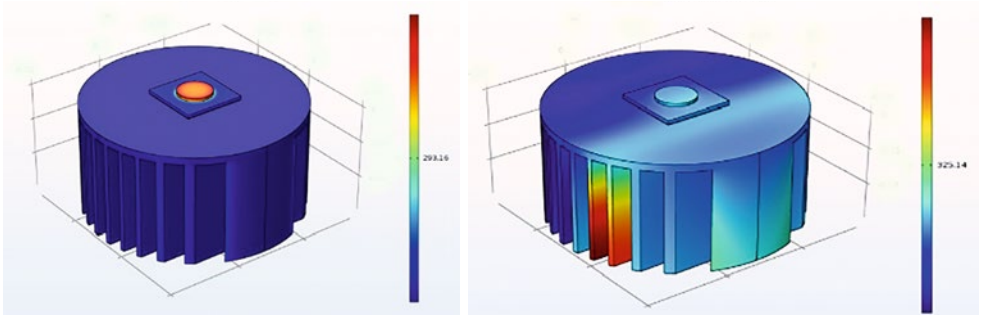

a) *b)*

Fig. 4. Temperature distributions of the COB-based LED by *COMSOL* software at the initial time (a) and after one-hour (b)

to the heat sink, which is defined by JEDEC in Eq. 2 as:

$$\psi_{JH} = (T_J - T_H) / P_d , \quad (2)$$

$$T_J = P_d \cdot \psi_{JH} + T_H , \quad (3)$$

where, T_J, T_H are the junction temperature and heat sink area temperature respectively at steady state and P_d is the power applied. The thermal characterization parameter ψ_{JH} has the unit of °C/W.

4.2. Simulation Results for the Selected Type of LED Module

The simulation calculates temperature distribution and heat fluxes in the structure. Therefore, a COB-based LED chip was designed with mounting pads, thermal interface material such as thermal paste (type 1 and type 2) and thermal pad (type 3), and an aluminium heat sink placed under each LED as shown in Fig. 4. Transient finite element simulations were performed using *COMSOL* software to simulate temperature increase over time through the LED module to heat sink. It was assumed that the heat flow is created by the conduction between the heat source (LED chips) and the heat sink and convection from the package to the air. The heat flow through the bottom/outer surface of the LED heat sink, as well as the junction temperature of the LED chip have been taken from the thermal analysis of the LED luminaire model. In this model, the heat transfer occurs through conduction in the subdomains. The simulated results have been noted over a time period of 1 hour.

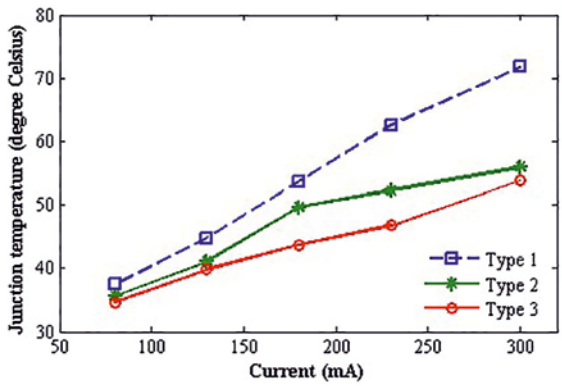

Fig. 5. The relationship between junction temperature and input current for 5 W COB-based LED module using three types of TIM material

4.3. Temperature Distribution of the COB-Based LED Luminaire with TIM as Thermal Pad

The temperature variations in the heat sink area (when using the TIM material as a thermal pad) over time, both for practical and software-simulation process are described in Table 6. The measured temperature in the sink area was taken when the device was in operation. The initial temperature of the LED was measured using an IR thermal imager. The initial value implies the minimum time taken to measure the value, but by this time, the temperature naturally begins to rise. For simulation, the initial temperature means that the device is exactly at the time when it is turned on. Therefore, the initial result of the simulation was an almost perfect position, that is at ambient temperature. Therefore, the measured initial temperature value was shown to be greater than the simulated results. The ambient temperature was set as 27 ˚C at the time of measurement. It is noticed that after 10 minutes when the almost steady state has observed, the percentage variation between the measured temperature and simulated temperature is in the range of about 6 %. A typical simulated diagram of heat distribution at the sink area has been illustrated in Fig. 4. The same thing appears as resemblance to actual nature.

Table 6. Measured and Simulated Temperature of the Sink Area over the Operation Time of COB-Based LED Module

Operation time (min)	Measured temperature (˚C)*	Simulated temperature (˚C)
Initial	39.8	33.1
1	43.7	43.9
10	50.6	47.4
15	51.5	47.3
20	51.3	49.0
25	51.5	49.5
30	51.9	49.7
35	51.8	50.5
40	52.0	50.9
45	51.8	51.8
50	51.7	52.1
55	51.8	52.5
60	51.7	53.1

***** The data given in this column and in Table 4 are puzzling. Indeed, as mentioned above, the radiator has a diameter of 7.7 cm and a height of 2.2 cm that is its volume V is approximately 97 cm^3. Even if we neglect the heat removal from the radiator, to heat it up to a temperature T_1 = 47.3 °C (which, according to Table 5, took place after 1 minute of LED module operation), energy $E_1 \leq C \cdot \rho \cdot V \cdot (T_1 - T_{amb})$. And since the radiator is made of aluminium, then $E_1 \leq 0.9$ J / (g · K) · 2.7 g / cm^3 · 97 cm^3 · (47.3–27) K ≈ 4785 J, and even if the entire consumed LED module power P = 5 W will be spent on heating the radiator, then on heating the radiator to the one given in Table 5 temperature of 47.3 °C, time t_1 will be required, not less than $E_1 / P \leq 4785/5 = 957$ s ≈ 16 min, not 1 min as follows from Table 5.

Remark from interpreter in Russian E. Rozovsky

4.4. Analysis of Simulation Results for a COB-Based LED Luminaire with Different Thickness of the TIMs and Drive Currents

The simulation was conducted in the two ways. First, the thickness of the TIMs was a fixed value while varied the drive current to get the value of junction temperature of the LED luminaires and, lastly, varied the thickness of the TIMs and drive current to monitor the junction temperature. The relationship between junction temperatures at different input drive current is shown in the Fig. 5. The curve shows that the junction temperature increases linearly (approximately) with increasing drive current of the LED. The junction temperature is highest for a type 1 TIM LED luminaire when the LED drive current is 300 mA and is nearly 72 ˚C. In the case of type 3 TIM LED luminaire, the junction temperature is 53.83 ˚C (drive current 300 mA), which is lower than other two TIMs.

Thus, it can be concluded that the heat dissipation from junction of the LED with the sink or the environment depends on the thermal conductivity of

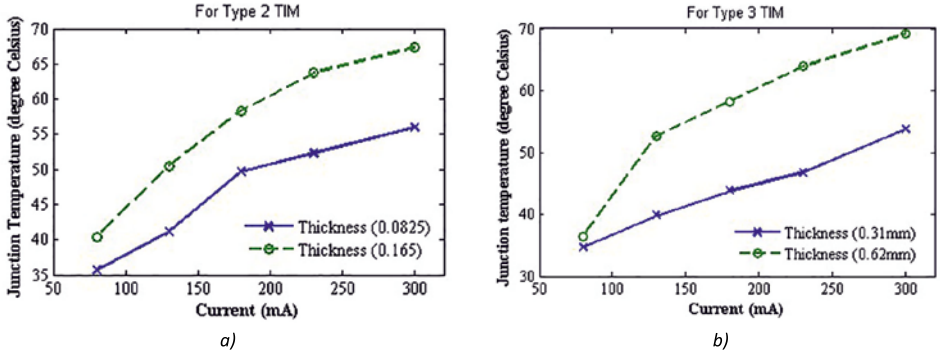

Fig. 6. The relationship between the junction temperature and the input current when varying the thickness of TIMs type 2 (a) and type 3 (b)

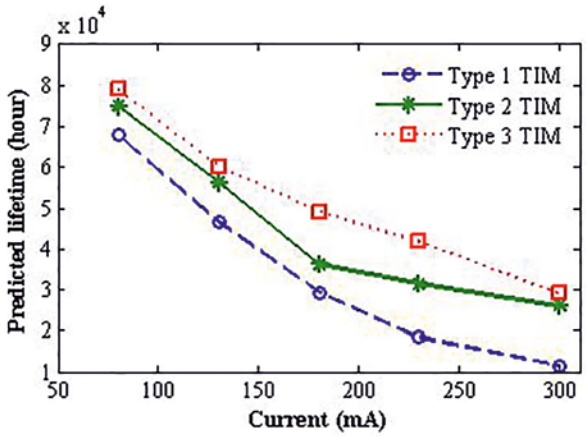

Fig. 7. Predicted lifetime depending on varying current for different TIMs

TIMs and other materials. Here the thermal conductivity of type 3 TIM is higher than other two.

The junction temperature of the LED luminaire changes when the thickness of the TIMs layer changes. In this experiment, the thickness of the type 2 and type 3 TIMs increases. When the thickness of the TIMs increases, the junction temperature of the LED also increases, as shown in Fig. 6. It can be seen that the junction temperature increases for a luminaire with an increased thickness of the TIM layer is higher, that is, up to the maximum at the drive current of 300 mA, the junction temperatures is 67.33 ˚C and 69.11 ˚C for type 2 and type 3 TIMs, respectively.

Therefore, it is assumed that increase in junction temperature of the LED luminaire depends not only on the increase in the drive currents, but also on the thickness of the TIM layers.

Predicting lifetime of a LED luminaire is the one of the important criteria for a LED manufacturer(s). In this experiment, a model based on inverse power law (exponential) is used to predict the lifetime for a LED luminaire [24]. From the model lifetime (L) of the LED:

$$L = \mathrm{A}_{T_j} \cdot e^{-n \cdot T_j}. \quad (4)$$

Here, according to the model [24], $A_{Tj} = 477337$, $n = 0.052$ and T_j is the junction temperature of the certain LED luminaire[1]. Using Eq. 4, you can calculate the predicted lifetime of the LED luminaire with the corresponding junction temperature with each type of TIM. The lifetime of the LED luminaire at different input drive currents is shown in Fig. 7. It can be seen that the lifetime of the LED luminaire is higher with a lower drive current. The type 3 TIM LED has the highest lifetime at various drive currents.

Similarly, the predicted lifetime of the LED luminaire with different thickness of type 2 and type 3 TIMs is calculated. Fig. 8 shows the predicted lifetime of the LED luminaire with different thickness of the TIMs at different input drive current. It can be seen that the lifetime of the LED luminaire decreases with increasing thickness of the TIM layer. As the thickness of the TIM layer increases, the heat release decreases, and as a result, the junction temperature increases. Therefore, the thickness of TIM layer is an important parameter for the designer or manufacturer.

5. CONCLUSION

The optical and thermal characteristics of these two types of LEDs with three types of TIM at dif-

[1] The article does not indicate the units of measurement for the parameters *L* and *Tj,* and at the same time the authors insist that the constants A_{Tj} and *n* are dimensionless.

– If we assume that A_{Tj} and *n* are measured, in hours and 1 / ºC respectively and substitute in formula (6), the temperature of the *p-n* – junction, which is quite acceptable for LEDs, equal to 80 °C, then we obtain a service life of 7450 h, which is somewhat small.

Remark from interpreter in Russian E. Rozovsky

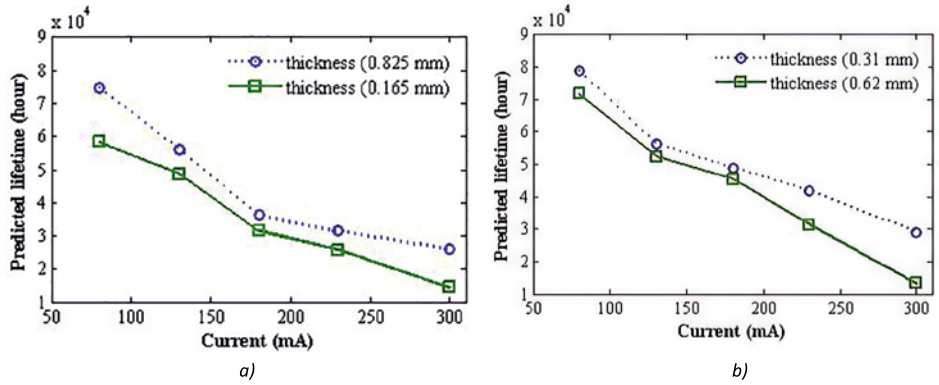

Fig. 8. Predicted lifetime depending on varying current when thickness TIM of the type 2 (a) and type 3 (b) changes

ferent thermal conductivity due to the same input current and power were initially studied using laboratory measurements. This study compares the thermal/ heat dissipation of LEDs with three different TIMs, and the measured results demonstrate that the thermal pad provides very efficient heat dissipation performance and better lumen output compared to the other two. The relationship between LED's heatsink temperature and luminaire operation time of the LED luminaires was obtained. Similarly, the relationship between the junction temperature and the temperature of the LED heat sink was also predicted. Thus, due to proper heat management of LED components, their reliability can be enhanced. This study has shown that, despite technological progress, thermal management is still an important element of luminaire design. A thermomechanical model of commercially available COB-based LED luminaires with three types of TIMs at different input drive currents was studied using finite element method. The junction temperature of COB-based LED luminaire at different drive current with three different TIMs are compared and analysed. Type 3 TIM gives a lower junction temperature than the other two due to its higher thermal conductivity properties, which gives the more heat dissipation through it to the heat sink. It is concluded that the junction temperature increases with an increases in the input drive current and the thickness of TIMs, which reduces the lifetime of the LED. The results can be explained as verification study necessary for the design and simulation of thermal effects and thermal management of COB-based LED luminaires. At the same time, LED manufacturers should take into account that the increase in the junction temperature of the LED luminaire depends not only on the increase in drive currents, but also on the thickness of the TIM layers.

ACKNOWLEDGEMENT

The first author wish to acknowledge the Government of West Bengal, India for providing the fellowship. Authors wish to acknowledge the support received from School of Illumination Sciences, Engineering & Design and Electrical Engineering Department of Jadavpur University, Kolkata, India for providing facilities with experimental set up to complete this work at the laboratory, therein.

REFERENCES:

1. N. Narendran, N. Maliyagoda, A. Bierman, R. Pysar and M. Overington. *Characterizing White LEDs for General Illumination Applications*, SPIE Photonics West Conference, San Jose, CA, SPIE paper 3938–39, Jan, 2000.

2. Mehmet Arika, Charles Beckerb, Stanton Weaverb and James Petroskic. *Thermal Management of LEDs: Package to System*, Third International Conference on Solid State Lighting, SPIE Vol. 5187, doi: 10.1117/12.512731(2004).

3. Guo-guang Lu, Ming-mingHao, Can-xiong Lai and Bin Yao. *Thermal analysis and reliability evaluation on high power Flip chip LED*, IEEE conference, China, ISBN: 978–1–5090–0175–0 (2015).

4. J.-M. Kang, J.-W. Kim, J.-H. Choi, D.-H. Kim, and H.-K. Kwon. *Lifetime estimation of high-power blue light-emitting diode chips*, Microelectron. Reliab. 49, 1231–1235 (2009).

5. M. Meneghini, A. Tazzoli, G. Mura, G. Meneghesso, and E. Zanoni. *A review on the physical mechanisms that limit the reliability of GaN-based LEDs*, IEEE Trans. Electron Devices 57, 108–118 (2010).

6. M. Meneghini, A. Tazzoli, G. Mura, G. Meneghesso, and E. Zanoni. *A review on the physical mechanisms that limit the reliability of GaN-based LEDs*, IEEE Trans. Electron Devices 57, 108–118 (2010).

7. B.-M. Song, B. Han, and J.-H. Lee. *Optimum design domain of LEDbased solid state lighting considering cost, energy consumption and reliability*, Microelectron. Reliab. 53, 435–442 (2013).

8. M. R. Krames, O.B. Shchekin, R. Mueller-Mach, G.O. Mueller, Ling Zhou, G. Harbers, and M.G. Craford. *Status and Future of High-Power Light Emitting Diodes for Solid-State Lighting*, J. Display Technol., 2007. V3, #2, p. 160.

9. Daren Alfred Lock, Simon R.G. Hall, A.D. Prins, B.G. Crutchley, S. Kynaston, and Stephen John Sweeney. *LED Junction Temperature Measurement Using Generated Photocurrent*, Journal of Display Technology, IEEE, May 2013. V9, #5.

10. Quan Chen, XiaobingLuo, Shengjun Zhou, and Sheng Liu. *Dynamic junction temperature measurement for high power light emitting diodes*, American Institute of Physics, Review of Scientific Instruments 82, 084904 (2011).

11. Chi-Yuan Lee, Ay Su, Yin-Chieh Liu, Wei-Yuan Fan and Wei-Jung Hsieh. *In Situ Measurement of the Junction Temperature of Light Emitting Diodes Using a Flexible Micro Temperature Sensor*, Sensors, 9, 5068–5075; ISSN1424–8220, 2009.

12. Minseok Ha, Samuel Graham. *Development of a thermal resistance model for chip-on-board packaging of high power LED arrays*, Microelectronics Reliability, 2012. V52, pp. 836–844.

13. A.E. Chernyakov et al. *Theoretical and Experimental Study of Thermal Management in High-Power AlInGaN LEDs*, IEEE Conference (EuroSimE2014), 978–1–4799–4790–4/14.

14. Kai HAN, Muqing LIU, Shenglong FAN, Haiping SHEN. *Improved Electrical Measurement Method for Junction Temperature of Light Emitting Diodes*, PRZEGLĄD ELEKTROTECHNICZNY (Electrical Review), ISSN0033–2097, R. 88 NR3b/2012.

15. Adam Christensen, Samuel Graham. *Thermal effects in packaging high power light emitting diode arrays*, Applied Thermal Engineering, 2009. V29, pp 364–371. doi:10.1016/j.applthermaleng.2008.03.019

16. A. Keppens, W.R. Ryckaert, G. Deconinck, and P. Hanselaer. *High power light-emitting diode junction temperature determination from current-voltage characteristics*, JOURNAL OF APPLIED PHYSICS104, 093104 (2008).

17. JaroslavFreisleben, Tomas Dzugan, Ales Hamacek. *Comparative Study of Printed Circuit Board Substrates used for Thermal Management of High Power LEDs*, IEEE38th Int. Spring Seminar on Electronics Technology, 978–1–4799–8860–0, 2015.

18. Lisa Mitterhuber et al., "*Investigation of the Temperature-Dependent Heat Path of an LED Module by Thermal Simulation and Design of Experiments*", IEEE Therminic 2016–22nd International Workshop, ISBN978–1–5090–5450–3, 2016.

19. Lu Guoguang, Yang Shaohuaa and Lei Zhifenga. *Failure analysis of LEDs*, IEEE2011 International Symposium on Advanced Packaging Materials (APM 2011), 978–1–4673–0149–7/11, 2011.

20. Y.C. Hsu et al. *Failure Mechanisms Associated with Lens Shape of High-Power LED Modules in Aging Test*, IEEE LEOS2007, 1092–8081, 2007.

21. Ghosh K, Raul D. *Performance analysis of various types of high power light emitting diodes*, Light and Engineering, 2018. V26, #1, pp. 91–98. doi.org/10.33383/2017–045.

22. D Raul and K Ghosh. *Performance of chip-on-board and surface-mounted high-power LED luminaires at different relative humidities and temperatures*, Lighting Research & Technology, 2018. doi: 10.1177/1477153518819040.

23. *Integrated Circuits Thermal Test Method Environmental Conditions – JEDEC Solid State Technology Association* – JESD51–2A, January 2008.

24. F.-K. Wang and T.-P. Chu, "*Lifetime predictions of LED-based light bars by accelerated degradation test*", Microelectron Reliability, July, 2012. V52, #7, pp. 1332–1336.

Debashis Raul
did his B.E. in Electronics & Communication Engineering from West Bengal University of Technology (WBUT). He passed M.E. from Jadavpur University in Electrical Engineering (Illumination Engg.). He has four years teaching experiences as an Assistant Professor at Camellia Institute of Engg. & Technology under WBUT. At present, he is Guest Faculty and Senior Research Fellow (SRF) at School of Illumination Science, Engineering & Design (SISED), Jadavpur University, Kolkata, India

Kamalika Ghosh
did her B.E., M.E. and Ph.D. from Jadavpur University, Kolkata. She has 20 years industrial experiences. At present, she is an Assistant Professor of School of Illumination, Science, Engineering and Design, Jadavpur University. Kolkata, India. She has about 56 nos. of published papers. She is a Life Fellow of Institution of Engineers, India and Indian Society of Lighting Engineers

CONTENTS

VOLUME 28 **NUMBER 6** **2020**

LIGHT & ENGINEERING
(SVETOTEKHNIKA)

PARTNERS OF LIGHT & ENGINEERING JOURNAL

Editorial Board with big gratitude would like to inform international lighting community about the Journal Partners Institute establishment. The list with our partners and their Logo see below. The description of partner's collaboration you can found at journal site *www.sveto-tekhnika.ru*

BL Group
International Lighting Engineering Corporation
BOOS LIGHTING GROUP

ВНИСИ

REFLUX
HID Lighting systems

interlight RUSSIA | intelligent building RUSSIA